INTRACELLULAR UNBOUND CONCENTRATIONS OF ATORVASTATIN AND BOSENTAN: PREDICTION USING MODELING AND SIMULATION, AND EFFECT OF METABOLISM AND TRANSPORT

A Dissertation

Submitted to the

Temple University Graduate Board

In Partial Fulfillment of the Requirements for the Degree

DOCTOR OF PHILOSOPHY

By

Priyanka R.Kulkarni

May 2017

Examining Committee Members:
Dr. Swati Nagar, Advisory Chair, Department of Pharmaceutical Science
Dr. Kenneth Korzekwa, Department of Pharmaceutical Science
Dr. Ho-Lun Wong, Department of Pharmaceutical Science
Dr. Donald Tweedie, External Member, Merck and Company, West Point, PA

ABSTRACT

Accurate prediction of target activity of a drug and rational design of dosing regimen requires knowledge of concentration-time course of the drug at the target. In vitro in vivo correlation (IVIVC) successfully predicts activity and pharmacokinetics of some drugs but is unsuccessful with many others due to poor permeability, transporter activity and use of plasma drug concentrations for determination of PK parameters. According to the free drug hypothesis, at steady state, the unbound drug concentration on either side of a biomembrane is equal. In this case, unbound plasma drug concentration acts as a good surrogate for unbound cell concentrations. However, presence of transporters coupled with poor membrane permeability result in violation of the free drug hypothesis. This results in failure of IVIVC and subsequent discrepancies in the prediction of target activity of pharmacokinetic predictions. Since it is the unbound drug that is capable of exerting the pharmacodynamic effect and available for intracellular metabolizing and transport machinery, knowledge of the unbound concentration inside the cell is very important. Experimental measurement of intracellular unbound concentration is very difficult due to the small size of the cell and complex cellular disposition resulting from activity of metabolizing enzymes, transporters, target binding and organelle binding within the cell. The present study, therefore, aims at predicting the intracellular unbound concentrations using modeling and simulation approach.

Liver perfusion experiments were conducted in male Sprague Dawley rats with uptake transporter substrates atorvastatin and bosentan, in presence and absence of inhibitors of active uptake and metabolism, to study tissue distribution of these drugs in presence of

uptake transport and metabolism. The outflow perfusate data thus obtained were used as input for the explicit membrane model for liver to predict the unbound intracellular concentrations of atorvastatin and bosentan. Similarly, in vivo pharmacokinetic experiments were also conducted in rats in presence and absence of inhibitors of active uptake and metabolism. The data obtained were used as input for hybrid compartmental models to predict unbound concentrations of these drugs upon intravenous dosing. Modeling exercises were also conducted to study the differential impact of inhibition of active uptake on plasma versus unbound cell concentrations. The effect of uptake transport on the induction potential of bosentan was studied in sandwich cultured rat hepatocytes and in in vivo studies in rats.

Inhibition of active uptake in the liver perfusion studies increased the outflow perfusate concentrations, decreased the amount recovered in the bile for atorvastatin and bosentan, and decreased the liver concentrations for atorvastatin. The liver concentrations for bosentan with inhibition of active uptake were not different than the control group. Inhibition of active uptake in the in vivo studies also decreased the systemic clearance of atorvastatin and bosentan. Inhibition of metabolism decreased the systemic clearance of bosentan. It was observed that the perpetrators for metabolism and transport used for this project were not specific for the pathway of interest.

Active uptake appeared to be of major significance for disposition of atorvastatin. The model predicted unbound concentrations of atorvastatin at the end of 50 min perfusion were about 7-fold higher in presence of active uptake than in absence of active uptake. On the other hand, inhibition of metabolism resulted in 1.26 fold increase in unbound

atorvastatin concentrations inside the cell. Modeling the in vivo data indicated that atorvastatin disposition was not affected until 90% inhibition of active uptake clearance was achieved. However, any further inhibition of active uptake clearance had a largely increased the exposure of this drug. The predicted unbound intracellular bosentan concentrations in presence of active uptake were only marginally higher than in the absence of active uptake, possibly due to inhibition of apical efflux of this drug by the uptake inhibitor, rifampin, used in this study. The modeling exercise showed that in the in vivo studies, BOS disposition was sensitive to intrinsic uptake clearance until 99% inhibition was achieved. However, any further inhibition resulted in minimal change in the exposure of this drug. The differential sensitivity of atorvastatin and bosentan exposure for active uptake clearance was thought to be due to the different diffusional clearance for these drugs. For both atorvastatin and bosentan, simulations indicated that any extent of inhibition of the active uptake clearance did not affect the cell exposure of these drugs.

In vitro induction of bosentan could not be characterized in sandwich cultured rat hepatocytes. Bosentan appeared to be a weak inducer of cyp3a mediated metabolism in rats.

In summary, the impact of uptake transport and metabolism on the systemic and intracellular disposition of atorvastatin and bosentan was studied. Liver perfusion and in vivo pharmacokinetic studies along with explicit membrane models were successfully used to predict unbound cell concentrations of atorvastatin and bosentan.

DEDICATION

To,

GURUMAI

Who always lead me through the right path

ACKNOWLEDGEMENTS

My journey as a Ph.D. student has completely transformed me as a person and as a scientist. The people I met along the path have been crucial to this transformation. I learnt valuable lessons from each one of them, and from the circumstances I faced here in the past 6 years. Few of the many valuable lessons I learnt along the path are be patient, handle failure sportively and emerge stronger, and be modest in success. It gives me great pleasure to express my gratitude towards all the people who made it possible for me to get through this program.

I am truly falling short of words to express my gratefulness towards my advisor, Dr. Swati Nagar. Dr. Nagar has been an amazing mentor. She has always been very supportive and patient with me in the difficult times. As a mentor, she provided ample creative space that was very important for the development of my critical thinking ability and scientific skills. She always ensured the development of not only my scientific skills, but also leadership and interpersonal skills by encouraging participation in organizations like AAPS. A person with very solid principles of life that she is, she has been and will always be a great source of inspiration for me. It was indeed a pleasure to pursue my doctoral studies under her guidance.

I would like to deeply thank Dr. Ken Korzekwa for being my co-advisor and a committee member. His valuable insights into my project from time to time were very helpful. I thoroughly enjoyed and learnt a lot from the several scientific discussions I had with him. Dr. Korzekwa has always inspired me for the great and very humble scientist that he is. I would also like to thank Dr. Ho Lun Wong and

Dr. Donald Tweedie for being a part of my committee. My special thanks to Dr. Tweedie for giving me valuable suggestions for career development. It was indeed a pleasure to interact with him at various conferences.

A friendly work atmosphere is crucial for success at a workplace and I am very thankful to my colleagues in the lab for providing me with one. My lab mates – Dr. Aneesh Argikar, Jaydeep, Kim, Dr. Chuong Pham and Min – helped me cope up with the at-times-bumpy ride of Ph.D. by providing constructive insights for troubleshooting. I thoroughly enjoyed all the discussions – ranging from scientific to political - that we had. The memories of room 423 C will always bring a smile to my face and remind me of the good times we had. I would like to specially thank my best friend, Jaydeep, for believing in me and for his immense support in the difficult times.

I would like to thank the past lab members – Dr. Vaishnavi Ganti, Dr. Satish Sharan and Dr. Amir Samaan for teaching me the experimental skills. I would like to thank Dr. Canney, Dr. Doukas and the faculty of School of Pharmacy for providing me with the financial support. I would also like to thank Almira Cutler for her administrative help. I would like to thank Feng Zhou from absorption systems for teaching me the liver perfusion surgery.

Finally, my special thanks to my family - Aai, Baba, Pranjali, Aji-Anna and Mangal Aji-Baba Ajoba. I love you all and would like to thank you so much for believing in me and for being by my side during the ups and downs in my life. I could not have become the person I am today without you all. Aai-Baba, I can imagine how

difficult it must have been for you to send your 21-year-old young daughter to a new country, thousands of miles away. But you never let the apprehension come in the way for the betterment of my future and I am very thankful for that!

TABLE OF CONTENTS

LIST OF FIGURES

LIST OF TABLES

ABBREVIATIONS

2-OH ATV: 2-hydroxy atorvastatin

3-C: 3-compartment

4-OH ATV: 4-hydroxy atorvastatin

5-C: 5-compartment

ABT: 1-aminobenzotriazole

ATV: Atorvastatin

AUC: Area under the curve

BCRP: Breast cancer resistance protein

BOS: Bosentan

BSEP: Bile salt export pump

C_a: Concentration in apical compartment

C_{am}: Concentration in apical membrane

C_b: Concentration in basolateral compartment

C_{bm}: Concentration in basolateral membrane

C_c: Concentration in cell

CE: Collision energy

CL: Clearance

CL_{aec}: Intrinsic apical efflux clearance from cell

CL_{aem}: Intrinsic apical efflux clearance from apical membrane

CL_{bu}: Intrinsic active uptake clearance

CL_i: Diffusional clearance into membranes

CL_m: Intrinsic metabolic clearance

CL_o: Diffusional clearance out of the membranes

CXP: Collision exit potential

CYP: Cytochrome P450

DDI: Drug-drug interaction

DILI: Drug induced liver injury

DMSO: Dimethyl sulfoxide

DP: Declustering potential

FBS: Fetal bovine serum

f_{um}: fraction unbound in microsomal membranes

HBSS: Hank's balanced salt solution

HLM: Human liver microsomes

HMG CoA: Hydroxymethylglutaryl CoA

HPLC: High performance liquid chromatography

IS: Internal standard

ITC: International transporter consortium

IVIVC: In vitro in vivo correlation

IVIVE: In vitro in vivo extrapolation

KETO: Ketoconazole

L: Liter

LC-MS/MS: Liquid chromatography tandem mass spectrometry

LLE: Liquid-liquid extraction

MAC: Macitentan

MATE: Multidrug and toxin extrusion protein

MCT: Monocarboxylate transporter

MDCK: Madine Darby canine kidney

MDR1-MDCK: Multidrug resistance protein- Madine Darby canine kidney

MDZ: Midazolam

Min: Minutes

MRP: Multidrug resistance associated protein

MTBE: Methyl Tertiary Butyl Ether

NMP: N-Methyl-2-pyrrolidone

OAT: Organic anion transporter

OATP: Organic anion transporting polypeptide

OCT: Organic cation transporter

OH-BOS: Hydroxy bosentan

OH-DM BOS: Hydroxy desmethyl bosentan

PD: Pharmacodynamics

P-gp: P-glycoprotein

PK: Pharmacokinetics

PS_{back}: Intrinsic efflux clearance into blood

PS_{bile}: Intrinsic apical efflux clearance into bile

PS_{up}: Total intrinsic uptake clearance

PTV: Pitavastatin

PXR: Pregnane X receptor

Q: Perfusion flow rate to liver

Q_{bile}: Biliary flow rate

QC: Quality control

Q_{Liver}: Blood flow to liver

RIF: Rifampin

RLM: Rat liver microsomes

SULT: Sulfotransferase

$t_{1/2}$: half life

UGT: Uridine-5'diphospho-glucuronosyltransferase

USFDA: United States food and drug administration

V_a: Volume of apical compartment

V_{am}: Volume of apical membrane

V_b: Volume of basolateral compartment

V_{bm}: Volume of basolateral membrane

V_c: Volume of cell

V_d: Volume of distribution

V_{ss}: Steady state volume of distribution

CHAPTER 1: INTRODUCTION

1.1 **Background**

In a drug development program, several factors influence the selection of specific molecules as potential drug candidates over others. Of particular significance are desirable pharmacodynamics (PD) response, optimum physicochemical properties like solubility, hydrophilic-lipophilic balance, minimal nonspecific target activity and the associated adverse reactions and desirable pharmacokinetic properties including but not limited to clearance (CL), volume of distribution (V_d) and in turn the half-life ($t_{1/2}$). Predicted target activities and pharmacokinetic (PK) properties play a large role in selecting drug candidates (Houston, 1994; Heimbach et al., 2009; Zou et al., 2012). It is unlikely that a compound will enter a drug development program without some knowledge of its target activity, metabolic stability, and drug-drug interaction (DDI) potential. Accurate prediction of CL and V_d is necessary for proper design of dosing regimen and predict the potential for DDIs. In order to select the appropriate candidate molecules early in a drug development program, it is important to be able to predict the above properties in vivo accurately using in vitro tools.

The drug concentration-response relationship at the target, determined in vitro along with plasma drug concentration-time profile in vivo, are used to predict the PD effect of a drug. This process of predicting the in vivo properties of a drug from in vitro parameters, called in vitro in vivo correlation (IVIVC), has limitations particularly for drugs that have poor permeability and are transporter substrates (Iwatsubo et al., 1997; Chiba et al., 2009;

Watanabe et al., 2009a; Watanabe et al., 2009b; Watanabe et al., 2009c; Watanabe et al., 2011; Maeda, 2015) . For such drugs, in vivo concentrations in clearance organs and at the target can be significantly different from the plasma concentrations that are typically used for IVIVC. When plasma concentrations are used for IVIVC, the underlying assumption is that the unbound concentration in plasma is equal to the unbound concentration inside the cell. This assumption is based on the free drug hypothesis. The free drug hypothesis states that at steady state, the unbound drug concentration on either side of the biomembrane is in thermodynamic equilibrium (Koch-Weser and Sellers, 1976; Israili, 1979; Pardridge et al., 1983). However, this does not hold true for drugs that are actively transported or poorly permeable (e.g. polar or charged compounds). Thus, the free drug hypothesis is violated in these scenarios. For example, cimetidine is poorly permeable (log D at pH 7.4 = -0.3). Due to this, the concentration of this drug in cerebrospinal fluid, which is an indication of the unbound drug concentration in brain, is 8 and 5 fold lower than the plasma concentration in dogs (Ziemniak et al., 1984) and humans (Somogyi and Gugler, 1983) respectively. Another example where unbound brain concentration is lower than plasma concentration is when the drug is a substrate for efflux transporter (Suzuki et al., 1997). Single-nucleotide polymorphisms in transporter *ABCB1* and *SLC28A2* genes correlated with the intracellular accumulation of the anti-hepatitis C virus drug boceprevir in peripheral blood mononuclear cells (Cusato et al., 2015).

Since the metabolic machinery for most drugs and target of action for some drugs are located inside the cell, it is the intracellular concentration and not the plasma

concentration that drives the metabolism, transport out of the cell, efficacy and/or toxicity of the drug. For example, bile salt export pump (BSEP/ ABCB11) is located on the canalicular side of the hepatocytes and is involved in efflux of monovalent bile salts and acids from the hepatocytes into the bile (Trauner and Boyer, 2003; Alrefai and Gill, 2007). Bile salts and acids are amphiphilic detergents in nature and are involved in solubilizing dietary lipids and assisting in their absorption. Because of their "detergent" nature, bile salts and acids can be tolerated by the cell only at very low concentrations. Elevations in the intracellular concentrations for any reason can result in cell death. BSEP protects the cell by removing the toxic bile acids and salts from the cell. A drug-drug interaction (DDI) involving inhibition of BSEP could, therefore, be fatal to the cell resulting in drug induced liver injury (DILI) (DeGorter et al., 2012). In order to predict the extent of BSEP inhibition by a perpetrator, it is necessary to have knowledge of the intracellular free concentration of the perpetrator, since this is the relevant concentration for the perpetrator's interaction with the transporter.

Under-prediction of cytochrome P 450 (CYP) mediated DDIs is observed when plasma concentrations of the perpetrators are used for predictions. This under prediction is likely due to intracellular perpetrator concentrations being higher than plasma concentrations. Inhibition of uptake or efflux transporters could result in decrease or increase in intracellular concentrations, respectively. For drugs with intracellular targets, this could subsequently cause decreased or increased target activity. For example, simulations indicated that multidrug resistance protein 2 (mrp2) inhibition increased pravastatin liver exposure while organic anion transporting polypeptide (oatp) inhibition increased

pravastatin plasma exposure in rats (Watanabe et al., 2009a). For this reason, the determination of free intracellular drug concentrations at the site of drug clearance or action is of significance. Accurate prediction of intracellular free concentrations can also explain and predict DDIs due to drug metabolizing enzyme inhibition or induction, since the concentration of the perpetrator at the enzyme location is of importance.

1.2 Intracellular disposition of drugs

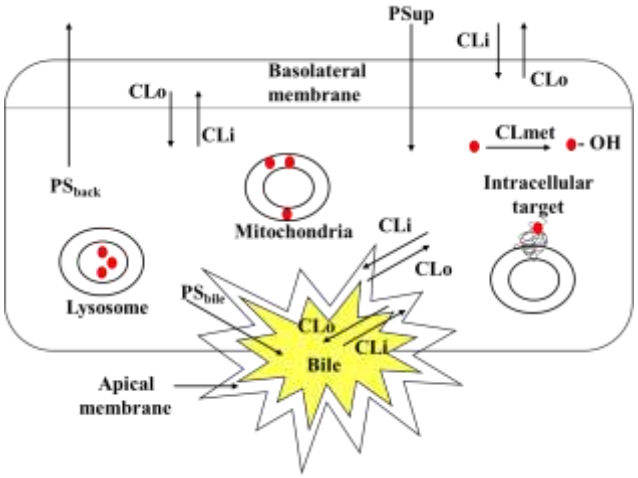

Figure 1.1 Intracellular disposition of drugs. Red solid circle represents a drug molecule

If a hepatocyte is considered as a representative type of cell, a drug molecule can have many possible intracellular disposition pathways within this cell (Fig. 1.1) (Chu et al., 2013). First, the drug has to be taken up into the hepatocytes by uptake clearance (PS_{up}) pathways. Uptake of the drug into the cell can be by transporter mediated active uptake or passive diffusion. For drugs that partition into membranes, membrane partitioning will occur before the drug is measured on the other side of the cell. The drug in membrane

then has an equal probability to diffuse out of the membrane either back into the blood or into the cell compartment (Nagar and Korzekwa, 2012).

Once inside the cell, the drug molecule can be

(a) Metabolized (CL_{met}) by drug metabolizing enzymes like CYPs, uridine glucuronosyl transferases (UGTs), sulfotransferases (SULTs), etc.

(b) Undergo canalicular efflux (PS_{bile}) mediated by apical efflux transporters like P-gp, MRP2, BCRP, etc.

(c) Undergo back efflux into the blood (PS_{back}) either mediated by basolateral efflux transporters like MRP3, MRP4, etc. located on the basolateral membrane of the hepatocytes, or simply by passive diffusion

(d) Get sequestered within cell organelles like lysosomes

(e) Bind to organelle membranes or plasma membrane

(f) Bind to pharmacological targets e.g. a statin binding to the endoplasmic reticulum bound enzyme, HMG-Co-A reductase.

1.2.1. Transporters

Membrane transporters are key players that control the elimination and/or distribution of many drugs thereby determining their pharmacokinetic, safety and efficacy profiles. P-glycoprotein (P-gp/ ABCB1), breast cancer resistant protein (BCRP/ ABCG2), multidrug resistance associated protein (MRP2/ ABCC2), organic anion transporting polypeptide 1B1 and 1B3 (OATP1B1/SLCO1B1 and OATP1B3/SLCO1B3), organic cation

transporter 2 (OCT2/ SLC22A2), organic anion transporters 1 and 3 (OAT1 / SLC22A6 and OAT3/SLC22A8), multidrug and toxin extrusion protein (MATE/ SLC47A) and bile salt export pump (BSEP/ ABCB11) are some of the important transporters that affect drug disposition and toxicity (Giacomini et al., 2010; Hillgren et al., 2013). The International Transporter Consortium (ITC) recommends that these transporters be studied in vitro to evaluate propensity for potential drug-drug interactions (DDIs) (Giacomini et al., 2010; Hillgren et al., 2013). Moreover, all of them transport endogenous molecules. For example, epinephrine, nor-epinephrine, serotonin, dopamine, histamine (Nies et al., 2011), tryptophan (Song et al., 2012), and creatinine (Koepsell, 2013) are endogenous substrates for OCT2. OATs are involved in transport of cortisol, estrone-3-sulfate, hormones and toxicants like organic mercury conjugates, perfluorooctanoic acid, etc. (VanWert et al., 2010). The endogenous substrates for BCRP are porphyrins (Krishnamurthy et al., 2004), folates, uric acid (Woodward et al., 2009), Aβ peptide, etc. BCRP was investigated for its protective role in Alzheimer's disease because of its ability to protect the brain from the entry of Aβ peptide (Pahnke et al., 2008; Xiong et al., 2009). As mentioned before, monovalent bile acids and salts are transported by BSEP (Trauner and Boyer, 2003; Alrefai and Gill, 2007). N^1-methylnicotinamide (NMN), choline, epinephrine, and dopamine are transported by MATEs (Roch-Ramel et al., 1992). Platelet activating factor, interferon γ, peptides, steroid hormones, interleukin-2, and interleukin-4 are substrates for P-gp (Eckford and Sharom, 2006). Sulfated steroids, leukotrienes, glutathione, bilirubin glucuronides are endogenous substrates for MRP2 (Wang et al., 2007).

These major transporters involved in drug disposition are, therefore, crucial for maintenance of normal physiology. Alteration in the function of any of these transporters due to genetic defects or DDIs could result in disturbance in normal physiology and the xenobiotic handling ability of the body may be compromised. As much as these transporters play an important role in transporting endogenous molecules and protecting cells from xenobiotics, they complicate drug disposition and prediction of pharmacokinetics (PK), safety and efficacy profiles of drugs. Uptake transporters increase while efflux transporters decrease the intracellular concentrations of their substrates. When transporters are involved in the disposition of a drug, prediction of in vivo clearance from in vitro data may not be accurate. Other in vitro experimental models like hepatocytes may improve the clearance predictions. The knowledge of various transporters involved in drug disposition apart from drug metabolizing enzymes then becomes important. Several excellent reviews and books cover details about various transporters (Wang et al., 2007; Giacomini et al., 2010; Hillgren et al., 2013), but OATPs are discussed in more detail below because this transporter family was the focus of the present work.

OATPs

Human organic anion transporting polypeptides (OATPs) are uptake transporters of significance in tissue distribution, renal and hepatic clearance, and intestinal absorption of drugs (Nozawa et al., 2005; Maeda et al., 2006; Kalliokoski and Niemi, 2009). OATPs are one of the most widely studied transport proteins (Tirona and Kim, 2007). The human OATPs are members of the ‘solute carrier’ family of transporters and are encoded by the

solute carrier *OATP (SLCO)* genes. The isoforms of OATPS found in humans are OATP1A2, OATP1B1, OATP1B3, OATP1C1, OATP2A1, OATP2B1, OATP3A1, OATP4A1, OATP4C1, OATP5A1, OATP6A1 (Tirona and Kim, 2007). Of these, OATP1B1, OATP1B3 and OATP2B1 are found in liver, where they are located on the basolateral or the blood side of hepatocytes. Other tissues where OATPs are expressed include small intestine, kidney, large intestine, brain, placenta and testes. The most important *SLCO1* family genes are found in the p12 locus on the shorter arm of chromosome 12 (Niemi et al., 2011). These transport proteins demonstrate characteristic sodium independent transport behavior. OATPs have broad substrate specificity. They are crucial in the disposition of drugs like endothelin receptor antagonists (Treiber et al., 2007), cardiac glycosides (Bossuyt et al., 1996), angiotensin II receptor antagonists (Yamashiro et al., 2006) and importantly, hydroxymethyl glutaryl (HMG) CoA inhibitors (statins) (Hsiang et al., 1999; Hirano et al., 2004; Schneck et al., 2004; Kameyama et al., 2005). Some of the classical OATP1B1 substrates are ATV, bosentan, rosuvastatin, pitavastatin, rifampin, valsartan, olmesartan, methotrexate, etc. (Tirona and Kim, 2007). Rifampin is also a competitive inhibitor for OATP transport and has been used in this study as an uptake inhibitor of OATP and BOS. Uptake transporters like OATPs increase the intracellular concentration of their substrates in the hepatocytes, and these concentrations can be many-fold higher than their plasma concentrations. Polymorphisms in OATPs result in differential hepatocyte versus plasma exposure of substrates and have significant impact on drug pharmacokinetics (PK) (Chung et al., 2005; Lee et al., 2005; Niemi et al., 2005; Katz et al., 2006; Xiang et al., 2006; Zhang et al., 2006). This is

crucial especially in the case of statins since rhabdomyolysis is a severe side effect associated with statin use. Cerivastatin was voluntarily withdrawn from the market in 2001 owing to cases of rhabdomyolysis followed by resultant renal failure (Furberg and Pitt, 2001).

1.2.2. Effect of transporter enzyme interplay

The intracellular drug concentration increases due to uptake into the cell, and decreases due to metabolism, apical or basolateral efflux of the drug out of the cell.

The overall intrinsic plasma clearance of the drug that is a substrate for metabolizing enzymes, uptake and efflux transporters is given by the following equation (Miyauchi et al., 1987):

$$CL_{int,all} = PS_{up} \times \frac{PS_{bile} + CL_{met}}{PS_{back} + PS_{bile} + CL_{met}} \quad \ldots\ldots\ldots\ldots\ldots\ldots (1.1)$$

Where, $CL_{int,all}$ is the overall intrinsic clearance, PS_{up} is the intrinsic uptake clearance, PS_{bile} is the biliary efflux clearance, CL_{met} is the metabolic clearance and PS_{back} is the basolateral efflux clearance back into the blood.

There are several scenarios where equation 1.1 can be reduced to a simpler form.

(1) When the sum of the metabolic and biliary clearances is much larger than the basolateral efflux clearance back into the blood, then the PS_{back} term can be ignored and the equation 1.1 simplifies to:

$$CL_{int,all} \approx PS_{up} \ldots\ldots\ldots\ldots\ldots\ldots\ldots (1.2)$$

In this case, the overall intrinsic clearance of the drug depends on the uptake clearance, and not on metabolic or biliary clearance. In other words, the uptake of the drug is the

rate determining step in its elimination. Therefore, metabolic clearance determined by in vitro experiments may not result in accurate clearance prediction.

(2) If a drug is not a substrate for uptake transporters and does not have permeability limitation, then unbound drug can freely pass the biomembrane. If the drug is not a substrate for basolateral efflux transporters, then the active uptake clearance in equation 1.1 becomes equal to the basolateral efflux term. Also, if the basolateral efflux term is much larger than the sum of metabolic and biliary efflux clearances, then equation 1.1 reduces to:

$$CL_{int,all} = PS_{bile} + CL_{met} \quad \text{..... (1.3)}$$

If the drug undergoes minimal biliary elimination, then microsomal clearance may result in good approximation of the in vivo clearance.

(3) If the drug is a substrate for uptake transporters, and the basolateral efflux clearance is much larger than the sum of metabolic and biliary clearances, then equation 1.1 takes the following form:

$$CL_{int,all} = PS_{up} \times \frac{PS_{bile} + CL_{met}}{PS_{back}} \quad \text{.....(1.4)}$$

In this case, the intrinsic clearance of the drug is dependent on all the pathways involved in the intracellular disposition. Similar to case 1, microsomal clearance determined in vitro may not be a good representation of the in vivo clearance.

It is important to note that increase in plasma concentrations due to DDIs may not be always reflected as a decrease in intracellular concentrations. For example, elevation in plasma concentrations of uptake transporter substrates due to inhibition of active uptake may not necessarily indicate a decrease in intracellular concentration. It has been shown

by simulations with pravastatin that inhibition of active uptake resulted in elevated plasma concentrations with minimal decrease in liver concentrations (Watanabe et al., 2009a). On the other hand, inhibition of MRP2 mediated apical efflux of pravastatin resulted in elevated liver concentrations with minimal change in plasma concentrations. Therefore, changes in drug concentrations in one physiological compartment (e.g. plasma) should be interpreted with caution to reflect changes in concentrations in other compartments (e.g. cell).

1.2.3. Intracellular binding

As mentioned before, once inside the cell, the drug can partition into the lipid components within the cell. This includes the organelle membranes or plasma membrane (Pfeifer et al., 2013). This is commonly known as nonspecific binding of drugs. The extent of drug partitioning into the cell and organelle membranes is governed by the physicochemical properties of the drug. The main contributing factors are the lipophilicity, polar surface area and the type of charges present in the drug molecule. It has been recently shown that certain drugs preferably partition into one organelle over another, possibly due to differences in lipid content of the organelle membranes resulting in varying affinities of the drug towards the membrane. For example, in perfused rat liver, subcellular localization of drugs was studied by differential centrifugation to separate various cell fractions (Pfeifer et al., 2013). The percentage of ritonavir present in cytosol, mitochondria and microsomes was 36%, 18% and 31% respectively. Rosuvastatin on the other hand was concentrated mostly in the cytosol (72%).

Furamidine was recovered in mitochondria (43%), nucleus (18%), lysosomes (15%) and cytosol (24%).

1.2.4. Lysosomal sequestration

Basic drugs enter the lysosomes and get sequestered within the organelle by a process called lysosomal trapping (De Duve et al., 1974; Macintyre and Cutler, 1988; Duvvuri and Krise, 2005; Kazmi et al., 2013). Entrapped weak bases can readily diffuse back into the cytosol via passive diffusion. However, moderate to strong bases get protonated in the acidic environment of lysosomes (pH = 4.5 - 5) and hence get entrapped permanently in their cationic state (Goldman et al., 2009). Lysosomal sequestration can also result in decreased free fraction of the drug inside the cell. For example, several anticancer drugs like sunitinib (Gotink et al., 2011), mitoxantrone (Smith et al., 1992), doxorubicin (Hurwitz et al., 1997; Herlevsen et al., 2007), daunorubicin, and imidazoacridinones (Adar et al., 2012) have been shown to accumulate in the lysosomes. Lysosomal sequestration is thought to decrease the drug induced cytotoxic effect on cancer cells since the unbound drug concentration at the target decreases. Lysosomal sequestration does not occur after cell lysis

1.3 Determination of intracellular unbound concentrations: current methods and challenges

Binding to or sequestration in cell organelles, or target binding, will reduce the free fraction of the drug in the cell. The resultant free fraction inside the cell is governed by the relative magnitudes of all of the above intracellular disposition pathways. Therefore,

it is necessary to have a thorough mechanistic understanding of each individual pathway and the effect of its interplay with other disposition pathways, in order to predict the unbound intracellular drug concentrations. While, the crosstalk between these interacting pathways is crucial for the survival of the cell, it also poses a challenge for the determination of intracellular unbound drug concentrations. Moreover, another aspect that makes the determination of unbound intracellular concentrations difficult is the size of the cell. With current technology, it is impossible to devise equipment that can probe the cell to give quantitative information about the unbound drug concentrations therein.

Current methods to indirectly determine intracellular free drug concentrations include microdialysis, fluorescence imaging, tomography imaging, capillary electrophoresis, equilibrium dialysis of tissues, microscopic imaging and particle induced photon emission (Chu et al., 2013), secondary ion MS (Dollery, 2013), and differential centrifugation in sandwich-cultured hepatocytes (Pfeifer et al., 2013). Most of these techniques have practical or financial limitations. Microdialysis is limited to preclinical species. Moreover, when microdialysis is used to measure unbound brain concentrations from cerebrospinal fluid, it is possible that unbound cell concentrations are not obtained since the free drug hypothesis may not hold true for some drugs due to involvement of transporters. Fluorescence imaging requires the drug to fluoresce, which is not a characteristic of every compound. Tissue homogenization does not consider the various compartments within the tissue and cell, like biliary compartment and subcellular organelles, and can give erroneous results when the drug preferentially distributes into one of the compartments e.g. lysosomal partitioning. Modification of molecules to

include moieties of radiolabeled elements for tomography imaging could modify their affinity towards enzymes and transporters. Equilibrium dialysis in hepatocytes is not useful when the drug is a substrate for one or more transporters. The imaging and particle induced photon emission techniques may give erroneous results due to artifacts arising as a result of freezing or fixation steps in tissue processing. Thus, experimental measurement of intracellular free drug concentration is very difficult.

Models to predict unbound intracellular concentrations in presence and absence of efflux transporters in Madin-Darby canine kidney (MDCK) and Multidrug Resistance Protein 1 -MDCK (MDR 1-MDCK) cell monolayers have been reported (Korzekwa et al., 2012). Compartmental models have also been described to study the P-gp mediated apical efflux of drugs (Korzekwa and Nagar, 2014). While experimental lag times have also been previously observed in the permeability experiments performed in cell monolayers (Knipp et al., 1997), the 3 compartment (3 C) model, composed of apical, cellular and basolateral compartments, did not predict the observed lag times. Since lag times could be a result of partitioning into membranes, the previous 3 C model was expanded into a 5 compartment (5 C) model to include explicit apical and basolateral membrane compartments (Korzekwa et al., 2012). Apart from predicting the lag times, the 5 C model gave lower systematic error. Processes such as membrane partitioning (and resulting experimental lag times) and transport out of the membrane can be accurately modeled with the inclusion of explicit membrane compartments (Knipp et al., 1997; Korzekwa et al., 2012).

1.4 Perfused liver to study effect of uptake and metabolism

The human liver is divided into four lobes, each of which is made up of several lobules. A lobule is a hexagonal sub-unit of a lobe (Fig. 1.2).

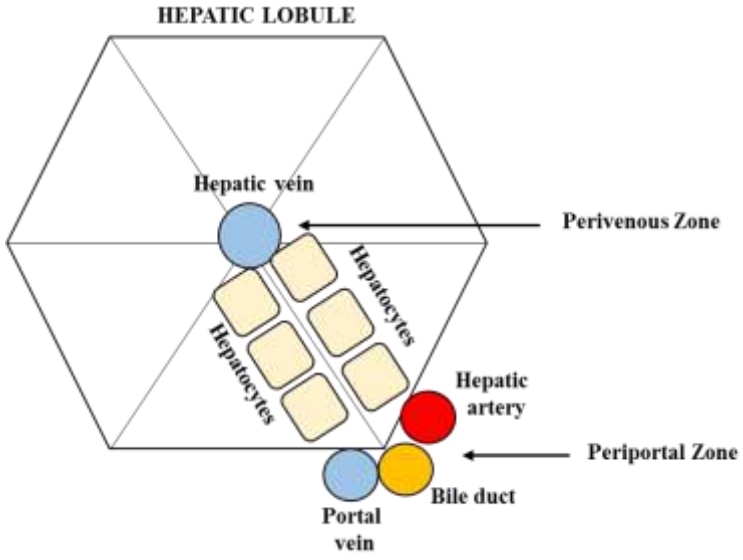

Figure 1.2 Schematic representation of a hepatic lobule, the functional subunit of liver

The blood enters a lobule through the area called the portal triad (Ternberg and Butcher, 1965). The portal triad is made up of branches of hepatic artery, portal vein and bile duct. The portal triad is located towards the periphery of the lobule. The blood entering through the peripheral portal triad flows towards the central vein, perfusing the hepatocytes along its path. The central vein ultimately empties into the hepatic vein. The part of the lobule where the central vein is located is called the perivenous zone. From the periportal zone to perivenous zone, the liver is heterogenous with respect to the oxygen and nutrient content of the blood, mitochondrial content of the hepatocytes, level of expression of enzymes and transporters, etc. Thus, in reality, the liver is not a well-stirred

organ. Therefore, a whole organ experimental model may be better to study drug disposition in liver as compared to the simpler cellular systems. Therefore, liver perfusion was selected as the experimental model for this project. However, this model is relatively tedious and impractical to use for faster data generation as compared to the cellular systems.

1.5 Drugs of interest

1.5.1. Atorvastatin (ATV)

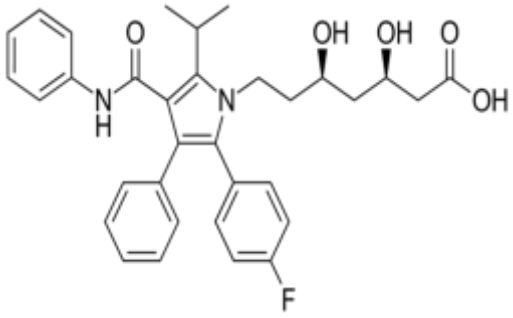

Figure 1.3 Structure of ATV

(https://pubchem.ncbi.nlm.nih.gov/compound/atorvastatin, accessed on 03/12/2017)

ATV (Fig. 1.3) is a member of the 'statin' class of drugs that are responsible for reducing the blood cholesterol level by inhibiting HMG Co A reductase, the rate limiting enzyme in cholesterol synthesis (Nawrocki et al., 1995). HMG Co A reductase is a membrane bound enzyme anchored to the endoplasmic reticulum with the active site facing the cytosol (Istvan et al., 2000).Upon oral administration ATV may be absorbed in the systemic circulation by passive diffusion or by various transporters like monocarboxylate transporters (MCTs) or OATPs. The oral bioavailability of ATV was found to be 14% in humans. The clearance and V_{ss} of ATV was 625 mL/min and 381 liters, respectively

(Gibson et al., 1997). The elimination $t_{1/2}$ of ATV has been reported to be 7 hours (Kantola et al., 1998; Lilja et al., 1999). In vivo, the ATV acid form exists in equilibrium with its lactone form.

Metabolism

The circulating metabolites of ATV detected in human plasma are 2-hydroxy atorvastatin (2-OH ATV) and 4-hydroxy atorvastatin (4-OH ATV) (Michniewicz et al., 1994; Kantola et al., 1998) (Jacobsen et al., 2000). Both hydroxy metabolites exist in equilibrium with their respective lactone forms. Both hydroxy metabolites were also observed in rats (Black et al., 1999). CYP3A4 is the primary enzyme involved in the formation of the hydroxy metabolites. Glucuronidation of ATV by UGTs has also been reported in human liver microsomes. Glucuronidation is a minor metabolic pathway for metabolism of ATV in human liver microsomes. In humans, ATV glucuronidation by UGTs 1A3, 1A4 and 1A9 yield the minor ATV ether glucuronide. UGTs 1A1, 1A3, 1A4, 1A8 and 2B7 form a major ATV acyl glucuronide, which is spontaneously converted to ATV lactone. UGTs 1A1, 1A3, 1A4, 1A8, 2B7 convert the ATV lactone to another ether glucuronide (Prueksaritanont et al., 2002; Goosen et al., 2007). The biliary route is the major route of elimination for ATV and its metabolites (Le Couteur, 1996), while only 1% of drug related material is excreted in the urine (Stern 1997).

Transport

Hepatic uptake transporters OATP1B1, OATP1B3, OATP2B1and NTCP have been reported to mediate transporter mediated uptake clearance of ATV into hepatocytes

(Hsiang et al., 1999; Grube et al., 2006; Choi et al., 2011; König, 2011; Karlgren et al., 2012). Active uptake of ATV in rats is mediated by uptake transporters oatp1a1, oatp1a4 and oatp1b2 (Lau et al., 2006a). Apical efflux transporters like MRP2 (Lau et al., 2006a; Ellis et al., 2013) and P-gp (Boyd et al., 2000; Hochman et al., 2004; Holtzman et al., 2006) also transport ATV.

DDIs

The most common type of DDIs observed for ATV are at the level of active uptake transport. ATV has been observed to be both a perpetrator as well as a victim for OATP mediated drug interactions. RIF significantly increased the exposure of ATV in healthy human subjects (Lau et al., 2007; Maeda et al., 2011) as well as rats (Lau et al., 2006b). Multiple dosing of RIF significantly decreased ATV exposure possibly due to induction of both OATPs and CYP3A4 (Backman et al., 2005).

Since disposition of ATV is limited by uptake, inhibition of metabolism should have no effect on the plasma exposure of ATV. Indeed, no change in ATV plasma exposure was observed in mice with co-administration of ketoconazole (a cyp3a inhibitor), while RIF significantly increased the plasma exposure of ATV in the same study (Chang et al., 2014). One clinical study reported a 3-fold increase in exposure of ATV upon co-administration with itraconazole (Kantola et al., 1998), while another study reported no change in ATV exposure with itraconazole co-administration (Maeda et al., 2011).

1.5.2 Bosentan (BOS)

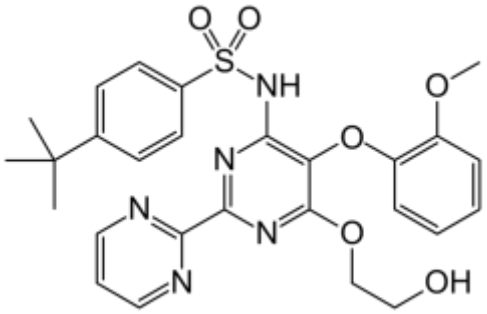

Figure 1.4 Structure of BOS

(Reference: https://pubchem.ncbi.nlm.nih.gov/compound/Bosentan, accessed on 03/12/2017)

BOS (Fig. 1.4) is an antihypertensive agent that exerts its pharmacological effect by acting as a competitive inhibitor of the endothelin receptors ET_A and ET_B. The oral bioavailability for BOS is 50% (Weber et al., 1996). The volume of distribution at steady state (Vss), CL and $t_{1/2}$ are 17.5 L, 145 mL/min and 4.5 hours, respectively (Weber et al., 1999b). BOS is highly bound to plasma proteins, mainly albumin. The fraction unbound in human plasma is 0.02 (Meyer and Brandt, 1996).

Metabolism

BOS undergoes CYP mediated oxidative metabolism in humans by CYP3A4 and CYP2C9. The contributions of CYP3A4 and CYP2C9 to the metabolism of BOS were found to be 60% and 40% respectively (Dingemanse and van Giersbergen, 2004). The exposure of metabolites in human plasma upon intravenous dosing of BOS was found to be 23% that of the parent (van Giersbergen et al., 2002). CYP3A4 and CYP2C9 mediate

aliphatic hydroxylation of BOS to form hydroxy BOS (OH-BOS) (Gasser R, 1995). Hydroxylation of BOS at a site (meta position of the phenol ring), other than the one involved in the formation of OH-BOS, has also been reported (Matsunaga et al., 2015). CYP3A4 also results in oxidative demethylation of BOS leading to the formation of desmethyl BOS. Both hydroxylation and demethylation can be followed by subsequent demethylation and hydroxylation, respectively, resulting in formation of hydroxy-desmethyl BOS (OH-DM-BOS) (van Giersbergen et al., 2002; Dingemanse and van Giersbergen, 2004). Recently, a BOS-glucuronide formed by UGT1A1 was also reported as one of the metabolites (Fahrmayr et al., 2013)

The three major BOS metabolites found in humans were also found to be present in Wistar rats (Treiber et al., 2004). Unlike in humans, the exposure of BOS metabolites in plasma was only 1-2% of the parent (Treiber et al., 2004). Upon intravenous dosing in rats, 98% of drug related material was excreted in the bile and 1% was found in urine. The drug related material found in bile comprised 6-8% unchanged BOS, 4-5% desmethyl BOS, 9-10% OH-DM BOS, and 62-64% OH-BOS. The drug related material in urine comprised OH-BOS and desmethyl BOS.

Transport

Active uptake of BOS into hepatocytes is mediated by OATP1B1 and OATP1B3 (Treiber et al., 2007). Uptake studies in hepatocytes demonstrated that active uptake contributed 48.9% to the total uptake of this drug (Yabe et al., 2011). BOS is known to induce cholestasis by inhibition of taurocholate efflux by BSEP, resulting in DILI (Fattinger et al., 2001; Mano et al., 2007; Lepist et al., 2014). BOS also inhibited taurocholate uptake

by OATP1B1, OATP1B3 and NTCP (Lepist et al., 2014). Whether BOS is a substrate/ inhibitor of P-gp is controversial. Some groups have reported it to be a weak P-gp substrate (Hartman et al., 2010), while others have reported that it is neither a substrate nor an inhibitor of P-gp (Weber et al., 1999b; Treiber et al., 2004). BOS is also a substrate for human (Fahrmayr et al., 2013) and rat MRP2 (Fouassier et al., 2002).

DDIs

Inhibition of active uptake mediated by OATP is one of the major interactions altering BOS PK. Rifampin (RIF), cyclosporine A, and sildenafil have been observed as inhibitors of OATP mediated BOS uptake (Treiber et al., 2007). Cyclosporine A increased exposure of BOS in rats (Treiber et al., 2004). Imatinib increased BOS exposure in humans (Renard et al., 2015). An increase in exposure of BOS was observed in clinic upon treatment with ketoconazole (KETO) (Van Giersbergen, 2001). In the same study, the exposure of desmethyl BOS and OH-DM BOS decreased, while exposure of OH-BOS increased. BOS is a known inducer of CYP3A4 (Weber et al., 1999b; van Giersbergen et al., 2002; Dingemanse and van Giersbergen, 2004; Shou et al., 2008). It induces its own metabolism as well as metabolism of other CYP3A4 substrates.

1.6 Hypotheses

The broader hypotheses of this dissertation are:

1) Inhibition of active uptake transport and metabolism can have differential impacts on the plasma and liver concentrations of drugs.

2) For an uptake transporter substrate, intracellular unbound concentration can better predict a pharmacological effect exerted by an intracellular target.

3) Experimental and modeling techniques can be successfully combined to predict intracellular unbound drug concentration in presence of metabolism and transport.

1.7 Goals

The broader goals of this project were

1) To generate in situ liver perfusion data for ATV and BOS with inhibition of metabolism and/or transport in the rat.

2) Use the 5-compartment explicit membrane model to model the data generated from the liver perfusion experiments, parameterize various clearances involved in intracellular drug disposition and thereby predict the intracellular unbound drug concentration.

3) Verify whether effects of intracellular targets can be better predicted by using intracellular unbound drug concentrations instead of plasma concentrations.

4) Predict unbound intracellular drug concentrations by using rat in vivo PK data.

In order to test the stated hypotheses and address the goals, the following specific aims were evaluated.

1.8 Specific Aims

1) Development and validation of a bio-analytical method for quantitation of ATV and BOS.

LC-MS/MS based bioanalytical methods were developed for quantitation of ATV, 2-OH ATV, and 4-OH ATV in perfusate, liver homogenate and bile. A bioanalytical method was developed for ATV analysis in Sprague Dawley rat plasma and hepatic microsomal matrix. Similarly, a bioanalytical method was developed for quantitation of BOS in perfusate, liver homogenate, bile, microsomal matrix and plasma, and for OH-BOS and OH-DM BOS in perfusate, liver homogenate and bile. Analysis of ATV, BOS and their metabolites from complicated biological matrices required extraction of these analytes from the matrices. Therefore, liquid-liquid extraction was performed for ATV, 2-OH ATV and 4-OH ATV using the organic solvent methyl-t-butyl ether. For BOS, OH-BOS and OH-DM BOS, dichloromethane was used as the extracting solvent. The analytical methods were validated by inter day and intraday evaluation with at least 3 quality control samples.

2) Liver perfusion to study the effect of inhibition of active uptake and metabolism of ATV and BOS on outflow perfusate, liver and bile concentrations.

An isolated perfused rat liver model was used to study the intracellular disposition of ATV and BOS. Liver perfusion was conducted to study the effect of uptake and metabolism of ATV and BOS. RIF was used as an uptake inhibitor. Metabolism inhibition was tested with the non-specific suicidal CYP inhibitor 1-aminobenzotriazole

(ABT) and the reversible cyp inhibitor KETO for ATV, and with ABT for BOS. The effect of passive diffusion was tested in presence of concomitant inhibition of metabolism and transport. For ATV, passive diffusion was also tested by conducting "cold" perfusions at 4 ºC. The perfusion medium consisted of modified Krebs' Hensleit buffer with dextran and sodium taurocholate. The drug combinations of interest were perfused through the cannulated portal vein and the outflow perfusate was collected at 0, 5, 10, 20, 30, 40 and 50 min through the cannulated hepatic vein. Cumulative bile samples were collected through the cannulated bile duct. After the end of the perfusion, the liver was homogenized. Perfusate, liver and bile samples were analyzed by the LC-MS/MS methods described in specific aim 1.

3) Modeling the liver perfusion data to predict unbound intracellular concentrations using the 5-compartment explicit membrane model.

The 5-compatment (5-C) explicit membrane model was fitted to the outflow perfusate data obtained from the liver perfusion experiments. A step wise approach was used to parameterize the various clearances using liver perfusion data obtained from different treatment groups. The parameterized clearances were used to simulate the unbound cell concentrations and study the effect of passive diffusion, active uptake and metabolic clearance on the unbound cell concentrations. The experimentally measured ATV and BOS liver concentrations and cumulative amount excreted in bile were compared to the model predicted values in order to check the correctness of the predictions.

4) Induction of cyp3a1 with BOS – in vitro and in vivo studies and use of unbound intracellular concentration to predict effect of induction.

BOS is an inducer of CYP3A4 and is highly bound to plasma proteins resulting in a very low unbound fraction of the drug in plasma. Since it is unlikely for a compound to be an inducer of drug metabolizing enzymes at this very low unbound plasma concentration, the role of active uptake transport in induction was evaluated. The goal of this chapter was to use the predicted unbound intracellular BOS concentration as the driving force for cyp3a1 induction in rats. In vitro induction studies were conducted in sandwich cultured rat hepatocytes with multiple dosing of BOS. In vitro studies were conducted in order to characterize the kinetics of induction (to determine E_{max} and EC_{50}). In vivo studies were conducted in rats to study the effect of multiple dosing of BOS on the PK of the cyp3a1 probe substrate midazolam (MDZ).

5) In vivo pharmacokinetic studies to assess the effect of metabolism and transport on systemic and intracellular disposition of ATV and BOS.

In vivo PK experiments were performed in rats to study effect of metabolism and transport on disposition of ATV and BOS. Uptake inhibition experiments were conducted by intravenous administration of the active uptake inhibitor RIF. Metabolism inhibition experiments were conducted by oral administration of the non-specific suicide inhibitor ABT. The PK data were then used as an input to a semi-physiological model to predict intracellular unbound ATV and BOS concentrations in the liver. The clearance parameters obtained in the modeling exercise from chapter 4 were used for unbound cell

concentration prediction. The model was used to study the effect of active uptake transport on intracellular disposition of ATV and BOS.

CHAPTER 2: DEVELOPMENT AND VALIDATION OF A BIO-ANALYTICAL METHOD FOR QUANTIFICATION OF ATV AND BOS

2.1 Rationale

The determination of intracellular free drug concentration requires a validated bioanalytical assay, which is reproducible and has high sensitivity. Numerous methods have been reported for liquid chromatography tandem mass spectrometric (LC-MS/MS) detection and quantification of atorvastatin (Bořek-Dohalský et al., 2006; Lau et al., 2006a; Shah et al., 2008) and BOS (Lausecker et al., 2000; Parekh et al., 2012). The aim of this study was to develop and validate in house LC-MS/MS assays for quantification of ATV, 2-OH ATV, 4-OH ATV, BOS, OH-BOS and OH-DM-BOS in various biological matrices like rat plasma, liver homogenate, bile and RLM.

2.2 Assay development: ATV, 2-OH ATV, and 4-OH ATV

2.2.1 Preparation of stock solutions and calibration standards samples

Stock solutions of ATV and internal standard (IS) pitavastatin (PTV) were prepared in dimethyl sulfoxide (DMSO). Stock solutions of 2-OH ATV and 4-OH ATV were prepared in methanol. Standard solutions for perfusate were prepared by serial dilution in blank perfusate. Standard solutions for all other matrices were prepared by spiking blank matrices with equal volume of standard sample in 1:1 acetonitrile: water. The calibration standards covered the range from 1.008 – 750 ng/mL in perfusate, 1.008 to 1000 ng/mL in liver homogenate, 1.37 – 1000 ng/mL in rat plasma and 4.1 to 8000 ng/ml in bile. The

calibration standards covered the range from 7.8 – 2000 ng/mL in suspensions of rat plasma in dialysis buffer, RLM in dialysis buffer and perfusate in dialysis buffer.

2.2.2 Sample preparation

Perfusion medium (Perfusate)

Method 1

To 250 µL of standard perfusate sample, 6.25 µL of 10,000 ng/mL PTV was added as IS along with 1 mL of methyl-t-butyl ether (MTBE). The mixture was vortexed for 5 min and centrifuged at 10,000 rpm. The organic phase was then separated and evaporated to dryness at 20 ºC under gentle stream of nitrogen. The sample was reconstituted in 25 µL of 1:1 acetonitrile: water. Five µL sample was injected for analysis into the LC-MS/MS system.

Method 2

To 250 µL of standard perfusate sample, 6.25 µL of 10,000 ng/mL PTV was added as IS along with 1 mL of MTBE. The mixture was vortexed for 5 min and centrifuged at 10,000 rpm for 10 min followed by immersion in dry ice for one hour to freeze the aqueous phase and precipitate dextran. The sample was centrifuged again at -5 ºC at 10,000 rpm for 10 min. The organic phase was then separated and evaporated to dryness at 20 ºC under gentle stream of nitrogen. The sample was reconstituted in 25 µL of 1:1 acetonitrile: water. Five µL sample was injected for analysis into the LC-MS/MS system.

Method 3

To 250 µL of standard perfusate sample, 12.5 µL of 1 M potassium monobasic phosphate (KH_2PO_4) was added along with 6.25 µL of 10,000 ng/mL PTV as IS and 1 mL of MTBE. The mixture was vortexed for 5 min and centrifuged at 10,000 rpm for 10 min followed by immersion in dry ice for one hour to freeze the aqueous phase and precipitate dextran. The sample was centrifuged again at -5 ºC at 10,000 rpm for 10 min. The organic phase was then separated and evaporated to dryness at 20 ºC under gentle stream of nitrogen. The sample was reconstituted in 25 µL of 1:1 acetonitrile: water. Five µL sample was injected for analysis into the LC-MS/MS system.

Liver homogenate, dialysis buffer with RLM and plasma, plasma and bile

Liver and bile samples were analyzed for ATV, 2-OH ATV and 4-OH ATV. Dialysis buffer with RLM and plasma, and plasma samples were analyzed only for ATV. Livers perfused with blank perfusion medium were homogenized with water in the ratio 1:2 using Polytron PT2100 apparatus by Kinematica. Blank liver homogenate (200 µL), dialysis buffer with RLM (200 µL), dialysis buffer with plasma (200 µL), plasma (100 µL) and bile (20 µL) were spiked with equal volume of standard ATV, 2-OH ATV or 4-OH ATV solutions in 1:1 acetonitrile: water followed by addition of 12.5 µL of KH_2PO_4, 6.25 µL of 10,000 ng/mL PTV as IS and 1 mL of MTBE. Further procedure for liquid-liquid extraction (LLE) has been followed as described for perfusate in method 3. For analysis of unknown liver samples, 20 µL of the liver homogenate sample was added to 180 µL blank liver homogenate spiked with 200 µL of 1:1 acetonitrile: water. For

analysis of unknown bile samples, 1 µL bile sample was added to 19 µL blank bile spiked with 20 µL of 1:1 acetonitrile: water. Dialysis buffer with RLM (total volume 200 µL), dialysis buffer with plasma (total volume 200 µL), dialysis buffer with perfusion medium (total volume 200 µL), 100 µL plasma were spiked with equal volume of 1:1 acetonitrile: water. Samples were reconstituted in 50 µL of 1:1 acetonitrile: water for liver samples and with 20 µL 1: 1 acetonitrile: water for dialysis buffer with RLM, dialysis buffer with plasma, dialysis buffer with perfusion medium, plasma and bile samples. Five µL sample was injected for analysis into the LC-MS/MS system.

2.2.3 LC-MS/MS conditions

An Agilent series 1100 high-performance liquid chromatography (HPLC) system coupled to an ABSciex API 4000 triple-quadrupole tandem mass spectrometer with electrospray ionization (ESI) source has been used for analysis. The mass spectrometer was operated in positive ionization mode. The LC-MS/MS data was acquired and processed using Analyst software version 1.6.

The mobile phase for HPLC separation consisted of water with 0.1% formic acid as the aqueous phase (A) and acetonitrile with 0.1%formic acid as the organic phase (B). The gradient used for ATV elution started with 90% A at 0 min to 5% A maintained from 0.5 min to 3 min, followed by gradual increase to 90 % A at 6.5 min maintained until 9 min. The gradient used for elution of 2-OH ATV and 4-OH ATV started with 60% A at 0 min to 5% A maintained from 0.5 min to 3 min, followed by gradual increase to 60 % A at 6.5 min maintained until 9 min. The analytical column used for HPLC was a Zorbax extend

C-18, 5 µm, 4.6 x 50 mm column (Agilent technologies) protected by a Zorbax SB C-18, 5 µm, 4.6 x 12.5 mm guard column (Agilent technologies). The column temperature was maintained at 20°C. The flow rate was 300 µL per min. The HPLC system was connected to an API 4000 mass spectrometer equipped with a Turbo ionspray source operating at 400°C. Nitrogen was used as ion source, curtain and collision gas. Optimum values for declustering potential (DP), collision energy (CE) and collision exit potential (CXP) were obtained for ATV and PTV upon direct infusion in to the mass spectrometer.

2.3 Assay development: BOS, OH-BOS and OH-DM-BOS

2.3.1 Preparation of stock solutions and calibration standards

Stock solutions of BOS and IS macitentan (MAC) were prepared in DMSO. Stock solutions of OH-BOS and OH-DM-BOS were prepared in methanol. Standard solutions for perfusate were prepared by serial dilution in blank perfusate. Standard solutions for all other matrices were prepared by spiking blank matrices with equal volume of standard sample in 1:1 acetonitrile: water. The calibration standards covered the range from 1.008 – 750 ng/mL in perfusate, 1.008 to 1000 ng/mL in liver homogenate, 1.37 – 1000 ng/mL in rat plasma and 4.1 to 8000 ng/ml in bile. The calibration standards covered the range from 7.8 – 2000 ng/mL in suspensions of rat plasma in dialysis buffer, RLM in dialysis buffer and perfusate in dialysis buffer.

2.3.2 Sample preparation

Perfusion medium

Perfusion samples were analyzed for BOS, OH-BOS and OH-DM-BOS.

Method 1

To 250 µL of standard perfusate sample, 10 µL of 500 ng/mL MAC in acetonitrile was added as IS along with 1 mL of MTBE, chloroform or dichloromethane. The mixture was vortexed for 5 min and centrifuged at 10,000 rpm for 10 min followed by immersion in dry ice for one hour to freeze the aqueous phase and precipitate dextran. The sample was centrifuged again at -5 ºC at 10,000 rpm for 10 min. The organic phase was then separated and evaporated to dryness at 20 ºC under gentle stream of nitrogen. The sample was reconstituted in 25 µL of 1:1 acetonitrile: water. Five µL sample was injected for analysis into the LC-MS/MS system.

Method 2

To 250 µL of standard perfusate sample, 20 µL of 1 M KH_2PO_4 was added along with 10 µL of 500 ng/mL MAC in acetonitrile as IS and 1 mL of dichloromethane. The mixture was vortexed for 5 min and centrifuged at 10,000 rpm for 10 min followed by immersion in dry ice for one hour to freeze the aqueous phase and precipitate dextran. The sample was centrifuged again at -5 ºC at 10,000 rpm for 10 min. The organic phase was then separated and evaporated to dryness at 20 ºC under gentle stream of nitrogen. The sample

was reconstituted in 25 µL of 1:1 acetonitrile: water. Five µL sample was injected for analysis into the LC-MS/MS system.

Liver homogenate and bile

Liver and bile samples were analyzed for BOS, OH-BOS and OH-DM-BOS. Livers perfused with blank perfusion medium were homogenized with water in the ratio 1:2 using Polytron PT2100 apparatus by Kinematica. Blank liver homogenate (200 µL) and bile (20 µL) were spiked with equal volume of standard BOS, OH-BOS and OH-DM-BOS solutions in 1:1 acetonitrile: water followed by addition of 20 µL of KH_2PO_4, 10 µL of 500 ng/mL MAC as IS and 1 mL of dichloromethane. Further procedure for liquid-liquid extraction (LLE) has been followed as described for perfusate in method 2. For analysis of unknown liver samples, 20 µL liver homogenate sample was added to 180 µL blank liver homogenate spiked with 200 µL of 1:1 acetonitrile: water. For analysis of unknown bile samples, 1 µL bile sample was added to 19 µL blank bile spiked with 20 µL of 1:1 acetonitrile: water. Samples were reconstituted in 50 µL of 1:1 acetonitrile: water for liver samples and with 20 µL 1: 1 acetonitrile: water bile samples. Five µL sample was injected for analysis into the LC-MS/MS system.

Plasma

Plasma samples were analyzed for BOS, OH-BOS and OH-DM-BOS. Blank plasma (10 µL) was spiked with equal volume of standard BOS in acetonitrile followed by addition of 20 µL of 500 ng/mL MAC as IS. Samples were centrifuged at 10000 rpm for 10 min. Five µL supernatant was injected for analysis into the LC-MS/MS system.

Plasma + dialysis buffer

Dialysis samples were analyzed for BOS. Standard plasma sample (10 µL) was spiked with equal volume of blank dialysis buffer followed by addition of 40 µL of 500 ng/mL MAC as IS. Samples were centrifuged at 10000 rpm for 10 min. Five µL supernatant was injected for analysis into the LC-MS/MS system.

RLM + dialysis buffer

Method 1

Dialysis samples were analyzed for BOS. Ten µL of the standard in 1mg/mL RLM in potassium phosphate buffer was spiked with equal volume of blank dialysis buffer followed by addition of 40 µL of 500 ng/mL MAC as IS. Samples were centrifuged at 10000 rpm for 10 min. Five µL supernatant was injected for analysis into the LC-MS/MS system.

Method 2

To 100 µL of standard sample in 1mg/mL RLM, equal volume of blank dialysis buffer was added along with 20 µL of 1 M KH_2PO_4, 10 µL of 500 ng/mL MAC in acetonitrile as IS and 1 mL of dichloromethane. The mixture was vortexed for 5 min and centrifuged at 10,000 rpm for 10 min followed by immersion in dry ice. The sample was centrifuged again at -5 ºC at 10,000 rpm for 10 min. The organic phase was then separated and evaporated to dryness at 20 ºC under gentle stream of nitrogen. The sample was

reconstituted in 20 µL of 1:1 acetonitrile: water. Five µL sample was injected for analysis into the LC-MS/MS system.

Method 3

Ten µL of the standard in 1mg/mL RLM in potassium phosphate buffer was spiked with equal volume of blank dialysis buffer and rat plasma followed by addition of 60 µL 500 ng/mL MAC as IS. Samples were centrifuged at 10000 rpm for 10 min. Five µL supernatant was injected for analysis into the LC-MS/MS system.

2.3.3 LC-MS/MS conditions

An Agilent series 1100 high-performance liquid chromatography (HPLC) system coupled to an ABSciex API 4000 triple-quadrupole tandem mass spectrometer with electrospray ionization (ESI) source has been used for analysis. The mass spectrometer was operated in positive ionization mode. The LC-MS/MS data was acquired and processed using Analyst software version 1.6.

The mobile phase for HPLC separation consisted of water with 0.1% formic acid as the aqueous phase (A) and acetonitrile with 0.1%formic acid as the organic phase (B). The gradient used for BOS, OH BOS and OH DM-BOS elution started with 90% A at 0 min to 5% A maintained from 0.5 min to 3 min, followed by gradual increase to 90 % A at 6.5 min maintained until 10 min. The analytical column used for HPLC was a Zorbax extend C-18, 5 µm, 4.6 x 50 mm column (Agilent technologies) protected by a Zorbax SB C-18, 5 µm, 4.6 x 12.5 mm guard column (Agilent technologies). The column temperature was

maintained at 20°C. The flow rate was 800 µL per min for perfusate, bile and liver homogenate. For analysis of plasma, dialysis buffer with plasma and dialysis buffer with RLM, flow rate of 450 µL per min was used. The HPLC system was connected to an API 4000 mass spectrometer equipped with a Turbo ionspray source operating at 400°C. Nitrogen was used as ion source, curtain and collision gas. Optimum values for declustering potential (DP), collision energy (CE) and collision exit potential (CXP) were obtained for ATV and PTV upon direct infusion in to the mass spectrometer.

2.4 Assay validation

In accordance with the recommendations made by Shah et al. (Shah et al., 2000), a full validation (inter day and intraday validation) has been performed for LC-MS/MS methods for ATV, 2-OH ATV and 4-OH ATV in perfusate, and for BOS, OH-BOS and OH-DM-BOS in plasma. For change of matrix within the same species, a partial validation is sufficient according to recommendations by Shah et al. Therefore, partial validation (inter day validation) was performed for all other matrices. Inter day and intraday accuracy and precision were determined using at least three quality control (QC) samples. The peak area ratio of analyte to IS was used to construct calibration curves with linear least squares regression method. A weighting factor of $1/x^2$ was used.

Precision (percentage coefficient variation) was calculated based on the following equation:

Precision = (Standard deviation / Mean) x 100

Calculation of accuracy was based on the following equation:

Accuracy = [(Mean observed – Theoretical) / Theoretical] x 100

2.5 Results

Assay development: ATV, 2-OH ATV and 4-OH ATV

Method 1 resulted in inadequate determination of concentrations less than 20 ng/mL. Immersing the analysis mixture in dry ice for one hour as described in method 2 improved the analytical ability of the method for lower concentrations. Increased signal to noise ratios at lower concentrations were achieved by method 3 upon acidification of the aqueous phase by 1 M KH_2PO_4. Acidification of aqueous phase also resulted in larger peak areas as compared to method 2. Therefore, method 3 was selected as the final method for further quantification. Figures 2.1 and 2.2 depict chromatograms upon sample preparation by method 3 described in section 2.2.2.

The retention time for ATV and PTV was ~6.07 and ~5.05 min respectively. The retention time for 2-OH ATV, 4-OH ATV and PTV was ~5.49, ~4.69 and ~2.87 minutes, respectively. The 9 min run was divided into 2 periods for the purpose of quantification- period 1 from t=0 min to t=5.15 min and period 2 from t=5.15 min to t=9 min. PTV and 4-OH ATV eluted in period 1, while 2-OH ATV eluted in period 2.

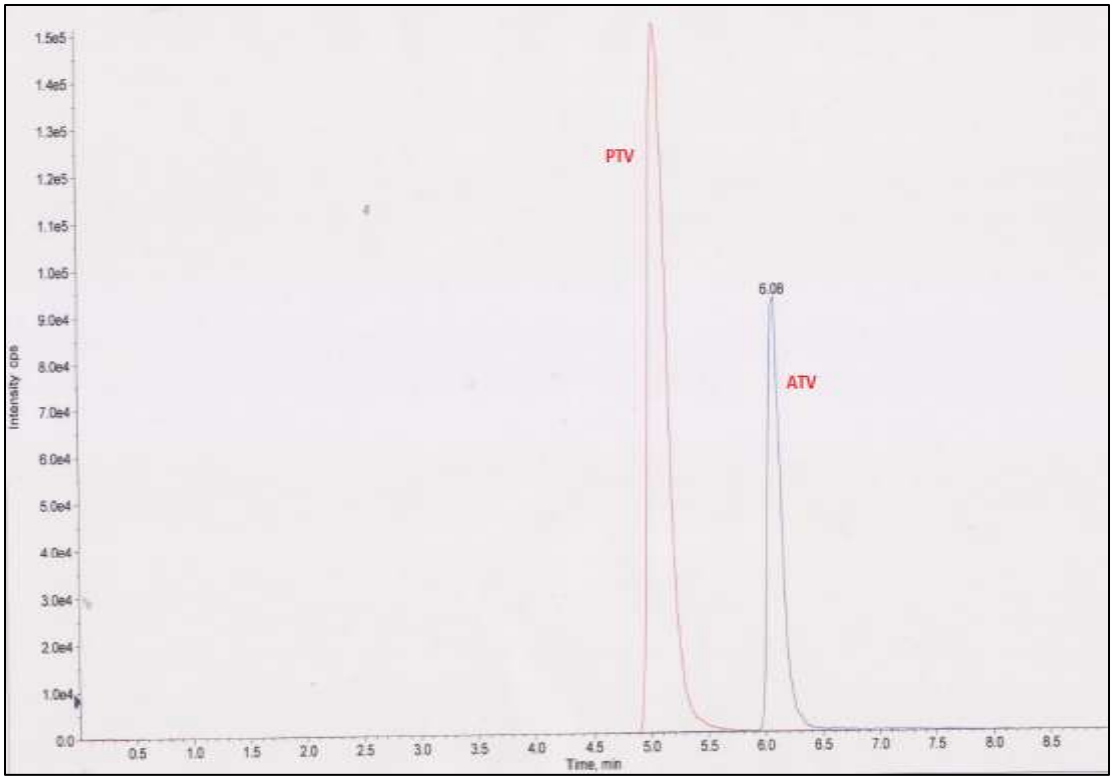

Figure 2.1 Representative chromatograms of ATV (blue) and PTV (red)

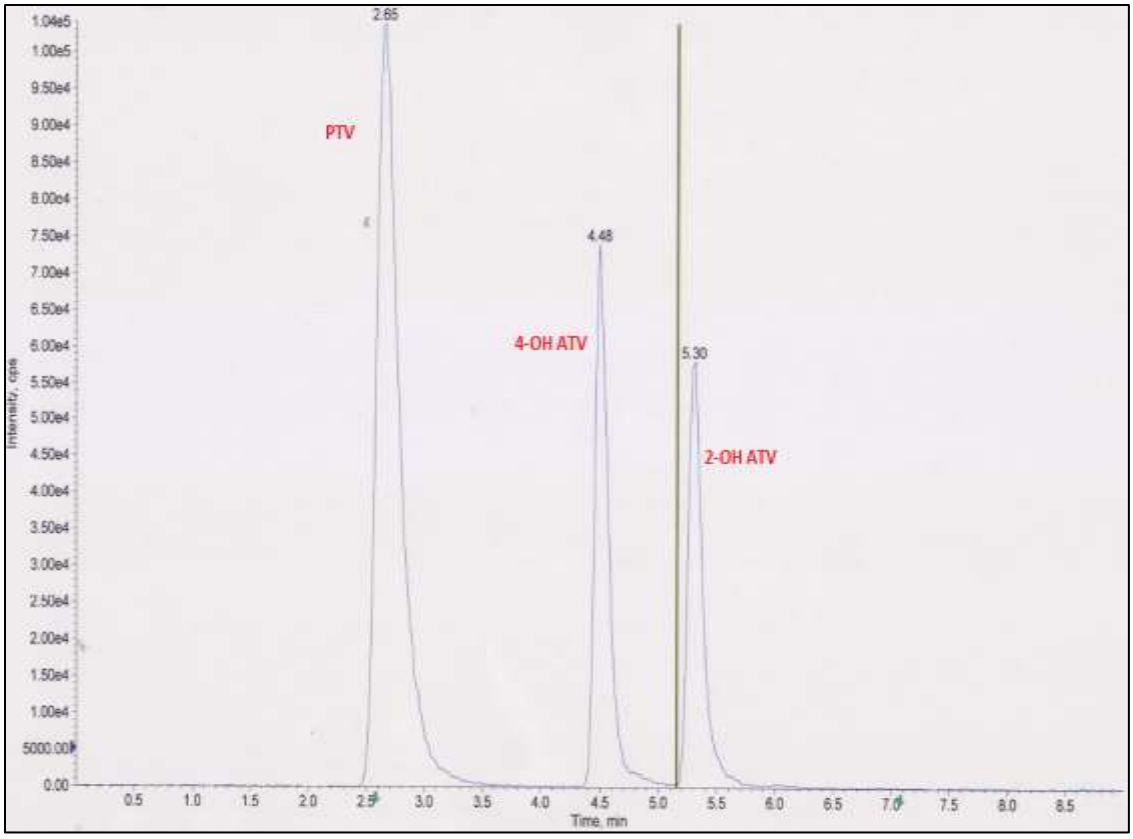

Figure 2.2 Representative chromatograms of 2-OH ATV, 4-OH ATV and PTV

Table 2.1 Optimized ESI-MS/MS operating, MRM and MS/MS parameters for ATV, 2-OH ATV, 4-OH ATV and PTV (IS)

Operating parameter	Value			
Collision gas (psi)	10			
Curtain gas (psi)	40			
Ion source gas 1 (psi)	40			
Ion source gas 2 (psi)	40			
Ion spray voltage (V)	4500			
Temperature (°C)	400			
	ATV	PTV	2-OH ATV	4-OH ATV
Precursor ion (m/z)	559.407	423.214	575.125	575.125
Product ion (m/z)	440.537	275.4	250.147	250.147
DP (V)	76	66	76	76
CE (V)	31	59	59	59
CXP (V)	12	28	6	6

The precursor → product ion transitions observed for ATV, 2-OH ATV, 4-OH-ATV and PTV were 559.407→440.537, 575.125→250.147, 575.125→250.147 and 423.214→275.4 respectively. The dwell time for each ion transition was 300 msec.

The relationship between ratio of ATV, 2-OH ATV and 4-OH ATV to PTV peak area and respective ATV, 2-OH ATV and 4-OH ATV nominal concentrations was linear and could be well represented by the equation y = mx + c.

Representative standard curves for ATV, 2-OH ATV and 4-OH ATV are shown in fig 2.3, 2.4 and 2.5, respectively.

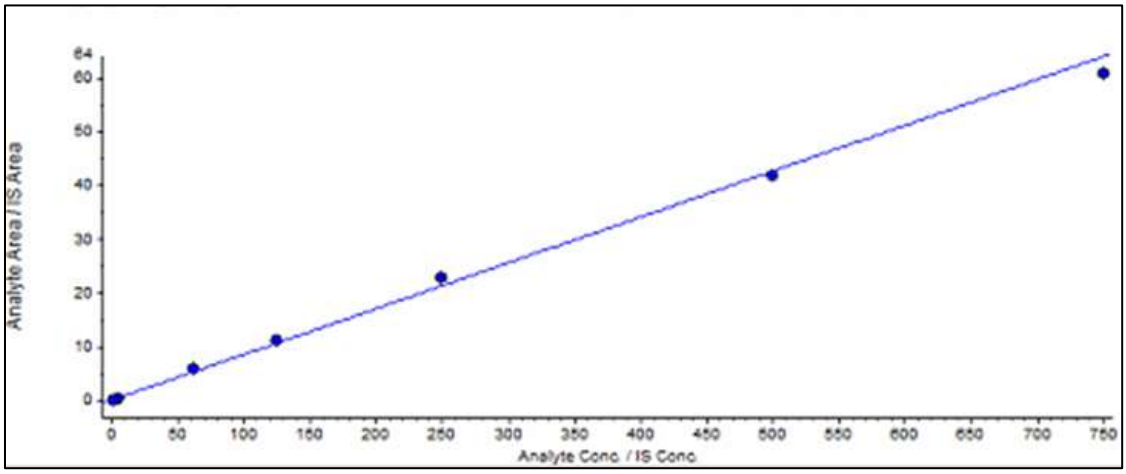

Figure 2.3 Representative standard curve for ATV

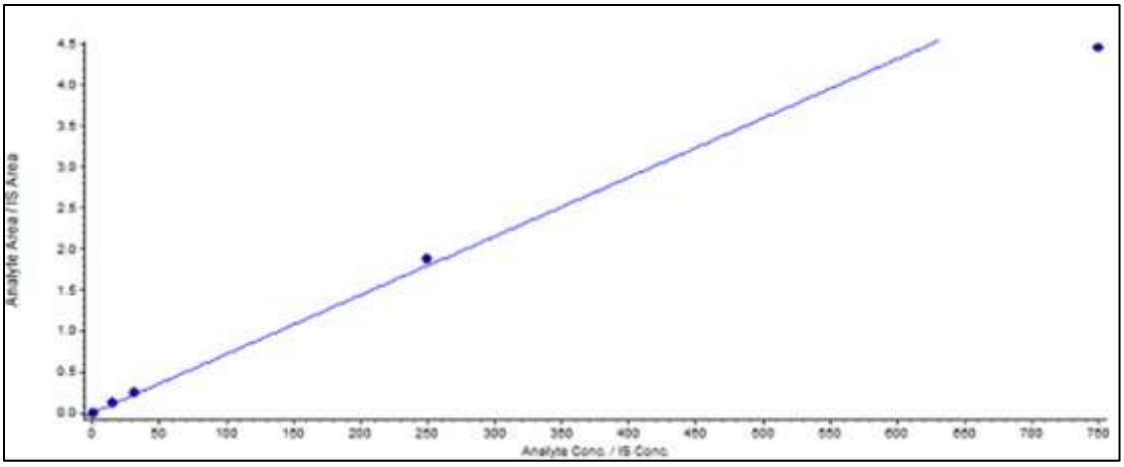

Figure 2.4 Representative standard curve for 2-OHATV

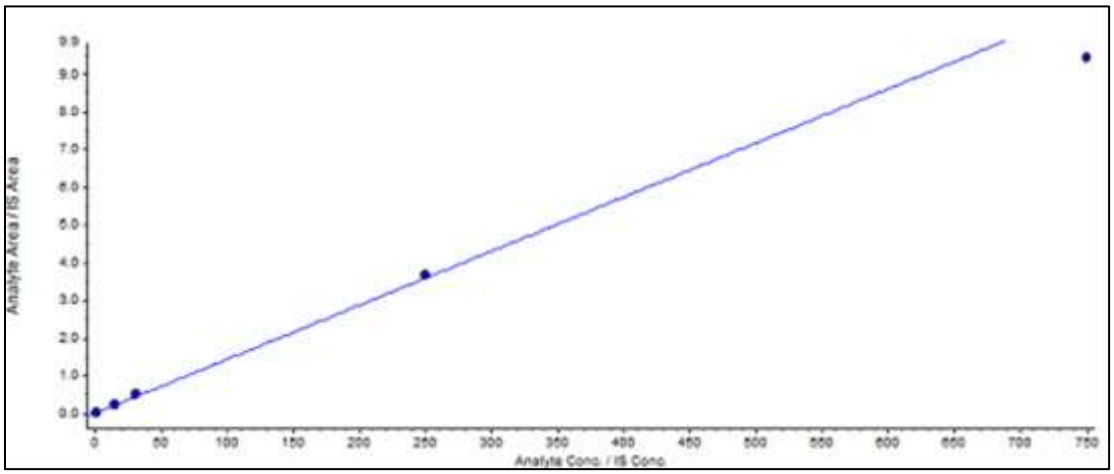

Figure 2.5 Representative standard curve for 4-OH ATV

The coefficients of determination (R^2) were > 0.99 by using a weighting factor of $1/x^2$ for all the matrices studied over varying concentration ranges: 1.008 – 750 ng/ml for perfusate and liver homogenate, 4.1-8000 ng/ml for bile, 1.37 – 1000 ng/ml for plasma, 7.8 – 2000 ng/ml for plasma + dialysis buffer, RLM + dialysis buffer and perfusion medium + dialysis buffer. The lowest point of each standard curve represents the limit of quantitation (LOQ) i.e., 1.008 ng/ml in perfusate and liver homogenate, 1.37 ng/ml in plasma, 4.1 ng/ml in bile, and 7.8 ng/ml in plasma + dialysis buffer, RLM + dialysis buffer and perfusion medium + dialysis buffer. The intraday and inter day % accuracy and % precision was within ± 15 % for the tested QC samples for ATV in (Tables 2.2, 2.3), 2-OH ATV (Table 2.4, 2.5) and 4-OH ATV (Table 2.6, 2.7) in perfusate. For partial validation with all other matrices, the inter day precision was less than 15 % and accuracy was within ± 15 % for the tested QC samples for all matrices except 7.8 ng/mL in plasma (precision = 16 %). Tables 2.2 – 2.7 summarize the results for inter day and intraday validation for ATV, 2-OH ATV and 4-OH ATV.

Table 2.2 Inter day (n = 3) precision and accuracy for ATV in different matrices

Matrix	Nominal concentration (ng/mL)	% Precision	% Accuracy
Perfusate	500	12.01	0.825
	125	9.25	1.025
	31.25	4.9	-12.15
	5.04	11.7	-7.1
Liver homogenate	500	4.9	-6.2
	125	4.6	-4.2
	31.25	2.3	14
	5.04	3.5	-6.6
Plasma	500	3.6	-1.8
	125	5.9	7.3
	31.25	5.9	-8.1
	7.8	16	3.8
Plasma + dialysis buffer	1000	11.5	-4.7
	500	12.6	3.4
	62.5	11.5	-9.7
RLM + dialysis buffer	1000	6.9	15
	250	10.1	2
	62.5	0.47	-11.7
Bile	4000	4.65	10.33
	1000	9.15	-6.6
	111	13.5	-2.2
	12.3	8.7	7.7

Table 2.3 Intra-day (n = 3) validation for ATV in perfusate

Nominal concentration (ng/mL)	**% Precision**	**% Accuracy**
500	14.6	2
125	9.6	2.5
31.25	9.17	-9.6
5.04	2.19	-14.6

Table 2.4 Inter day (n = 3) precision and accuracy for 2-OH ATV in different matrices

Matrix	**Nominal concentration (ng/mL)**	**% Precision**	**% Accuracy**
Perfusate	500	7.17	5.9
	125	15	-0.4
	62.5	9.49	10
	5.04	4.7	-12.7
Liver homogenate	500	10.2	3.23
	125	11.5	4.8
	31.25	7.7	3.7
	5.04	4.5	-4.9
Bile	4000	12.2	4.63
	1000	7.85	-1.86
	111	4.06	-5.26
	12.3	5.43	1.33

Table 2.5 Intra-day (n = 3) validation for 2-OH ATV in perfusate

Nominal concentration (ng/mL)	% Precision	% Accuracy
500	7.63	6.06
125	7.37	1.2
62.5	4	-3.43
5.04	5.2	-8.26

Table 2.6 Inter day (n = 3) precision and accuracy for 4-OH ATV in different matrices

Matrix	**Inter day validation (n=3)**		
	Nominal concentration (ng/mL)	**% Precision**	**% Accuracy**
Perfusate	500	6.1	-3.6
	125	7.4	7.73
	62.5	6.5	11.3
	5.04	12.6	2.4
Liver homogenate	500	13.23	5.5
	125	15	-3.1
	31.25	11.6	-7.4
	5.04	11	-5.7
Bile	4000	8.8	2
	1000	3.84	-0.13
	111	1.96	-4
	12.3	10	-0.23

Table 2.7 Intra-day (n = 3) validation for 4-OH ATV in perfusate

Nominal concentration (ng/mL)	% Precision	% Accuracy
500	3.05	2.2
250	6.5	0.8
125	0.96	-1.73
62.5	5.6	-1.4

Assay development: BOS, OH-BOS and OH-DM-BOS

Extraction of BOS, OH-BOS and OH-DM-BOS could not be achieved with MTBE or chloroform. Dichloromethane could successfully extract all three analytes. Acidification of the aqueous phase by 1 M KH_2PO_4 resulted in better signal. Therefore, method 2 was selected as the final method for further quantification. Representative chromatograms for BOS, 2-OH BOS and 4-OH BOS are shown in fig 2.6.

Use of method 1 and 2 for analysis of RLM + dialysis buffer resulted in quadratic standard curves. Addition of blank plasma to analytical samples resulted in linear standard curves. Therefore, method 3 was selected as the final method for further quantification for RLM + dialysis buffer samples.

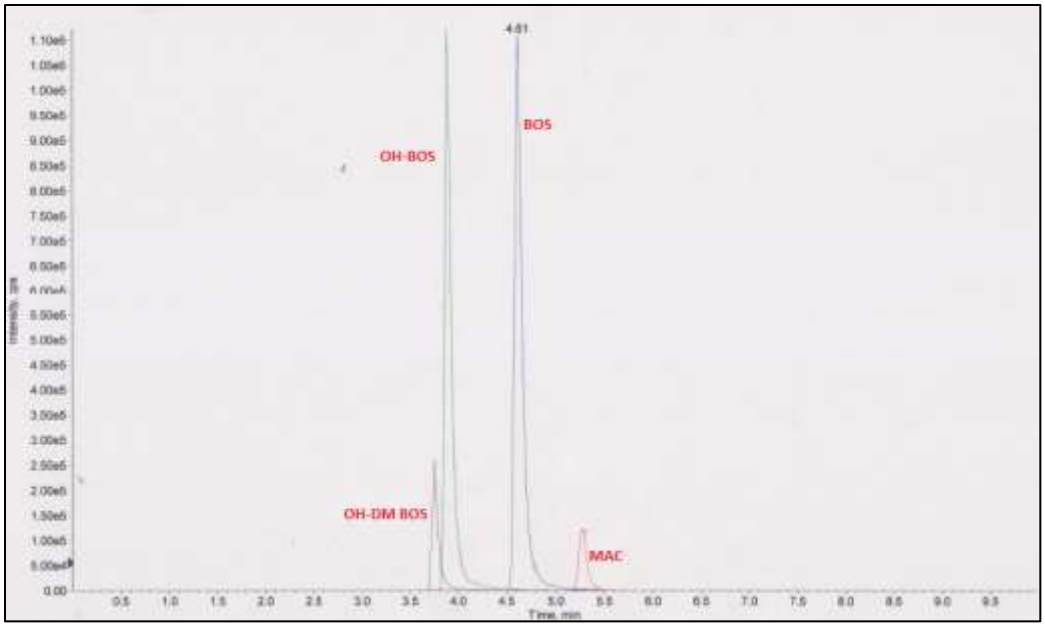

Figure 2.6. Representative chromatograms of BOS (Blue), OH-BOS (Green), OH-DM BOS (Grey) and MAC (Red)

In plasma, dialysis buffer with plasma and dialysis buffer with RLM, the retention time for BOS, OH-BOS, OH-DM-BOS and MAC was ~4.61 min, ~3.67 min, ~3.64 min and ~5.07 min respectively. In perfusate, bile and liver homogenate, the retention time for BOS, OH-BOS, OH-DM-BOS and MAC was ~2.47 min, ~2.11 min, ~2.05 min and ~2.78 min respectively. Table 2.8 summarizes the operating conditions for the tandem mass spectrometer.

The precursor → product ion transitions observed for BOS, OH-BOS, OH-DM-BOS and MAC were 552.028→202.19, 568.466→202.184, 554.092→189.297 and 587.283→201.114 respectively. The dwell time for each ion transition was 300 msec.

Table 2.8 Optimized ESI-MS/MS operating, MRM and MS/MS parameters BOS, OH-BOS, OH-DM-BOS and MAC (IS)

Operating parameter	Value			
Collision gas (psi)	10			
Curtain gas (psi)	40			
Ion source gas 1 (psi)	40			
Ion source gas 2 (psi)	40			
Ion spray voltage (V)	4500			
Temperature (°C)	400			
	BOS	OH-BOS	OH-DM-BOS	MAC
Precursor ion (m/z)	552.028	568.466	554.092	587.283
Product ion (m/z)	202.19	202.184	189.297	201.114
DP (V)	96	36	121	36
CE (V)	49	45	47	23
CXP (V)	10	4	16	12

The relationship between ratio of BOS, OH-BOS and OH-DM-BOS to MAC peak area and respective BOS, OH-BOS and OH-DM-BOS nominal concentrations was linear and could be well represented by the equation y = mx + c. Representative standard curves for BOS, OH-BOS and OH-DM-BOS are depicted in fig 2.7, 2.8 and 2.9, respectively.

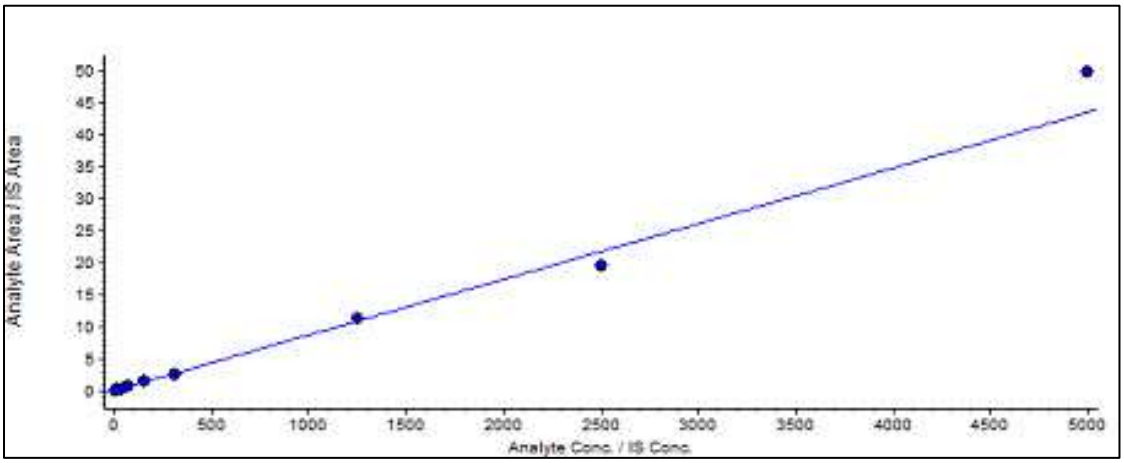

Figure 2.7 Representative standard curve for BOS

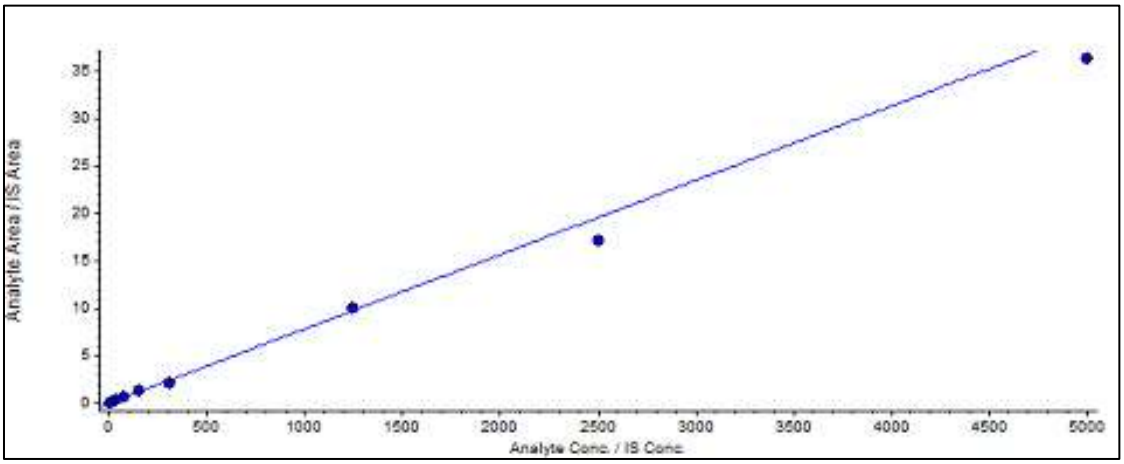

Figure 2.8 Representative standard curve for OH-BOS

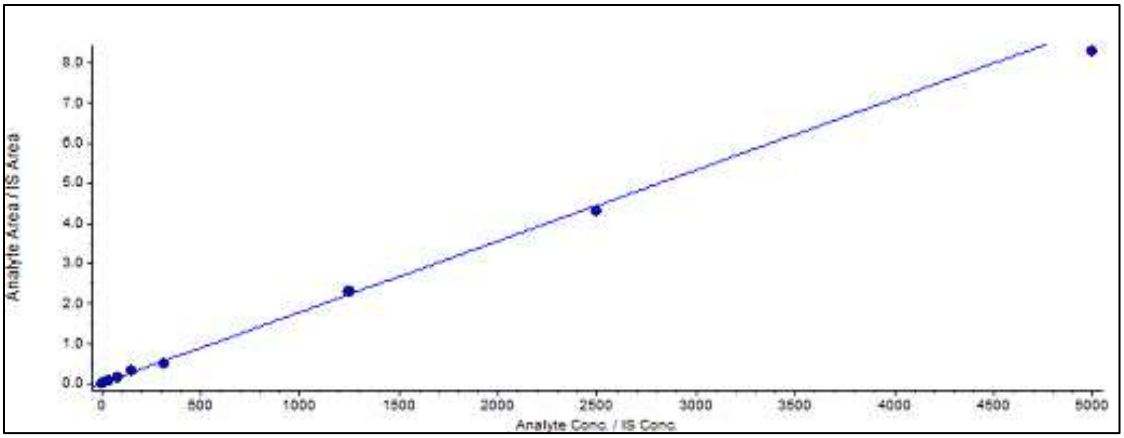

Figure 2.9 Representative standard curve for OH-DM-BOS

The coefficients of determination were > 0.99 by using a weighting factor of $1/x^2$ for all the matrices studied over varying concentration ranges: 1.008 – 750 ng/ml for perfusate and liver homogenate, 4.1-8000 ng/ml for bile, 2.4 – 5000 ng/ml for plasma, 7.8 – 2000 ng/ml for plasma + dialysis buffer, RLM + dialysis buffer. The lowest point of each standard curve represents the limit of quantitation (LOQ) i.e., 1.008 ng/ml in perfusate and liver homogenate, 1.37 ng/ml in plasma, 4.1 ng/ml in bile, 7.8 ng/ml in plasma + dialysis buffer, RLM + dialysis buffer and perfusion medium + dialysis buffer. Tables 2.9 to 2.14 summarize the results for inter day and intraday validation for BOS, OH-BOS and OH-DM-BOS respectively. The intraday and inter day % accuracy and % precision was within ± 15 % for the tested QC samples for BOS in (Table 2.9, 2.10), OH-BOS (Table 2.11, 2.12) and OH-DM-BOS (Table 2.13, 2.14) in plasma. For partial validation with all other matrices, the inter day precision was less than 15 % and accuracy was within ± 15 % for the tested QC samples for all matrices.

Table 2.9 Inter day (n = 3) precision and accuracy for BOS in different matrices

Matrix	**Nominal concentration (ng/mL)**	**% Precision**	**% Accuracy**
Perfusate	500	4.12	11
	125	8.01	8.03
	62.5	11.06	-11.06
	5.04	13.03	-8.7
Liver homogenate	3333	0.34	-14.8
	370	8.3	-4.6
	121	8.5	-9.2
Plasma	5000	12.3	-3.3
	1250	7.5	8
	78	10.2	-3.16
	19.5	12.1	-2.56
	4.87	9.7	-6.93
Plasma + dialysis buffer	2500	6.4	-12.1
	625	13.3	4.8
	156	5.27	4.33
	39	12.2	11.6
RLM + dialysis buffer	2500	12.7	3
	625	5.36	3.63
	156	7.8	5.5
Bile	1111	15	-2.3
	370	13.6	-5.5
	121	3.1	11

Table 2.10 Intra-day (n = 3) validation for BOS in plasma

Nominal concentration (ng/mL)	% Precision	% Accuracy
5000	14.8	-6
1250	15.6	2.8
78	11.6	6.5
19.5	12.5	4
4.87	11.22	3.7

Table 2.11 Inter day (n = 3) precision and accuracy for OH-BOS in different matrices

Matrix	Nominal concentration (ng/mL)	% Precision	% Accuracy
Perfusate	500	9.09	-1.83
	125	5.07	8.67
	62.5	8.82	-0.17
	5.04	6.08	-0.57
Liver homogenate	3333	9.4	9.53
	370	9.5	4.36
	121	6.5	10
Bile	1111	3.9	-5
	370	0.62	-7.6
	121	12.4	-1.6
Plasma	5000	7.3	-4
	1250	3.4	2.1
	78	5.6	-3.2
	19.5	13.3	-1.13
	4.87	14.3	-0.13

Table 2.12 Intra-day (n = 3) validation for OH-BOS in plasma

Nominal concentration (ng/mL)	**% Precision**	**% Accuracy**
5000	12.9	-7.9
1250	7.7	-4.4
78	12	-5.5
19.5	14.6	-2.2
4.87	5.3	12.6

Table 2.13 Inter day (n = 3) precision and accuracy for OH-DM-BOS in different matrices

Matrix	Nominal concentration (ng/mL)	% Precision	% Accuracy
Perfusate	500	10	8.4
	125	9.02	1.43
	62.5	5.8	-10.7
	5.04	12.9	8.56
Liver homogenate	3333	14.9	-1.56
	370	2.5	5
	121	13.9	3.9
Bile	1111	12	-4.2
	370	1.1	-3.7
	121	3.4	11.6
Plasma	5000	5.9	8.33
	1250	3	7.6
	78	5.3	-5.23
	19.5	7.3	-5.9
	4.87	7.14	8.6

Table 2.14 Intra-day (n = 3) validation for OH-DM-BOS in plasma

Nominal concentration (ng/mL)	% Precision	% Accuracy
5000	1.76	13
1250	2.38	11
78	12.8	-0.56
19.5	12.3	2.9
4.87	5.5	9.6

2.6 Discussion and Conclusion

An LC-MS/MS method for ATV, 2-OH ATV and 4-OH ATV has been successfully developed and validated using PTV as IS in different biological matrices. Insensitivity of method 1 (section 2.2.2) for lower concentrations could have resulted from interference due to dextran present in the perfusion medium. Immersion of the analytical mixture in dry ice precipitated the dextran and a relatively cleaner organic phase could be achieved. Acidification of the aqueous phase as in method 3 (section 2.2.2.1) resulted in increased un-ionized fraction of both ATV (pKa 4.33) and PTV (pKa 4.13), resulting in more efficient extraction in organic phase. This explains the larger peak areas obtained in method 3.

Similarly, an LC-MS/MS method has been successfully developed and validated for BOS and its metabolites, OH-BOS and OH-DM-BOS, using MAC as IS in different biological matrices. Successful extraction of BOS and its metabolites from biological matrices could be achieved by using dichloromethane as the organic solvent. MTBE and chloroform did

not prove successful in extracting the desired analytes. Similar to ATV, acidification of the aqueous phase as in method 2 resulted in increased unionized fraction of BOS (pKa 5.8), resulting in more efficient extraction in organic phase.

Ionic interference is expected at greater intensity at lower concentrations, resulting in lower than proportional signal at lower concentrations as compared to that at higher concentrations. Quadratic standard curves in RLM + dialysis buffer could have resulted from ionic interference due to the ions present in dialysis buffer. However, if the non-linearity of standard curves were due to ionic interference, liquid-liquid extraction with dichloromethane should have resolved the issue. Moreover, standard curves obtained in plasma + dialysis buffer were linear. This suggests that solubility limitation and/or nonspecific binding to the apparatus could be a reason for quadratic standard curves. Addition of plasma proteins is expected to resolve both the problems for a highly protein bound compound like bosentan. This explains the linearity of standard curves for plasma + dialysis buffer and RLM + dialysis buffer (method 3, see section 2.3.2).

The results from the validation experiments prove that the developed methods demonstrate the desired sensitivity and are suitable for analysis of ATV, BOS and their metabolites in perfusate, liver homogenate, plasma, plasma + dialysis buffer, RLM + dialysis buffer and bile.

CHAPTER 3: LIVER PERFUSION TO STUDY THE IMPACT OF ACTIVE UPTAKE AND METABOLISM OF ATV AND BOS ON OUTFLOW PERFUSATE, LIVER AND BILE CONCENTRATIONS

3.1 Background and rationale

As described in chapter 1, the experimental determination of unbound intracellular drug concentration is very difficult. Since the metabolic machinery for most drugs and the targets for many drugs are located inside the cell, it is the unbound intracellular concentration, and not the plasma concentration, that drives the metabolism and efficacy of many drugs.

The active uptake of ATV from plasma to hepatocytes in humans is mediated by various SLC transporters – OATP1B1, OATP1B3, OATP2B1 (Choi et al., 2011; König, 2011; Karlgren et al., 2012; Vildhede et al., 2014) and NTCP (Choi et al., 2011). The average contribution of these transport proteins in the active uptake of ATV was reported to be in the order OATP1B1> OATP1B3>>OATP2B1>NTCP (Vildhede et al., 2014). Similarly, the active uptake of ATV in rat hepatocytes is mediated by oatp1a1, oatp1a4 and oatp1b2 (Lau et al., 2006a). Transporter mediated hepatic uptake has been confirmed as the rate determining step in the disposition of ATV in humans (Watanabe et al., 2009a; Maeda et al., 2011). ATV is metabolized mainly by CYP3A4 to ortho-hydroxy atorvastatin (2-OH ATV) and para-hydroxy atorvastatin (4-OH ATV) (Michniewicz et al., 1994; Kantola et al., 1998; Jacobsen et al., 2000). Similar metabolic pathways are also observed in rats (Black et al., 1999). Glucuronidation is a minor metabolic pathway for metabolism of

ATV in human liver microsomes. In humans, ATV glucuronidation by UGTs 1A3, 1A4 and 1A9 yield the quantitatively minor metabolite, ATV ether glucuronide. UGTs 1A1, 1A3, 1A4, 1A8 and 2B7 form a major ATV acyl glucuronide, which is spontaneously converted to ATV lactone. UGTs 1A1, 1A3, 1A4, 1A8, 2B7 convert the ATV lactone to another ether glucuronide (Prueksaritanont et al., 2002; Goosen et al., 2007). ATV is also a substrate for apical efflux transporters like MRP2 (Lau et al., 2006a; Ellis et al., 2013) and P-gp (Boyd et al., 2000; Hochman et al., 2004; Holtzman et al., 2006). The reported Km values for formation of 2-OH ATV and 4-OH ATV, and transport by oatp1a4 and oatp1b2 are 23.8 µM, 19.8 µM, 22.2 µM and 7.12 µM, respectively (Lau et al., 2006a). The Km value for ATV uptake in rat hepatocytes has been reported to be 4.03 µM.

For a transporter or enzyme mediated process, linear range is defined as the range of substrate concentration within which the rate of the reaction increases linearly with the substrate concentration. When the substrate concentration becomes greater than the Km for the process, the pathway begins to saturate. Whenever a disposition pathway saturates, the assumptions of linearity do not hold true and hence the less than proportional decrease in clearance can occur. Hence it is critical to maintain the working ATV concentration in the linear range for both metabolism and active uptake. Therefore, a low working concentration is desired. However, the concentrations obtained post-uptake should be above the quantitation limit for the analytical method. Therefore, the working concentration of ATV was chosen to be 1 µM for the present study.

Similar to ATV, BOS is also a substrate for various active transporters and metabolizing enzymes. OATP1B1 and OATP1B3 are responsible for active uptake of BOS in human

hepatocytes (Treiber et al., 2007). Rifampin (RIF), cyclosporine A and sildenafil inhibited the OATP1B1 mediated active uptake of BOS with IC50 values of 3.2 ± 1.6, 0.3± 0.1, and 1.5 ± 0.5, respectively, in OATP1B1 overexpressing CHO cells (Treiber et al., 2007). Similarly, the IC50 values for inhibition of OATP1B3 mediated BOS uptake in CHO cells were 1.6 ± 0.8, 0.8 ± 0.2 and 0.8 ± 0.3 for RIF, cyclosporine A and sildenafil, respectively (Treiber et al., 2007). BOS is also a substrate of human and rat NTCP as demonstrated with experiments from HEK cells overexpressing ntcp (Leslie et al., 2007). The Km and Vmax for transport of BOS by human NTCP are 2.1 ± 1.4 µM and 814 ± 278 pmol/min/mg protein. The Km and Vmax for transport of BOS by rat ntcp are 2.6 ± 1.6 µM and 357 ± 134 pmol/min/mg protein. The contribution of active uptake of BOS relative to passive diffusion in suspended rat hepatocytes was 48.9% (Yabe et al., 2011). BOS is metabolized to hydroxy BOS (OH-BOS) by both CYP3A4 and CYP2C9 by aliphatic hydroxylation. Oxidative demethylation of BOS by CYP3A4 results in formation of desmethyl BOS. Both hydroxylation and demethylation can be followed by subsequent demethylation and hydroxylation, respectively, resulting in formation of hydroxy-desmethyl BOS (OH-DM-BOS) (van Giersbergen et al., 2002; Dingemanse and van Giersbergen, 2004). Another group has reported a novel metabolite of desmethyl BOS formed by its hydroxylation at a site that is different than that involved in the formation of OH-DM-BOS (Matsunaga et al., 2015). OH-BOS, desmethyl-BOS and OH-DM-BOS were also detected as BOS metabolites in rats (Treiber et al., 2004). BOS inhibited taurocholate transport mediated by human OATP1B1, OATP1B3, NTCP and BSEP with IC_{50} values of 5, 5.2, 35.6 and 42.1 µM, respectively in sandwich cultured

human hepatocytes (Lepist et al., 2014). Another group has reported the IC_{50} values for human and rat BSEP inhibition to be 76.8 and 101 µM, respectively (Mano et al., 2007). A mixture of 40 µM RIF and 5 µM cyclosporine reduced the cellular accumulation of BOS by 46 % (Lepist et al., 2014). Similar results for altered disposition of taurocholate by BOS have been observed in sandwich cultured rat hepatocytes (Kemp et al., 2005). BOS caused reversible dose dependent liver injury in humans and rats with increased levels of serum bile salts, indicating BSEP inhibition (Fattinger et al., 2001). BOS is neither a substrate nor an inhibitor for human P-gp according to some groups (Weber et al., 1999b; Treiber et al., 2004), while other groups have reported it to be a weak P-gp substrate (Hartman et al., 2010). The reported Km for active uptake of BOS in hepatocytes is 5.24 µM (Yabe et al., 2011). Another group has reported the unbound Km in rat hepatocytes to be 6.39 µM (Ménochet et al., 2012). Therefore, a working concentration of 1 µM was selected for the present study. Cellular BOS disposition has been studied in a quadruple transfected MDCK II-OATP1B1-CYP3A4-UGT1A1-MRP2 cell line (Fahrmayr et al., 2013). In that study, BOS was observed to be a substrate of MRP2. Also, UGT1A1 mediated formation of a BOS-glucuronide has been observed in the same study. Mrp2 mediated increase in bile flow in rats was observed with BOS (Fouassier et al., 2002).

RIF is a competitive inhibitor of OATPs (Fattinger et al., 2001; Vavricka et al., 2002). RIF has demonstrated inhibition of rat oatp1a4 and oatp1b2 mediated ATV active uptake. The IC_{50} values for oatp1a4 and oatp1b2 mediated ATV uptake by RIF were 3.05 and 0.95 µM, respectively (Lau et al., 2006a). Therefore, in the current study, inhibition of

ATV uptake was tested at 10µM and 20µM RIF. Inhibition of BOS uptake has been tested at 20µM RIF.

ABT is a mechanism based (nonspecific suicidal) inhibitor of CYPs. It acts by destruction of prosthetic haem group of the enzymes (De Montellano and Mathews, 1981). Incubation of RLM with 10 mM ABT for 30 min resulted in 81% reduction in the activity of the enzyme (De Montellano and Mathews, 1981). It is a very efficient tool to inhibit activity of majority of CYPs. Recent reports do suggest that ABT might be less effective in inhibiting certain CYPs like CYP2C9 (Linder et al., 2009). Moreover, it was not possible to achieve complete inhibition of cyp3a1 mediated metabolism even at a very high dose of 300 mg/Kg and 26 hours post ABT administration in rats (Parrish et al., 2016). Similarly, more than 15 % CYP activity was remaining in RLM and 5-10% CYP activity was remaining in rat hepatocytes suspended in rat plasma upon 60 min preincubation of 2 mM ABT. It has been previously reported that up to 1 mM ABT does not interfere with the uptake transport by human OATP, P-gp, BCRP, and MRP2 (Plise et al., 2010). Therefore, 1 mM ABT treatment for 30 min was chosen to be the regimen for the liver perfusion studies described in this chapter.

Ketoconazole (KETO) is a potent noncompetitive inhibitor of CYP3A4 and CYP3A5 (Brown et al., 1985; Mosca et al., 1985; Ball et al., 1992). The Ki for recombinant CYP3A4 and CYP3A5 was observed to be 26.7 nM and 109 nM respectively (Gibbs et al., 1999). The IC_{50} for testosterone-6-β hydroxylation in rat liver microsomes was found to be 0.29 ± 0.09 µM (Eagling et al., 1998). Literature reports suggest that ketoconazole is not a substrate for OATP1B1 (Higgins et al., 2014), but weakly inhibits olmesartan

uptake in oocytes transfected with OATP1B1 with a Ki of 66.1 µM (Choi et al., 2011). A working concentration of 1 µM KETO was selected for the experiment.

Compounds with high passive permeability and non-substrates for transporters and metabolizing enzymes are expected to have a ratio of unbound intracellular concentrations to unbound plasma concentrations (KP_{uu}) equal to 1 (Koch-Weser and Sellers, 1976; Israili, 1979; Pardridge et al., 1983; Choi et al., 2011). Uptake transporters like OATPs increase the intracellular concentration of their substrates in the hepatocytes, and these concentrations can be many-fold higher than their plasma concentrations. Contrarily, metabolism and apical or basolateral efflux decrease the intracellular concentrations. Thus, the magnitude and time course of unbound intracellular concentrations is governed by the interplay between active uptake, passive diffusion, metabolism and efflux. BOS is a known inducer of CYP3A4 (Weber et al., 1999b; van Giersbergen et al., 2002) and is an inhibitor of BSEP. Inhibition of BSEP has been linked to the liver injury caused by this drug (Fattinger et al., 2001). Both these effects are driven by the intracellular concentration of BOS. As mentioned before, several statins including ATV are OATP substrates. Drug interactions due to OATP inhibition result in elevated plasma concentrations of these compounds leading to muscle toxicity (rhabdomyolysis) (Chapman and Carrie, 2005). Moreover, unbound intracellular concentrations will also be affected.

Single pass liver perfusion studies have been performed with ATV and BOS, alone and in combination with inhibitors of CYP mediated metabolism (ABT and KETO) and transport (RIF) to study the effect of active uptake, passive diffusion, metabolism and

efflux on unbound intracellular concentrations, tissue concentrations and bile concentrations of ATV and BOS. Passive diffusion for ATV was also studied by performing cold liver perfusions at 4°C.

3.2 Materials

ATV calcium trihydrate, 2-OH ATV and 4-OH ATV were obtained from Tokyo Chemical Industry America, OR. BOS, OH-BOS, OH-DM-BOS were obtained from Toronto Research Chemicals, Ontario, Canada. RIF for injection USP was obtained from Sanofi-Aventis, NJ. ABT, dextran, sodium bicarbonate ($NaHCO_3$), sodium taurocholate, glucose and dexamethasone were obtained from Sigma Aldrich, MO. KETO, Sodium chloride (NaCl), potassium chloride (KCI), calcium chloride ($CaCI_2$), magnesium chloride ($MgCI_2$), sodium monobasic phosphate (NaH_2PO_4), sucrose, potassium phosphate monobasic (KH_2PO_4), potassium phosphate dibasic (K_2HPO_4) were obtained from Fisher Scientific, NH. Sodium sulfate (Na_2SO_4) was obtained from EMD Chemicals, PA. Male Sprague Dawley rat plasma was obtained from BioChemed Services, VA. Isoflurane was obtained from University Laboratory Animal Resources (ULAR), Temple University. Intravenous (IV) catheter was purchased from Terumo Corporation, NJ. Polyethylene (PE) 20 tubing (0.11'' x 0.024'' x 0.0065'') and PE 100 tubing (0.055'' x 0.075'' x 0.01'') were purchased from AM systems, WA. HSE UNIPER UP-100 Type 834 perfusion apparatus was obtained from Harvard Apparatus, MA.

3.3 Methods

3.3.1 Animals

Male Sprague Dawley rats were maintained in the American Association for the Accreditation of Laboratory Animal Care-accredited University Laboratory Animal Resources of Temple University. Animals were provided with a normal rodent diet. Food and water was available to the animals as required. The animals were housed in a standard 12-hour dark/light cycle. Animal studies were approved by the Institutional Animal Care and Use Committee.

3.3.2 Perfusion set up

In situ liver perfusion was performed with the HSE UNIPER UP-100 Type 834 for isolated organ perfusion in rodents, as depicted in Fig 3.1 below.

Figure 3.1 HSE Uniper UP-100 Perfusion apparatus

The drug reservoir is connected to a peristaltic roller pump, which pumps the drug solution at a fixed flow rate. A flow rate of 20 mL/min was used. The windkessel acts as a bubble trap and reduces the pulsations caused by the roller pump. The heat exchanger receives water warmed at 37 ºC from the thermocirculator, which circulates around and heats up the perfusate. The warmed perfusate is then pumped into the organ of interest.

The perfusion medium consisted of modified Kerbs-Hensleit buffer with 3% dextran 40 and 30 μM sodium taurocholate. The modified Krebs'-Hensleit buffer consisted of the following: 109 mM NaCl, 4 mM KCI, 1.6 mM $CaCI_2$, 0.5 mM $MgCI_2$, 0.5 mM Na_2SO_4, 1 mM NaH_2PO_4, 12 mM sucrose, 10 mM glucose, and 25 mM $NaHCO_3$. The perfusion medium was warmed to 37°C or cooled to 4°C, depending on the type of the experiment, and aerated with oxygen containing 5% carbon dioxide throughout the experiment.

Surgery and perfusion: The rat was anesthetized by placing in isoflurane chamber at 1 L/min oxygen and 3% isoflurane for at least 5 minutes until breathing became regular and muscles were completely relaxed. The isoflurane supply was then switched to the tray mask. The rat was placed on the dissection tray with abdomen facing upward, head placed inside the isoflurane mask and legs secured to the tray with adhesive tape. Before proceeding with the surgery, adequate sedation was ensured by squeezing the paw with tweezers. A vertical incision was made on the lower abdomen followed by two forty degree incisions to the left and right. The abdomen was cut open to expose the viscera. Upon moving the intestine aside and exposing the liver, the inferior vena cava was sutured with a loose knot. Then the bile duct was isolated, a small incision was made and the PE 20 tubing was inserted into the duct and secured by a suture. Bile was collected on

ice. Thereafter, the portal vein was isolated and cannulated using the 18G IV catheter. The outlet from the perfusion apparatus was then connected to the catheter after allowing the blood from liver to drain out to avoid generation of air bubbles. The catheter was quickly secured with a suture and the inferior vena cava was cut. At this point, the liver blanches and turns into a light beige color (See results and fig 3.2). The hepatic vein was given a small cut and PE 100 tubing was inserted for sampling. After the loosely tied knot around the inferior vena cava was tightened, perfusate started coming out from the PE 100 tubing used for hepatic vein cannulation. The liver was allowed to equilibrate with blank perfusion medium for 20 min before beginning perfusion of drug combinations of interest. The perfusion time was decided on the basis of data obtained from preliminary experiments with ATV with longer perfusion times up to 100 min. For the purpose of final experiments with both ATV and BOS, the perfusion was continued for 50 min. Experiments were conducted with the following treatment groups for ATV: ATV alone at 4°C (n = 4), ATV alone at 37°C (n = 3), +10 µM RIF (n=5), + 20 µM RIF (n = 3), +ABT (n = 3), + ABT +20 µM RIF (n = 3), +KETO (n = 3) and +KETO+20 µM RIF (n = 3). Effect of RIF on BOS was tested at only 20 µM concentration. Experiments were conducted with the following treatment groups for BOS: BOS alone at 37°C (n = 4), +RIF (n = 4), +ABT (n=4) and +ABT+RIF (n = 4). ATV solution in methanol (1 mg/ml) or BOS solution in DMSO (1mg/mL) was added to the perfusate reservoir to give 1 µM final concentration. The final concentration of methanol and DMSO in the perfusion medium was 0.05 % v/v. For experiments with RIF, 10mg/mL RIF solution in water was added to the perfusate reservoir 5 min prior to addition of ATV or BOS to give the

desired final concentration (10 or 20 µM). Stock solution of ABT was prepared in ethanol (50 mg/mL) to give a final concentration of 1mM. The final concentration of ethanol in the perfusion medium was 0.25 % v/v. Stock solution of KETO was prepared in DMSO (1 mg/mL) to give a final concentration of 1 µM. The final concentration of DMSO in the perfusion medium was 0.05 % v/v.

3.3.3 Passive Diffusion Study for ATV in Cold Perfused Liver

Cold perfusions (4°C) were performed to determine passive diffusion of ATV and as a negative control for uptake and metabolism experiments. The perfusion medium was cooled down to 4°C, and the liver was covered with ice to maintain the temperature at 4°C. ATV solution in methanol (1 mg/ml) was added to the perfusate reservoir to give a final concentration of 1 µM. The final concentration of methanol in the perfusion medium was 0.05% v/v.

3.3.4 Passive Diffusion, Uptake, and Metabolism Studies for ATV and BOS in Perfused Liver at 37°C

The perfusion medium was warmed to 37°C, and a heating lamp was used to maintain the liver temperature at 37°C. ATV (1 µM) was perfused alone, with either RIF, ABT or KETO, or with a combination of either +ABT+RIF or +KETO+RIF. Since ABT is a non-specific CYP inactivator, it could also inhibit the enzymes involved in metabolism of bile salts, in turn affecting the bile flow and apical efflux process. Therefore, metabolism inhibition was tested with a specific cyp3a inhibitor, KETO. Passive diffusion was also determined at 37°C by combined inhibition of uptake and metabolism. To determine

passive diffusion at 37°C, ABT (1mM) was perfused for 20 minutes, followed by switching the reservoir to rifampin (RIF, 20 µM) for 5 minutes, followed by the addition of ATV (1 µM), which was then co-perfused with RIF for 50 minutes. Alternatively, passive diffusion was determined by combined treatment with KETO and RIF. KETO (1 µM) was perfused for 5 minutes followed by perfusion with 20 µM RIF for 5 min before the addition of ATV (1 µM). KETO and RIF were then co-perfused along with ATV 50 minutes. Passive diffusion for BOS was determined in a similar manner at 37°C. However, based on the results for ATV, passive diffusion for BOS was determined only with ABT as the inhibitor of metabolism instead of KETO. BOS solution in DMSO (1 mg/ml) was added to the perfusate reservoir to give a final concentration of 1 µM. The final concentration of DMSO in the perfusion medium was 0.05% v/v.

For uptake inhibition studies, RIF (10 µM or 20 µM) was perfused 5 minutes before the addition of ATV (1 µM). Inhibition of BOS uptake was tested with 20 µM RIF in a similar manner, based on results obtained from ATV experiments. RIF was then co-perfused along with ATV or BOS for 50 minutes.

For metabolism inhibition studies, ABT (1mM) was perfused for 20 minutes, followed by switching of the reservoir solution to 1 µM ATV or 1 µM BOS. Inhibition of ATV metabolism was also tested by co-perfusion with KETO (1 µM) along with ATV. KETO (1 µM) was perfused 5 minutes before the addition of ATV (1 µM). KETO was then co-perfused along with ATV for 50 minutes. Bile flow was used as a measure of viability of the hepatocytes.

Bile was collected on ice over intervals of 0–15, 15–30, and 30–50 minutes. Propagation of errors in the calculation of cumulative amount in bile was performed using the following equation.

$$Error = \sqrt{{\sigma_A}^2 + {\sigma_B}^2}$$

Outlet perfusate from hepatic veins was sampled at 0, 5, 10, 20, 30, 40, and 50 minutes. During the entire course of the experiment, the liver was covered with sterile gauze kept moist by occasional spraying of saline. Inlet reservoir concentration was also sampled for analysis. The liver was removed at the end of 50 minutes, flash frozen on dry ice and homogenized with water in the ratio 1:2 before analysis. All perfusate, liver samples, and bile samples were stored at -80°C until further analysis.

3.3.5 Control experiments to determine normal bile flow

In order to determine normal bile flow in rat livers perfused with modified Krebs'-Hensleit buffer with sodium taurocholate and dextran 40, blank perfusion medium was perfused in the same manner as that for the above experiments. Briefly, after completion of the surgery, the liver was allowed to equilibrate for 20 min and blank perfusion medium was allowed to pass through the liver for 50 min. Cumulative bile samples were collected from 0-15, 15-30 and 30-50 min and bile flow was measured.

3.3.6 Statistical analysis

Statistical analysis was conducted using SigmaStat software, version 3.5. A t-test was used to compare groups. One-way ANOVA was used for comparison between multiple

groups. Post hoc analysis was conducted using Tukey's test. A p value less than 0.05 was considered statistically significant.

3.4 Results

The difference between a perfused and an un-perfused liver can be observed in fig 3.2 below. An un-perfused liver has vasculature filled with blood, and therefore, appears red in color (fig 3.2A). On the contrary, a perfused liver appears beige in color due to draining of blood and presence of perfusate in the vascular spaces. A well perfused liver should be devoid of any unevenly colored spots on its surface (fig 3.2B). Fig 3.2C below is an example of an inadequately perfused liver. Here, the encircled area has not been well perfused and hence appears red.

(A) **(B)** **(C)**

Unperfused liver **Well perfused liver** **Inadequately perfused liver**

Figure 3.2 Comparison between an un-perfused, well perfused and inadequately perfused liver

Perfusion time was decided from the preliminary results obtained with extended perfusion periods using ATV. In order to reach steady state, longer perfusion periods were desired. Fig 3.3 shows ATV outflow perfusate concentrations normalized to inflow concentration versus time profile for perfusions carried out for longer duration (110 min).

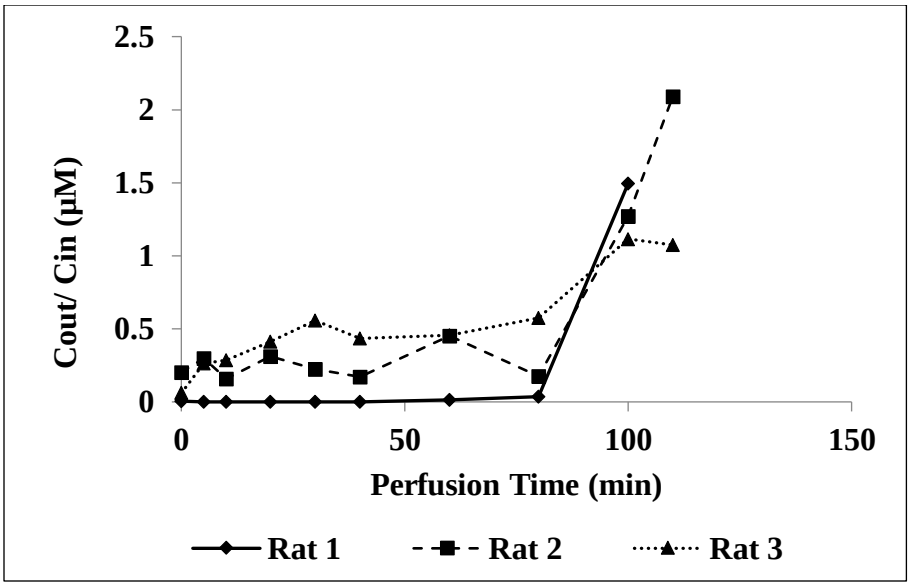

Figure 3.3 ATV outflow perfusate concentrations normalized to inflow concentration versus time for longer perfusion period (110min)

It is evident that in all the three animals, the outflow concentrations after about 60 min started increasing and surpassed the inlet concentration of 1µM at 100 min. This could be an indication of the hepatocytes losing their viability. Hence, perfusion was discontinued at 50 min for subsequent experiments.

3.4.1 Comparison of bile flow across different groups

Normal bile flow in rats is 20 - 22 µL/min (Guerrier et al., 2014). Bile flow in rats perfused with Krebs'-Ringer buffer with 3% bovine serum albumin has been reported to be 10-12 µL/min (Akita et al., 2001). The bile flow rate in the control experiments to determine normal bile flow upon liver perfusion was 7.4 µL/min from 0-15 min, 8.1 µL/min from 15-30 min and 7.97 µL/min from 30-50 min. Therefore, 8-10 µL/min was

considered as the normal bile flow for the current experimental procedure. Data from the surgeries in which the bile flow rate was less than 3 µL/min were considered to be of poor quality and not used for subsequent modeling exercises. The average bile flow rate from successful surgeries in various treatment groups is summarized in Table 3.1. No significant difference was observed between control group and any other groups.

It can be observed in the current study that the treatment groups with RIF demonstrate a slightly higher mean bile flow as compared to the groups without RIF treatment. This is in accordance with the previous findings in isolated perfused rat livers. It was observed that 100 µg/mL RIF increased the bile flow to 134 % of the control (Oliven and Bassan, 1986). Also, the BOS treated groups demonstrated a higher bile flow than the control group. An additive effect of BOS and RIF on bile flow can be observed in groups treated with both drugs. The difference in bile flow for the BOS + RIF treated groups was significantly different than the control group.

Table 3.1 Average bile flow rates across different experimental groups treated with ATV Data are represented as mean ± SD, a t-test was used to compare control group with other groups, *p < 0.05, **p < 0.01

Group	**Sub - group**	**Average bile flow rate (µL/min)**
Untreated	Control	7.84 ± 1.62
ATV treated	ATV	7.58 ± 1.06
	ATV + RIF	9.92 ± 1.86
	ATV + ABT	6.19 ± 1.03
	ATV + ABT + RIF	8.23 ± 1.3
	ATV + KETO	6.73 ± 0.55
	ATV + KETO + RIF	10.3 ± 1.1
BOS treated	BOS	10.5 ± 0.87
	BOS + RIF	15.6 ± 0.42*
	BOS + ABT	10 ± 0.96
	BOS + ABT + RIF	13.9 ± 0.62**

3.4.2 Effect of bile flow on ATV outflow perfusate concentrations and liver concentrations

The bile flow in some experiments was lower than others. Comparison of the data from low bile flow groups to normal bile flow groups revealed that the lower bile flow groups showed elevated ATV outflow perfusate concentrations as compared to the normal bile flow (Fig 3.4). This effect was independent of inhibition of active uptake transport. Outflow perfusate concentrations were elevated with decrease in bile flow irrespective of the presence or absence of RIF. Decreased bile flow rates resulted in lower average liver concentrations in both ATV only and +RIF groups. The liver concentrations were 1.7 and 2.6 fold higher in the groups with normal bile flow as compared to those with low bile flow in the ATV only and + RIF groups, respectively, as demonstrated by fig 3.5.

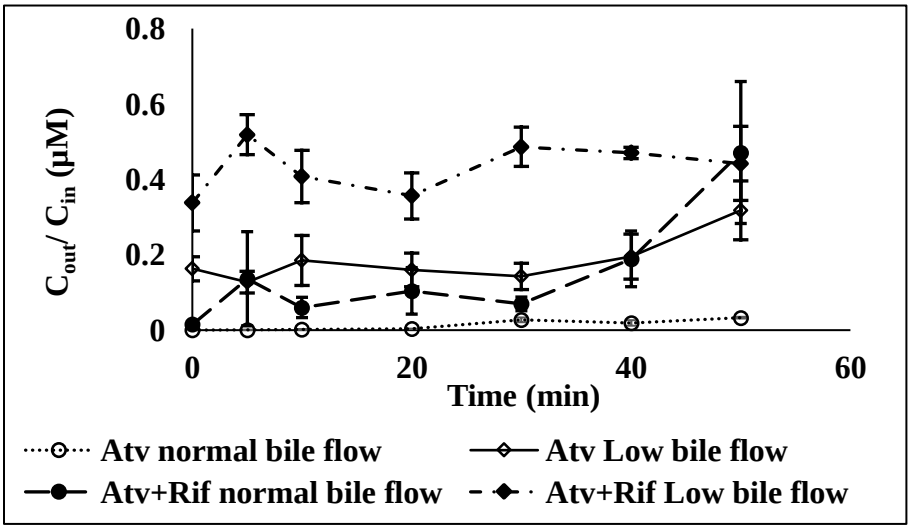

Figure 3.4 Effect of bile flow on outflow perfusate concentrations. Data are represented as mean ± SEM

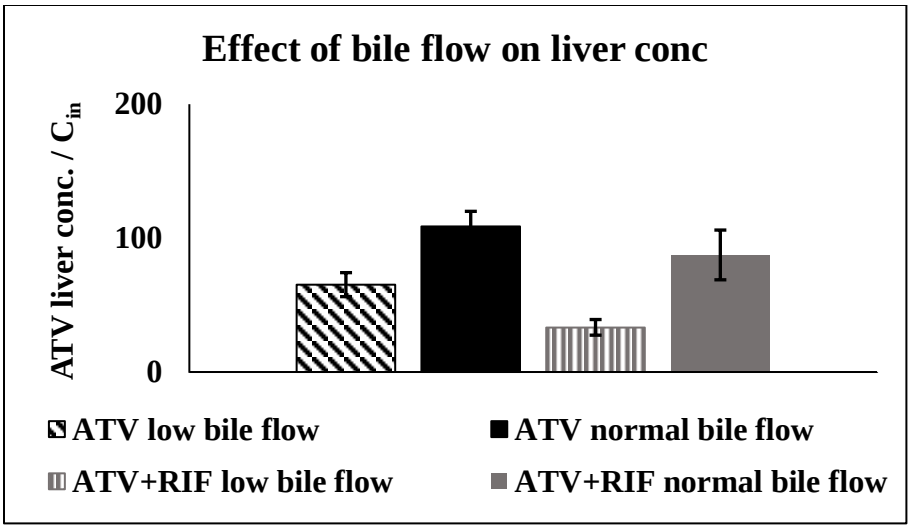

Figure 3.5 Effect of bile flow on liver concentrations. Data are represented as mean ± SEM

In the ATV only groups, 122 – 304 fold difference was observed in outflow concentrations with decrease in bile flow. In the +RIF groups, the fold difference was 0.8 to 21.4 fold (Table 3.2).

Table 3.2 Ratio of outflow perfusate concentrations in normal versus decreased bile flow groups

Time (min)	ATV only	ATV+RIF
0	156	21.4
5	122	3.8
10	177	6.4
20	153	3.3
30	137	5.6
40	187	2.1
50	304	0.8

3.4.3 Optimization of RIF concentration for ATV uptake and passive diffusion studies

RIF demonstrated a dose dependent decrease in ATV liver concentrations (Fig 3.6). Mean ATV concentrations for livers perfused with ATV only, ATV + 10 µM RIF and ATV + 20 µM RIF were 65.2 µM, 45.43 µM and 33.34 µM respectively**.** The ATV only demonstrated significant difference ($p < 0.05$) in liver concentrations as compared to 20 µM RIF treated group. However, there was no significant difference in liver concentrations between ATV only and 10 µM RIF treated groups, and 10 versus 20 µM RIF treated groups.

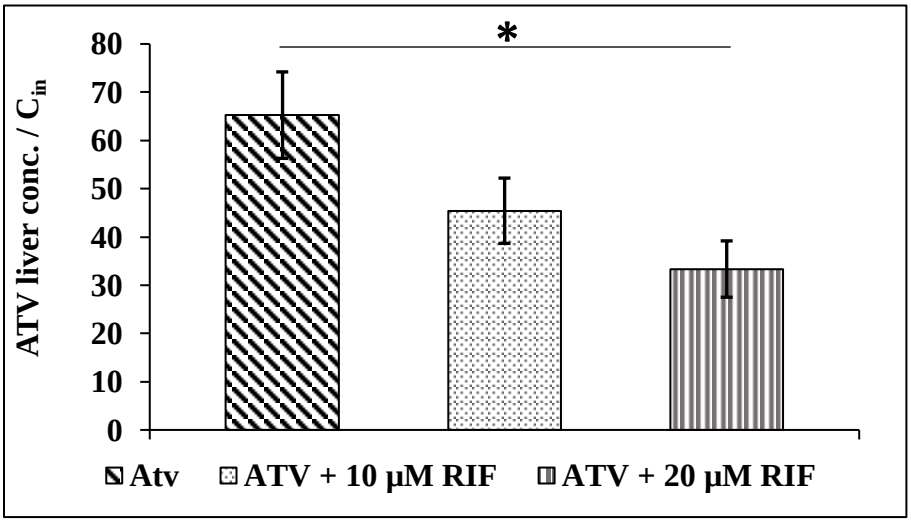

Figure 3.6 Effect of RIF on ATV liver concentrations. Data are represented as mean ± SEM

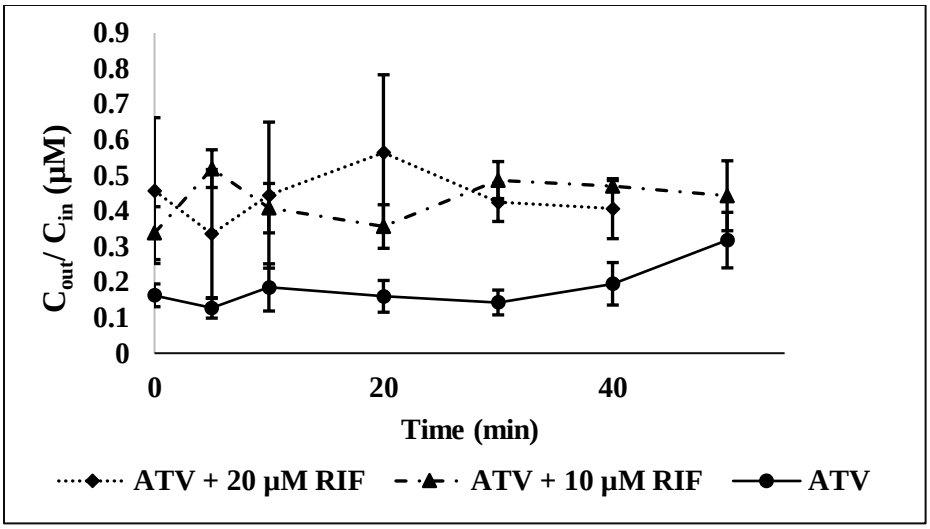

Figure 3.7 Effect of rifampin treatment on ATV outflow perfusate concentrations. Data are presented as mean ± SEM

The C_o/C_{in} ratio achieved a steady state almost immediately and ranged between 0.2 to 0.35 for animals treated with ATV only, whereas this ratio increased to 0.4 to 0.55 for animals treated with ATV + 10 µM RIF (Fig 3.7). A statistically significant difference was observed in the C_o/C_{in} ratio between ATV only and 10 µM RIF groups at 0 and 30 min, ATV only and 20 µM RIF groups at 5, 30 and 40 min, and 10 µM and 20 µM RIF groups at 5 min ($p < 0.05$). Therefore, 20 µM RIF concentration was selected for further studies with ATV and BOS.

All the three experimental groups demonstrated low bile flow. However, as demonstrated by Fig 3.4 above, effect of inhibition of active uptake on the outflow perfusate concentrations is qualitatively similar across the low versus normal bile flow groups. Hence, although these data have discrepancy, they can be used for the purposes of optimization of RIF concentrations for future studies.

3.4.4 Passive Diffusion of ATV in the Perfused Liver

The outflow perfusate concentrations of ATV upon inhibition of active transport and metabolism are shown in Fig. 3.8 A. The outflow perfusate ATV concentration in 4°C studies achieved steady state by 10 minutes after the start of the perfusion, with an average steady-state outflow concentration of 1–1.5 µM (essentially equal to the inlet concentration). The outflow perfusate concentrations in the +ABT + RIF group were generally lower than the 4°C group and were significantly lower at 5 ($p < 0.001$), 10 and 20 ($p < 0.05$) min. The outflow perfusate concentrations in the +KETO + RIF group were significantly lower than both the +ABT + RIF group and the 4°C group at all times ($p < 0.05$). The mean liver concentration at the end of the 50-minute perfusion was 12.3 µM in the 4°C group, which was significantly lower than 60.1 µM observed in the +KETO + RIF group ($p < 0.001$) and 56.8 µM observed in the +ABT + RIF group ($p < 0.001$) (Fig. 3.8 B). The total amount of the parent drug excreted in bile was 0.00012 µmol in 4°C studies. Both the hydroxy metabolites were undetectable in outflow perfusate as well as bile in 4°C studies. The liver concentration of 2-OH ATV at the end of the 50-minute perfusion was 0.005 µM, whereas 4-OH ATV was undetectable in liver in 4°C studies. The average bile flow was 5-fold lower than the +ABT + RIF group and 6.7 fold lower than +KETO + RIF group at 37°C. Based on these results and modeling efforts described subsequently in chapter 4, the +ABT + RIF group was selected as the control group for all subsequent studies.

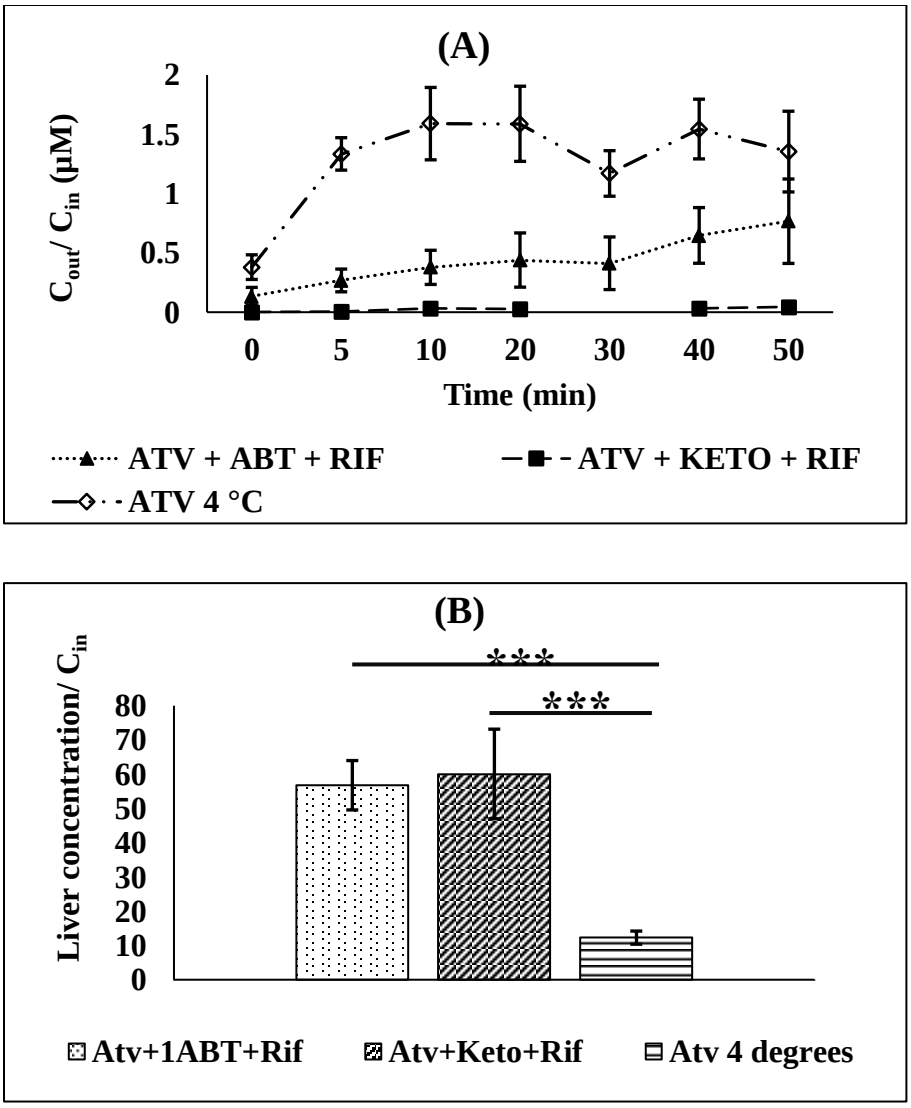

Figure 3.8 Passive diffusion experiments. (A) ATV outflow perfusate concentrations normalized to inlet concentration and (B) ATV total liver concentrations normalized to inlet concentration, in the absence of active transport and metabolism. Data are presented as mean ± S.E.M.; ATV 4°C: n = 4, ATV + ABT + RIF: n = 3; A t test was performed to compare the two groups. ***$p < 0.001$.

3.4.5 Uptake and Metabolism of ATV in the Perfused Liver

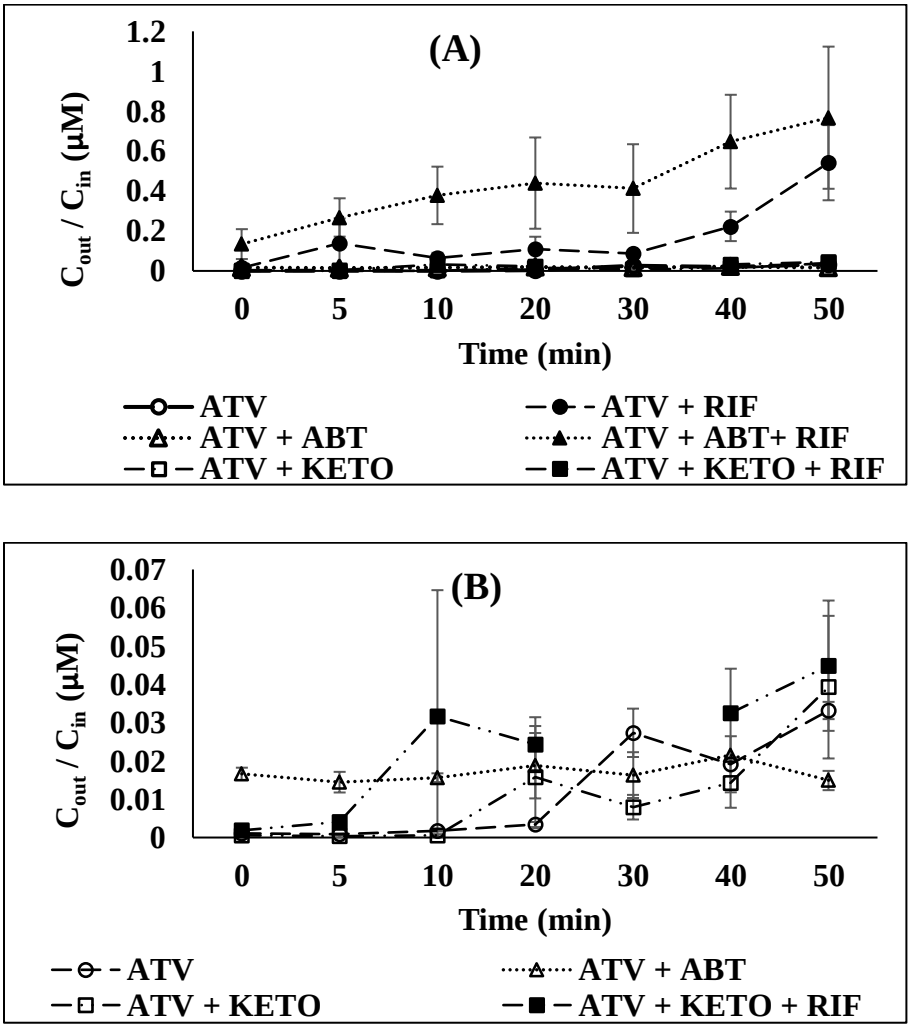

Figure 3.9 ATV data collected with single pass liver perfusions (A) Outflow perfusate concentration normalized to inflow concentration versus time profiles for 50 min perfusion; (B) Outflow perfusate concentration normalized to inflow concentration versus time profiles on a magnified scale for selected groups. Data are presented as mean ± SEM; ATV: n=3, ATV + RIF: n=3, ATV + ABT: n=3, ATV + ABT + RIF: n=3, ATV + KETO: n=3, ATV + KETO + RIF: n=3

ATV outflow perfusate concentration normalized to inlet concentration (C_{out} / C_{in}) versus time profiles for 50 min perfusion in various experimental groups can be seen in fig 3.9. The outflow perfusate concentrations in the +ABT + RIF and +KETO + RIF groups demonstrated a continued increase over 50 minutes when both uptake and metabolism were inhibited at 37°C. The outflow concentrations from +ABT + RIF group were generally higher than the other groups at 37°C (Fig. 3.9 A). For the +KETO + RIF group, the outflow perfusate concentrations were 70-fold lower at 0 min and 17 fold lower at 50 min, as compared to the +ABT + RIF group. The average outflow concentrations were lowest in the ATV alone group and ranged between 0.001 µM at the start of the perfusion and 0.03 µM at the end of the 50-minute perfusion (Fig. 3.9 B). Inhibition of uptake transport on RIF co-perfusion significantly increased the ATV outflow perfusate concentrations compared with the ATV-alone group ($p < 0.05$ at 30 and 40 minutes). The outflow concentrations were significantly higher than the ATV-alone group upon inhibition of metabolism by ABT during the first half of the perfusion ($p < 0.01$ at 0, 5, 10 minutes; Fig. 3.9 B) and significantly lower than the ATV group at 50 minutes ($p < 0.01$; Fig. 3.9 B); however, no significant difference in concentrations was seen at 30 and 40 minutes. In the +KETO group, the mean outflow concentrations were lower than ATV group at all time points except 20 and 50 minutes, and were significantly different than the ATV group at 10 and 30 minutes ($p < 0.05$).

The ATV liver concentrations at the end of the 50-minute perfusion in various groups are shown in Fig. 3.10.

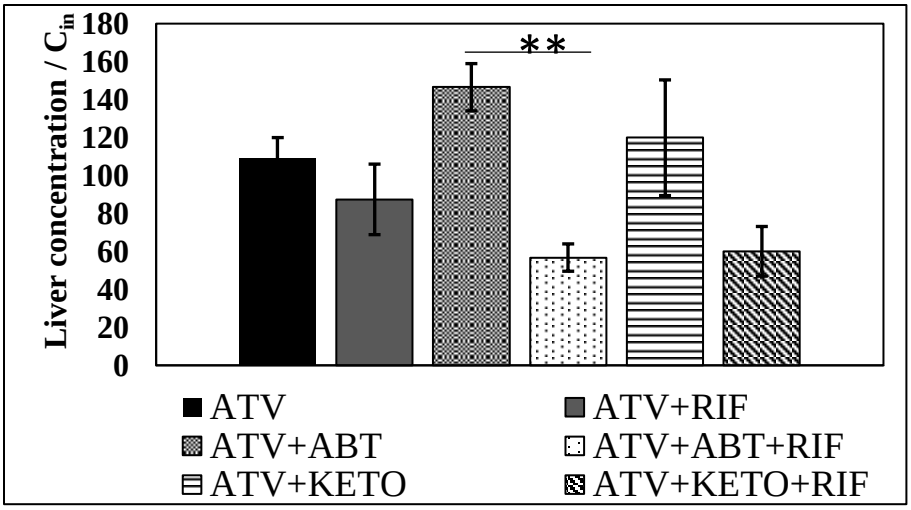

Figure 3.10 ATV data collected with single pass liver perfusions. ATV total liver concentrations normalized to inlet concentration. t-tests were performed to compare the ATV alone group with +RIF or with +ABT and to compare +ABT with +ABT + RIF; **$p < 0.01$. Data are presented as mean ± SEM; ATV: n=3, ATV + RIF: n=3, ATV + ABT: n=3, ATV + ABT + RIF: n=3, ATV + KETO: n=3, ATV + KETO + RIF: n=3

The mean ATV liver concentrations at the end of a 50-minute perfusion in the ATV-alone group were 108.9 µM. A decrease in ATV liver concentration was observed on treatment with RIF; however, the decrease was not statistically significant. Inhibition of metabolism by ABT resulted in a 1.3-fold increase in ATV liver concentration, while no significant difference in liver concentrations was observed upon treatment with KETO. The lowest mean ATV liver concentration was observed in the +ABT + RIF group when both uptake and metabolism were inhibited. A statistically significant decrease ($p < 0.01$) was observed in the liver concentrations between the +ABT group and the +ABT + RIF

group. The cumulative amount excreted in bile at the end of 15, 30, and 50 minutes is shown in Fig. 3.11.

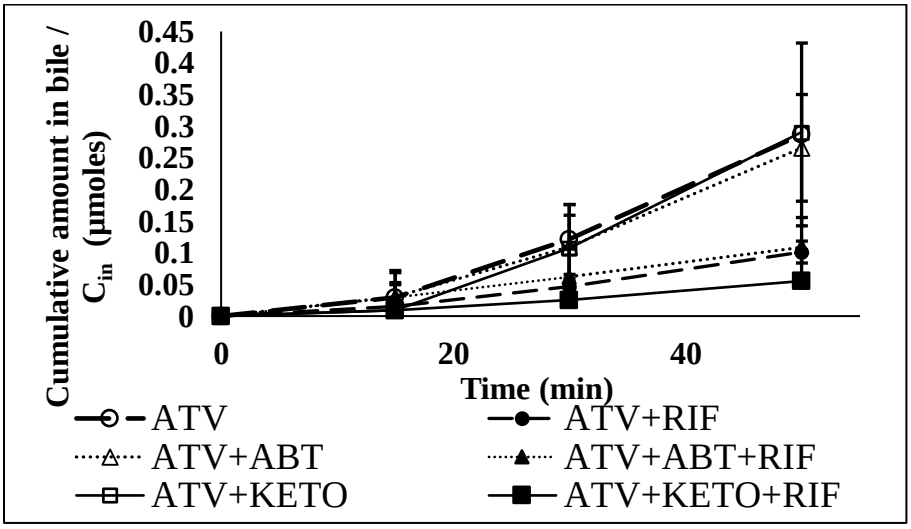

Figure 3.11 ATV data collected with single pass liver perfusions: Cumulative amount of ATV excreted in bile. Data are presented as mean ± S.E.M. ATV: n = 3, ATV + RIF: n = 3, ATV + ABT: n = 3, ATV + ABT + RIF: n = 3.

A steady increase in the amount excreted over time was observed in all groups. The amount in bile and the rate of appearance of ATV in bile were higher in all groups without RIF treatment. There was a lag in the appearance of drug in the bile in all groups. The percentage of total dose recovered in the bile as parent drug was 28.7%, 11.2%, 26.6%, 10.7%, 29% and 5.5% in the ATV alone, +RIF, +ABT, +ABT + RIF, +KETO and +KETO + RIF groups, respectively.The concentrations of 2-OH ATV and 4-OH ATV in the outflow perfusate were below the limit of quantitation. The highest liver metabolite concentrations were observed in the ATV group (Fig. 3.12, A and B).

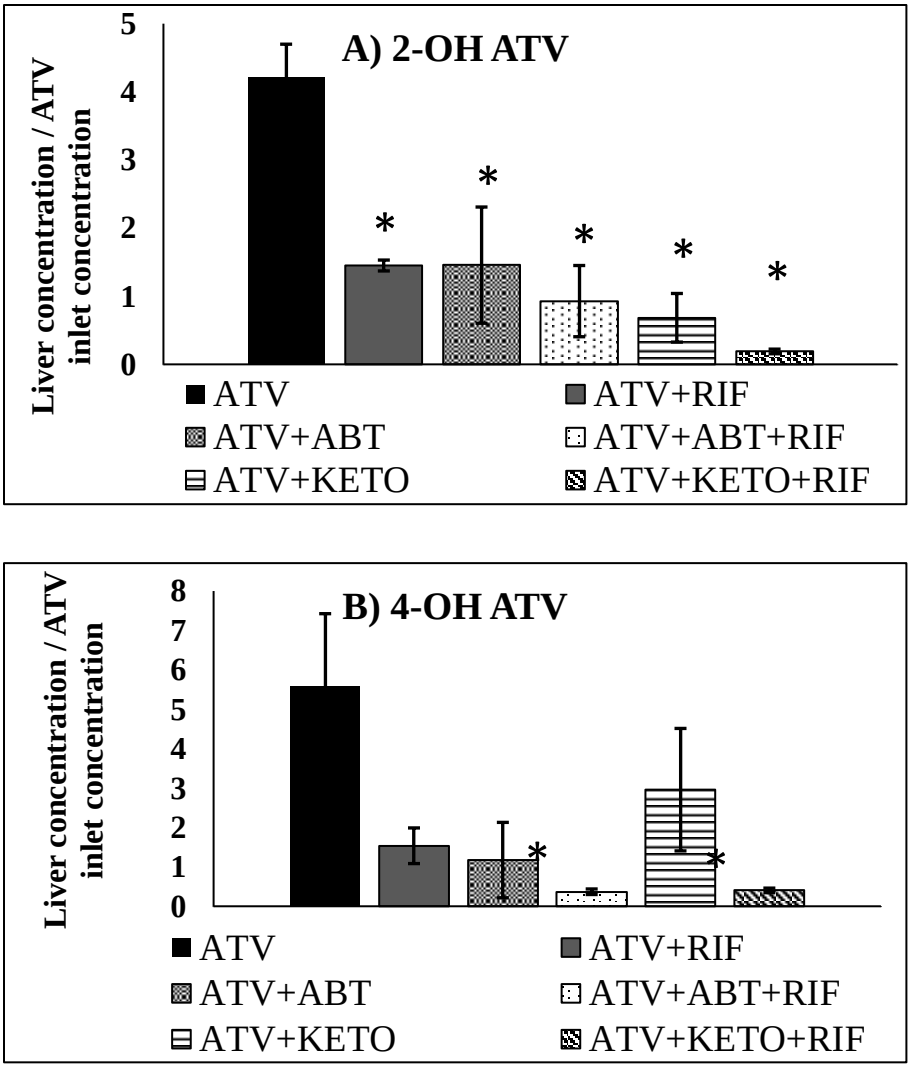

Figure 3.12 ATV metabolite data from single-pass liver perfusion studies: Liver concentrations normalized to ATV inlet concentration for (A) 2-OH ATV, (B) 4-OH ATV. One-way analysis of variance followed by post hoc Tukey's test was performed; *Groups statistically different from ATV ($p < 0.05$) are marked. Data are presented as mean ± S.E.M.; ATV: n = 3, ATV + RIF: n = 3, ATV + ABT: n = 3, ATV + ABT + RIF: n = 3, ATV + KETO: n=3, ATV + KETO + RIF: n=3.

RIF treatment decreased the mean liver concentration of 2-OH ATV by 2.9-fold and 4-OH ATV by 3.62-fold. A 2.9- and 4.7-fold decrease was observed on inhibition of metabolism by ABT in the mean liver concentrations of 2-OH ATV and 4-OH ATV, respectively, as compared to the ATV group. Similarly, a 6.17- and 1.88-fold decrease was observed in the mean liver concentrations of 2-OH ATV and 4-OH ATV, respectively, upon treatment with KETO, as compared to the ATV group. The +ABT + RIF and +KETO + RIF –treated groups demonstrated lowest metabolite liver concentrations (Fig. 3.12, A and B).

The cumulative amount of metabolites in bile over time is shown in Fig. 3.13, A and B. The ATV group demonstrated the highest amount of metabolites recovered in bile, with 2-OH ATV and 4-OH ATV accounting for 4.8% and 5.06% of the parent in bile, followed by the +RIF group. The amount of metabolites in bile in the +ABT, +ABT + RIF, +KETO and +KETO + RIF groups was lower than the other two groups but could not be compared statistically owing to high variability in the data. These data were not used for subsequent modeling efforts.

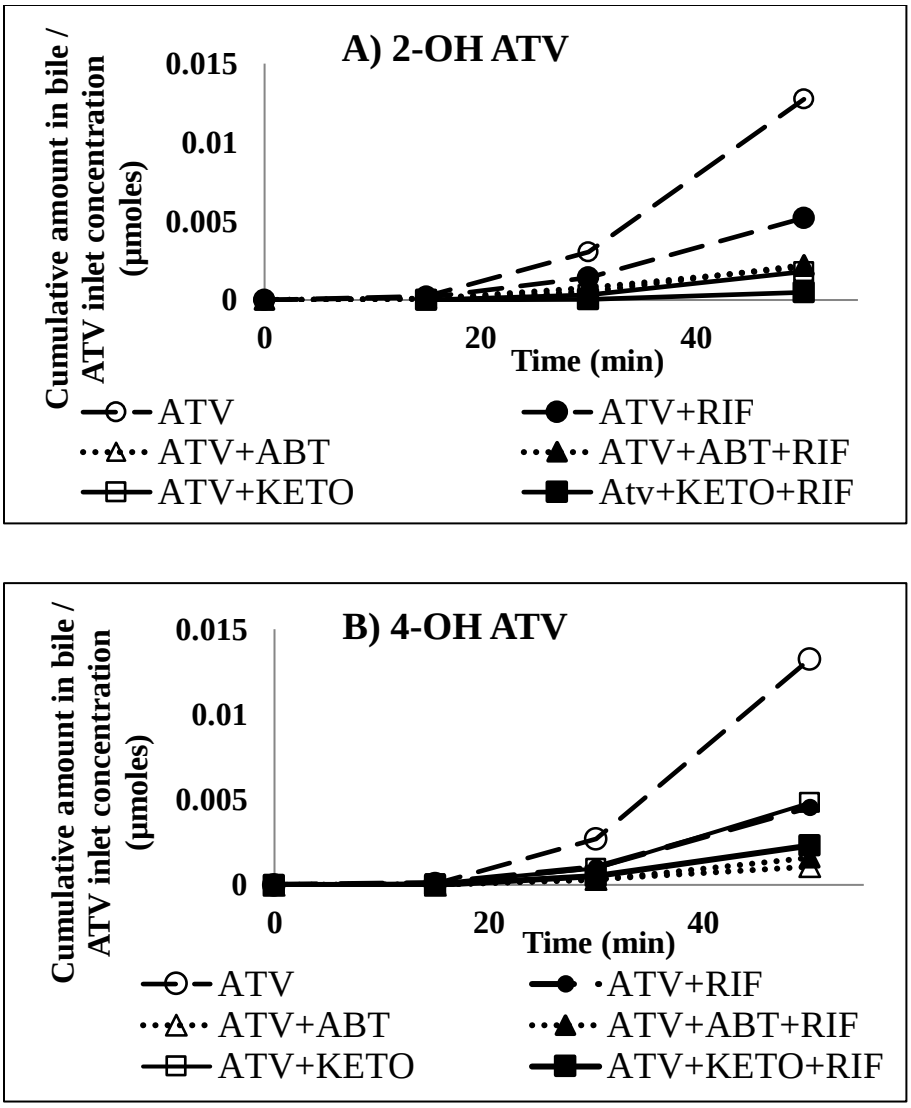

Figure 3.13 ATV metabolite data collected from single-pass liver perfusion studies: Cumulative amount excreted in bile normalized to ATV inlet concentration of (A) 2-OH ATV and (B) 4-OH ATV. ATV: n = 3, ATV + RIF: n = 3, ATV + ABT: n = 3, ATV + ABT + RIF: n = 3, ATV + KETO: n=3, ATV + KETO + RIF: n=3.

The total metabolite-to-parent ratios were calculated as the ratio of sum of the two hydroxy metabolite concentrations to the total parent concentration in the liver at the end of the 50-minute ATV perfusion are presented in Fig. 3.14.

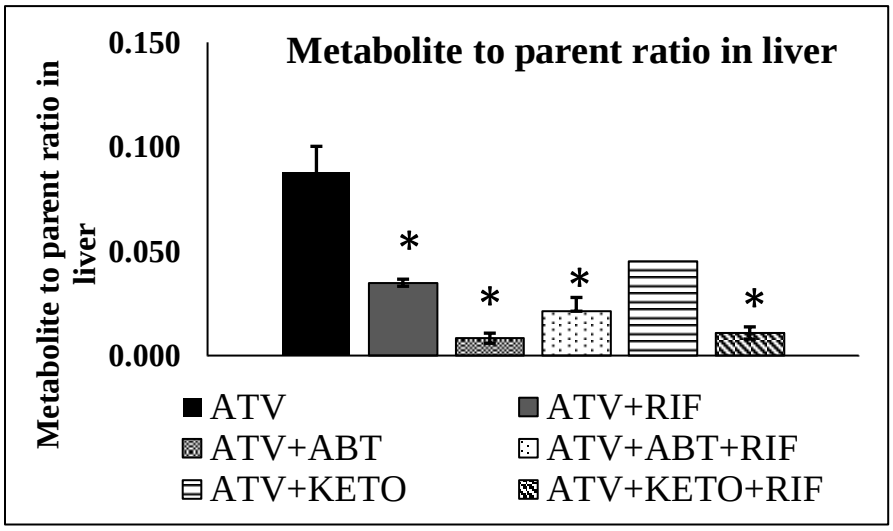

Figure 3.14 Metabolite-to-parent ratio for ATV in liver. t tests were performed to compare each treatment group to ATV alone *P < 0.05. Data are presented as mean ± S.E.M.; ATV: n = 3, ATV + RIF: n = 3, ATV + ABT: n = 3, ATV + ABT + RIF: n = 3, ATV + KETO: n=3, ATV + KETO + RIF: n=3.

The metabolite-to- parent ratio in the +RIF group was 37.7% of that in the ATV alone group, and the difference was statistically significant (p = 0.012). Inhibition of metabolism by ABT significantly decreased the metabolite-to-parent ratio as expected, to 19.3% of that in the ATV alone group (p = 0.012). This is in agreement with the previous observations by De Montellano and coworkers that preincubation of RLM with 1 mM ABT for 30 minutes resulted in a 77% loss of P450 activity (De Montellano and Mathews, 1981). No significant difference was found in the metabolite to parent ratio

between +ABT and +ABT + RIF groups. The metabolite-to-parent ratio in the +KETO and +KETO + RIF groups was 51 % and 12.5 % as compared to that in ATV group.

3.4.6 Passive diffusion, Uptake and Metabolism of BOS in the Perfused Liver:

According to the results obtained for ATV passive diffusion studies as summarized previously, uptake and passive diffusion studies for BOS were performed only in presence of 20 µM RIF at 37°C.

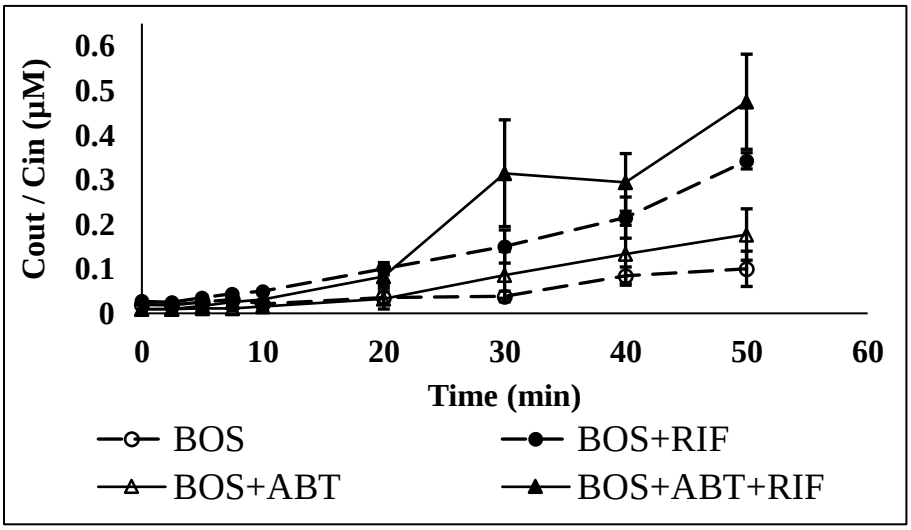

Figure 3.15 BOS data collected with single pass liver perfusions: outflow perfusate concentration normalized to inflow concentration versus time profiles
Data are presented as mean ± SEM; BOS –Bosentan, RIF –Rifampin, ABT–1-aminobenzotriazole; BOS: n=4, BOS + RIF: n=4, BOS + ABT: n=4, BOS + ABT + RIF: n=4

For passive diffusion studies of BOS with +ABT + RIF, the highest mean outflow perfusate concentrations were obtained at 30, 40 and 50 min as compared to all other

experimental groups (Fig 3.15). At 0, 2.5, 5, 7.5, 10 and 20 min, the BOS + RIF group demonstrated the highest concentrations. The difference between BOS + RIF and BOS + ABT + RIF groups was statistically significant from 0 to 7.5 min ($p < 0.05$). The BOS only group had the lowest outflow concentrations of all groups followed by the inhibition of metabolism in BOS + ABT group. The difference between BOS and BOS + ABT groups was not statistically significant throughout the experiment. Inhibition of active uptake by RIF, however, demonstrated a significant increase in outflow concentrations from 10 to 50 min ($p < 0.05$) as compared to the BOS only group.

The mean BOS liver concentrations at the end of 50 min perfusion are summarized in fig 3.16. The mean BOS liver concentrations in the BOS only group were 92 µM. Inhibition of active uptake by RIF increased the mean liver concentrations to 136.6 µM. The difference in the liver concentrations in BOS only versus BOS + RIF groups was not statistically significant. Inhibition of cyp3a mediated metabolism by ABT resulted in mean liver concentrations of 85 µM, which were not significantly different than the BOS only group. The lowest mean liver concentrations of 76.7 µM were demonstrated by the BOS + ABT + RIF group. The liver concentrations obtained from this group were significantly different only from the BOS + RIF group ($p < 0.01$)

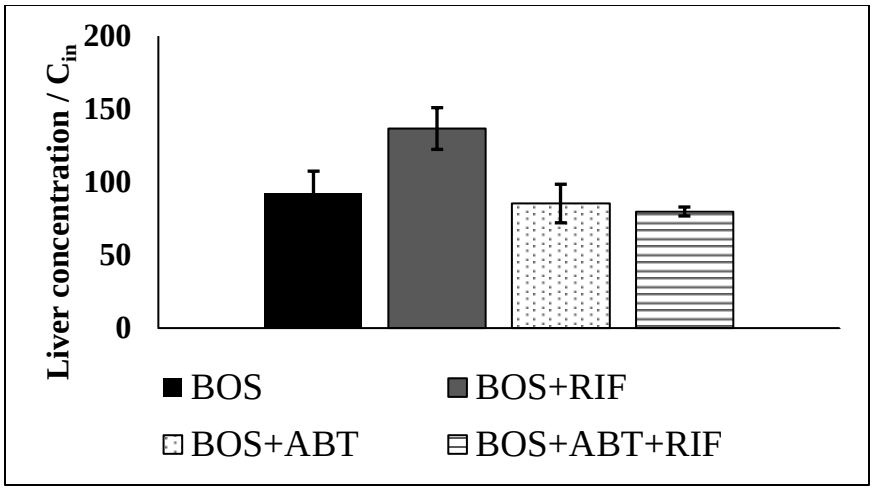

Figure 3.16 BOS data collected with single pass liver perfusions: BOS total liver concentrations normalized to inlet concentration. t-tests were performed to compare the BOS alone group with +RIF or with +ABT and to compare +ABT with +ABT + RIF; Data are presented as mean ± SEM

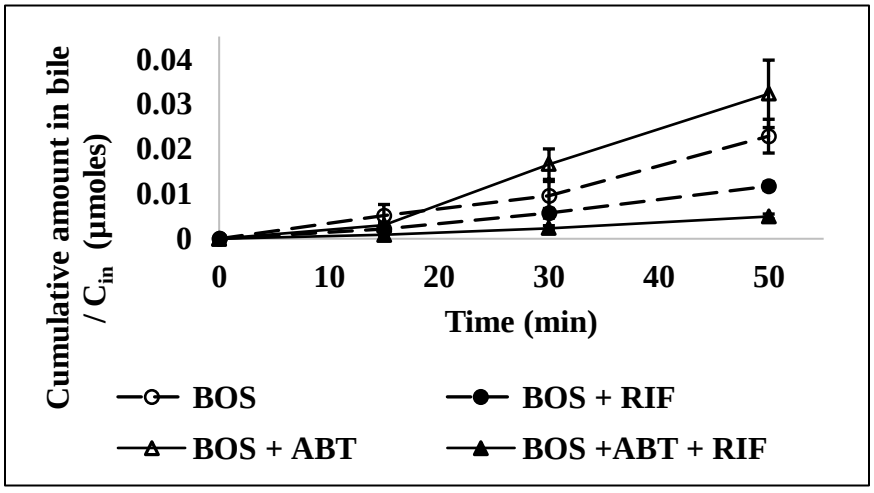

Figure 3.17 BOS data collected with single pass liver perfusions: Cumulative amount of BOS excreted in bile. Data are presented as mean ± SEM

Fig 3.17 shows the cumulative amount of BOS excreted in bile at the end of 15, 30 and 50 minutes. All the groups demonstrated a steady increase in the cumulative amount excreted over time, similar to ATV. A lag was observed in the appearance of BOS in bile in all treatment groups. The highest rate of appearance and cumulative amount excreted in bile at each time point was observed for the BOS + ABT group. The cumulative amount in bile for the BOS group was significantly lower than that for BOS + ABT group at all time points. The RIF treated groups demonstrated the lowest rate of appearance and the cumulative amount of drug excreted in bile. The cumulative amount of BOS excreted in bile was significantly lower in the BOS + RIF group as compared to the BOS only group ($p < 0.05$) and in BOS + ABT + RIF group as compared to the BOS + ABT group ($p < 0.01$). The mean percentage dose recovered from BOS only, BOS + RIF, BOS + ABT and BOS + ABT + RIF groups was 2.28 %, 1.17 %, 4.39 % and 0.49 %, respectively.

Metabolites of BOS could not be detected in the outflow perfusate. The mean OH-BOS liver concentrations were similar in the BOS and BOS + RIF groups (0.3 µM and 0.29 µM, respectively (Fig 3.18). OH-BOS liver concentrations in the BOS + ABT and in BOS + ABT + RIF groups were 2.28 and 1.28 fold lower than the BOS only group, but not significantly different. RIF treatment had no effect on mean liver concentrations of OH-DM-BOS (0.97 µM and 0.93 µM in BOS and BOS + RIF groups, respectively). ABT treatment decreased the OH-DM liver concentrations by 1.33 fold and 1.73 fold in the BOS + ABT and BOS + ABT + RIF groups, respectively. The difference was, however, not statistically significant.

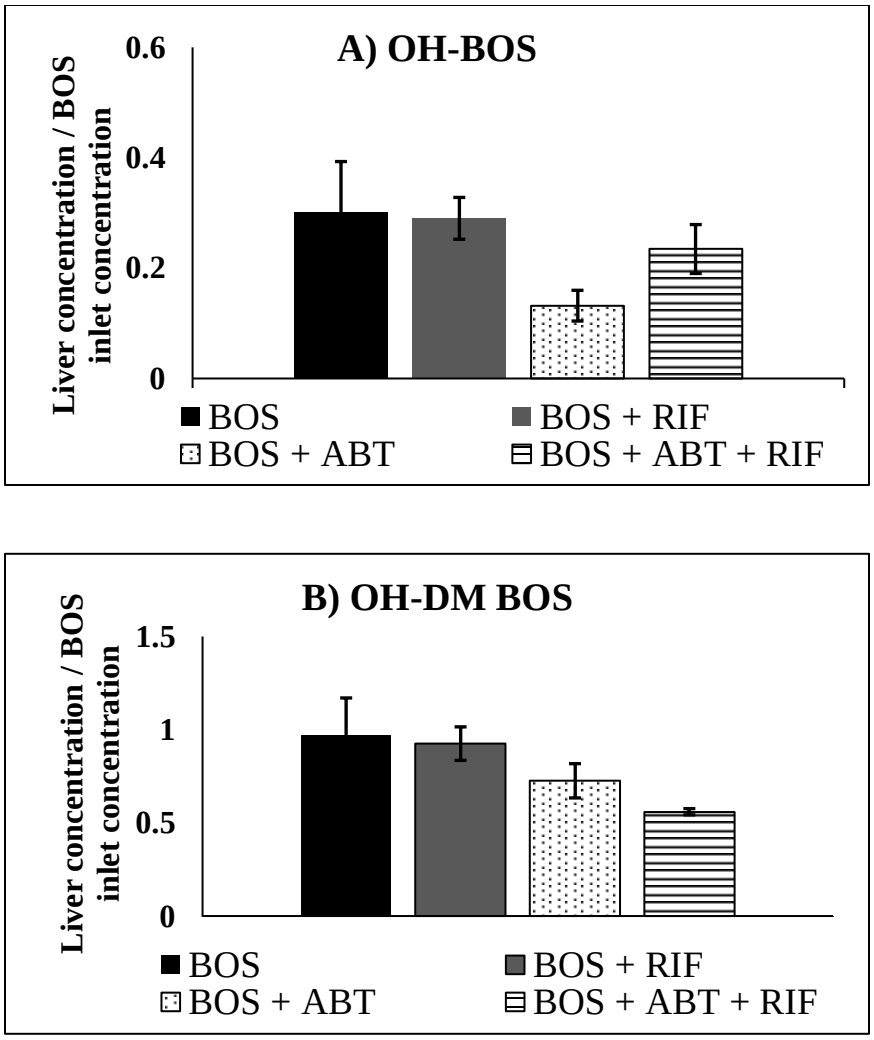

Figure 3.18 BOS metabolite data collected from single-pass liver perfusion studies: Liver concentrations normalized to BOS inlet concentration for (A) OH-BOS and (B) OH-DM-BOS. One-way analysis of variance was performed; Data are presented as mean ± SEM; BOS: n=4, BOS + RIF: n=4, BOS + ABT: n=4, BOS + ABT + RIF: n=4

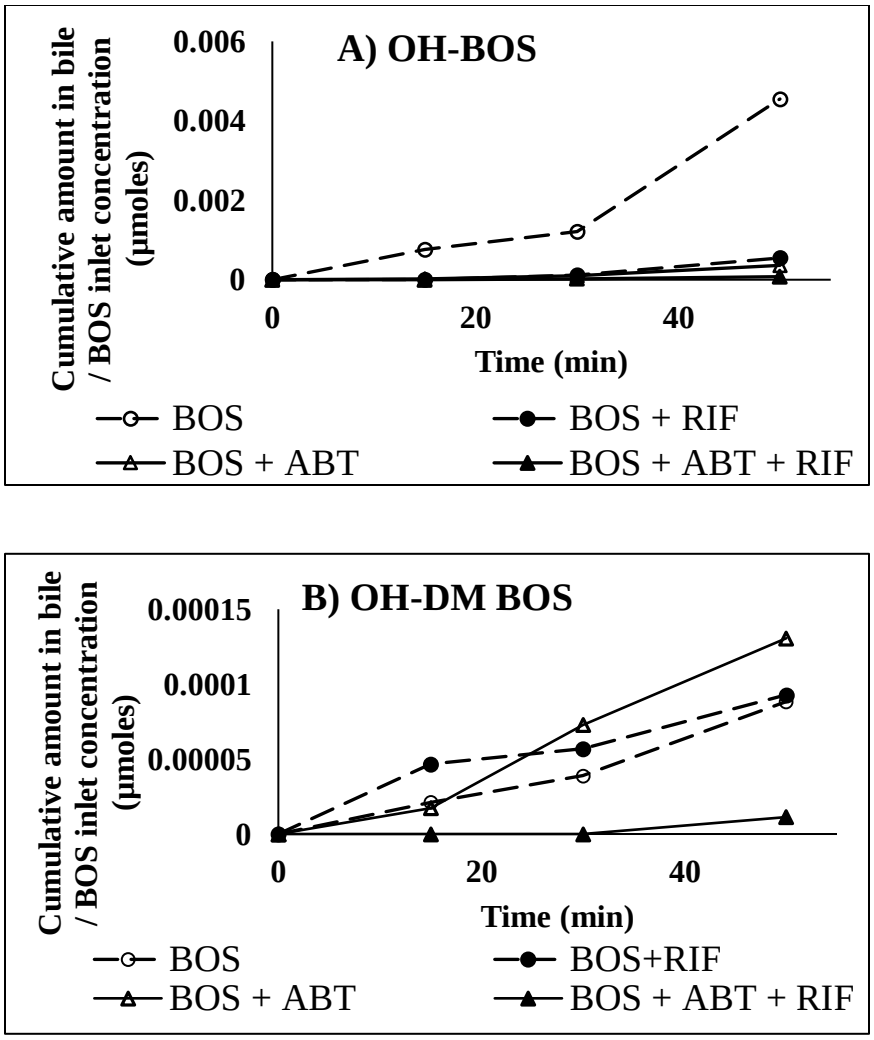

Figure 3.19 BOS metabolite data collected from single-pass liver perfusion studies: Cumulative amount excreted in bile of normalized to BOS inlet concentration for (A) OH-BOS and (B) OH-DM-BOS. One-way analysis of variance was performed; BOS – Bosentan, RIF – Rifampin, ABT – 1-aminobenzotriazole; BOS: n=4, BOS + RIF: n=4, BOS + ABT: n=4, BOS + ABT + RIF: n=4

The cumulative amounts of OH-BOS in bile in various treatment groups are shown in Fig 3.19A. OH-BOS was undetectable in bile in the BOS + ABT + RIF group at 15 min. RIF and ABT treatments, each alone ($p < 0.05$) and in combination ($p < 0.01$) significantly decreased the cumulative amount of OH-BOS excreted in bile at 50 min. No significant difference was observed in cumulative amount of OH-BOS excreted in bile at 50 min in BOS + ABT + RIF and BOS + ABT groups. The percentage of parent drug excreted as OH-BOS in bile at the end of 50 min was 0.45 %, 0.05 %, 0.036 %, and 0.0076 % in BOS only, BOS + RIF, BOS + ABT and BOS + ABT + RIF groups, respectively.

Fig 3.19 B depicts the cumulative amount of OH-DM BOS excreted in bile in various treatment groups. OH-DM-BOS was detectable in bile only at 50 min in the BOS + ABT + RIF group. The mean percentage of parent drug excreted as OH-DM BOS was 0.009 %, 0.0092 %, 0.013 % and 0.0013 % in BOS only, BOS + RIF, BOS + ABT and BOS + ABT + RIF groups, respectively. The difference was not statistically significant except between BOS and BOS + ABT + RIF groups.

3.5 Discussion

3.5.1 Comparison of bile flow across different groups

Bile is a solution made up of bile salts, and other bile acid related materials in water. As chemicals are secreted in to the canaliculi, water is dragged with them by osmosis. Bile flow is comprised of two portions: bile salt dependent bile flow and bile salt independent bile flow (Fouassier et al., 2002). Bile salt dependent bile flow is generated by excretion of bile salts mediated by BSEP. Bile salt independent bile flow is generated by excretion

of bicarbonates, glutathione, bilirubin diglucuronides and other anions mediated by MRP2. Drugs that are MRP2 substrates are also capable of increasing the bile salt independent flow. Strong stimulation of MRP2 activity was observed by substrates of MRP2 in transfected cells (Bakos et al., 2000; Evers et al., 2000). Rifampin was co-transported by both OATP1B1 and OATP1B3 on the basolateral side and MRP2 on the apical side, as demonstrated by experiments using MDCK-II and LLC-PK1 cell lines (Cui et al., 2001; Spears et al., 2005). RIF was shown to inhibit rat Mrp2 mediated 5(6)-carboxy-29,7-dichlorofluorescein (CDCF) and tritiated taurocholic acid ([^{3}H] TCA) uptake in membrane vesicles (Watanabe et al., 2015). BOS is also a MRP2 substrate, as mentioned previously in the introduction. Therefore, increase in bile flow in presence of RIF and/or BOS could be explained by increase in MRP2 mediated bile salt independent bile flow.

3.5.2 Effect of bile flow on ATV outflow perfusate concentrations and liver concentrations

Low bile flow (<3 µL/ min) in certain experiments could be explained by change of perfusion medium from blood to perfusion buffer or effect of drugs used in the experiments. However, if these possibilities were true, it would not have been possible to achieve a close to normal bile flow in any other surgeries. Since an average bile flow of 7.8 µL/min was obtained in control experiments with blank perfusion medium, the above possibilities can be ruled out. Another situation where the bile flow could be lower than expected is when the surgery was flawed or the angle of placing the cannula in the bile duct was incorrect resulting in only a part of the liver being alive. In this case, the lesser

than normal number of alive hepatocytes would produce less amount of bile, hence, reduce the bile flow. This can be further explained by the fact that the liver concentrations in animals with low bile flow are lower than in those with normal flow, since fewer hepatocytes are alive to perform active uptake of ATV (Fig 3.5). It should be noted that even if the number of alive hepatocytes in the low bile flow groups are low, different treatment groups can be compared to observe effects of drug treatments, as long as the bile flow rates are similar. The underlying assumption would be that similar number of hepatocytes is alive in both groups.

3.5.3 Optimization of RIF concentration for uptake and passive diffusion studies

RIF is a potent inhibitor of oatp1b2 and oatp1a4 in rats, which are functionally analogous to OATP1B1 and OATP1B3 in humans. The IC_{50} and Ki values for RIF using ATV as a substrate have been reported as 0.95 ± 0.25 µM and 0.79 ± 0.13 µM respectively for oatp1b2 and 3.04 ± 1.44 µM and 2.88 ± 1.33 µM respectively for oatp1a4 (Lau et al., 2006a). Hence, the uptake of ATV was potently inhibited in a dose dependent manner by 10 and 20 µM RIF, resulting in higher outflow perfusate concentrations in presence of RIF as compared to livers perfused with ATV alone (Fig. 3.6). Inhibition of ATV uptake by RIF also explains the dose dependent decrease in ATV liver concentrations. To test inhibition of uptake with BOS, experiments were conducted with 20 µM RIF.

3.5.4 Passive Diffusion of ATV in the Perfused Liver

Complete inhibition of a specific disposition pathway could be challenging due to several reasons. Overlapping specificity of the inhibitors of metabolizing enzymes and

transporters limits generation of clearer data to study drug disposition by a specific pathway. For example, several oatp substrates are also substrates for the efflux transporter mrp2 (Suzuki and Sugiyama, 2002). Similarly, as previously demonstrated by the data, RIF is a potent competitive inhibitor for the rat uptake oatp transporters and also for cyp3a1/3a2. Moreover, it may not be possible to achieve a high enough concentration of an inhibitor due to solubility limitations thereby making complete inhibition of certain proteins difficult. Involvement of multiple proteins in the same disposition pathway e.g. multiple uptake transporters or metabolizing enzymes which are inhibited by a common perpetrator, makes it difficult to study the contribution of any single pathway.

Estimation of passive diffusion is widely performed at 4°C since the proteins relevant to drug disposition, enzymes, and transporters, are functionally inactive at this temperature (Shigehara et al., 1992; Ismair et al., 2001; Shimada et al., 2003; Lancon et al., 2004). The aforementioned issues of inability to achieve complete inhibition of transporters and enzymes, and lack of specific inhibitors, could be addressed by passive diffusion studies at 4°C. Literature reports suggest that the cell membranes undergo temperature related changes (Quinn, 1988; Kandušer et al., 2008). In plants, changes in lipid composition have been observed with changes in growth temperature. These changes are manifested as alterations in chain length of lipids, the position of acylation of the fatty acid chains and change in degree of unsaturation. While these changes are of significance for the adaptability of plants, temperature exposures beyond the normal range can result in stunted plant growth due to irreversible phase separation of membrane constituents and subsequent loss of transport and permeability processes (Quinn, 1988).

As temperature decreases, the membrane fluidity decreases as observed in experiments on V-79 (Chinese hamster lung fibroblasts) and B16F-1 (murine melanoma) cell lines (Kandušer et al., 2008). Electro-permeabilization of stratum corneum was affected by changes in temperature influencing membrane fluidity (Gallo et al., 2002).

Difference in membrane fluidity at 37°C versus 4°C can significantly affect the estimates for passive diffusion obtained at 4°C. In fact, there was minimal drug partitioning into the liver at 4°C (Fig. 3.8 B). Therefore, estimation of passive diffusion for liver perfusion studies at 37°C with concomitant use of inhibitors of enzymes and transporters is a better approach than the use of 4°C data. The +KETO + RIF group demonstrated outflow concentrations lower than the +ABT + RIF group. One of the possible explanations for this is that KETO is somehow assisting the uptake of ATV, perhaps by another transporter that is not inhibited by RIF. ATV and/or RIF, being stronger uptake substrates, could also be inhibiting the entry of KETO into the liver. The molecular weight of KETO is 531.43, while that of ABT is 134.14. From the size of KETO, it is possible that this compound may require some assistance in crossing the membrane. As mentioned previously, KETO is known to inhibit olmesartan uptake. Since KETO is capable of interfering with transport processes, the data from +KETO + RIF were not used in modeling the passive permeability of ATV.

3.5.5 Uptake and Metabolism of ATV in the Perfused Liver

The liver perfusion experiments demonstrated that inhibition of hepatic uptake of ATV increased the outflow perfusate concentrations, and decreased the liver concentrations

and amount of parent drug eliminated in the bile (Fig. 3.9-3.11). Conversely, inhibition of metabolism by ABT had little effect on the outflow perfusate concentrations, but it increased the liver concentration of ATV in the +ABT group. This finding is in agreement with the previous reports in which inhibition of OATP had a profound effect on the plasma concentration of OATP substrates, whereas inhibition of metabolism had a lesser impact on increasing the plasma concentration of the drug (Kantola et al., 1998; Maeda et al., 2011; Chang et al., 2014). This is because uptake is the rate determining step in the elimination of ATV from liver (Watanabe et al., 2009a). These results further highlight the importance of determining the effect of transporter enzyme interplay on intracellular unbound concentrations, since inhibition of metabolism of an uptake limited drug may not result in increased parent plasma concentrations.

As mentioned previously in the +KETO + RIF group, it is possible that KETO is assisting the entry of ATV in the liver by interference with some transport processes. This is further supported by the outflow concentration data from the +KETO group, since the mean concentrations in the +KETO groups were lower than the ATV group for most time points. Also, ABT appears to inhibit ATV metabolism more efficiently than KETO based on the metabolite-to-parent ratios in the liver (Fig 3.14). KETO was tested as an inhibitor of metabolism because ABT could cause changes in bile flow due to interference in bile salt metabolism. However, it can be seen from Table 3.1 that the bile flow in +KETO and +ABT groups is not different.

The decrease in liver concentrations of ATV in the presence of RIF was not significant. Moreover, the decrease in formation of metabolites in the RIF-treated group (2.9-fold for

2-OH ATV and 3.62-fold for 4-OH ATV) was greater than the decrease in the parent liver concentrations (1.24-fold) as illustrated by the metabolite to parent ratios (Fig. 3.14). Single pass perfusions of 20 µM RIF for 50 min could result in very high intracellular RIF concentrations. This concentration could be sufficient for competitively inhibiting cyp3a1-mediated metabolism of any other substrate. This is in agreement with literature reports that RIF inhibits ATV metabolism (Lau et al., 2006a). Rifampin inhibited the formation of both 2- and 4- OH metabolites of ATV in a concentration dependent manner. The formation of 2-OH ATV was decreased by approximately 8% of control while that of 4-OHATV was not affected by 25 µM rifampin. Because of the confounding effect of RIF on ATV metabolism, it was not possible to model the data from +RIF studies.

The decreased cumulative amount of drug excreted in the bile upon RIF treatment could be explained by inhibition of uptake into the cell and decreased intracellular accumulation.

Pretreatment with ABT and KETO did not completely inhibit ATV metabolism; however, there was a significant decrease in the liver concentration of 2-OH ATV at the end of the 50-minute perfusion compared with the ATV group (Fig. 3.12A). The liver concentration of 4-OH ATV was not significantly different than the ATV group except for the +KETO + RIF group ($P < 0.05$; Fig. 3.12B). The metabolite to-parent ratio in the liver decreased significantly with ABT treatment, indicating inhibition of metabolism (Fig. 3.14). Similarly, the cumulative amounts of metabolites excreted in bile were considerably lower after ABT and KETO treatment (Fig. 3.13, A and B).

Inhibition of metabolism, however, significantly increased the liver/bile ratio of ATV. A similar fold increase was observed in the RIF-treated group, presumably owing to inhibition of metabolism. The increase in ATV liver to-bile ratio upon inhibition of metabolism could be a result of saturation of efflux transport resulting from elevated intracellular ATV concentrations. Although this increase in the ATV liver-to-bile ratio is consistently observed in the +ABT group (where the liver concentrations are higher than ATV group), an increase is also observed in the +ABT + RIF or +RIF groups (where the liver concentrations are lower than the ATV group). Inhibition of apical efflux by ATV cannot by itself explain these results. This phenomenon appears to be associated with inhibition of metabolism instead of apical efflux transport saturation by ATV. Another possibility is that the concentration of an endogenous efflux transporter substrate is increased by P450 inhibition. It is possible that the apical efflux transport of ATV is inhibited by the endogenous substrate. Since P-gp has been reported to have multiple binding sites (Ruth et al., 2001; Mayer et al., 2002; Ledwitch et al., 2016), cooperative binding of endogenous substrates or metabolites could be involved.

3.5.6 Passive Diffusion, Uptake and Metabolism Studies for BOS in Perfused Liver

As illustrated in Fig 3.15, BOS outflow perfusate concentrations increased and amount of parent drug excreted in bile decreased upon inhibition of active uptake of the drug by RIF. Surprisingly, the mean total liver concentrations of BOS did not change significantly in presence of RIF. (Fig. 3.16). The mean liver concentrations for both OH-BOS and OH-DM BOS were not significantly different in the RIF treated and untreated groups. Therefore, inhibition of cyp3a mediated metabolism resulting in elevated parent liver

concentrations seems unlikely. RIF and BOS are both substrates for mrp2. The increased liver concentrations in presence of RIF could be explained by competitive inhibition of mrp2 mediated BOS efflux by RIF. Similar to ATV, RIF could also be inhibiting the cyp3a1 mediated metabolism of BOS, thus increasing the BOS liver concentrations. However, this possibility seems less likely than the efflux inhibition by RIF. This is because BOS is also a substrate for other metabolizing enzymes like cyp2c9 and ugt1a1. Therefore, inhibition of one pathway can divert the disposition of a drug to other pathways. Further studies with dual inhibition of cyp2c9 along with cyp3a1 are required to achieve complete inhibition of metabolism and test the aforementioned possibilities. The significant decrease in the amount of BOS and OH-BOS recovered in the bile could be attributed to decreased intracellular concentrations resulting from inhibition of active uptake.

Inhibition of cyp3a mediated metabolism by ABT did not significantly increase the BOS outflow perfusate concentrations (Fig. 3.15), nor were the liver concentrations (Fig 3.16) affected. There was a significant increase in the amount of BOS recovered in bile (Fig. 3.17), which could be attributed to increased intracellular concentrations owing to inhibition of CYP mediated metabolism. Furthermore, the amount of OH-BOS recovered in bile upon ABT treatment was significantly lower (Fig 3.19). The liver concentrations for OH-BOS were, however, not significantly lower. BOS is metabolized by CYP3A4, CYP2C9 and UGT1A1 in humans. Same metabolites for the CYP mediated metabolism as those observed in humans were also observed in rats (Treiber et al., 2004). If similar enzymes are responsible for metabolism of BOS in rats, it is possible that ABT treatment

may not be completely inhibiting BOS metabolism. It has been reported that ABT does not effectively inhibit CYP2C9 (Linder et al., 2009). A 30 min preincubation of HLM with 1 mM ABT could inhibit only 40 % activity of CYP2C9. Therefore, inhibition of one pathway could be shunting the metabolism to another pathway in case of BOS. OH-BOS is formed by both CYP3A4 and CYP2C9. Inhibition of cyp3a1, therefore, may not inhibit formation of OH-BOS completely. The lower amount of OH-BOS recovered in the bile as compared to the BOS only group could be result of either inhibition of formation of OH-BOS by ABT or inhibition of apical efflux of OH-BOS by ABT. A decreasing trend is observed in the liver concentrations of OH-DM BOS from BOS only to BOS + ABT to BOS + ABT + RIF which could be attributed to inhibition of cyp3a1. Insignificant difference in the liver concentrations and amount recovered in bile of OH-DM BOS can be explained by the formation of this metabolite partly by cyp3a1 and partly by cyp2c9. It is also possible that inhibition of cyp3a mediated pathway could be diverting the metabolism of BOS to a ugt mediated pathway.

3.6 Conclusion

Liver perfusion studies were performed with ATV and BOS to study the effect of passive diffusion, active uptake and metabolism on liver-mediated disposition of these drugs. Bile flow can be affected due to transporter mediated apical efflux of some drugs like RIF and BOS. Passive diffusion studies conducted at 4°C suggested that the drug partitioning into tissues at this temperature may be affected by temperature mediated changes in membrane fluidity. However, to perform these studies at 37°C with concomitant inhibition of metabolism and transport, the availability of cleaner and highly

potent inhibitors is crucial. Thus, the limitations of passive diffusion determination by either method should be considered during data interpretation. Active uptake appeared to be the major contributor in ATV disposition as compared to metabolism. Inability of RIF to decrease liver concentrations could be related to the inhibition of apical efflux of BOS by this drug. In summary, liver perfusion is a good experimental tool to study liver disposition of drugs and has been successfully used in this project to study disposition of ATV and BOS.

CHAPTER 4: MODELING THE LIVER PERFUSION DATA TO PREDICT UNBOUND INTRACELLULAR CONCENTRATIONS USING THE 5-COMPARTMENT EXPLICIT MEMBRANE MODEL

4.1 Introduction

Pharmacokinetic modeling is the process of representing the body, organ or experimental system of interest (e.g. hepatocytes) by one or more compartments and deriving mathematical expressions to describe the processes of interaction between those compartments. A mathematical model describes the processes that are thought to be involved in the course of data generation. The simplest way to describe a cellular system involved in drug disposition is a 3 compartment (3-C) model, as described in Fig 4.1.

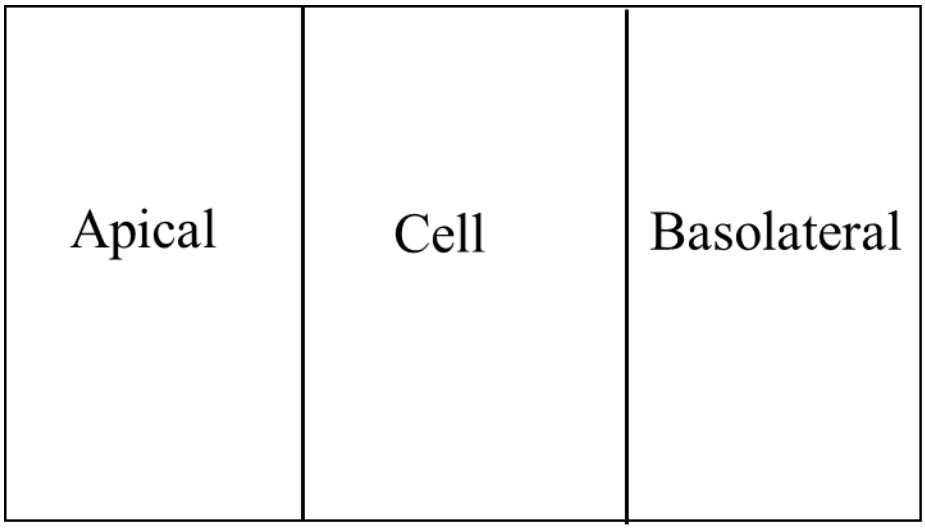

Figure 4.1 A 3-compartment model consisting of apical, cell and basolateral compartments

The 3 compartments in this model consist of apical compartment, basolateral compartment and cellular compartment. The intracellular disposition of a drug can be described by a 3-C model. There are several reports in the literature describing the effect of active uptake, metabolism and apical efflux on the disposition of drugs from in vitro systems. For example, Ménochet et al. utilized a mechanistic modeling approach for simultaneous assessment of metabolism, active uptake and passive diffusion of 7 drugs (Ménochet et al., 2012). A 3-C model as described in fig 4.1 was used to study the permeability, transport and metabolism of a set of drugs in Caco-2 cells (Sun and Pang, 2008). A structural model to study kinetics of P-gp transport in Caco-2 cell monolayers has been described (Bentz and Ellens, 2014).

The mechanistic modeling approaches reported in the literature do not consider the membrane partitioning of drugs, since explicit membrane compartments are absent in these models. Membrane partitioning could be of importance for compounds with low permeability. Experimental lag times have been reported during permeability experiments for both high and low permeability compounds (Knipp et al., 1997; Korzekwa et al., 2012).The 3-C model failed to accurately predict the experimental lag times. For high permeability compounds like verapamil, the 3-C model predicted a very short lag time due to rapid equilibration among compartments. This predicted lag time was inconsistent with the experimentally observed much larger lag time. For low permeability compounds like labetalol, significant lag time was experimentally observed, and also predicted by the 3-C model, in MDCK experiments when apical efflux was absent. However, no lag time was predicted in MDR1-MDCK experiments when apical efflux was present, even

though lag was observed experimentally. This is because the apical efflux in the 3-C model was modeled from the cell compartment due to absence of membranes. The apical efflux from the cell compartment allowed equilibrium to be reached rapidly in the simulations, resulting in disappearance of lag in the receiver compartment. The 5-compartment (5-C) model consisted of explicit membrane compartments (Fig 4.2).

The 5-C explicit membrane model could incorporate membrane partitioning and therefore, could accurately predict the experimentally observed lag times (Korzekwa et al., 2012). Moreover, apical efflux for P-gp substrates could be modeled from the apical membrane instead of cell compartment. It has been reported that substrate binding site of P-gp is located in the apical membrane (Gottesman et al., 1995; Gottesman et al., 1996; Hennessy and Spiers, 2007). Hence, membrane concentrations, and not the cell concentrations, would serve as the driving concentrations for apical efflux of P-gp substrates.

The goal of this chapter was:

a) To determine membrane partitioning and plasma protein binding of ATV and BOS using equilibrium dialysis

b) To model the data obtained in chapter 3 using the 5-C explicit membrane model along with the membrane partitioning parameter obtained in this chapter, and predict intracellular unbound concentrations of ATV and BOS

c) To study the effect of inhibition of metabolism versus inhibition of transport on the intracellular unbound concentrations of ATV and BOS

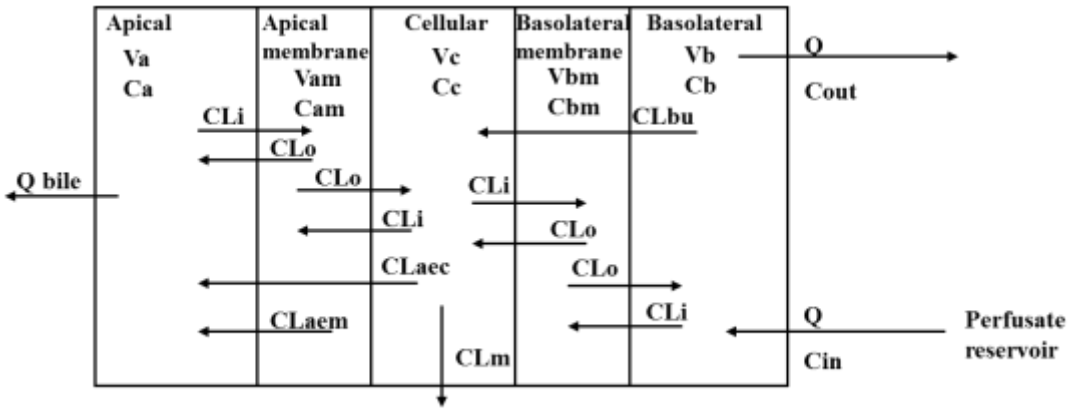

Figure 4.2 A 5-C model with explicit membrane compartments for rat liver. V_A, V_B, V_C, V_{AM}, V_{BM}: volumes of apical, basolateral, cellular, apical membrane and basolateral membrane compartments, respectively; C_A, C_B, C_C, C_{AM}, C_{BM}: concentration in apical, basolateral, cellular, apical membrane, and basolateral membrane compartments, respectively; CL_i, CL_o: diffusional clearance into and out of the membrane respectively; CL_{bu}, active basolateral uptake clearance into the cell; CL_{aem}, apical efflux clearance from the apical membrane into the apical compartment; CL_{aec}, apical efflux clearance from the cell into the apical compartment; Q, perfusion flow rate; Q_{bile}, biliary flow rate; C_{in}, inlet concentration; C_{out}, outlet concentration.

4.2 Methods

4.2.1 Equilibrium dialysis

Unbound fractions of ATV and BOS were determined in rat plasma (f_{up}) and rat liver microsomes (RLM) (f_{um}). Equilibrium dialysis was performed using a 96-well equilibrium dialyzer with MW cutoff of 5K and placed in dual-plate rotator set to maximum speed (25 rpm) located in a 37 °C incubator with a 10% CO_2 atmospheric environment. Dialysis Buffer consisted of 0.1 M phosphate buffer containing 3mM MgCl2, pH =7.4. Frozen male Sprague Dawley rat plasma was thawed and the pH was adjusted to 7.4 using a pH meter and 1 N HCl. Plasma (495µL) was spiked with 5 µL of 200 µM ATV or BOS stock solution to give 2 µM in pH-adjusted plasma. Plasma samples (200 µL) and buffer were added to the respective sides of the 96-well dialysis plate and wells were capped. The plate was then placed in the rotator and incubator and allowed to dialyze for 22 h. Following 22 hours of dialysis, 100 µL of buffer and plasma were removed from each side of dialysis plate and mixed with 100 µL of the opposite matrix in a 96-deep well plate. Samples were then stored at -80 °C for future analyte quantitation. Plasma was replaced with 1mg/ml RLM and liver homogenate diluted 1:2 in water. To determine the fum, 495 µL RLM suspension in 1 mM potassium phosphate buffer (1mg/mL) was spiked with 5 µL of 200 µM ATV or BOS stock solution to give 2 µM. Further procedure was similar as that described above to determine f_{up}.

4.2.2 Modeling

The data obtained from the liver perfusion experiments were modeled using the 5-C model depicted in Fig. 4.2 to predict the intracellular unbound concentration of ATV and BOS. This model has been described previously for cell-based systems (Korzekwa et al., 2012). In the present study, perfusate and bile flow rates were included from the experiment, and clearance pathways were modeled. Wolfram Mathematica (version 10.1) was used for modeling. The five compartments in Fig. 4.2 represent a rat liver. The basolateral compartment represents the blood compartment, and the apical compartment represents the biliary compartment within the liver. Hepatocytes have been further divided into apical membrane, basolateral membrane, and cytosolic compartments.

The following assumptions were made for the 5-C explicit membrane model:

1) The volume of membranes was assumed to be 10% of the total cell volume, with the apical and basolateral membranes each comprising 5% (Korzekwa and Nagar, 2014).

2) Of the total liver volume, 10.6% was assumed to be the sinusoidal volume (Blouin et al., 1977).

3) The volume of hepatocytes in liver was calculated by using a rat liver hepatocellularity of 120 million cells per gram of liver (Sohlenius-Sternbeck, 2006) and a volume of 3.9 µL for one million hepatocytes (Reinoso et al., 2001)

4) Volume of the intrahepatic biliary tree was set to 50 µl (Blouin et al., 1977; Masyuk et al., 2001).

5) Apical efflux was assumed to occur from the apical membrane only (e.g., P-gp) for ATV, and from both the apical membrane (e.g., P-gp) and cell (e.g., MRP2) for BOS.

6) Intracellular unbound concentrations were assumed to drive the metabolic clearance of both ATV and BOS.

7) Back diffusion from the bile into the liver was assumed to be minimal.

The interaction between various compartments within the model can be described by equations 4.1 to 4.5.

$$\frac{dC_B}{dt} = \frac{QC_{in} + CL_o C_{BM} - CL_i C_B - CL_{bu} C_B - QC_B}{V_B} \quad (4.1)$$

$$\frac{dC_{BM}}{dt} = \frac{CL_i C_C + CL_i C_B - 2CL_o C_{BM}}{V_{BM}} \quad (4.2)$$

$$\frac{dC_C}{dt} = \frac{CL_{bu} C_B + CL_o C_{BM} + CL_o C_{AM} - 2CL_i C_C - CL_m C_C - CL_{aec} C_C}{V_C} \quad (4.3)$$

$$\frac{dC_{AM}}{dt} = \frac{CL_i C_C - 2CL_o C_{AM} - CL_{aem} C_{AM} + CL_i C_A}{V_{AM}} \quad (4.4)$$

$$\frac{d C_A}{dt} = \frac{-Q_{bile} C_A + CL_{aem} C_{AM} + CL_{aec} C_C + CL_o C_{AM} - a CL_i C_A}{V_A} \quad (4.5)$$

Where, V_A, V_B, V_C, V_{AM}, V_{BM}: volumes of apical, basolateral, cellular, apical membrane and basolateral membrane compartments, respectively; C_A, C_B, C_C, C_{AM}, C_{BM}: concentration in apical, basolateral, cellular, apical membrane, and basolateral membrane compartments, respectively; CL_i, CL_o: diffusional clearance into and out of the membrane respectively; CL_{bu}, active basolateral uptake clearance into the cell; CL_{aem}, apical efflux clearance from the apical membrane into the apical compartment; CL_{aec}, apical efflux clearance from the cell into the apical compartment; Q, perfusion flow rate; Q_{bile}, biliary flow rate; C_{in}, inlet concentration; C_{out}, outlet concentration; a, fraction of diffusional clearance from the bile into the apical membrane.

The ratio of CLi and CLo, defined as the Kp of the drug into the membrane, is given by equation 4.6.

$$\frac{CL_i}{CL_o} = \frac{V_A(1-fu_m)}{V_m fu_m} \qquad (4.6)$$

In the above equation, f_{um}, V_A, and V_m represent the unbound fraction in the membrane, volume of the partitioning incubation, and volume of the membrane, respectively. In 1 ml of microsomal solution with 1 mg/ml microsomal protein concentration, the volume of lipids is assumed to be 0.7 µL (Nagar et al., 2014). Therefore, the ratio of V_m to V_A was set to 0.0007. Since V_m was obtained from the amount of microsomes used in the equilibrium dialysis experiment, and the membrane volume was defined as 10% of cell volume in the model, f_{um} used in this exercise was not corrected for dilution during the modeling procedure.

This model allowed us to simulate perfusate, membrane, unbound intracellular, and biliary concentrations.

a) ATV modeling:

For modeling the ATV liver perfusion data, an initial estimate for the apical efflux clearance from the membrane (CL_{aem}) back diffusion from the bile were iteratively optimized with the +ABT + RIF data set to obtain the observed amount of parent drug recovered in bile. CL_{aem} was then scaled based on hepatocellularity for subsequent modeling. The fraction of CL_i from bile to apical membrane (back diffusion) was set to 0.03. CL_{aec} was set to zero since apical efflux was assumed to occur only from the apical

membrane. Initial estimates for metabolic clearance (CL_m), diffusional influx clearance into the membrane (CL_i), and active basolateral uptake clearance (CL_{bu}) were obtained from the literature and scaled up to the organ level for ATV (Lau et al., 2006a; Watanabe et al., 2009a; Korzekwa et al., 2012). Table 4.1 summarizes the experimental values and initial estimates of model parameters for ATV studies.

Table 4.1 Initial estimates for model parameters for ATV studies.

Parameter	**Symbol**	**Units (per liver)**	**Value**
Volume of bile (apical compartment) (Masyuk et al., 2001)	V_A	mL	0.05
Volume of intrahepatic vasculature (basolateral compartment) (Blouin et al., 1977)	V_B	mL	0.8
Volume of hepatocytes (Sohlenius-Sternbeck, 2006)	V_C	mL	5[a] 4.7[b] 4.1[c]
Volume of apical membrane	V_{AM}	mL	0.05 x 5[a] 0.05 x 4.7[b] 0.05 x 4.1[c]
Volume of basolateral membrane	V_{BM}	mL	0.05 x 5[a] 0.05 x 4.7[b] 0.05 x 4.1[c]
Diffusional clearance into the membrane (Korzekwa et al., 2012)	CL_i	mL/min	2.5
Active uptake clearance (Lau et al., 2006a)	CL_{bu}	mL/min	8
Metabolic clearance (Watanabe et al., 2009a)	CL_m	mL/min	12.15
Apical efflux clearance from the apical membrane	CL_{aem}	mL/min	88[a] 82[b] 70[c]
Perfusion flow rate[d]	Q	mL/min	20
Fraction unbound in RLM	f_{um}		0.84[d]
Fraction of CLi from bile to apical membrane (Back diffusion)	a		0.03

[a]ATV + ABT + RIF, [b]ATV + ABT, [c]ATV. [d]Experimental values.

The modeling exercise was started with the use of the +ABT + RIF dataset for CL_i estimation. Initially, for CL_i estimation, CL_m and CL_{bu} were set to 0 and CL_{aem} was iteratively optimized. However, the model over predicted the outflow perfusate concentrations. Therefore, CL_{bu} was set to 0.26 L/min, CL_m was set to 0 and CL_i was estimated. In order to study effect of passive diffusion alone on ATV unbound and tissue concentrations, simulations were performed with the previously estimated CL_i and CL_{bu} = 0. Upon obtaining model-fitted estimates for CL_i, CL_{bu} was parameterized next using average outflow perfusate concentration data obtained from the +ABT experiments with CL_m set to 0. Average outflow perfusate concentration data from experiments with ATV alone were then used to parameterize CL_m using the previously optimized values of CL_i and CL_{bu}. Finally, intracellular ATV concentrations were predicted using all the optimized clearance values.

b) BOS modeling:

BOS + ABT and BOS + ABT + RIF experimental data for parent and metabolite liver concentrations and amounts excreted in bile could have multiple possible explanations as discussed in chapter 3. It is difficult to model such data unless more mechanistic information about the interaction is available. Therefore, ABT treated experimental data were not used for modeling.

Modeling the BOS liver perfusion data was started with BOS + RIF dataset to estimate CL_i. Here, CL_{bu} was set to 0 since RIF inhibits BOS uptake. Initial estimates of apical efflux from the membrane (CL_{aem}), apical efflux from the cell (CL_{aec}) and metabolic

clearance (CL_m), and back diffusion from the bile were iteratively optimized with the BOS + RIF dataset to obtain the experimentally observed BOS liver concentrations and amount of BOS recovered in the bile.

Since there were multiple iteratively fixed parameters for BOS, it was important to verify whether there could be multiple solutions to the model. In other words, it was important to confirm whether there were other combinations of the fixed parameters that also resulted in similar predicted BOS liver concentration and amount of BOS recovered in bile. Therefore, CL_m was varied from 0.0072 to 0.144 L/min with CL_{aec}, CL_{aem} and the fraction of diffusional clearance from the bile into the apical membrane (a) set to 49.9 L/min, 0.00045 L/min and 0.2, respectively. Later, CL_{aec} was varied from 8.3 to 200 L/min. CL_{aem} was varied from 0 to 0.0045 L/min. The fraction of diffusional clearance back from the bile into the apical membrane (a) was varied from 0.05 to 1.
Next, CL_m and "a" were fixed to 0.028 L/min and 0.2, respectively for modeling the data from BOS only perfusions. CL_i, CL_{aec} and CL_{aem} were iteratively optimized to parameterize CL_{bu} and predict liver concentrations and amount of BOS recovered the bile.

Initial estimates for diffusional influx clearance into the membrane (CL_i), and active basolateral uptake clearance (CL_{bu}) were obtained from the literature and scaled up to the organ level (Yabe et al., 2011). Table 4.2 summarizes the experimental values and initial estimates of model parameters for BOS studies.

Table 4.2 Initial estimates for model parameters for BOS studies

Parameter	**Symbol**	**Units (per liver)**	**Value**
Volume of bile (apical compartment) (Masyuk et al., 2001)	V_A	mL	0.05
Volume of intrahepatic vasculature (basolateral compartment) (Blouin et al., 1977)	V_B	mL	0.833
Volume of hepatocytes (Sohlenius-Sternbeck, 2006)	V_C	mL	5.85[a] 4.61[b]
Volume of apical membrane	V_{AM}	mL	0.05 x 5.85[a] 0.05 x 4.61[b]
Volume of basolateral membrane	V_{BM}	mL	0.05 x 5.85[a] 0.05 x 4.61[b]
Diffusional clearance into the membrane (Yabe et al., 2011)	CL_i	mL/min	13.12[a] 9.74[b]
Active uptake clearance (Yabe et al., 2011)	CL_{bu}	mL/min	28[a] 20.8[b]
Metabolic clearance	CL_m	mL/min	7.2 to 144
Apical efflux clearance from the apical membrane	CL_{aem}	mL/min	0 to 4.5
Apical efflux clearance from the cell	CL_{aec}	L/min	8.3 to 200
Perfusion flow rate[c]	Q	mL/min	20
Fraction unbound in RLM	f_{um}		0.5943
Fraction of CLi from bile to apical membrane (Back diffusion)	a		0.05 to 1

[a]BOS, [b]BOS + RIF, [c]Experimental values.

The "NonlinearModelFit" function in Mathematica was used with 1/Y weighting to parameterize various clearances. To get numeric solutions of the ordinary differential equations, the NDSolve function was used with MaxSteps → 100,000, and PrecisionGoal → Infinity. To check the robustness of the optimizations, the initial estimates were varied 10-fold from the final parameter estimates.

4.3 Results

4.3.1 Equilibrium dialysis

The unbound fraction for ATV in plasma was determined as 0.08 ± 0.0032 using equilibrium dialysis under 10% CO2. The unbound fraction in 1 mg/mL RLM was determined to be 0.84 ± 0.074. Similarly, the fup and fum determined for BOS were 0.01086 ± 0.003 and 0.5943 ± 0.066, respectively.

4.3.2 ATV modeling

The parameter estimates for various clearances are summarized in table 4.3. Model predicted tissue concentrations and amounts recovered in bile as compared to the experimental values are summarized in tables 4.4 and 4.5, respectively. Table 4.6 summarizes the model predicted unbound cell concentrations at 50 min and steady state.

Table 4.3 Parameter estimates for CL_i, CL_{bu}, CL_m and CL_{aem} represented as estimate ± standard error

Parameter	Value (L/min)
CL_i	0.135 ± 0.029
CL_{bu}	20.04 ± 4.8
CL_m	0.00125*
CL_{aem}	0.08**

*Obtained from simulations in ATV only group
**Iteratively optimized from the +ABT + RIF dataset and scaled based on hepatocellularity for subsequent groups

Table 4.4 Observed and predicted ATV tissue concentrations (µM) at 50 min and steady state

Group	**Observed**	**Predicted, at 50 min**	**Predicted, at steady state**
ATV	109	119	160
ATV + ABT	146.5	151	366
ATV + ABT + RIF	56.8	70	78.99* (25.6**)

*Simulated with residual 0.26 Liter/ min active uptake clearance
**Simulated without residual 0.26 Liter/ min active uptake clearance

Table 4.5 Observed and predicted ATV amount recovered in bile at 50 min

Group	**Observed (µmoles)**	**Predicted, at 50 min (µmoles)**
ATV	0.287	0.229
ATV + ABT	0.266	0.211
ATV + ABT + RIF	0.107	0.153* (0.056**)

*Simulated with residual 0.26 Liter/ min active uptake clearance
**Simulated without residual 0.26 Liter/ min active uptake clearance

Table 4.6 Model predicted ATV unbound cell concentrations at 50 min and at steady state

Group	**At 50 min (µM)**	**At steady state (µM)**
ATV	5.69	7.56
ATV + ABT	7.17	17.25
ATV + ABT + RIF	3.11* (0.9**)	3.49* (0.91**)

*Simulated with residual 0.26 Liter/ min active uptake clearance
**Simulated without residual 0.26 Liter/ min active uptake clearance

The average outflow perfusate concentrations from 4°C perfusions were used to calculate the passive diffusion of ATV; however, since the average steady-state concentrations were greater than the inlet concentration (1 µM) (Chapter 3, section 3.4.4, Fig 3.8), CL_i could not be estimated. Therefore, subsequent CL_i estimation was performed using the data from +ABT + RIF experiments. The results from the modeling exercise for ATV are summarized in Fig. 4.3

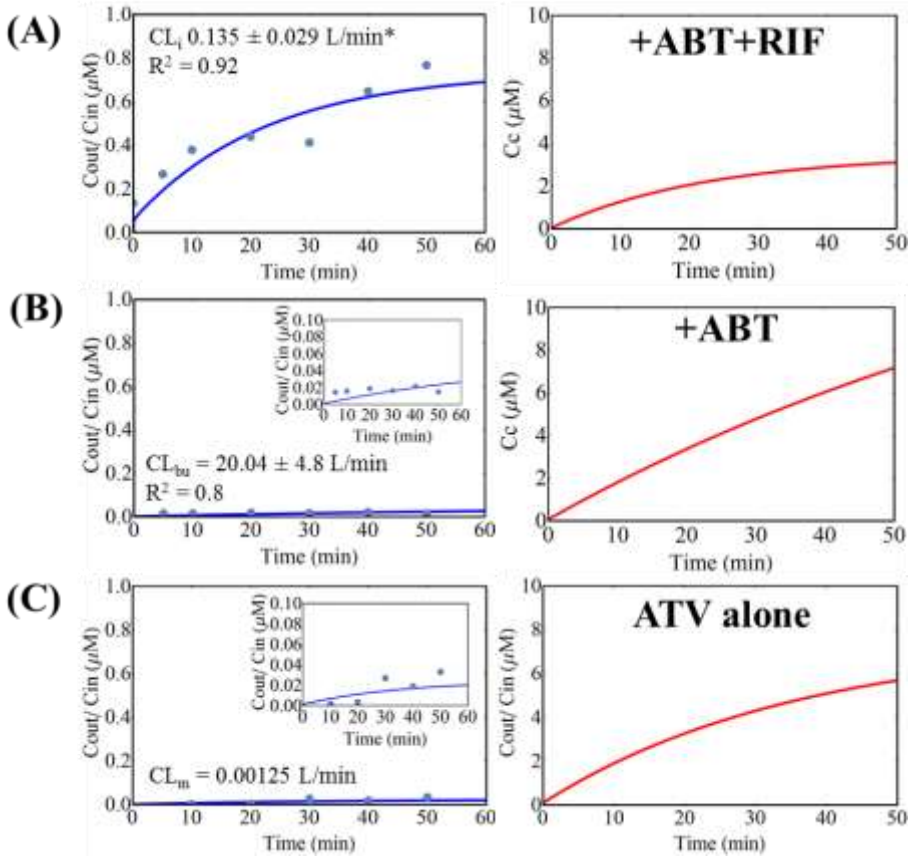

Figure 4.3 Modeling ATV liver perfusion data with the 5-C explicit membrane model. Model fitted outflow perfusate-concentration time profiles (blue) and simulated unbound intracellular concentration-time profiles (red) for (A) ATV + ABT + RIF group and (B) ATV + ABT group. Inset shows data on magnified scale. Model-fitted parameter ± standard error values are listed, along with the R^2 of the fit. (C) Simulated outflow perfusate concentration-time profile (blue) and cell concentration-time profile (red) for ATV group. Inset shows fitted outflow perfusate concentration-time profile. The CL_m value was obtained from the simulation as detailed in Results. Mean experimental data are depicted as solid circles, and model fitted or simulated results are depicted as solid lines. *Residual CL_{bu} of 0.26 L/min was used to parameterize CL_i

In the estimation of CL_i, an over prediction of the outflow perfusate concentrations was observed when both CL_m and CL_{bu} were set to 0. An improvement in the fitting for predicted outflow concentrations was observed when a residual intrinsic uptake clearance (CL_{bu}) of 0.26 L/min was included (R^2 = 0.922, Fig 4.3 A). A CL_i estimate of 0.135 ± 0.029 L/min was obtained. The predicted total liver concentration of 70 µM at the end of 50 minutes was obtained using this CL_i estimate and the residual uptake clearance of 0.26 liter/ min (Table 4.4), and the predicted steady-state liver concentration was 79 µM. Similarly, the predicted drug amount recovered in bile was 0.153 µmol. These predictions compared well with the observed values. The predicted unbound intracellular concentration at the end of 50 minutes was 3.11 µM (Fig. 4.3 A). Next, the 5-C model was fit to the +ABT C_{out} data (Fig. 4.3 B), with the CL_i fixed from the previous step, and a CL_{bu} of 20.02 ± 4.8 liters/min was estimated. The predicted total liver concentration obtained using the estimated CL_i and CL_{bu} values was 151 µM, compared with the mean observed value of 146.5 µM. The predicted total amount of drug recovered in bile was 0.211 µmoles. The predicted unbound intracellular ATV concentration in this group was 7.17 µM at the end of the 50-minute perfusion (Fig. 4.3 B). With the previously obtained estimates for CL_i and CL_{bu}, a CL_m value of 0.00125 L/min was able to predict the liver concentrations and amount of drug recovered in the bile in the ATV only group (Fig. 4.3 C). The simulation predicted a total liver concentration and the amount of drug recovered in bile of 119 µM and 0.229 µmoles, respectively, comparing well with the experimental mean values of 109 µM and 0.287 µmoles, respectively. The predicted unbound intracellular concentration at the end of 50 minutes was 5.69 µM (Table 4.4).

Fig 4.4 summarizes the results for simulations with CL_i = 0.135 L/min without any residual active uptake. This exercise is helpful to study the theoretical effect of passive diffusion alone on intracellular unbound and tissue concentrations of ATV.

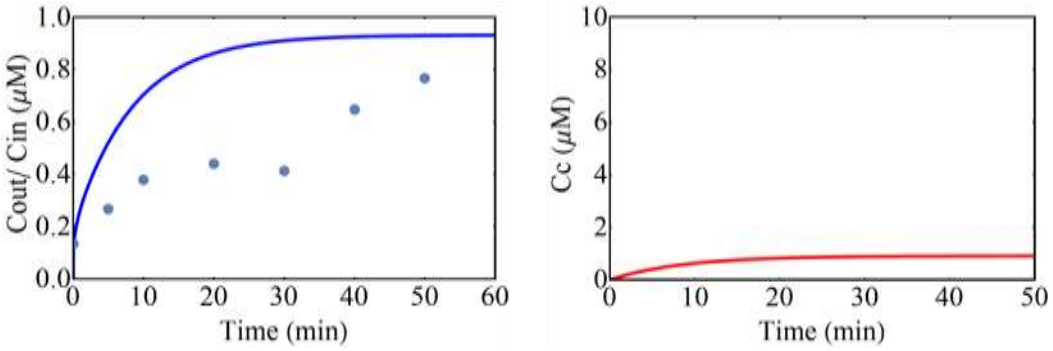

Figure 4.4 Simulated outflow perfusate concentration-time profile (blue) and cell concentration-time profile (red) with CL_i = 0.135 L/min and CL_{bu} = 0. Solid circles represent the data for ATV + ABT + RIF group.

When no residual active uptake was present, an over prediction of the outflow perfusate concentrations was observed as mentioned previously (Fig 4.4). The predicted tissue concentrations and amount recovered in bile were 25.6 µM and 0.056 µmoles, respectively (Table 4.4). These predictions were inconsistent with the observed liver concentrations (72 µM) and amount recovered in bile (0.107 µmoles). The predictions improved when a residual uptake clearance of 0.26 L/min was added. With the residual active uptake clearance, the predicted liver concentrations were 78.99 µM and the predicted amount recovered in bile was 0.153 µmoles. The simulations revealed that in the absence of residual active uptake clearance and with only diffusional clearance of 0.135 L/min, the predicted unbound cell concentrations at the end of 50 min and at steady

state were 0.909 µM and 0.911 µM, respectively. The predicted outflow perfusate concentrations at the end of 50 min and at steady state were 0.93 µM and 0.932 µM, respectively (Fig 4.4). Hence, the Kp_{uu} at 50 min and steady state were 0.97742 and 0.97746, respectively.

4.3.3 BOS modeling

Data from liver perfusion studies with BOS were modeled similar to ATV data as described before. Fig 4.5 summarizes the modeling exercise for BOS.

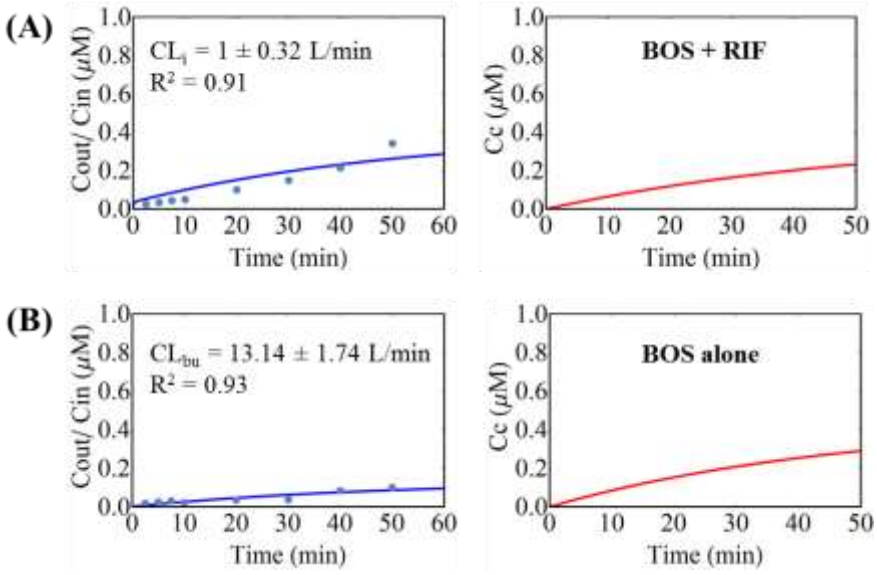

Figure 4.5 Modeling the BOS liver perfusion data with the 5-C explicit membrane model Model fitted outflow perfusate-concentration time profiles (blue) and simulated unbound intracellular concentration-time profiles (red) for (A) BOS + RIF group, with CL_m, CL_{aec} and CL_{aem} and "a" equal to 0.28 .L/min, 9.98 L/min, 0 L/min and 0.2, respectively, and (B) BOS alone group, with CLm and "a" fixed from BOS + RIF, CL_i parameterized to be 11 L/min, CL_{aec} and CL_{aem} fixed to 63.36 L/min, 0.0574 L/min, Model-fitted parameter ± standard error values are listed, along with the R^2 of the fit.

Model predicted tissue concentrations with a representative combination of various clearances, as compared to the experimental values are summarized in table 4.7. The respective predicted and observed amounts recovered in bile are summarized in table 4.8. Table 4.9 summarizes the model predicted unbound cell concentrations at 50 min and steady state for this specific combination of clearances. Please refer to appendix A for sensitivity analysis and model predicted values with other combinations of clearances.

The CL_m, CL_{aec}, CLaem and a values of 0.028 L/min, 9.98 L/min, 0 L/min and 0.2 resulted in a CL_i estimate of 1 ± 0.32 L/min using the BOS + RIF dataset (Fig 4.5 A). This combination of various clearances resulted in a predicted liver concentration of 136.3 µM and the amount of BOS recovered in bile was predicted to be 0.0109 µmoles (Tables 4.6 and 4.7). The R^2 for the fitting of outflow perfusate concentration-time data was 0.911. At 50 min, the predicted unbound intracellular BOS concentration and the predicted outflow perfusate concentration were 0.233 µM and 0.262 µM, respectively. Thus the Kp_{uu} at 50 min was 0.89. At steady state, the predicted unbound intracellular BOS concentration and the predicted outflow perfusate concentration were 0.387 µM and 0.411 µM, respectively, resulting in a KP_{uu} of 0.942.

Table 4.7 Observed and predicted BOS tissue concentrations (µM)

Group	Observed	Predicted, at 50 min	Predicted, at steady state
BOS**	92	105	161.33
BOS + RIF*	136	136.3	226.6

*CL_m, CL_{aec} and CL_{aem} and "a" equal to 0.28 L/min, 9.98 L/min, 0 L/min and 0.2, respectively
**CL_m and "a" fixed from BOS + RIF, CL_i parameterized to be 11 L/min, CL_{aec} and CL_{aem} fixed to 63.36 L/min, 0.0574 L/min

Table 4.8 Observed and predicted BOS amount recovered in bile at 50 min

Group	Observed (µmoles)	Predicted, at 50 min (µmoles)
BOS**	0.02	0.021
BOS + RIF*	0.012	0.0109

*CL_m, CL_{aec} and CL_{aem} and "a" equal to 0.28 L/min, 9.98 L/min, 0 L/min and 0.2, respectively
**CL_m and "a" fixed from BOS + RIF, CL_i parameterized to be 11 L/min, CL_{aec} and CL_{aem} fixed to 63.36 L/min, 0.0574 L/min

Table 4.9 Model predicted BOS unbound cell concentrations at 50 min and at steady state

Group	At 50 min (µM)	At steady state (µM)
BOS**	0.29	0.446
BOS + RIF*	0.233	0.387

*CL_m, CL_{aec} and CL_{aem} and "a" equal to 0.28 L/min, 9.98 L/min, 0 L/min and 0.2, respectively
**CL_m and "a" fixed from BOS + RIF, CLi parameterized to be 11 L/min, CL_{aec} and CL_{aem} fixed to 63.36 L/min, 0.0574 L/min

As mentioned in the methods section, CL_m, CL_{aec}, CL_{aem} and 'a' were varied to perform sensitivity analysis using the BOS + RIF dataset. Upon varying the CL_m from 0.0072 to 0.144 L/min, and fixing CL_{aec} (50 L/min), CL_{aem} (0.00045 L/min) and a (0.2), it was observed that CL_m from 0.014 to 0.028 L/min resulted in reasonable CL_i estimates ranging from 4.62 to 8 L/min. The predicted tissue concentrations and amount in bile were within 20% of the observed values (Appendix A). The CL_i parameter was very sensitive to changes in CL_{aec}. Increasing the CL_{aec} from 9.98 to 200 L/min increased the CL_i estimate from 0.992 to 22.7 L/min, yet resulted in liver concentration and biliary amount predictions within 20% of the observed value. The model failed to converge at the CL_{aec} value of 8.3 L/min. From the tested range for CL_{aem}, 0.00045 to 0.0027 L/min resulted in predictions for liver concentrations and biliary amounts within 20% of the observed value. However, CL_i was not very sensitive to changes in CL_{aem} since changing CL_{aem} from 0.00045 to 0.0027 L/min resulted in CL_i estimates ranging from 5.52 to 5.65 L/min. The CL_{aem} of 0.0045 L/min resulted in predicted biliary amount greater than 20% of the observed value. The amount of BOS recovered in bile was very sensitive to the fraction of diffusional clearance back into the apical membrane (a). Within the range of 'a' values tested, only 0.2 appeared to accurately predict the amount of BOS in bile. 'a' value less than 0.2 over-predicted, while greater than 0.2 under-predicted the biliary amount of BOS. However, varying the 'a' value from 0.05 to 1 had a minor influence on the predicted liver concentrations and amount of BOS recovered in bile.

One of the purposes to model the BOS + RIF data was to obtain an estimate for CL_i. Based on the tested range of various clearance values, multiple combinations of these

clearances could result in predictions with less than 20% error compared to the observed data. Thus, any of the resulting CL_i parameter estimates (0.992 to 22.7 L/min) could be real. Therefore, it was necessary to test this range of CL_i for the BOS only dataset.

To model the BOS only data, CL_m was fixed to 0.0365 L/min, as optimized previously with BOS + RIF and scaled based on hepatocellularity of the BOS only group. With the BOS only dataset, the model did not converge for values of CL_i less than 8.2 L/min, irrespective of the fixed values of CL_{aec} and CL_{aem}. The range of CL_i from 9.5 to 12.5 L/min with CL_{aec} and CL_{aem} values fixed to 63.36 and 0.0574 L/min respectively resulted in predictions of liver concentrations and amount of BOS in bile within 20% of the experimental values. A 5-fold higher value of CL_{aec} than BOS + RIF group and 0.0574 L/min CL_{aem} (as opposed to "0" L/min for BOS + RIF group) was required to explain the experimental BOS amount in bile. The CL_i of 11 L/min (mean of the acceptable range) resulted in the CL_{bu} parameter estimate of 13.14 ± 1.74 L/min (Fig 4.5 B). The predicted liver concentration was 105 µM and the amount of BOS recovered in bile was predicted to be 0.021 µmoles (Tables 4.6 and 4.7). The R^2 for the fitting of outflow perfusate concentration-time data was 0.94. At 50 min, the predicted unbound intracellular BOS concentration and the predicted outflow perfusate concentration were 0.29 µM and 0.086 µM, respectively. Thus the Kp_{uu} at 50 min was 3.35. At steady state, the predicted unbound intracellular BOS concentration and the predicted outflow perfusate concentration were 0.446 µM and 0.132 µM, respectively, resulting in a Kp_{uu} of 3.37. Thus, the steady state unbound intracellular BOS concentrations were 1.15 fold higher in the presence of active uptake. Similarly, the steady state Kp_{uu} of BOS in presence of

active uptake was 3.4 fold higher in the BOS only group as compared to BOS + RIF group.

4.4 Discussion

Experimental measurement of intracellular unbound drug concentrations is difficult. Modeling and simulation is a powerful tool for studying the mechanistic interaction of various components involved in drug disposition. A mechanistic model designed for the cell could give insights into intracellular drug disposition. Inhibition of one or more disposition processes could result in differential impact on intracellular drug concentrations. The magnitude of impact may depend on the magnitude of the clearance pathways themselves along with the extent of inhibition or induction of the specific pathways involved. In this chapter, the data obtained from ATV and BOS liver perfusion experiments in chapter 3 were modeled with the 5-C explicit membrane model for perfused rat liver along with the membrane partitioning values obtained in this chapter. The impact of inhibition of active uptake and metabolism on intracellular unbound concentrations of the respective drugs was studied.

4.4.1 Equilibrium dialysis

Unbound fraction in plasma has been previously determined for ATV by ultrafiltration (Watanabe et al., 2009a) or equilibrium dialysis without 10% CO_2 (Paine et al., 2008) as 0.0567 and 0.04 respectively. It is well known that ultrafiltration is conducted for short duration which is insufficient for allowing adequate equilibration between binding and debinding. Equilibrium dialysis when conducted without 10% CO_2 over predicts plasma

protein binding due to change in pH of plasma (Kochansky et al., 2008). Over predicting plasma protein binding under predicts the toxicity potential of drugs which can be hazardous. Therefore, in this study, the unbound fraction of drugs was determined with 10% CO_2. ATV (Log P 5.7) is more lipophilic than BOS (Log P 3.7). Interestingly however, the f_{um} for ATV is higher than BOS. This is because the membrane partitioning of a compound may not depend just on its lipophilicity. The interaction between the functional groups in the compound to those in the membrane lipids is also an important factor in membrane partitioning.

4.4.2 ATV modeling

Since the unbound intracellular concentration determined by the modeling exercise cannot be measured experimentally, it can be argued whether the model predicted unbound concentrations are the actual unbound intracellular concentrations. Therefore, the model predicted total liver concentrations and cumulative amount recovered in bile at the end of 50 min were used as endpoints to verify the predictive ability of the model. The total liver concentrations and total amounts of ATV recovered in the bile during perfusion in all groups could be successfully predicted by the model within 0.94- to 1.3-fold of the experimental value. This increases the confidence in the predicted unbound ATV cell concentrations Also, since the R^2 for fitting the outflow perfusate concentrations was > 0.8, the 5-C explicit membrane model can reasonably account for the variance across the experimental groups. The increase in Kp_{uu} over time could be explained by the fact that the system has not reached equilibrium. In absence of any transporter or metabolizing enzyme activity, the Kp_{uu} of a drug is expected to be 1.

However, in case of ATV, Kp_{uu} is less than 1 in the +ABT + RIF group. This can be explained by the ongoing apical efflux of the drug in this experimental group.

The unbound intracellular concentration in presence of active uptake was 5 to 6-fold higher than the inlet concentration, which is typical for a strong active uptake transporter substrate. Inhibition of active uptake had a larger impact on the unbound intracellular concentrations as compared to inhibition of metabolism. This is because of the larger magnitude of the active uptake clearance (20 L/min) compared to the metabolic clearance (0.00125 L/min). If the metabolic clearance was much higher in magnitude, such that its magnitude was now comparable to the uptake clearance, then inhibition of metabolism would also have a significant impact on the intracellular disposition of ATV. This situation is analogous to a DDI, which results in induction of CYP enzymes. Although, there would have to be 1000 to 2000-fold induction of CYPs to experimentally reproduce the aforementioned scenario. Due to toxicity limitations for inducers, it may never be practically possible to achieve this magnitude of induction. Another situation that may result in equal impact of metabolism and transport on intracellular disposition is if the intrinsic uptake clearance were much smaller than the current value (20 L/min) and comparable to the metabolic intrinsic clearance of 0.00125 L/min.

It is generally accepted that for uptake limited drugs like statins, inhibition of active uptake will have higher impact on the plasma concentrations, but minimal impact on the intracellular concentrations (Watanabe et al., 2009b). Similarly, inhibition of metabolism or apical efflux clearance will have higher impact on the intracellular concentrations, but minimal impact on the plasma concentrations. This is because most uptake limited drugs

have a very high intrinsic uptake clearance which is limited by the blood flow to the respective organ. ATV demonstrated a very high intrinsic uptake clearance of 20 L/min. In a preclinical or clinical setting, there are limitations on the dose of the uptake inhibitor compound due to toxicity limitations. Therefore, the perpetrator may not be able to completely inhibit the uptake of the victim drug. In such a situation, if the residual intrinsic uptake clearance after inhibition is still higher than the blood flow to the relevant organ, one may not see a significant change in the intracellular concentration. However, plasma concentrations will increase due to uptake inhibition. This concept is further illustrated in chapter 6.

4.4.3 BOS modeling

Similar to ATV, the predictive ability of the 5-C model for BOS was verified by comparing the experimental total tissue concentrations and amount of BOS recovered in bile to the model predicted values. The model predicted BOS total tissue concentrations and amount recovered in bile were within 0.8 to 1.2 fold of the observed values, increasing confidence in the predicted unbound concentrations. The predicted steady state Kp_{uu} in the BOS + RIF group was 0.942. The ongoing metabolism and apical efflux in this group could explain the Kp_{uu} less than 1. In reality, for a drug undergoing passive diffusion only, the Kp_{uu} would equal to 1 according to the free drug hypothesis (Koch-Weser and Sellers, 1976; Israili, 1979; Pardridge et al., 1983). As discussed in chapter 3, the higher BOS liver concentrations in presence of RIF as compared to the BOS only group could be a result of inhibition of mrp2 mediated apical efflux of the drug by RIF. RIF was shown to inhibit rat Mrp2 mediated 5(6)-carboxy-29,7-dichlorofluorescein

(CDCF) and tritiated taurocholic acid ([^{3}H] TCA) uptake in membrane vesicles (Watanabe et al., 2015). Indeed, a 5-fold higher CL_{aec} as well as presence of CL_{aem} were required for the BOS only group to explain the experimental data. This supports the hypothesis that it is the inhibition of apical efflux that results in higher BOS tissue concentrations in the RIF treated group than in the RIF untreated group. The CL_i estimates obtained from the BOS + RIF group could, therefore, be confounded by the inhibited apical efflux clearance. In other words, if an uninhibited apical efflux clearance were present, a true sink condition would prevail and hence, a larger value of CL_i may be required to explain the decrease in the outflow perfusate concentrations. As mentioned in the results section, CL_i was very sensitive to the initial estimate of CL_{aec}. A high initial estimate of CL_{aec} resulted in a large estimate for CL_i. Therefore, the CL_i of 1 ± 0.32 L/min obtained from the BOS + RIF group could be an under-estimate. Indeed, for the BOS only group, the model did not converge for CL_i values less than 8.2 L/min. The range of CL_i that predicted the experimental data from BOS only group within 20% of observed values was 9.5 to 12.5 L/min. This higher value of CL_i for the BOS only group as compared to what was obtained from the BOS + RIF group (1 ± 0.32 L/min) is not surprising considering the dependence of CL_i on CL_{aec}, as discussed before. Also, sensitivity analysis of the BOS + RIF group (Appendix A) showed that the CL_i estimate could range between 0.992 to 22.7 L/min. The CL_i values required to correctly predict the experimental data for BOS only group are within this range of 0.992 to 22.7 L/min. The predicted steady state Kp_{uu} in the BOS only group was 3.37. The presence of active uptake clearance in this group could explain the Kp_{uu} greater than 1. It should be noted

that the ratio of predicted unbound intracellular BOS concentrations in the BOS only group to that in BOS + RIF group was 1.15 at steady state. This indicates that there is minimal increase in the intracellular unbound BOS concentrations in presence of active uptake.

The model assumed minimal back diffusion from the bile. This is because for lipophilic compounds, once the molecule enters the biliary compartment, it is sequestered in the bile due to the presence of amphiphilic lipid solubilizing bile salts and acids (Graham and Northfield, 1987). These components of the bile act like detergents solubilizing the lipophilic compounds into micelles. The more hydrophilic the compound, the less sequestered it is and a greater fraction is then available for diffusing back into the apical membrane. Hence, the fraction of diffusional clearance from the bile back into the apical membrane ('a') is dependent on the lipophilicity of the compound of interest. The measured log P values for ATV and BOS are 5.7 and 3.7 (https://www.drugbank.ca/drugs/DB01076, accessed on 03/13/2017; https://www.drugbank.ca/drugs/DB00559, accessed on 03/ 13/2017). Thus, ATV is expected to diffuse back to a lesser extent than BOS. Therefore, the 'a' term was required to be fixed to 0.03 for ATV and 0.2 for BOS in order to explain the experimental data. Interestingly, the CL_i for BOS is approximately two orders of magnitude higher than ATV, even though the log P for BOS is lower. This is because while log P gives a reasonable approximation of the affinity of drugs for lipids in the biomembrane, several other physicochemical interactions amongst the drugs and the membrane components are

also important in deciding the affinity of the drugs towards the membranes. The net affinity will be a resultant of all these interacting forces.

4.5 Conclusion

The 5-C explicit membrane model along with liver perfusion data were successfully used to predict the experimental tissue concentrations, amount recovered in bile and unbound intracellular concentrations for ATV and BOS. Presence of active uptake increased the Kp_{uu} and the unbound intracellular concentrations for both ATV and BOS. Inhibition of metabolism demonstrated a marginal increase in the unbound intracellular ATV concentrations indicating that the magnitude of the clearance pathway, relative to other clearance pathways and the organ blood flow, is an important determinant of the resultant impact upon inhibition of that specific pathway. The intracellular unbound drug concentrations are influenced by the intracellular disposition pathways. The resultant intracellular unbound concentrations are dependent upon the net effect of all these intracellular disposition pathways.

CHAPTER 5: INDUCTION OF CYP3A1 WITH BOS – IN VITRO AND IN VIVO STUDIES AND USE OF UNBOUND INTRACELLULAR CONCENTRATION TO PREDICT EFFECT OF INDUCTION

5.1 Introduction

Drug drug interactions (DDIs) can lead to serious problems in drug development. One type of unfavorable DDIs are those that can result in toxicity leading to adverse drug reactions (Honig et al., 1993; Gomez et al., 1995; Floren et al., 1997; Greenblatt et al., 1999; Backman et al., 2002; Backman et al., 2006). This interaction is anticipated when one of the drugs involved in the interaction is a metabolism or transport inhibitor of the other drug. Another type of unfavorable DDI occurs when one of the drugs is an inducer of metabolism and transport of another drug. This can result in inadequate pharmacological activity of the desired drug (Back et al., 1979; Heimark et al., 1987; Dickinson et al., 2001; Grub et al., 2001). It is, therefore, important to predict the effect of DDIs in vivo from in vitro metabolism data in the early stages of drug development. Induction of CYP3A4 is thought to occur by the following mechanism mediated by the orphan nuclear receptor – Pregnane X receptor (PXR) (Moore and Kliewer, 2000). The inducer compound binds to PXR in the cytosol. The complex then translocates to the nucleus and binds to the DNA responsive element of the *CYP3A4* gene. This causes activation of the promotor resulting in transcription of *CYP3A4*. The duration of exposure to the inducer and the concentration of the inducer determine the extent of induction.

Predictive models have been described in the literature for IVIVE of induction-based DDIs (Shou et al., 2008). The most common modeling approach used to predict induction is the Hill equation (Hill, 1910).

$$\frac{E=E_{max}.[Ind]^n}{EC_{50}^n+[Ind]^n} \quad (5.1)$$

where E_{max} is the maximum response (net maximum fold increase), EC_{50} is the inducer concentration at 50% E_{max}, [Ind] is the inducer concentration, and *n* is the sigmoidicity of the fitted curve.

The induction parameters obtained as described above can be used to predict the change in exposure of a victim drug upon induction of a disposition protein by a perpetrator drug using the following equation (Shou et al., 2008)

$$\frac{AUC_{iv}'}{AUC_{iv}} = \frac{1}{f_h.f_{m,CYP3A4}.\frac{CL'_{int,CYP3A4}}{CL_{int,CYP3A4}}+(1-f_h.f_{m,CYP3A4})} \quad (5.2)$$

or

$$\frac{AUC_{iv}'}{AUC_{iv}} = \frac{1}{f_h.f_{m,CYP3A4}.(1+\frac{E^{max}.[Ind]^n}{EC_{50}+[Ind]^n}+(1-f_h.f_{m,CYP3A4})} \quad (5.3)$$

In the above equations, AUC'_{iv} and AUC_{iv} are the AUCs of the victim drug in presence and absence of the perpetrator drugs, respectively. $f_{m,CYP3A4}$ is the fraction of the drug metabolized by CYP3A4. f_h is the fraction of the drug escaping hepatic metabolism. $CL'_{int,CYP3A4}$ and $CL_{int,CYP3A4}$ is the intrinsic clearance of the victim drug in the presence

and absence of the inducer or perpetrator drug. [Ind] is the steady state plasma concentration of the inducer.

The induction potential of BOS has been previously reported by several groups (Weber et al., 1999b; van Giersbergen et al., 2002; Dingemanse and van Giersbergen, 2004; Shou et al., 2008). Bosentan has been listed as a moderate CYP3A inducer by the United States Food and Drug Administration (USFDA) (https://www.fda.gov/Drugs/DevelopmentApprovalProcess/DevelopmentResources/DrugInteractionsLabeling/ucm093664.htm#table1-3). A moderate inducer is defined to be a compound that decreases the AUC of a probe substrate by > 50% but < 80%.

BOS is highly bound to plasma proteins in humans. The range of fraction unbound in human plasma for BOS has been reported from 0.0053 to 0.041 (Lave et al., 1996; Weber et al., 1999b; Dingemanse and van Giersbergen, 2004; Shou et al., 2008). It is unlikely that BOS would result in 50 – 80% change in exposure of CYP3A4 substrates at low unbound BOS plasma concentrations upon low doses. Since the machinery for metabolism and hence induction is located inside the cell, it would be the intracellular concentration of the inducer that would be of relevance for prediction of induction potential of a drug by IVIVE. For uptake transporter substrates like BOS, the intracellular BOS concentration may be higher than the plasma concentration. This could explain the observed in vivo degree of induction.

The goal of this chapter was to use the predicted unbound intracellular BOS concentration as the driving force to model cyp3a1 induction in rats. The use of intracellular unbound BOS concentration instead of plasma concentration was expected

to improve the prediction of induction. In vivo studies were conducted in rats to study the effect of multiple dosing of BOS on the PK of the cyp3a1 probe substrate, midazolam (MDZ). In vitro induction studies were conducted in sandwich cultured rat hepatocytes with multiple dosing of BOS. In vitro studies were conducted in order to characterize the kinetics of induction (i.e. to determine E_{max} and EC_{50}).

5.2 Materials

Matrigel^{TM} was obtained from Corning Life Sciences, NJ. Collagenase, MDZ and dexamethasone were obtained from Sigma Aldrich, MO. Insulin, William's E medium and Hank's balanced salt solution (HBSS) were obtained from Gibco, NH. Penicillin, streptomycin, L-glutamine and fetal bovine serum (FBS) were obtained from Life Technologies, CA. Isoflurane was obtained from University Laboratory Animal Resources (ULAR), Temple University. BOS was obtained from Toronto Research Chemicals, Ontario, Canada. Bovine serum albumin was obtained from Fisher Scientific, NH. EDTA was obtained from Ambion, CA.

5.3 Methods

5.3.1 Animals

Male Sprague Dawley rats were maintained per conditions approved by the American Association for the Accreditation of Laboratory Animal Care-accredited University Laboratory Animal Resources of Temple University. Animals were provided with a normal rodent diet. Food and water was available to the animals as required. The animals

were housed in a standard 12 hour dark/light cycle. Animal studies were approved by the Institutional Animal Care and Use Committee at Temple University.

5.3.2 In vitro induction experiments in sandwich cultured hepatocytes

In vitro experiments for BOS induction were performed in sandwich cultured hepatocytes in order to obtain the kinetic parameters (E_{max}, EC_{50}) for BOS induction in rat hepatocytes.

a) Hepatocyte isolation

Primary hepatocytes were isolated from male Sprague Dawley rats as follows. In situ liver perfusion was performed with the HSE UNIPER UP-100 Type 834 for isolated organ perfusion in rodents. Perfusion conditions and protocol for liver perfusion surgery was followed as in chapter 3 (section 3.3.2) except that the inferior vena cava was not sutured and the bile duct and hepatic vein were not cannulated. The perfusion buffer consisting of 500 µL calcium and magnesium free HBSS, 500 µL insulin (4mg/ml), 500 µL EDTA (0.5 M pH 8.0), 2.5 g bovine serum albumin was pre warmed at 37 °C and perfused for 10 min at 20 mL/min. After 10 min, the inlet was switched to digestion buffer consisting of HBSS, 500 µL insulin (4mg/ml), 100 mg collagenase (approximately 3U/mg) and 2.5 g bovine serum albumin perfused for 10 min at 20 mL/min. The softened and disintegrating liver was then carefully dissected from its connections to the stomach and duodenum. Care was taken to avoid cuts to the intestine since this could have led to bacterial contamination.

b) Sandwich culture

On day 1, 24-well plates were seeded with 0.5mL of cells/well at a cell density of 0.7 X 10^6 viable cells/mL in complete William's E media for plating. Complete Williams E media for plating consisted of 500mL Williams E media supplemented with 5mL of pen-strep (5,000 units/mL penicillin, 5 mg/mL streptomycin, 0.9% sodium chloride), 5mL of L-glutamine (200mM), 500µL of insulin (4mg/mL in 1% v/v glacial acetic acid to sterile water), 50µL of dexamethasone (10mM), and 5% final concentration FBS. Plates were placed in an incubator at 37°C, 5% CO_2, 95% relative humidity and cells were allowed to attach for 1-3 hrs. The William's E media was changed, aspirating the unattached cells, taking care not to disturb the cell layer. On day 2, the cells were inspected for proper density. Cuboidal cells achieving ~80% confluency were the desired characteristics to achieve maximum canalicular formation. Matrigel was diluted to 0.25mg/mL protein concentration in cold, complete William's E media for cell maintenance. Complete Williams E media for cell maintenance consisted of 500mL Williams E media without phenol red supplemented with 5mL of pen-strep (5,000 units/mL penicillin, 5 mg/mL streptomycin, 0.9% sodium chloride), 5mL of L-glutamine (200mM), 5mL Insulin transferrin selenium+ and 5µL of dexamethasone (10mM). The medium was aspirated to remove floating dead cells and 0.5mL diluted matrigel was added to each well and plates were returned to incubator. On day 3 and day 4, the cells were treated with BOS (0 – 100 µM).

Two treatment regimens with different experimental conditions were tested for treatment of cells with BOS on days 3 and 4:

A) At the start of day 3, the previous medium was aspirated and fresh BOS solution was added every 12 hours at 0, 12, 24 and 36 hours. 0 – 100 mM stock solutions of BOS were prepared by serial dilution in 50:50 N-methyl pyrrolidone (NMP): DMSO. The working solutions of BOS were prepared by dilution of stock solutions in William's E medium for maintenance. The final concentrations of BOS ranged from 0- 100 µM. The final concentration of the organic solvents NMP and DMSO was 0.1% each (total 0.2% organic).

B) At the start of day 3, the previous medium was aspirated and fresh BOS solution was added every 24 hours at 0 and 24 hours. Stock solutions and working solutions were prepared as described in (A).

RIF was used as a positive control for the induction experiments. The stock solution of RIF (20 mM) was prepared in 50:50 NMP: DMSO. The stock solution was diluted 1000 fold in William's E medium for maintenance to prepare working solution of 20 µM. The final concentration of the organic solvents NMP and DMSO was 0.1% each (total 0.2% organic, same as that for BOS solutions).

Activity measurement assay for cyp3a1 was conducted on day 5 with MDZ as cyp3a1 probe substrate. A stock solution of 150 mM MDZ was prepared in NMP and diluted in HBSS to prepare the working solution. The Km for formation of 4-hydroxy MDZ is reported to be 22 µM (Kotegawa et al., 2002). It is recommended that the substrate concentration should be at least 10 fold higher than the Km to avoid substrate depletion. Therefore, the working concentration of MDZ in the activity assay was 300 µM. The previously added BOS solution was aspirated and cells were washed with pre warmed

HBSS to remove any residual BOS. The reaction was started by adding MDZ solution in HBSS. Upon incubating the plates at 37 °C for 60 min, the reaction was stopped by aspirating the MDZ solution and adding ice-cold acetonitrile containing diltiazem as IS to the cell layer. The cells were scraped and the cell suspension was centrifuged at 10000 rpm. The supernatant was analyzed by LC-MS/MS for measurement of the MDZ metabolite, 4-hydroxy MDZ. The previously aspirated MDZ solution was also analyzed for 4-hydroxy MDZ by adding diltiazem as IS. It has been observed that this reaction was catalyzed by cyp3a1 in rat liver microsomes (Kobayashi et al., 2002).

5.3.3 In vivo induction experiments rats

The induction potential of BOS was tested in vivo in single jugular cannulated male Sprague Dawley rats. After multiple dosing of BOS, MDZ was administered to test cyp3a1 induction. The weight range of animals used in this study was 290 – 340 grams.

The following treatment regimens were tested for BOS administration.

1) Stock solution of BOS (20 mg/mL) was prepared in DMSO. To 10% of the 20 mg/mL stock solution, 15% NMP and 75% saline were added to prepare a working solution of 2 mg/mL. BOS (4mg/Kg) was administered to treatment group of animals (n=3) at 0, 12, 24 and 36 hours. For the 12 hour dosing of BOS, precipitation of BOS in the dosing solution was observed. The dosing solution was warmed to dissolve the precipitated drug. Therefore, for BOS administration at 24 and 36 hours, formulation of BOS had to be changed to 30% NMP and 70% saline to ensure complete dissolution. The control group was administered an equal volume of solvent mix i.e. 10% DMSO, 15%

NMP and 75% saline at 0 and 12 hours, and 30% NMP and 70% saline at 24 and 36 hours. MDZ (2 mg/Kg) was then administered at 48 hours. MDZ was formulated as 1 mg/mL solution in 30% NMP and 70% saline.

2) Stock solution of BOS (5 mg/mL) was prepared in NMP. To 30% of this solution, 70% saline was added to obtain a working solution of 1.5 mg/mL. BOS was dosed at 3 mg/kg every 24 hours for 7 days. The control group received an equal volume of solvent every 24 hours for 7 days. MDZ (5mg/Kg) was administered on day 8. MDZ was formulated as 2.5 mg/mL solution in 30% NMP and 70% saline.

Blood samples (100 μL) were collected at 2, 5, 10, 15, 30, 60, 120, 180, 240, 360, 480 and 600 minutes in heparinized tubes and centrifuged at 10000 rpm for 10 min. Equal volume saline was injected as replacement. Supernatant plasma was collected and analyzed by LC-MS/MS with the protocol described in chapter 2. Compartmental analysis of the PK data was carried out with SAAM II (Version 2.3). Statistical analysis was performed on the data using a t test. A p value < 0.05 was considered to be statistically significant.

5.4 Results

5.4.1 In vitro induction experiments in sandwich cultured hepatocytes

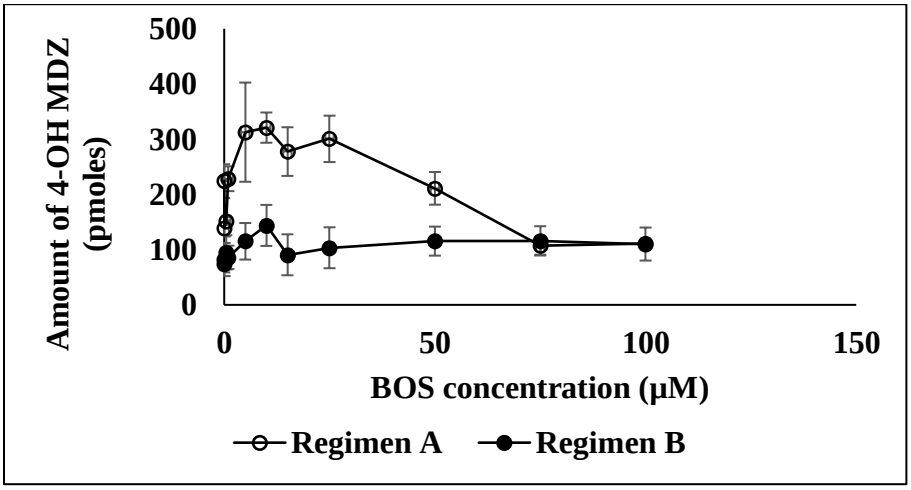

Figure 5.1 Effect of BOS treatment on amount of 4-hydroxy MDZ formed in sandwich cultured rat hepatocytes

Fig 5.1 summarizes the results for induction experiments performed in sandwich cultured rat hepatocytes. For both treatment regimens, a dose dependent linear increase was observed in the amount of metabolite 4-hydroxy MDZ with increasing incubation concentration of BOS until 10 µM. For the experiment with regimen A, a higher extent of product formation was observed as compared to regimen B. BOS incubation concentrations higher than 10 µM demonstrated decreased amounts of 4-hydroxy MDZ formed as compared to the concentrations lower than 10 µM. With regimen A, the decrease in amount of 4-hydroxy MDZ BOS was concentration dependent for concentrations higher than 10 µM. With regimen B, the amount of 4-hydroxy MDZ formed at concentrations higher than 10 µM BOS dropped drastically at 15 µM and

remained constant thereafter until 100 µM. Interestingly, for both regimens, the amounts of 4-hydroxy MDZ formed plateaued at similar values for higher BOS concentrations. Neither regimen A nor regimen B demonstrated the typical sigmoidal concentration-response curve.

Normally, the presence of intact matrigel layer is confirmed by glossy appearance of the bottom of the well. Dull patches indicate that the matrigel has been washed off. Experimentally, with regimen A, there could be observed areas within several wells, where matrigel was not present. With regimen B, the matrigel was intact in most wells. However, the layer became thinner over time.

5.4.2 In vivo induction experiments in rats

MDZ, when dosed alone or after BOS treatment, followed 3 compartment PK in rats (Fig 5.2 and 5.3). The compartmental parameter estimates are listed in Table 5.1.

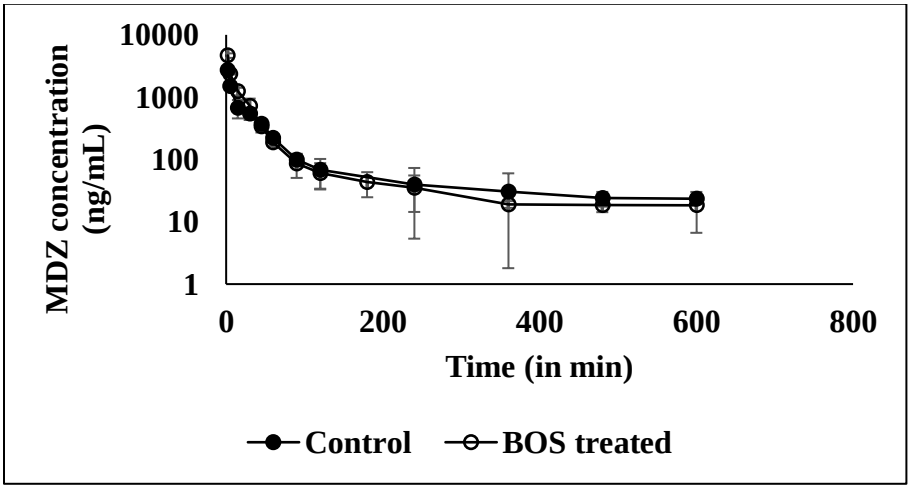

Figure 5.2 Effect of BOS treatment (Regimen 1; 4mg/Kg every 12 hours for 2 days) on MDZ PK. MDZ dose 2 mg/Kg; Control group: n=3, BOS treated group: n=3; Data are presented as mean ± SD.

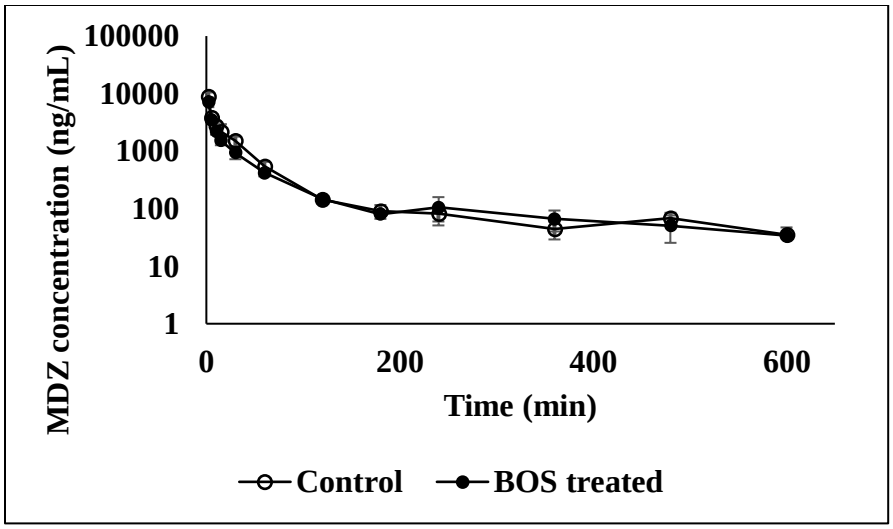

Figure 5.3 Effect of BOS treatment (Regimen 2; 4mg/Kg every 24 hours for 7 days) on MDZ PK. MDZ dose 5 mg/Kg; Control group: n=3, BOS treated group: n=3; Data are presented as mean ± SD

Table 5.1 Compartmental analysis of MDZ PK

Parameter	Units	Treatment regimen 1	
		Control group	BOS treated group
CL	mL/min	7.88 ± 0.64	7 ± 0.54
V_{ss}	mL	2726 ± 820	928 ± 241*
$t_{1/2}$	min	513 ± 164	299 ± 67
		Treatment regimen 2	
		Control group	BOS treated group
CL	mL/min	7.8 ± 0.27	9.45 ± 0.52*
V_{ss}	mL	1230 ± 128	1834 ± 321
$t_{1/2}$	min	323 ± 28	316 ± 58

Values reported as estimate ± SE.
t-test was conducted for statistical analysis
* Significantly different from the respective control group ($p < 0.05$),

With treatment regimen 1 for BOS, no difference was observed in the clearance of MDZ. However, BOS treatment significantly decreased the volume of distribution of MDZ in this group. The half-life ($t_{1/2}$) of MDZ was 1.85 fold lower in the BOS treated group, presumably due to the decrease in $V_{ss.}$

With treatment regimen 2, the mean systemic clearance of MDZ in the BOS treated group was 1.2 fold higher than the respective control group. The mean V_{ss} in the BOS treated group was slightly higher than the control group, but the difference was not significant. There was no change in the $t_{1/2}$ of MDZ with BOS treatment with regimen 2. Within the control groups, the CL was similar with either treatment regimen, the V_{ss} was significantly lower with regimen 1 and the $t_{1/2}$ was not significantly different. The decrease in V_{ss} could be due to experimental variability.

5.5 Discussion

As discussed in previous chapters, unbound target site concentration is responsible for the pharmacological effect mediated by that target. For induction as the pharmacological effect, the relevant concentration is, therefore, the unbound intracellular concentration. Intracellular concentrations can be influenced by interplay between metabolizing enzymes and uptake transporters. Therefore, use of unbound plasma concentrations may significantly under predict the extent of induction, especially for a compound like BOS which is highly bound to plasma proteins and is a substrate for uptake transporters. In vitro and in vivo induction studies were performed in order to use the unbound

intracellular BOS concentrations to predict the extent of in vivo induction of cyp3a1 in rats.

The concentration dependent linear increase followed by plateauing of the response was not observed in the in vitro experiments. There could be multiple plausible explanations for this result. There were visible patches in the culture wells where matrigel was not present in regimen A. The matrigel is crucial for maintenance of the 3-D cuboidal structure and proper distribution of cytoskeletal proteins of the hepatocytes (Rubin et al., 1981; Lindblad et al., 1991). This further controls the formation and maintenance of bile ducts (LeCluyse et al., 1994; Liu et al., 1998). The biliary route is an important disposition pathway for BOS and its metabolites (Weber et al., 1999a). It is possible that the transporter-enzyme interplay may have been disrupted in this experiment. The data obtained should, therefore, be interpreted with caution. Frequent change of the culture medium in regimen A (every 12 hours, for 2 days) and the associated shock from aspiration and dispensing of the culture medium can create weak spots in the matrigel layer. This can result in faster than normal matrigel dissolution in the medium.
Apart from affecting the matrigel layer, frequent incubation with fresh BOS solution could also result in saturation of clearance pathways of BOS, thereby causing intracellular accumulation. BOS is metabolized by cyp3a1, the same enzyme responsible for the formation of 4-hydroxy MDZ. MDZ is a better substrate for cyp3a1 and is used at a very high concentration of 300 µM. However, BOS is an uptake transporter substrate and could have intracellular concentration several fold higher than the incubation concentration. Therefore, BOS can compete for metabolism with MDZ, especially at

higher concentration. The decrease in the amounts of this metabolite at higher BOS concentrations could, therefore, be explained by saturation of cyp3a1 by BOS.

In order to resolve the possible issues arising from frequent dosing in regimen A, regimen B was designed to decrease the dosing frequency. Interestingly, regimen A demonstrated higher amount of 4-hydroxy MDZ formation as compared to regimen B, possibly due to higher extent of induction resulting from more frequent dosing. BOS is known to induce hepatotoxicity through inhibition of BSEP as discussed earlier in chapter 3 (section 3.1). Dose dependent BOS toxicity in hepatocytes could also explain the bell shaped appearance of the concentration-response curve. The different profiles obtained from two different regimens could also be due to inter-experiment variability.

In the in vivo studies, failure of regimen 1 to demonstrate difference in systemic clearance of MDZ could be attributed to competitive inhibition due to frequent BOS dosing. Intracellular accumulation of BOS at concentrations high enough to compete with cyp3a1 mediated MDZ metabolism could mask the induction effect. Therefore, in regimen 2, less frequent administration at a lower dose for a longer duration was tested. This resulted in a very small but significant increase in clearance of MDZ, indicating that BOS is a very weak inducer in rats. BOS has been assigned as a moderate inducer by the FDA (https://www.fda.gov/Drugs/DevelopmentApprovalProcess/DevelopmentResources/DrugInteractionsLabeling/ucm093664.htm#table1-3). Species differences in enzyme induction are well known (Jones et al., 2000; Moore and Kliewer, 2000). Major differences have been observed in the degree of responses in induction across different species. While RIF

is a very potent PXR activator in rabbits and humans, it has minimal effect in mice and rats (Jones et al., 2000; Vignati et al., 2004). These literature reports along with the results presented here further highlight the limitations of preclinical models in predicting human clearance and effect of induction on the drug metabolizing enzyme activity. Since the kinetic parameters for induction could not be obtained from in vitro experiments, it was not possible to predict the effect of in vivo cyp3a1 induction on MDZ exposure. Similar induction studies could be conducted in vitro with inhibition of uptake transport in order to check if uptake transport has a role to play in BOS induction. Induction studies could be performed with inhibition of active uptake with concomitant incubation with a potent uptake inhibitor like rosuvastatin. Rosuvastatin is a better choice over RIF for uptake inhibition since it is minimally metabolized. Alternatively, hepatocytes isolated from uptake transporter knockout rats could be used.

5.6 Conclusion

BOS was a weak cyp3a1 inducer in vivo in rats. A linear, BOS-concentration-dependent increase in the activity of cyp3a1 was observed initially in the in vitro induction experiments. However, the activity decreased at higher BOS concentrations possibly due to saturation of metabolism, or toxicity. IVIVC for induction could not be conducted due to inability to generate kinetic parameters for induction in vitro. The choice of dosing regimen for BOS was important to avoid confounding effects of competitive inhibition on induction, for both in vitro and in vivo studies.

CHAPTER 6: IN VIVO PHARMACOKINETIC STUDIES TO ASSESS THE EFFECT OF METABOLISM AND TRANSPORT ON SYSTEMIC AND INTRACELLULAR DISPOSITION OF ATV AND BOS

6.1 Introduction

The well stirred model has been described for estimation of hepatic clearance as follows (Pang and Rowland, 1977).

$$CL_H = \frac{Q\, f_u\, CL_{int}'}{Q + f_u\, CL_{int}'} \quad \ldots\ldots\ldots\ldots\ldots\ldots (6.1)$$

In equation 6.1, CL_H is the hepatic clearance, Q is the hepatic blood flow, f_u is the fraction unbound in the blood and CL_{int}' is the intrinsic clearance of the unbound drug. In this model, the CL_{int}' can be obtained from in vitro metabolism studies using human liver microsomes (HLM). Prediction of in vivo hepatic clearance of compounds has been routinely performed in the past from in vitro metabolic clearance measured in HLM. While in vivo hepatic clearance could be well predicted from in vitro estimates obtained from HLM for most compounds, large discrepancies were observed in predicted versus observed clearance for others (Iwatsubo et al., 1997; Chiba et al., 2009). A possible explanation for this discrepancy could be the lack of incorporation of transporters in predictive models. Transporters are important determinants of the kinetics of drug disposition. The various processes involved in the disposition of a drug are passive diffusion into the cell, active uptake into the cell, metabolism in the cell, passive diffusion out of the cell, active efflux back into the blood or active efflux into the apical chamber. The overall intrinsic clearance is, therefore, a combination of all these

processes, and not just metabolism. The overall intrinsic clearance ($CL_{int,all}$)is given by the following equation (Miyauchi et al., 1987)

$$CL_{int,all} = PS_{up} \times \frac{PS_{bile} + CL_{met}}{PS_{back} + PS_{bile} + CL_{met}} \quad \ldots\ldots\ldots\ldots\ldots\ldots (6.2)$$

Where,

PS_{up} is the sum of active and passive uptake clearances,

PS_{bile} is the active efflux clearance in the bile,

CL_{met} is the metabolic clearance,

PS_{back} is the sum of active and passive efflux back into the blood

Inhibition of each individual pathway can have a differential impact on the disposition of a drug. The magnitude of impact will depend on the contribution of that pathway to the overall intrinsic clearance of the drug of interest. For example, in an in vivo clinical microdosing study, ATV plasma exposure was significantly increased by active uptake inhibition by RIF, but not by the CYP3A4 inhibitor itraconazole (Maeda et al., 2011). In the same study, itraconazole significantly increased the plasma AUC of MDZ, while RIF had no effect on MDZ plasma AUC. While RIF increased the plasma AUC of pravastatin, itraconazole had no effect on pravastatin plasma exposure. This is because the contributions of different pathways in equation 6.2 to the disposition of these drugs are different. MDZ is not a substrate for transporters and is only metabolized. Hence, uptake transport inhibition has no effect, while metabolism inhibition has significant effect on MDZ exposure. ATV and pravastatin on the other hand are substrates for uptake

transporters OATP1B1 and 1B3. Therefore, RIF significantly influences exposure to these drugs. The inability of itraconazole to affect ATV plasma exposure is because uptake is the rate determining step in the elimination of ATV (Watanabe et al., 2009a; Maeda et al., 2011). Similar results were obtained for ATV in mice where RIF demonstrated elevated plasma exposure, while KETO had no significant effect on ATV plasma exposure (Chang et al., 2014). Interestingly, RIF had no significant effect on ATV liver concentrations while KETO demonstrated a significant increase in liver concentrations. This indicates that for drugs like ATV, plasma concentrations may not be reflective of tissue concentrations. Hence, changes in plasma exposure due to DDIs should be translated into changes in tissue exposure with caution.

Clinical (Lau et al., 2007; Maeda et al., 2011) and preclinical (Lau et al., 2006b; Chang et al., 2014) DDIs for ATV with uptake transporter inhibitors have been reported in the literature. Similarly, inhibition of uptake transport has been determined to be the major pathway involved in several reported interactions with BOS in vivo (Treiber et al., 2004) and in vitro (Treiber et al., 2007). Similar observations were made for ATV and BOS disposition during the liver perfusion studies conducted for this project. These results are described in detail in chapters 3 and 4.

Use of semi-physiological mathematical models to study the effect of enzyme inactivation by perpetrators on PK of victim drugs has been reported (Quinney et al., 2009; Zhang et al., 2010). In these models, the central compartment is connected to peripheral compartments by distribution rate constants like a normal mammillary model. The central compartment is also connected to physiological organ compartments (gut or

liver) by organ blood flows. The mechanistic interaction between the perpetrator and the victim within the organs is then modeled using in vitro data to predict the in vivo effect. A semi-physiological modeling approach like this is usually an over-simplification of the actual physiological scenario However, the simpler model structure offers advantage i.e. fewer parameters to estimate, as compared to a full physiologically based pharmacokinetic model.

The goals of this chapter were

1) To perform in vivo experiments in rats to study the effect of metabolism and transport on the PK of ATV and BOS

2) To use PK data and the semi-physiological model to predict unbound intracellular ATV and BOS concentrations.

3) To study the effect of inhibition of uptake transport, on the predicted unbound intracellular concentrations of ATV and BOS.

Inhibition of uptake transport has been tested with administration of 20 mg/Kg RIF 5 minutes before ATV or BOS administration. Inhibition of cyp3a1 mediated ATV metabolism in mice has been tested with KETO. KETO administered at a dose of 35 mg/Kg, 30 min before ATV administration was shown to effectively inhibit ATV metabolism in mice. Therefore, in the current study, 20 mg/Kg RIF was dosed 5 min before, and 35 mg/Kg KETO was dosed 30 min before administration of ATV or BOS. The recommended treatment regimen for inhibition of cyp mediated metabolism by ABT in rats is 100 mg/Kg, 2 hours before administration of the substrate (Balani et al., 2002). However, another literature report suggested that inhibition of cyp mediated metabolism

in rats was not complete at this dose (Parrish et al., 2016). In fact, increased extent of inhibition was observed at doses of 200 mg/Kg and 300 mg/Kg. However, 300 mg/Kg was not well tolerated in rats. Parrish *et al* also observed that maximum inactivation had been achieved at 2 hours and that subsequent increase in inactivation time up to 26 hours did not achieve any additional inhibition. Therefore, in the current studies, 200 mg/Kg ABT was dosed 2 hours prior to ATV or BOS administration.

6.2 Materials

ATV calcium trihydrate was obtained from Tokyo Chemical Industry America, OR. BOS was obtained from Toronto Research Chemicals, Ontario, Canada. RIF for injection USP was obtained from Sanofi-Aventis, NJ. ABT was obtained from Sigma Aldrich, MO. KETO was obtained from Fisher Scientific, NH. Single jugular cannulated male Sprague Dawley rats were obtained from Charles River, PA.

6.3 Methods

6.3.1 Animals

Male Sprague Dawley rats were maintained in accordance with guidelines of the American Association for the Accreditation of Laboratory Animal Care-accredited University Laboratory Animal Resources of Temple University. Animals were provided with a normal rodent diet. Food and water was available to the animals as required. The animals were housed in a standard 12-hour dark/light cycle. Animal studies were approved by the Institutional Animal Care and Use Committee at Temple University.

In vivo PK studies were conducted in male Sprague Dawley rats for ATV and BOS. In order to investigate the effect of uptake transporters on ATV and BOS PK, studies were conducted in presence and absence of the uptake inhibitor RIF. To study the effect of inhibition of CYP mediated metabolism, PK experiments were conducted with administration of the non-specific suicide CYP inhibitor ABT (for ATV and BOS) and with the reversible CYP inhibitor KETO (for ATV). Experiments were also conducted to test the effect of inhibition of both metabolism and transport by co-administration of RIF and ABT (for ATV and BOS) or KETO and ABT (for ATV) along with the drugs of interest, ATV or BOS. Single jugular vein cannulated rats were used. Animals were dosed and samples were withdrawn from the same cannula.

6.3.2 PK studies with ATV

Animals were dosed intravenously with ATV (2mg/Kg) as a 1mg/mL solution in 10% DMSO and 90% saline (n=3). For uptake inhibition studies, RIF (20 mg/Kg) was administered as a 10mg/mL solution in 10% DMSO and 90% saline (n=4). RIF was administered 5 min before administration of ATV. ABT (200mg/Kg) was administered as a 50 mg/mL solution in 2% DMSO, 2% ethanol and 96% saline. ABT was administered orally, 2 hours before administration of ATV (n=12). ATV + ABT PK experiment was performed four times with an n=3 each time, on account of inability to reproduce experimental data. For studies with ABT + RIF, 20 mg/Kg was administered intravenously 5 min before ATV administration to ABT dosed rats (n=3). Metabolism inhibition was also tested with oral administration of KETO (35 mg/Kg), 30 minutes before ATV administration, with or without 20 mg/Kg RIF. In summary, the 6

experimental groups for ATV PK studies were – ATV alone, ATV + RIF, ATV+ ABT (4 subgroups), ATV + ABT + RIF, ATV + KETO and ATV + KETO + RIF. Blood samples (200 μL) were collected at 2, 5, 10, 20, 30, 45, 60, 75, 90, 120, 180, 240, 360, 480 and 600 min. Blood was replaced with equal volume of saline. Blood was collected in heparinized tubes and centrifuged at 10000 rpm for 5 min. Supernatant plasma was collected and analyzed by LC-MS/MS with the protocol described in chapter 2. Compartmental analysis of the PK data was carried out using SAAM II (Version 2.3). Statistical analysis was performed on the data using one-way Analysis of Variance with Tukey's posthoc test. A p value < 0.05 was considered to be statistically significant.

6.3.3 PK studies with BOS

Animals were dosed intravenously with BOS (2mg/Kg) as a 1mg/mL solution in 10% DMSO, 15% NMP and 75% saline (n=3). For uptake inhibition studies, RIF (20 mg/Kg) was administered as a 10mg/mL solution in 10% DMSO and 90% saline (n=3). RIF was administered 5 min before administration of BOS. ABT (200mg/Kg) was administered as a 50 mg/mL solution in 2% DMSO, 2% ethanol and 96% saline. ABT was administered orally, 2 hours before administration of BOS (n=3). For studies with ABT + RIF, 20 mg/Kg RIF was administered intravenously 5 min before BOS administration to ABT dosed rats (n=3). In summary, the four experimental groups for BOS PK were – BOS alone, BOS + RIF, BOS + ABT and BOS + ABT + RIF. Blood samples (100 μL) were collected at 2, 5, 10, 20, 30, 45, 60, 75, 90, 120, 180, 240, 360, 480 and 600 min. Blood was replaced with equal volume of saline. Blood was collected in heparinized tubes and centrifuged at 10000 rpm for 5 min. Supernatant plasma was collected and analyzed by

LC-MS/MS with the protocol described in chapter 2. Compartmental analysis of the PK data was carried out using SAAM II (Version 2.3). Statistical analysis was performed on the data using one-way Analysis of Variance with Tukey's posthoc test. A p value < 0.05 was considered to be statistically significant.

The data obtained from PK studies conducted for ATV and BOS were analyzed by 2-compartment (Fig 6.1) and 3-compartment (Fig 6.2) mammillary models. The drug was dosed to and sampled from the central compartment.

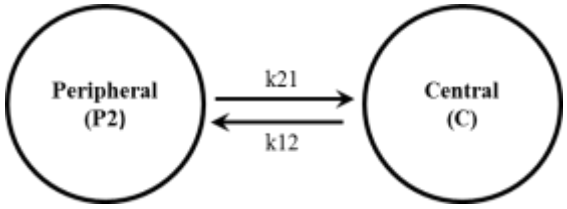

Figure 6.1 2-compartment mammillary model

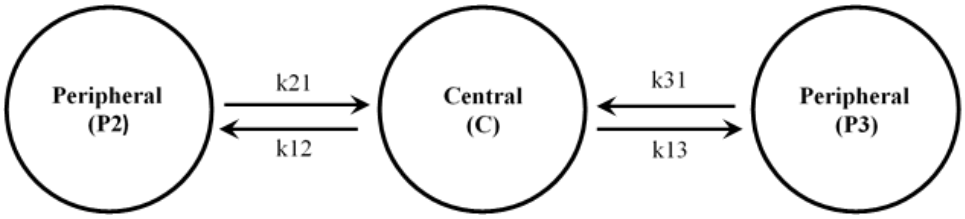

Figure 6.2 3-compartment mammillary model

6.3.4 Prediction of ATV unbound intracellular concentration

In order to predict the intracellular unbound ATV concentration upon intravenous dosing, a semi-physiological or hybrid modeling approach was tested. The 5-C explicit membrane model (described in chapter 4, section 4.1) was linked to the central

compartment of the 3-C mammillary model by the liver blood flow as described in Fig 6.3.

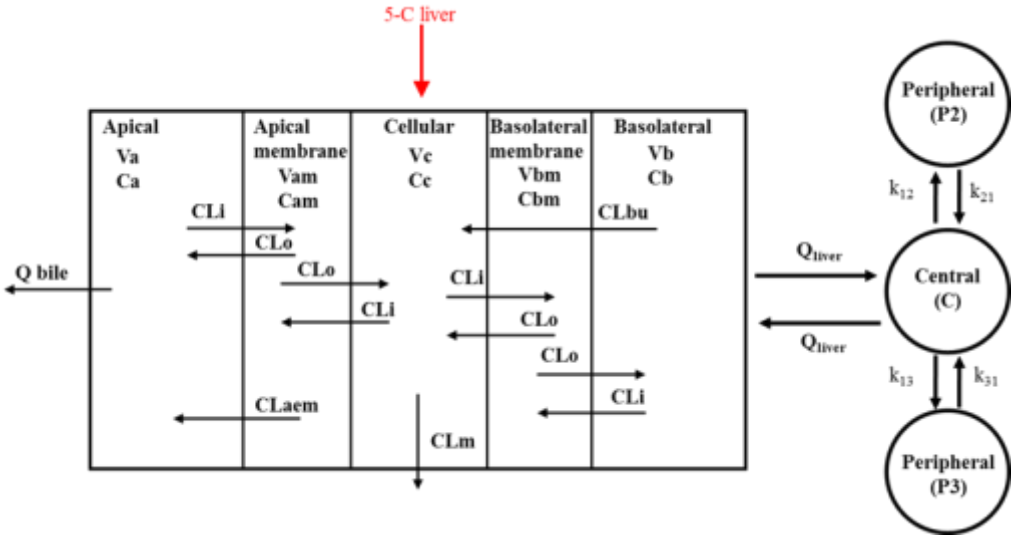

Figure 6.3 A 3-C hybrid model including a 5-C model with explicit membrane compartments for rat liver. C, P_1, P_2: amounts of drug in central, peripheral 2 and peripheral 3 compartments, respectively; V_A, V_B, V_C, V_{AM}, V_{BM}: volumes of apical, basolateral, cellular, apical membrane and basolateral membrane compartments, respectively; C_A, C_B, C_C, C_{AM}, C_{BM}: concentration in apical, basolateral, cellular, apical membrane, and basolateral membrane compartments, respectively; CL_i, CL_o: diffusional clearance into and out of the membrane respectively; CL_{bu}, active basolateral uptake clearance into the cell; CL_{aem}, apical efflux clearance from apical membrane into the apical compartment; Q_{liver}, liver blood flow; Q_{bile}, biliary flow rate

The interaction between various compartments of the semi-physiological model can be described by the following equations:

$$dC/dt = -K_{12}C + K_{21}P_2 + K_{31}P_3 - K_{13}C - QC/V_{central}B/P + QC_bB/P \quad (6.1)$$

$$dP_2/dt = K_{12}C - K_{21}P_2 \quad (6.2)$$

$$dP_3/dt = K_{13}C - K_{31}P_3 \quad (6.3)$$

$$dC_B/dt = (QC/V_{central}\,B/P + CL_oC_{BM} - fup\,CL_iC_B - A\,fup\,CL_{bu}C_B - QC_BB/P)/V_B \quad (6.4)$$

$$dC_{BM}/dt = (CL_i\,C_C + CL_iC_B - 2CL_oC_{BM})/V_{BM} \quad (6.5)$$

$$dC_C/dt = (A\,CL_{bu}C_B + CL_oC_{BM} + CL_oC_{AM} - 2CL_iC_C - CL_mC_C)/V_C \quad (6.6)$$

$$dC_{AM}/dt = (CL_i\,C_C - 2CL_oC_{AM} - CL_{aem}\,C_{AM} + CL_i\,C_A)/V_{AM} \quad (6.7)$$

$$d\,C_A/dt = (-Q_{bile}\,C_A + CL_{aem}C_{AM+} + CL_oC_{AM} - a\,CL_i\,C_A)/V_A \quad (6.8)$$

CLo was defined by equation 6.9

$$\mathrm{CL_i/CL_o} = \mathrm{V_A}(1 - \mathrm{fu_m})/\mathrm{V_m fu_m} \quad (6.9)$$

The clearance parameters involved in the intracellular disposition of ATV were fixed as obtained from modeling the data from the liver perfusion experiments in chapter 4 (section 4.3.2), and are listed in Table 6.1, along with values used for various volume terms.

Table 6.1 Parameter initial estimates for ATV

Parameter	**Symbol**	**Units (per liver)**	**Value**
Volume of bile (apical compartment) (Masyuk et al., 2001)	V_A	mL	0.05
Volume of intrahepatic vasculature (basolateral compartment) (Blouin et al., 1977)	V_B	mL	1.108 [a] 1.08[b]
Volume of hepatocytes (Sohlenius-Sternbeck, 2006)	V_C	mL	5.76[a] 5.63[b]
Volume of apical membrane	V_{AM}	mL	0.05 x 5.76[a] 0.05 x 5.63[b]
Volume of basolateral membrane	V_{BM}	mL	0.05 x 5.76[a] 0.05 x 5.63[b]
Diffusional clearance into the membrane[d]	CL_i	mL/min	154.8[a] 151.3[b]
Active uptake clearance [d]	CL_{bu}	mL/min	24480[a] 23920[b]
Metabolic clearance [d]	CL_m	mL/min	1.8[a] 1.73[b]
Apical efflux clearance from the membrane[d]	CL_{aem}	mL/min	100.3[a] 98[b]
Fraction of viable active uptake clearance	A	-	1[a] 0.05[b]
Blood flow (Richardson and Withrington, 1982)	Q	mL/min	16.56[a] 16.56[b]
Fraction unbound in RLM[c]	f_{um}		0.84
Fraction unbound in rat plasma[c]	f_{up}		0.08
Blood to plasma ratio (Lau et al., 2006b)	B/P	-	1.47
Fraction of CL_i from bile to apical membrane (Back diffusion)	a		0.03

[a]ATV group, [b]ATV + RIF group, [c]Experimental values, [d]Fixed from liver perfusion modeling

For the ATV only group, all the parameters described in table 6.1 were fixed and the distribution rate constants (k_{12}, k_{21}, k_{13}, k_{31}) and volume of the central compartment were parameterized. For the ATV + RIF treated group, the viable fraction of the intrinsic active uptake clearance (A) in the liver was additionally parameterized. This exercise was performed to address the possibility that since ATV is a potent uptake transporter

substrate, the concentration of RIF (20mg/mL) used in this study may not be able to completely inhibit the active uptake of ATV. Upon satisfactory explanation of the intravenous PK data by the model, the cell concentration-time profile was simulated using the parameterized numbers. Sensitivity analysis was conducted by varying the CL_{bu} from 0.1% to 100%. The effect of CL_{bu} on plasma and simulated cell concentrations was studied. Wolfram Mathematica (Version 10.0) was used for semi-physiological modeling.

6.3.5 Prediction of BOS unbound intracellular concentration

A semi-physiological modeling approach similar to the one described for ATV was tested for BOS in order to predict the intracellular unbound BOS concentration upon intravenous dosing. The 5-C explicit membrane model (described in chapter 4, section 4.1) was linked to the central compartment of the 2-C model by the liver blood flow as described in Fig 6.4.

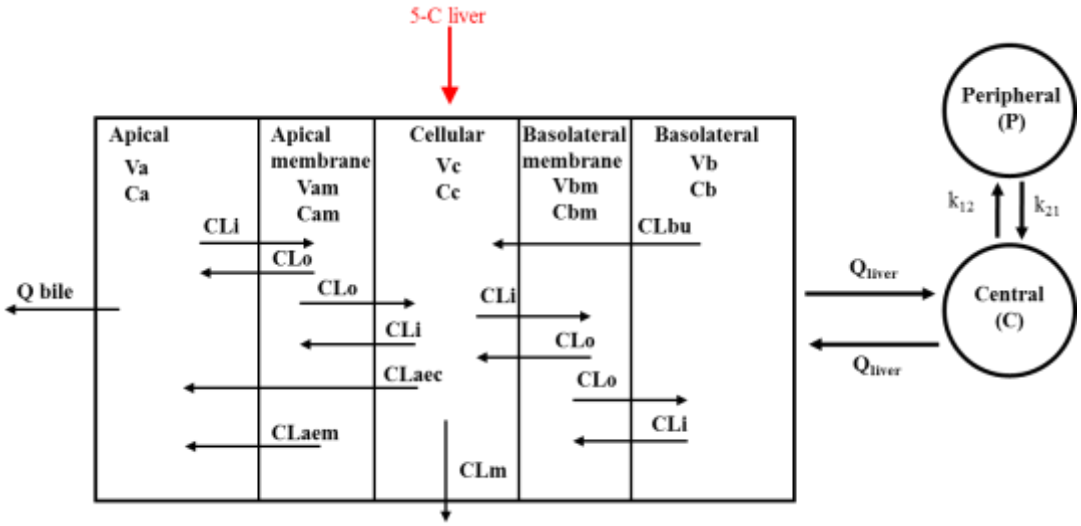

Figure 6.4 A 2-C hybrid model including a 5-C model with explicit membrane compartments for rat liver. C, P: amounts of drug in central and peripheral compartments, respectively; V_A, V_B, V_C, V_{AM}, V_{BM}: volumes of apical, basolateral, cellular, apical membrane and basolateral membrane compartments, respectively; C_A, C_B, C_C, C_{AM}, C_{BM}: concentration in apical, basolateral, cellular, apical membrane, and basolateral membrane compartments, respectively; CL_i, CL_o: diffusional clearance into and out of the membrane respectively; CL_{bu}, active basolateral uptake clearance into the cell; CL_{aem}, apical efflux clearance from apical membrane into the apical compartment; CL_{aec}, apical efflux clearance from cell into the apical compartment; Q_{liver}, liver blood flow; Q_{bile}, biliary flow rate

The interaction between various compartments of the semi-physiological model can be described by the following equations:

$$dC/dt = -K_{12}C + K_{21}P_2 + K_{31}P_3 - K_{13}C - QC/V_{central}B/P + QC_bB/P \quad (6.10)$$

$$dP_2/dt = K_{12}C - K_{21}P_2 \quad (6.11)$$

$$dC_B/dt = (QC/V_{central}B/P + CL_oC_{BM} - fup\ CL_iC_B - A\ fup\ CL_{bu}C_B - QC_BB/P)/V_B \quad (6.12)$$

$$dC_{BM}/dt = (CL_i\ C_C + CL_iC_B - 2CL_oC_{BM})/V_{BM} \quad (6.13)$$

$$dC_C/dt = (A\ CL_{bu}C_B + CL_oC_{BM} + CL_oC_{AM} - 2CL_iC_C - CL_mC_C - CL_{aec}C_C)/V_C \quad (6.14)$$

$$dC_{AM}/dt = (CL_i\ C_C - 2CL_oC_{AM} - CL_{aem}\ C_{AM} + CL_i\ C_A)/V_{AM} \quad (6.15)$$

$$d\ C_A/dt = (-Q_{bile}\ C_A + CL_{aem}C_{AM+} + CL_{aec}C_C + CL_oC_{AM} - a\ CL_i\ C_A)/V_A \quad (6.16)$$

CL_o in the above equations has been previously defined by equation 6.9.

The clearance parameters involved in the intracellular disposition of BOS were fixed as obtained from modeling the data from the liver perfusion experiments in chapter 4 (section 4.3.3), and are listed in Table 6.2, along with values used for various volume terms. A scaling factor of 1 to 2.25 was tested for the transporter mediated clearances (i.e. CL_{bu}, CL_m, CL_{aec} and CL_{aem}) obtained from the liver perfusion data.

Table 6.2 Parameter initial estimates for BOS

Parameter	**Symbol**	**Units (per liver)**	**Value**
Volume of bile (apical compartment) (Masyuk et al., 2001)	V_A	mL	0.05
Volume of intrahepatic vasculature (basolateral compartment) (Blouin et al., 1977)	V_B	mL	1.154[a] 1.127[b]
Volume of hepatocytes (Sohlenius-Sternbeck, 2006)	V_C	mL	6.674
Volume of apical membrane	V_{AM}	mL	6.674 x 0.05[a] 5.63 x 0.05[b]
Volume of basolateral membrane	V_{BM}	mL	6.674 x 0.05[a] 5.63 x 0.05[b]
Diffusional clearance into the membrane[d]	CL_i	Liter /min	12.54_a 10.58[b]
Active uptake clearance [d]	CL_{bu}	Liter /min	15[a] 13.11[b]
Metabolic clearance [d]	CL_m	mL/min	41.6[a] 35.1[b]
Apical efflux clearance from the cell[d]	CL_{aec}	Liter /min	72.3[a] 12.18[b]
Apical efflux clearance from the membrane[d]	CL_{aem}	mL/min	65.4[a] 0[b]
Scaling factor for transporter mediated clearances (CL_{bu}, CL_m, CL_{aec} and CL_{aem})			1 to 2.25
Fraction of viable active uptake clearance	A	-	1[a] 0.1[b]
Blood flow (Richardson and Withrington, 1982)	Q	mL/min	17.48[a] 17.07[b]
Fraction unbound in RLM[c]	f_{um}		0.5943
Fraction unbound in rat plasma[c]	f_{up}		0.01086
Blood to plasma ratio (Gehin et al., 2016)	B/P	-	0.6
Fraction of CLi from bile to apical membrane (Back diffusion)	a		0.2

[a]BOS group, [b]BOS + RIF group, [c]Experimental values, [d]Fixed from liver perfusion modeling

For the BOS only group, all the parameters described in table 6.2, except the scaling factor for transporter mediated clearances, were fixed and the distribution rate constants (k_{12}, k_{21}) and volume of the central compartment were parameterized. The scaling factor for CL_{bu}, CL_m, CL_{aec} and CL_{aem} was varied from 1 to 2.25. For the BOS + RIF treated group, the viable fraction of the intrinsic active uptake clearance (A) in the liver was additionally parameterized. For BOS + RIF group, it was assumed that RIF causes inhibition of apical efflux clearances of BOS to similar extent as observed in the liver perfusion experiments. For the BOS + RIF group, modeling was also performed with fully viable apical efflux clearances i.e. without assuming inhibition of apical efflux by RIF. This exercise was performed to address the possibility that intracellular RIF concentrations upon single dose intravenous administration of RIF may not be high enough to inhibit apical efflux of BOS, as opposed to single pass continuous liver perfusion with RIF. Upon satisfactory explanation of the intravenous PK data by the model, the cell concentration-time profile was simulated using the parameterized numbers. Sensitivity analysis was conducted by varying the CL_{bu} from 0.1% to 100%. The effect of CL_{bu} on plasma and simulated cell concentrations was studied. Wolfram Mathematica (Version 10.0) was used for semi-physiological modeling.

Due to the complications involved in PK data with the use of ABT, the ABT treated datasets for both ATV and BOS were not used for modeling.

6.4 Results

6.4.1 PK studies with ATV

ATV demonstrated multi-compartment disposition behavior from observation of the PK profile. Compartmental models described in Fig 6.1 (2-C) and Fig 6.2 (3-C) were tested for ATV. The model fitted PK profiles for ATV alone along with the residual analysis plots are shown in Fig 6.5 and 6.6 for a 2-C and 3-C model, respectively.

The 2-C model was unsuccessful in describing the disposition of the first compartment resulting in under prediction of the concentration at 0 minute. The 3-C model predicted the concentration at 0 minute well, and could also describe the behavior of the first compartment. The AIC for the 3-C model (4.04) was lesser than that for 2-C model (4.51). However, the difference in the AICs was not conclusive. Therefore, residual analysis was performed to confirm random distribution of residuals. It was observed that with the 2-C model, there was a pattern in the distribution of residuals, while with the 3-C model, the residual distribution was random. Therefore, the 3-C model was confirmed as the final model to describe the PK of ATV. Fig 6.7 shows the effect of inhibition of active uptake by RIF on ATV PK. Fig 6.7 describes the effect of inhibition of metabolism by ABT and KETO on PK of ATV. Fig 6.8 shows the effect of concomitant inhibition of metabolism and transport by ABT + RIF and KETO + RIF on ATV PK. Table 6.4 summarizes the results from compartmental analysis of ATV in all groups.

(A)

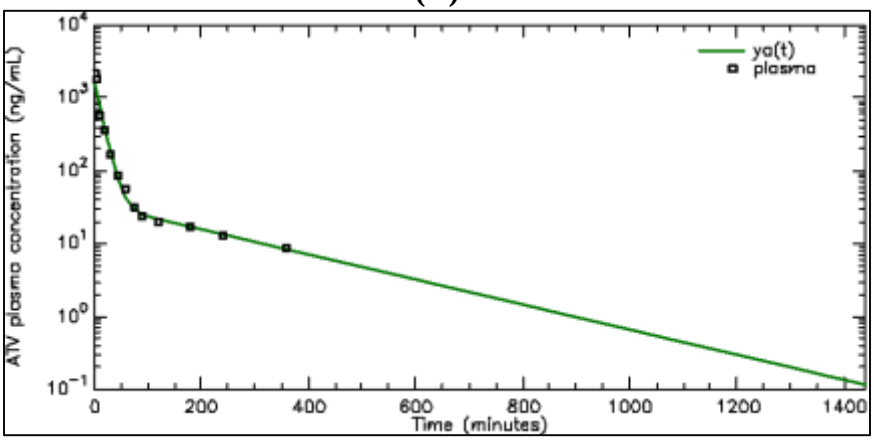

(B)

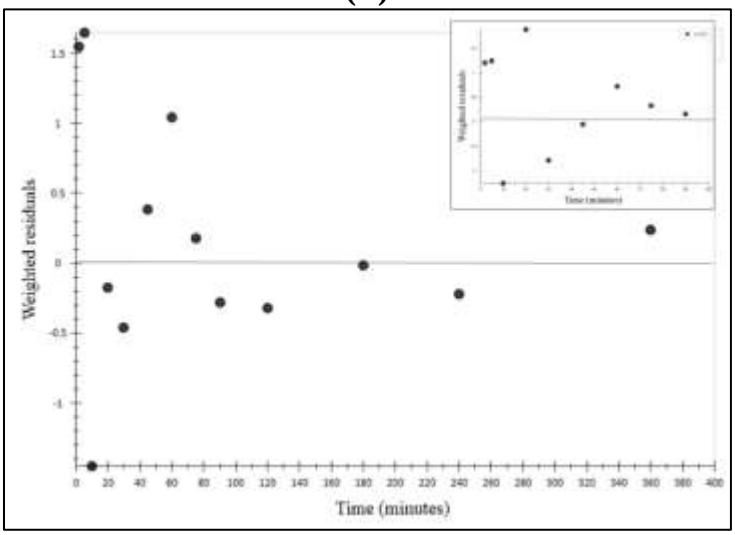

Figure 6.5 2-C model analysis of ATV PK data. (A) ATV PK profile predicted by 2-C model (green line) overlaid on experimental PK data (Open squares) (B) Residual analysis for 2-C model, inset shows residual analysis from 0 – 100 min.

(A)

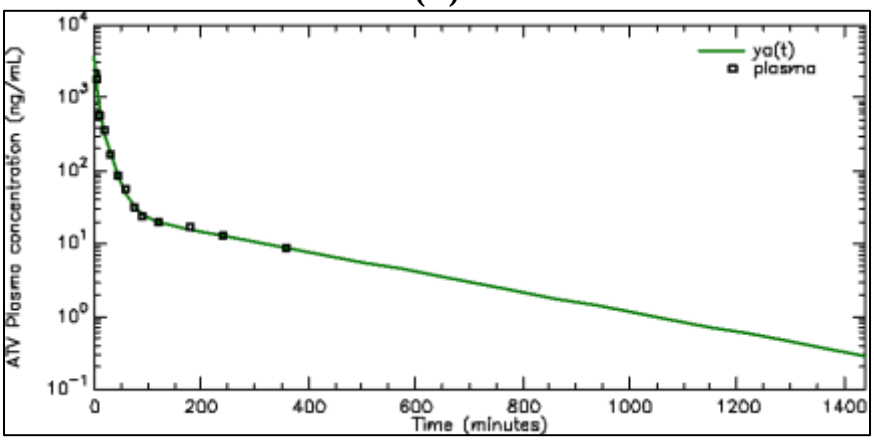

(B)

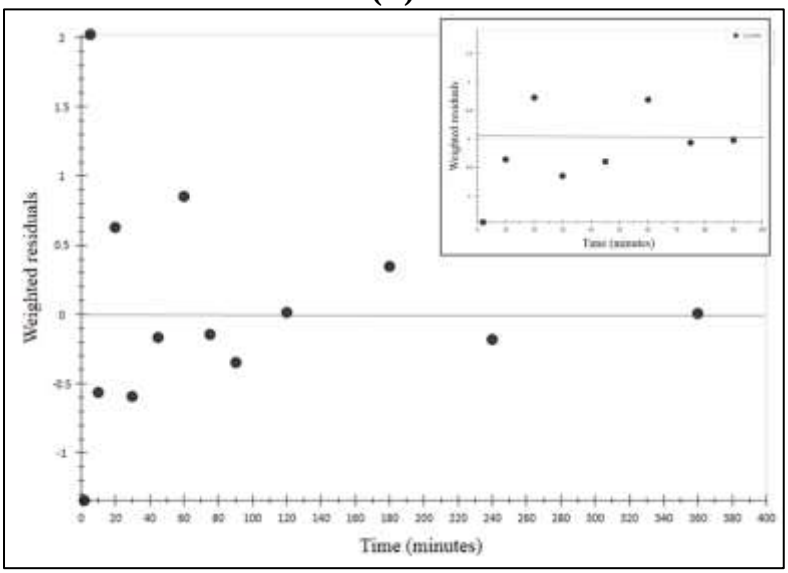

Figure 6.6 3-C model analysis of ATV PK data. (A) ATV PK profile predicted by 3-C model (green line) overlaid on experimental PK data (Open squares) (B) Residual analysis for 3-C model, inset shows residual analysis from 0 – 100 min.

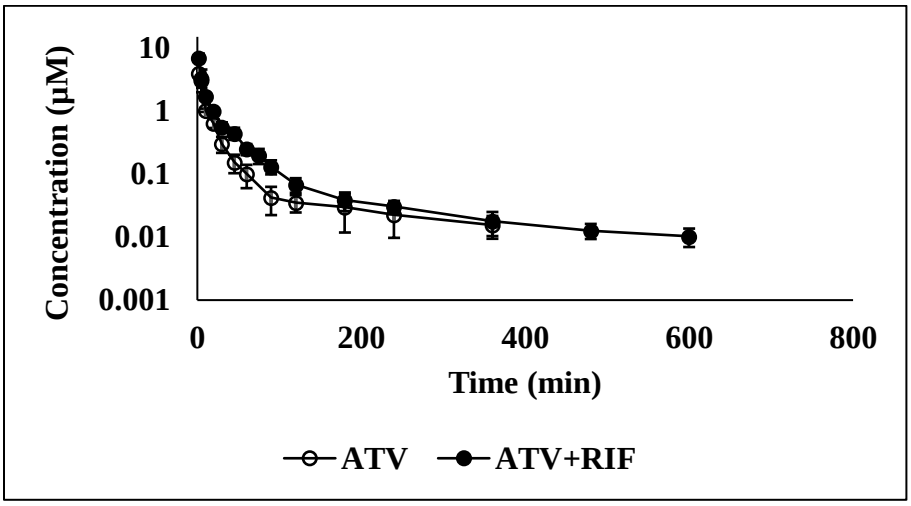

Figure 6.7 Effect of inhibition of uptake transport by RIF on ATV PK. ATV: n=3, ATV + RIF: n=4; Data are presented as mean ± SD

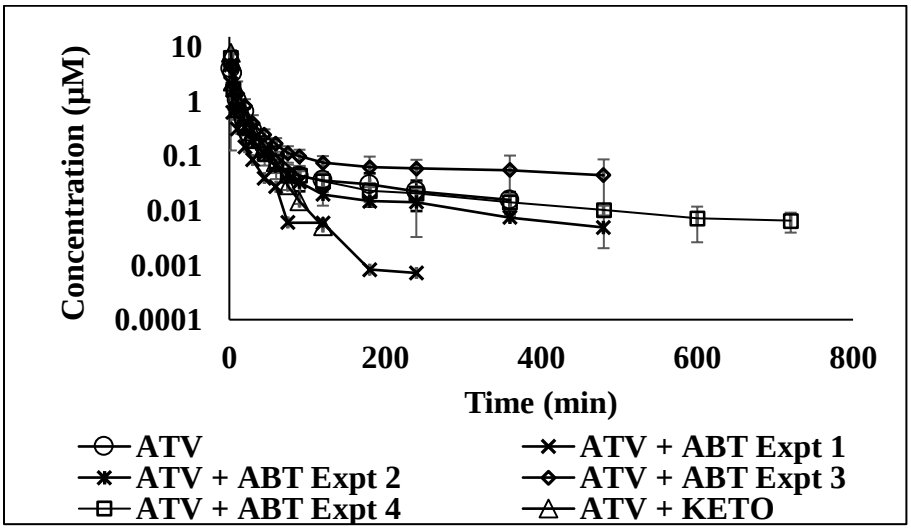

Figure 6.8 Effect of inhibition of ATV metabolism by ABT and KETO on ATV PK ATV: n=3, ATV + ABT Experiment 1: n=3, ATV + ABT Experiment 2: n=3, ATV + ABT Experiment 3: n=3, ATV + ABT Experiment 4: n=3; ATV + KETO: n=3; Data are presented as mean ± SD (Individual PK profiles for all groups are shown in appendix B)

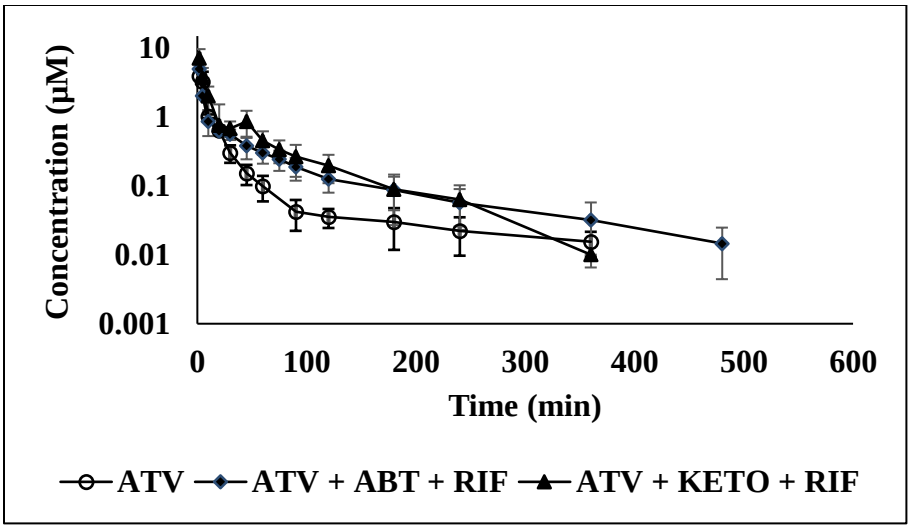

Figure 6.9 Effect of concomitant inhibition of metabolism and transport by ABT + RIF and KETO + RIF on ATV PK. ATV: n=3, ATV + ABT +RIF n=3, ATV + KETO + RIF: n=3; Data are presented as mean ± SD

Table 6.3 Compartmental analysis of ATV PK

Group	CL (mL/min)	V_{ss} (mL)	$t_{1/2}$ (min)
ATV	11.8 ± 0.75	1574 ± 440	219 ± 58
ATV + RIF	7.5 ± 0.29***	905 ± 103	235 ± 29
ATV + ABT Experiment 1	35 ± 1.8***	987 ± 99	56 ± 2.6*
ATV + ABT Experiment 2	18 ± 0.9***	2670 ± 520*	291 ± 4.63
ATV + ABT Experiment 3	7.3 ± 0.4**	3168 ± 539***	436 ± 70**
ATV + ABT Experiment 4	14.6 ± 0.9*	1822 ± 262	225 ± 17.5
ATV + ABT + RIF	7.3 ± 0.2***	926 ± 51	136 ± 8.7
ATV + KETO	10.7 ± 0.58	689 ± 125	201 ± 22
ATV + KETO + RIF	4.6 ± 0.44***	1295 ± 492	378 ± 122*

*Groups significantly different from the ATV group are marked; Data are presented as estimate ± SD for a 3-C model. Statistical analysis was performed with one-way analysis of variance followed by posthoc Tukey's test; *$p < 0.05$, **$p < 0.01$, ***$p < 0.001$

The B/P ratio of ATV is 1.47 (Lau et al., 2006b), indicating that the drug partitions into red blood cells. The mean CL of ATV corrected using the B/P ratio of 1.47 was 11.8 ± 0.75 mL/min (Table 6.3). RIF treatment significantly decreased the CL of ATV by 1.57 fold due to uptake inhibition. The mean V_{ss} of the RIF treated groups was lower than the ATV only group, but the difference was not statistically significant. The $t_{1/2}$ of ATV was unaffected with RIF treatment. Inhibition of cyp mediated metabolism with ABT had a variable impact on ATV PK. It was observed that the PK data obtained for ATV in presence of ABT could not be reproduced during the 4 times this experiment was repeated. The systemic clearance in the ABT treated group was significantly higher for experiment numbers 1, 2 and 4, and significantly lower for experiment number 3. A significant difference in the V_{ss} was observed between ATV only and experiments 2 and 3 for the ABT treated groups. No other groups showed significant difference in V_{ss} when compared to the ATV only group. There was a significant decrease in $t_{1/2}$ for ATV + ABT experiment 1 group, and a significant increase in $t_{1/2}$ for ATV + ABT experiment 3 group, as compared to the ATV only group. The decrease in $t_{1/2}$ for the ATV + ABT experiment 1 group could be attributed to a significant increase in clearance and an unchanged Vss. However, in ATV + ABT experiment 3 group, decrease in $t_{1/2}$ was influenced by both decrease in clearance and increase in V_{ss}. Thus, ABT treatment did not result in consistent impact on ATV PK. Inhibition of metabolism by KETO had no effect on the systemic clearance of the drug as compared to the ATV only group. Concomitant inhibition of metabolism and transport by ABT + RIF decreased the systemic clearance of ATV to 7.3 ± 0.2 mL/min (comparable to that observed in the RIF treated group).

Concomitant inhibition of metabolism and transport by KETO + RIF demonstrated a systemic clearance lower than the ABT + RIF group. In the ATV + KETO + RIF group, decreased clearance and increased V_{ss} resulted in increased $t_{1/2}$. The data from metabolism inhibition experiments with ABT and KETO were not interpretable. Therefore, only ATV and ATV + RIF datasets were used for modeling with the semi-physiological model described earlier.

6.4.2 Prediction of ATV unbound intracellular concentration

The model fitted concentration-time profiles generated by using ATV plasma PK data as an input for the 3-C hybrid model depicted in fig 6.3, are shown in fig 6.10 and 6.11. The fig 6.10 shows ATV PK and unbound cell concentrations in absence of RIF and fig 6.11 shows ATV PK and unbound cell concentrations in the presence of RIF. The parameter estimates obtained in the modeling exercise are summarized in table 6.4.

Table 6.4 Parameter estimates obtained by analysis of ATV data with the 3-C hybrid model

Parameter	**Group**	
	ATV only	**ATV + RIF**
k_{12} (min^{-1})	0.08 ± 0.04	0.13 ± 0.03
k_{21} (min^{-1})	0.096 ± 0.027	0.07 ± 0.009
k_{13} (min^{-1})	0.041 ± 0.008	0.025 ± 0.004
k_{31} (min^{-1})	0.0026 ± 0.0006	0.0036 ± 0.00045
$V_{central}$ (L)	0.145 ± 0.03	0.089 ± 0.017
A	-	0.069 ± 0.0085

Data are listed as parameter estimate ± SE.

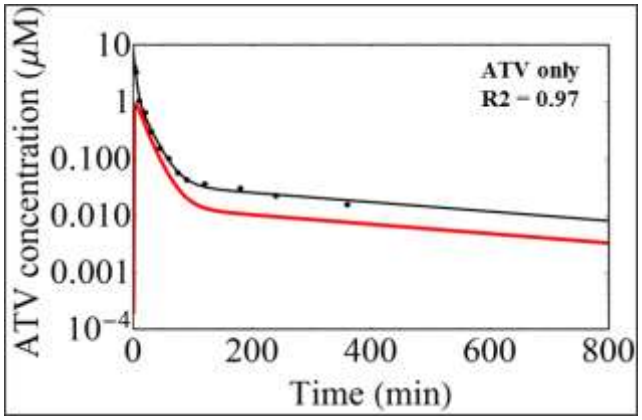

Figure 6.10 Fitted ATV concentration-time profiles for ATV only group using the 3-C hybrid model. Solid circles are mean experimental data for plasma concentrations, black solid line represents model fitted plasma profile, and the red solid line represents model predicted unbound intracellular concentration-time profile.

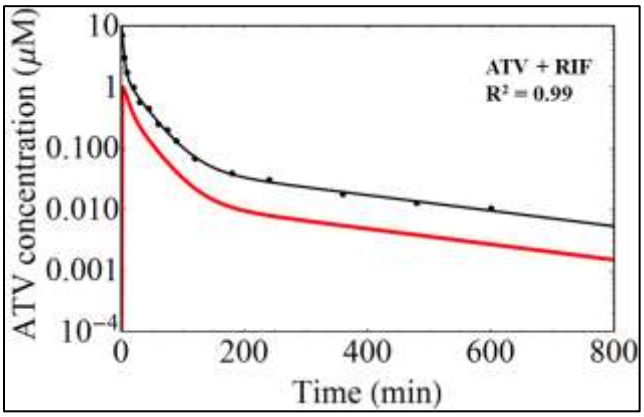

Figure 6.11 Fitted ATV concentration-time profiles for ATV + RIF group using the 3-C hybrid model. Solid circles are mean experimental data for plasma concentrations, black solid line represents model fitted plasma profile, and the red solid line represents model predicted unbound intracellular concentration-time profile.

The model predicted the ATV plasma PK data very well, both for the ATV only and ATV + RIF groups. The R^2 for fitting was 0.97 and 0.99 in absence and presence of RIF, respectively. The predicted unbound cell concentration of ATV demonstrated a sharp increase followed by gradual decrease in both groups. The maximum peak unbound ATV concentration in the cell was ~ 1 µM in both groups. The total ATV plasma concentration was higher than the unbound cell concentration at all times. However, the unbound cell concentration of ATV was consistently higher than the unbound plasma concentration after C_{max} for the unbound cell concentrations (f_{up} = 0.08). The parameter estimates for distribution rate constants, volume of central compartment and fraction of viable intrinsic uptake clearance are summarized in table 6.4. The volume of the central compartment for ATV decreased from 0.145 L to 0.089 L upon treatment with RIF. The modeling exercise with ATV + RIF group resulted in an estimate of 0.069 for "A", the fraction of viable intrinsic clearance.

The results for sensitivity analysis with CL_{bu} are summarized in fig 6.12.

(A)

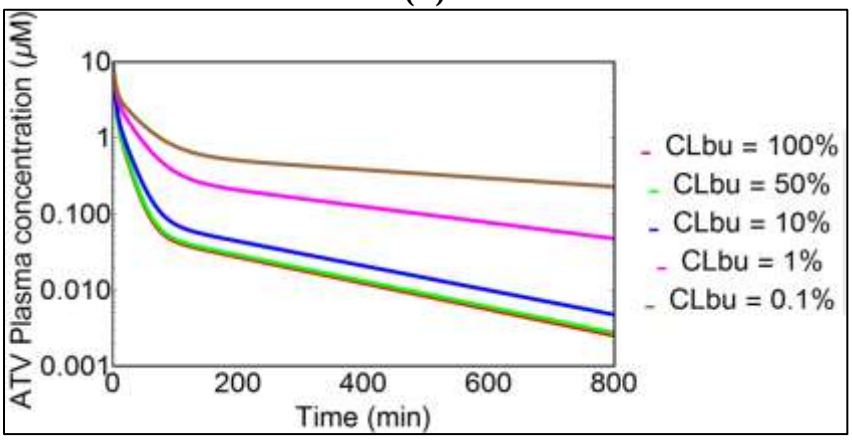

(B)

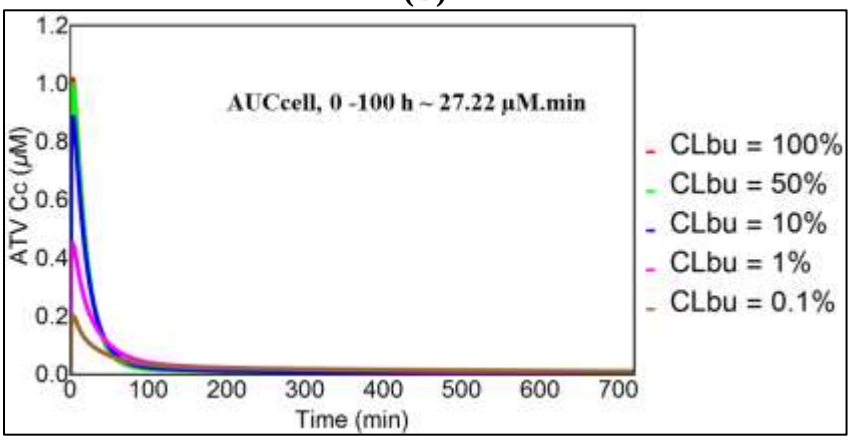

Figure 6.12 Sensitivity analysis with CL_{bu} for ATV. Simulated (A) plasma and (B) unbound cell concentration-time profiles for CL_{bu} = 100% (red), 50% (green), 10% (blue), 1% (pink) and 0.1% (brown) of the actual value of 24.4 L/min

Decrease in CL_{bu} increased the plasma concentrations and decreased the unbound cell concentrations of ATV. Decreasing the CL_{bu} from 100% (24.4 L/min) to 50% (12.2 L/min) resulted in a marginal increase in plasma concentrations and a corresponding small decrease in unbound cell concentrations. Decreasing the CL_{bu} from 50% to 10% resulted in a larger increase in plasma concentrations as compared to the increase obtained upon reducing the CL_{bu} from 100% to 50%. Similar trend in decrease in ATV unbound cell concentration was observed. Much larger effects on plasma and cell concentrations were observed when CL_{bu} was decreased from 10% to 1 and 0.1%. More than 100-fold increase in plasma exposure and a 5-fold lower unbound cell C_{max} was observed when CL_{bu} was decreased from 100% to 0.1%. However, the cell exposure remained unchanged irrespective of the CL_{bu} value. The AUC_{cell} from 0 to 100 hours was approximately equal to 27.22 µM.min from CL_{bu} = 0.1% to 100%.

6.4.3 PK studies with BOS

BOS demonstrated multi-compartment disposition behavior from observation of the PK profile. Compartmental models described in Fig 6.1 (2-C) and Fig 6.2 (3-C) were tested for BOS. The model fitted PK profiles for BOS alone along with the residual analysis plots are shown in Fig 6.13 and 6.14 for a 2-C and 3-C model, respectively.

(A)

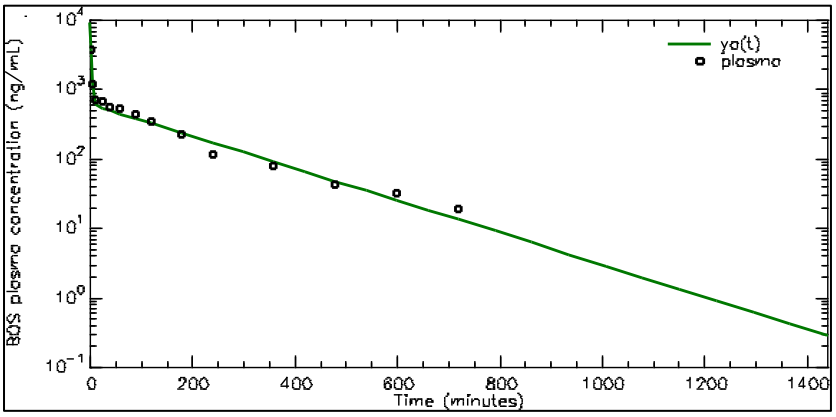

(B)

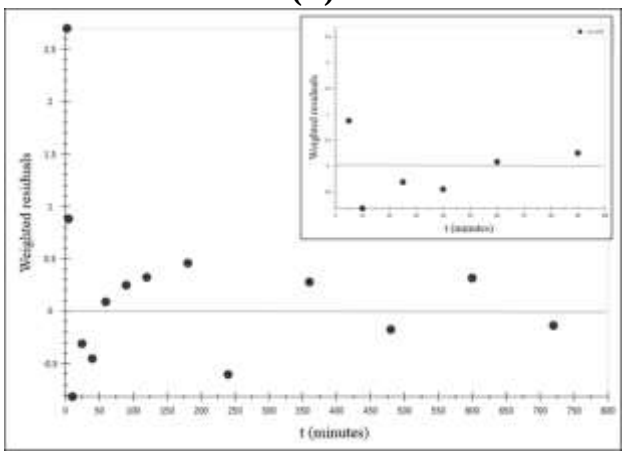

Figure 6.13 2-C model analysis of BOS PK data. (A) BOS PK profile predicted by 2-C model (green line) overlaid on experimental PK data (Open squares) (B) Residual analysis for 2-C model, inset shows residual analysis from 0 – 100 min.

(A)

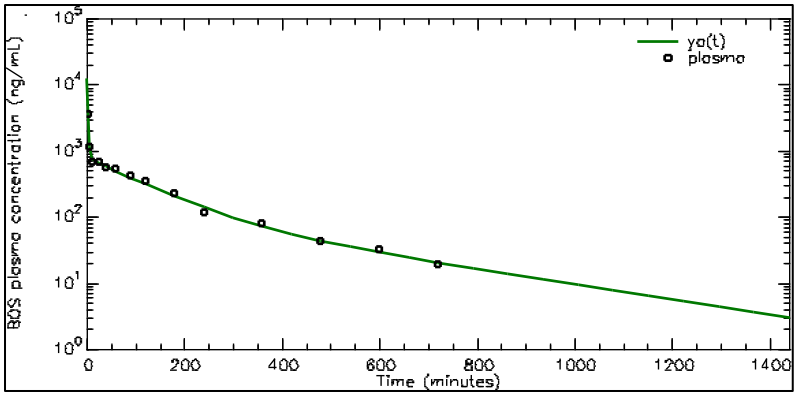

(B)

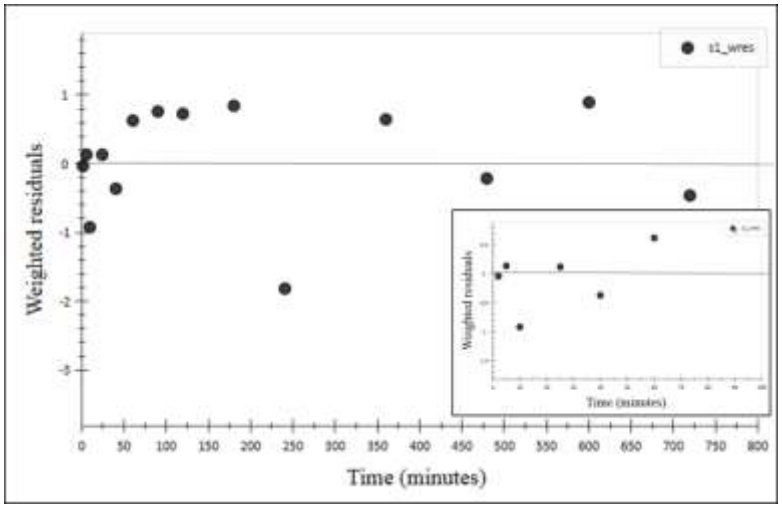

Figure 6.14 3-C model analysis of BOS PK data. (A) BOS PK profile predicted by 2-C model (green line) overlaid on experimental PK data (Open squares) (B) Residual analysis for 3-C model, inset shows residual analysis from 0 – 100 min.

Both, the 2-C and 3-C models well predicted the concentration-time profile of BOS. The AIC for the 3-C model (4.95) was lesser than that for 2-C model (5.68). However, the difference in the AICs was not conclusive. Residual analysis demonstrated random residual distribution for both models. The PK parameters predicted by both models were not significantly different. A 3-C model was required to explain the experimental data for BOS+ABT group. The $t_{1/2}$ obtained from 3-C model was significantly greater than that by a 2-C model. The compartmental analysis of the BOS + ABT data are presented in detail in Appendix C.

Fig 6.15 shows the experimental results for BOS PK in absence and presence of RIF and/or ABT.

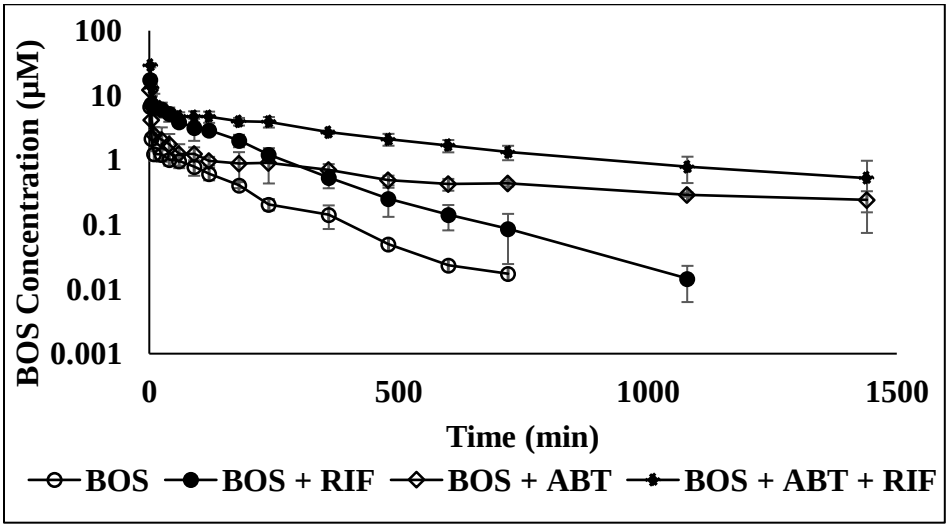

Figure 6.15 Effect of inhibition of uptake transport by RIF and inhibition of metabolism by ABT on BOS PK. BOS: n=3, BOS +RIF: n=3, BOS + ABT: n=3, BOS + ABT + RIF: n=3; Data are presented as mean ± SD.

Table 6.5 Compartmental analysis of BOS PK

	CL (mL/min)	V_{ss} (mL)	$t_{1/2}$ (min)
BOS	8.1 ± 0.6	801 ± 97	130 ± 9
BOS + RIF	1.86 ± 0.1***	177 ± 12.5***	116 ± 4
BOS + ABT	1.9 ± 0.16***	758 ± 80	479 ± 65***
BOS + ABT + RIF	0.61 ± 0.018***, ##	199 ± 8***, ###	389± 6***, #

Groups significantly different than the BOS group (*) and BOS + ABT group (#) are marked; Data are presented as mean ± SD
Statistical analysis was performed with one-way analysis of variance followed by posthoc Tukey's test, *$p < 0.05$, ***$p < 0.001$, #$p < 0.05$, ##$p < 0.01$, ###$p < 0.001$

The metabolites of BOS were not detectable in plasma. A similar observation has been made by Treiber and co-workers (Treiber et al., 2004). The B/P ratio of BOS is 0.6 (Gehin et al., 2016) indicating that the drug has minimal partitioning into red blood cells. The mean CL of BOS corrected using the B/P ratio of 0.6 was 8.1 ± 0.6 mL/min (Table 6.5). RIF treatment significantly decreased the CL of BOS by 4.3 fold due to uptake inhibition. The mean V_{ss} of BOS was also decreased significantly by 4.5 fold with RIF treatment, possibly since the distribution of the drug was now limited due to uptake inhibition. Since RIF treatment decreased both CL and V_{ss} of BOS, the $t_{1/2}$ remained unchanged (130 ± 9 min and 116 ± 4 min, without and with RIF, respectively). Inhibition of cyp mediated metabolism with ABT decreased the mean CL of BOS by 4.1 fold from 8.1 ± 0.6 mL/min to 1.9 ± 0.16 mL/min, however, the V_{ss} was not affected. Since the CL decreased and the V_{ss} was unaffected, the $t_{1/2}$ in this group increased by 3.7 fold from 130 ± 9 min to 479 ± 65 min, as compared to the BOS only group. The systemic CL and V_{ss} of BOS decreased by 13.3 -fold and 4 -fold, respectively, when both uptake and

metabolism of BOS were inhibited when compared to the BOS only group. This resulted in a 3 -fold increase in the $t_{1/2}$ of BOS as compared to the BOS only group. Within the ABT treated groups, a significant decrease was observed in both CL, V_{ss} and $t_{1/2}$ of BOS with RIF treatment possibly due to uptake inhibition. Due to the complicated results obtained with ATV, metabolism inhibition for BOS was not tested with KETO.

6.4.4 Prediction of BOS intracellular unbound concentration

The model fitted concentration-time profiles generated by using BOS plasma PK data as an input for the 2-C hybrid model depicted in fig 6.4 are shown in fig 6.16 and 6.17. Of the scaling factors tested (1 to 2.25), the scaling factor of 1.75 best explained the experimental data. Also, the best R^2 was obtained for both BOS and BOS + RIF groups when this scaling factor of 1.75 was used. The model predicted BOS plasma PK data accurately, both for the BOS only and BOS + RIF groups. The R^2 for fitting was 0.975 and 0.98 in absence and presence of RIF, respectively. The predicted unbound cell concentration of BOS demonstrated a sharp increase followed by gradual decrease in both groups. The decline in unbound cell concentrations was parallel to the decline in plasma concentrations. The maximum peak unbound BOS concentration in the cell was ~ 0.1 µM in the BOS only group and 0.125 µM in the BOS + RIF group. Similar to ATV, the total BOS plasma concentration was higher than the unbound cell concentration at all times. However, the unbound cell concentration of BOS was consistently higher than the unbound plasma concentration after C_{max} for the unbound cell concentrations (f_{up} = 0.01086). The parameter estimates for distribution rate constants, volume of central compartment and fraction of viable intrinsic uptake clearance are summarized in table

6.6. The volume of the central compartment for BOS decreased from 0.059 liters to 0.024 liters upon treatment with RIF. The modeling exercise with BOS + RIF group resulted in an estimate of 0.022 for "A", the fraction of viable intrinsic clearance. The results for modeling the BOS + RIF data without assuming inhibition of apical efflux of BOS by RIF are presented in detail in appendix D. It was observed that when inhibition of apical efflux of BOS with RIF was not assumed, nonreal estimates for k12 and volume of central compartment were obtained.

Table 6.6 Parameter estimates obtained by analysis of BOS data with the 2-C hybrid model

Parameter	**Group**	
	BOS only	**BOS + RIF**
k_{12} (min^{-1})	0.3 ± 0.06	0.44 ± 0.2
k_{21} (min^{-1})	0.04 ± 0.011	0.087 ± 0.022
$V_{central}$ (L)	0.059 ± 0.02	0.024 ± 0.012
A	-	0.022 ± 0.011

Data are represented as mean ± standard error

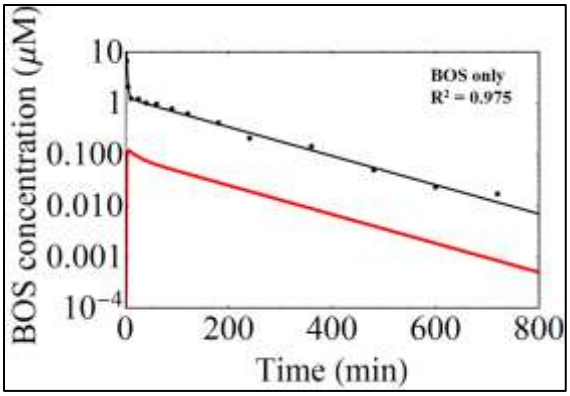

Figure 6.16 Fitted BOS concentration-time profiles for BOS only group using the 2-C hybrid model. Solid circles are experimental data for plasma concentrations, black solid line represents model fitted plasma profile, and red solid line represents model predicted unbound intracellular concentration-time profile.

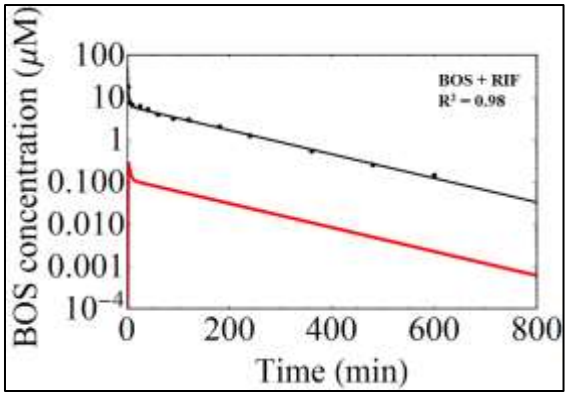

Figure 6.17 Fitted BOS concentration-time profiles for BOS + RIF group using the 2-C hybrid model. Solid circles are experimental data for plasma concentrations, black solid line represents model fitted plasma profile, and red solid line represents model predicted unbound intracellular concentration-time profile.

The results for sensitivity analysis with CL_{bu} are summarized in fig 6.18. Decrease in CL_{bu} increased the plasma concentrations and decreased the unbound cell concentrations of BOS. Decreasing the CL_{bu} from 100% (21.95 L/min) to 50% (11 L/min) resulted in increase in plasma concentrations and corresponding decrease in unbound cell concentrations. Decreasing the CL_{bu} from 50% to 10% resulted in further increase in plasma concentrations and decrease in unbound cell concentrations. Decreasing the CL_{bu} from 10% to 1% resulted in a smaller increase in plasma concentrations as compared to the increase obtained upon reducing the CL_{bu} from 100% to 50% or 50% to 10%. Similar trend in decrease in BOS unbound cell concentration was observed. Changing CL_{bu} from 1% to 0.1% neither affected the plasma concentrations, nor the unbound cell concentrations of BOS. Similar to ATV, the cell exposure remained unchanged irrespective of the CL_{bu} value. The AUC_{cell} from 0 to 100 hours was approximately equal to 14.51 µM.min from CL_{bu} = 0.1% to 100%.

(A)

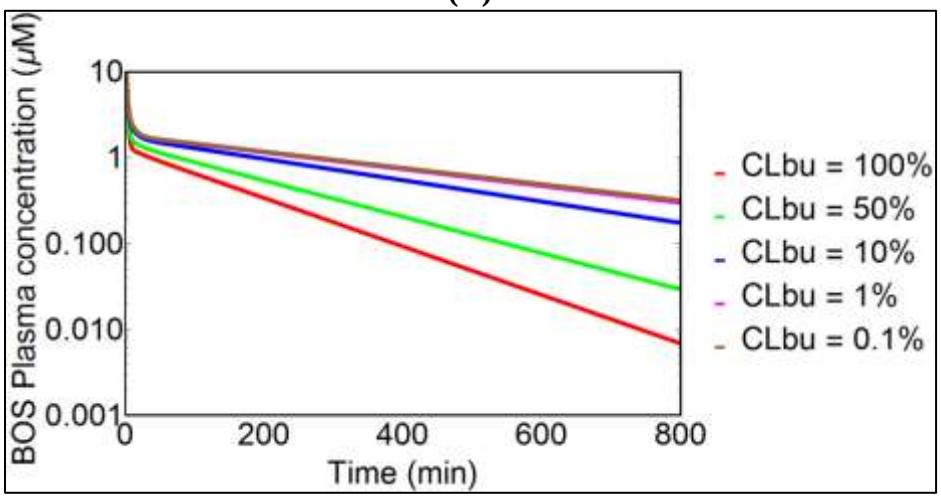

(B)

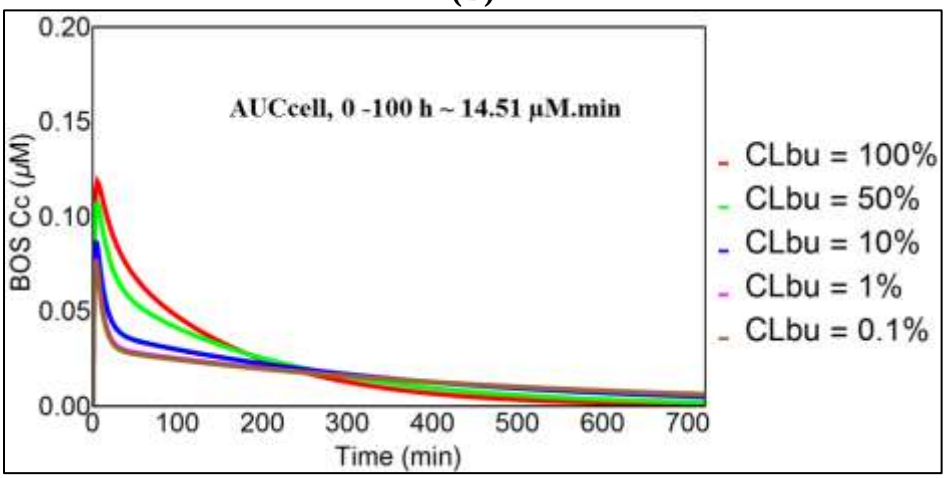

Figure 6.18 Sensitivity analysis with CL_{bu} for BOS. Simulated (A) plasma and (B) unbound cell concentration-time profiles for CL_{bu} = 100% (red), 50% (green), 10% (blue), 1% (pink) and 0.1% (brown) of the actual value of 21.95 L/min

The impact of inhibition of CL_{bu} on its contribution to the net uptake clearance for both ATV and BOS is summarized in table 6.7. The net intrinsic uptake clearance, defined as a sum of the active clearance and passive diffusion, decreased with inhibition of active uptake. The decrease was consistent from 0% to 99.9% inhibition (or 100% to 0.1% viable CL_{bu}) for ATV, while the decrease plateaued for BOS at 99% inhibition. For ATV the fractional contribution of CL_{bu} towards this total intrinsic clearance approximated 1 until 90% inhibition (10% viable CL_{bu}), and decreased drastically with any further inhibition. For BOS, the fractional contribution of CL_{bu} to net uptake clearance decreased consistently from 100% viable CL_{bu} to 0.1% viable CL_{bu}.

Table 6.7 Effect of inhibition of active uptake of ATV and BOS on its contribution to the total clearance

	ATV			**BOS**		
CL_{bu}* (L/min)	24.4			21.95		
CL_i * (L/min)	0.155			12.54		
$CL_d = CL_i/2$ (L/min)	0.0775			6.25		
	% viable CL_{bu}	**Fractional contribution of CL_{bu} to net uptake clearance**	**Net intrinsic uptake clearance (L/min) (viable CL_{bu} + CL_d)**	**% viable CL_{bu}**	**Fractional contribution of CL_{bu} to net uptake clearance**	**Net intrinsic uptake clearance (L/min) (viable CL_{bu} + CL_d)**
	100%	0.997	24.47	100%	0.77	28.2
	50%	0.96	12.27	50%	0.63	17.22
	10%	0.955	2.51	10%	0.26	8.44
	1%	0.76	0.32	1%	0.034	6.47
	0.1%	0.239	0.10	0.1%	0.0034	6.27

*from tables 6.1 and 6.2

6.5 Discussion

Drug transporters can complicate drug disposition, prediction of PK properties, and safety and efficacy profiles of drugs. Evaluating transporter enzyme interplay is crucial in understanding the disposition of drugs. Inhibition of drug transporters versus inhibition of drug metabolism can have different effects on drug PK and intracellular drug disposition. Semi-physiological or hybrid PK models have been previously used to study DDIs (Quinney et al., 2009; Zhang et al., 2010). The current chapter summarizes the PK studies performed to test the effect of active uptake versus metabolism on the PK of ATV and BOS. Data from PK studies were used as input for the semi-physiological model to predict the unbound intracellular concentrations and study the effect of inhibition of active uptake.

Inhibition of active uptake of ATV decreased the clearance because uptake is the rate limiting step in the disposition of ATV (Watanabe et al., 2009a). Also, since the uptake is inhibited, the drug distribution in the peripheral compartments is also decreased. Thus it is expected that the steady state volume of ATV should also decrease. However, the decrease in the mean V_{ss} upon RIF dosing was not statistically significant since the error in estimation of V_{ss} was high (Table 6.3). Unchanged $t_{1/2}$ of ATV upon inhibition of uptake with RIF could be explained by decrease in both clearance and V_{ss} of the drug.

Inhibition of ATV metabolism by ABT resulted in highly variable profiles (Fig 6.8). The clearance and V_{ss} values obtained from these profiles bracketed the clearance value from ATV only group. Only experiment 3 resulted in a clearance value lower than the ATV

only group. This phenomenon can have multiple possible explanations. The variability of experimental data could result from batch to batch variability in the ABT purchased. ABT is a very potent nonspecific suicidal CYP inhibitor and may affect CYPs involved not only in the metabolism of drugs, but also the ones involved in the maintenance of normal physiology. Hence the variable effect of ABT on ATV PK could also be an indirect effect resulting from interference with one or more normal physiological functions. Poorly water soluble drugs can result in highly variable PK profiles due to precipitation. This seems unlikely in case of ABT since it has reasonable water solubility (25 mg/mL). Moreover, if precipitation of ABT were actually occurring, there would be less or no inhibition of ATV metabolism instead of decreased exposure. Therefore, the variable effect of ABT on ATV PK appears to be related to the complex nature of ABT. Previous studies optimizing ABT treatment regimen in rats recommend pretreatment with ABT 2 hours before administration of the drug of interest (Balani et al., 2002; Parrish et al., 2016). These studies were optimized with the cyp3a probe substrate MDZ. It is possible that the treatment regimen used in the current study for ATV may not be appropriate. Instead, multiple dosing with ABT to ensure complete inactivation of the enzymes could be performed in the future. Glucuronidation has also been reported as a minor route of ATV metabolism (Prueksaritanont et al., 2002; Goosen et al., 2007). In absence of cyp mediated metabolism, it is possible that an alternative pathway could be taking over at a higher efficiency resulting in increased clearance. It would be helpful to quantitate the hydroxy metabolites of ATV in the future to confirm the inhibition of cyp mediated metabolism.

The clearance of ATV + KETO group was not significantly different than the ATV only group (Table 6.3). KETO has been shown to be an inhibitor of cyp3a mediated testosterone metabolism in rat liver microsomes (Eagling et al., 1998). It was observed from the liver perfusion data with KETO perfusions that KETO is somehow assisting the uptake of ATV (Chapter 3, section 3.5.5). A similar phenomenon could be occurring in the in vivo PK experiments with KETO, resulting in masking the metabolism inhibition effect of KETO. The treatment regimen for inhibition of metabolism with KETO has been chosen based on a literature report for similar experiment with ATV in mice (Chang et al., 2014). Another possibility for unchanged clearance in the KETO group as compared to the ATV only group is that the chosen dosing regimen for metabolism inhibition by KETO is not appropriate for rats. The significant decrease in clearance upon concomitant administration of KETO and RIF or ABT and RIF could have resulted from inhibition of uptake clearance by RIF.

Using the PK data as an input for the 3-C hybrid model described in fig 6.3 indicated that the model predicted maximum unbound intracellular ATV concentrations in the presence and absence of RIF were not different (~ 1 µM). The sensitivity analysis performed for CL_{bu} indicated that the inhibition of intrinsic active uptake clearance from 100% viable clearance to 10% viable clearance results in minimal change in both plasma and unbound cell concentrations for ATV. This explains the similar ATV C_{max} obtained for unbound intracellular ATV concentration in presence and absence of RIF, since the parameter estimate for the fraction of viable intrinsic active uptake clearance ("A") was 6.9. This means that even in presence of RIF, 6.9% active uptake clearance is still viable. The

reason there is minimal change in plasma and unbound cell concentrations from 100% and 10% viable active uptake clearance is the relative magnitudes of the intrinsic uptake clearance (~24 L/min) and the blood blow (~17.5 mL/min). No matter how high the magnitude of the intrinsic uptake clearance is, the blood flow is restricting the uptake of ATV into the cell, resulting in a certain cell concentration. Therefore, the inhibition of uptake will not make a difference in this case unless the inhibition occurs to such an extent that the intrinsic active uptake clearance is comparable to the blood flow. Thus, in the +RIF group, even though 93.1% of the intrinsic uptake clearance was inhibited, a 6.9% was still viable, and this value is still higher than the blood flow in this group. Therefore, no change in the unbound intracellular ATV concentrations can be seen (Fig 6.11), even though the plasma exposure of ATV in this group has increased (clearance significantly decreased). Therefore, increase in plasma concentrations of uptake transporter substrates may not necessarily imply a decrease in unbound cell concentrations. Hence, interpretations regarding the effect on intracellular pharmacological targets or DDIs should be made with caution. In case of strong uptake substrates like ATV, in order to achieve complete inhibition of active uptake, a very high concentration of the perpetrator may be required. Toxicity limitations may never allow testing of uptake perpetrator concentrations high enough to completely inhibit active uptake of drugs like ATV. Hence, drug interactions due to decreased unbound cell concentrations may not be a concern for such drugs. However, increased plasma exposure could result in extra-hepatic drug interactions like rhabdomyolysis in case of statins. It can be seen from fig 6.12 B that the C_{max} of the unbound ATV cell concentrations

decreases at CL_{bu} values of 1% and more so for 0.1%. However, the overall exposure of the cell is not affected irrespective of the percentage of viable CL_{bu} (AUC ~ 27.22 µM.min). This is because for drugs like statins, if liver is the only eliminating organ, then DDIs with uptake transporter inhibitors can result in decreased unbound cell C_{max} and the drug will gain entry to the cell slower than that in the absence of the perpetrator of uptake transport. However, all the drug will eventually enter the cell to be eliminated therefrom, resulting in unchanged exposure. Similar observation has also been made by other groups (Patilea-Vrana and Unadkat, 2016).

For uptake inhibition studies with BOS using RIF, significant decrease in clearance of BOS could be explained by the inhibition of uptake mediated clearance of the compound (Fig 6.15/Table 6.5). The decrease in V_{ss} is possibly due to limitation in the distribution of the compound into tissues when uptake was not inhibited. Since both clearance and V_{ss} decreased significantly, there was no change in the $t_{1/2}$, which is defined as a function of both clearance and volume of distribution of a drug. Inhibition of metabolism by ABT demonstrated a similar decrease in clearance of BOS as obtained by uptake inhibition with RIF (Fig 6.15, Table 6.5), indicating that active uptake and metabolism are both crucial to the disposition of this drug. Concomitant inhibition of uptake transport and metabolism by both ABT and RIF demonstrated an additive effect in the decrease in clearance. Also, the decrease in V_{ss} in this group was similar to that observed in the BOS + RIF group (Table 6.5), indicating that this decrease is due to inhibition of active uptake.

Unlike ATV, BOS followed a 2-compartment model for all groups except BOS + ABT group. This could be due to the differences in lipophilicities of the two drugs. ATV is

more lipophilic than BOS. The measured log P of ATV and BOS is 5.7 and 3.7, respectively (https://www.drugbank.ca/drugs/DB01076, accessed on 03/13/2017; https://www.drugbank.ca/drugs/DB00559 accessed on 03/13/2017). Recall from chapter 4 that for ATV, the fraction diffusing back from the bile compartment was smaller (0.03) than BOS (0.2) (Chapter 4, section 4.4.4). Therefore, ATV may distribute deeper and more extensively in the tissues as compared to BOS. Thus an additional compartment was required to explain ATV PK as compared to BOS. The 3-C behavior of the BOS + ABT group could be explained by the possibility that the inactivation of cyps by ABT is not complete yet, resulting in the appearance of a third phase.

Similar to ATV, unbound intracellular BOS concentrations were determined using the PK data as an input for the 2-C hybrid model described in fig 6.4. Unlike ATV, the model predicted maximum unbound intracellular BOS concentrations in the presence of RIF (~ 0.125 µM) were slightly higher than that in the absence of RIF (~ 1 µM) (Fig 6.16, 6.17). This could be explained by the lower apical efflux clearances used in the RIF treated group as compared to BOS only group. Lower apical efflux clearances were used assuming that RIF causes inhibition of apical efflux clearance of BOS, as was observed with the liver perfusion data with RIF co-perfusions. The failure of the modeling exercise without apical efflux inhibition to give real parameter estimates further supports the hypothesis that apical efflux is indeed occurring with RIF. Similar to ATV, the overall BOS exposure of the cell is not affected irrespective of the percentage of viable CL_{bu} (AUC ~ 14.51 µM.min), for reasons similar to those described for ATV.

The sensitivity analysis performed for CL_{bu} indicated that the disposition of BOS is sensitive to inhibition of active uptake until the CL_{bu} value reaches 1% of the actual intrinsic clearance (Fig 6.18). This is in contrast to the observation for ATV, where the disposition was relatively insensitive between CL_{bu} values of 10% and 100% (Fig 6.12). This difference in sensitivity for CL_{bu} by ATV and BOS may be due to the different diffusional clearances into membrane (CL_i ~ 0.15 L/min for ATV versus ~ 12.5 L/min for BOS), although the CL_{bu} values are comparable (~ 24 L/min for ATV versus ~26 L/min for BOS).

In case of ATV, the fractional contribution of active uptake clearance towards total clearance is approximately 1 when active uptake is between 100% viable and 10% viable, since the diffusional clearance contributes very little to the uptake of ATV (Table 6.7). When the active uptake is 99% inhibited (i.e. 1% viable), this contributing fraction decreases to 0.76. Thus, of the total hepatic clearance, 76% is contributed by active uptake and 24% by passive diffusion. With further inhibition to 99.9% (or 0.1% viable CL_{bu}), the fractional contribution of active uptake further decreases to 0.24. Since the contribution of the inefficient pathway (diffusional clearance) in the uptake of ATV increases, the efficiency of the overall uptake process decreases, thus decreasing the clearance and increasing the exposure of ATV. However, this is not the case until 0 to 90% CL_{bu} inhibition (or when CL_{bu} is 100 to 10% viable), since active uptake is still an equal contributor in the clearance.

In case of BOS, the fractional contribution of active uptake clearance towards total clearance is 0.77 when active uptake is 100% viable. This fraction decreases to 0.63,

0.26, 0.034 and 0.0034 as the viable intrinsic uptake clearance decreases to 50%, 10%, 1% and 0.1% of the original value (original CL_{bu} = 21.95 L/min). Thus it can be seen that in contrast to ATV, the fractional contribution of active uptake decreases significantly with any degree of inhibition of this process. As a result the plasma concentrations become very sensitive to inhibition of active uptake at high CL_{bu} values. The net uptake including passive and active clearances does not differ much when CL_{bu} is 1% viable (net uptake clearance = 6.47 L/min) versus when CL_{bu} is 0.1% viable (net uptake clearance = 6.27 L/min). Thus the exposure of BOS does not change with an inhibition of active uptake higher than 99%.

6.6 Conclusion

In vivo PK studies were performed to study the effect of metabolism and uptake on disposition of ATV and BOS. Inhibition of active uptake resulted in decreased clearances for both drugs. Inhibition of metabolism of ATV with ABT resulted in highly variable PK profiles, while with KETO resulted in unchanged clearance. Concomitant inhibition of metabolism and uptake transport of ATV resulted in decrease in clearance equivalent to that obtained with inhibition of active uptake. Inhibition of BOS metabolism with ABT resulted in significant decrease in clearance of BOS, while V_{ss} was unaffected, since inhibition of metabolism does not alter drug distribution. Concomitant inhibition of metabolism and uptake of BOS resulted in additive effect on decrease in clearance, compared to inhibition of each pathway alone. A semi physiological modeling approach was successfully used to predict unbound intracellular ATV and BOS concentrations using PK data as input. The results from the modeling exercise indicated that increase in

plasma concentrations may not always result in decrease in unbound cell concentrations. If liver is the only eliminating organ, decrease in intrinsic uptake clearance due to DDIs with uptake inhibitors will not change the overall cell exposure (AUC) of the drug, however, the unbound C_{max} may decrease.

CHAPTER 7: CONCLUSIONS AND FUTURE DIRECTIONS

This chapter summarizes the studies conducted to predict unbound intracellular ATV and BOS concentrations, and to study the effect of metabolism and transport on these predictions. Liver perfusion and in vivo PK experiments were conducted in rats for ATV and BOS in presence of perpetrators of drug metabolism and transport. The 5-C explicit membrane model was modified to describe in situ liver disposition and was connected to compartmental mammillary models to describe liver disposition upon intravenous dosing of ATV and BOS. The liver perfusion and in vivo PK data were used as inputs for these modeling exercises.

Robust LC-MS/MS methods were required for analysis of ATV, BOS and their metabolites from complex biological matrices. LC-MS/MS based bioanalytical methods were developed and validated for quantitation of ATV, BOS and their metabolites i.e. 2-OH ATV, 4-OH ATV, OH-BOS and OH-DM BOS in perfusate and biological matrices like liver homogenate, bile, plasma and rat liver microsomal suspension in buffer.

In order to study the effect of metabolism and transport on ATV and BOS liver concentrations, liver perfusion studies were conducted in Sprague Dawley rats. RIF caused a dose-dependent decrease in ATV liver concentrations due to inhibition of active uptake. Passive diffusion studies for ATV at 4°C showed that there was minimal drug partitioning into liver at this temperature as compared to studies conducted with concomitant inhibition of metabolism and transport at 37°C, possibly due to decrease in membrane fluidity at lower temperatures. Hence, data obtained from passive diffusion

studies conducted at 4°C should be interpreted with caution. However, RIF inhibited ATV metabolism and possibly also inhibited BOS apical efflux. Thus, careful choice of inhibitors for specific pathways of interest is important. From the present results, active uptake appeared to the more important for the disposition of ATV as compared to metabolism. Inhibition of ATV active uptake by RIF demonstrated a higher increase in the outflow perfusate concentrations as compared to inhibition of metabolism. The concentration of RIF used in the present study did not result in a significant decrease in liver concentration of ATV. Inhibition of metabolism by RIF as seen in the decreased metabolite-to parent ratios in the ATV+RIF group as compared to the ATV only group, could explain this lack of change. Pre-treatment with ABT resulted in significant decrease in ATV liver concentrations, further confirming the possibility of metabolism inhibition by RIF. Metabolism inhibition studies for ATV with KETO resulted in complicated data that could be explained by interference on ATV transport by KETO. Inhibition of active uptake increased the BOS outflow perfusate concentrations and decreased the amount of BOS recovered in the bile, although the BOS liver concentrations were unaffected. This could be a result of inhibition of apical efflux of BOS by RIF, in addition to inhibition of active uptake. ABT treatment resulted in no change in BOS liver concentrations, probably due to diversion of BOS metabolism to other non-cyp3a1 mediated pathways. Due to the complicated nature and limited mechanistic understanding of the experiments conducted with KETO for ATV and with ABT for BOS, these datasets could not be used for modeling. It was also observed that in

the liver perfusion experiments, BOS and RIF resulted in increased bile flow, possibly due to stimulation of mrp2 mediated bile salt independent bile flow.

The 5-C model was successfully used along with the liver perfusion data to predict unbound intracellular concentrations of ATV and BOS. A step-wise modeling approach was used to parameterize clearance for a single disposition pathway at a time, for ATV. The model predicted 8-fold higher unbound ATV concentrations at steady state in presence of active uptake as compared to in absence of active uptake, supporting the generally accepted idea that unbound intracellular concentrations for uptake transporter substrates could be several fold higher than their unbound plasma concentrations. Inhibition of metabolism predicted only a 2.3 fold increase in the unbound ATV concentrations. BOS disposition was more complicated than ATV since an additional apical efflux clearance from the cell was also involved. Moreover, as mentioned previously, ABT did not efficiently inhibit BOS metabolism completely due to probable involvement of multiple metabolic pathways that still remained viable in presence of ABT. Hence, BOS data from ABT treated animals could not be used for modeling. Thus, multiple parameters like CL_m, CL_{aec}, CL_{aem} and back diffusion from bile "a" were required to be fixed, making the modeling more challenging. The model predicted only slightly lower unbound cell concentrations in the presence of RIF, even when active uptake was inhibited in the modeling exercise. This was probably due to inhibition of apical efflux by RIF. Once again, this highlights the importance of "clean" inhibitors, i.e. inhibitors specifically targeting only the pathway of interest. Since it is not possible to experimentally measure the unbound cell concentration, it can be argued whether the

predictions resulting from these modeling exercises are real. The model accurately predicted the outflow perfusate concentrations, liver concentrations and amount of ATV and BOS recovered in the bile, thus increasing confidence in the predicted unbound intracellular concentrations.

BOS appeared to be a weak inducer of cyp3a1 activity in rats from in vivo studies. The choice of in vivo BOS treatment regimen was found to be critical to see the induction effect. Less frequent administration of lower doses for extended periods of time could help avoid confounding effects of competitive inhibition of the probe substrate by the perpetrator used for the induction study. Initial increase followed by a decrease in activity of cyp3a1 during in vitro induction experiments could be saturation of metabolism or toxicity at higher BOS concentrations.

Inhibition of active uptake in vivo with RIF decreased the systemic clearance of both ATV and BOS and decreased the V_{ss} of BOS due to uptake inhibition. Inhibition of metabolism of ATV by ABT resulted in highly variable, complicated data that could not be clearly explained, thus limiting the use of these data for future modeling exercises. ABT treatment decreased the clearance of BOS to a similar extent as that observed with inhibition of active uptake by RIF. This indicates that in addition to active uptake, metabolism is also an equally important pathway in the disposition of BOS. ABT treatment resulted in a tri-exponential plasma profile for BOS, whose disposition could otherwise be described by a bi-exponential profile. This probably indicates that the ABT mediated-enzyme inactivation is not complete for the duration of the PK experiment for BOS. In summary, ABT appeared to be a very complicated perpetrator for ATV

disposition in vivo and for BOS disposition in both liver perfusion and in vivo PK experiments.

The modeling exercise indicated that the relative magnitudes of active uptake clearance, diffusional clearance into membranes and the blood flow are important determinants of the disposition of a drug. Even though a perpetrator inhibits the intrinsic active uptake of a victim drug, if the inhibition is not complete, and the residual uptake clearance is higher in magnitude than the blood flow to the organ, the unbound cell C_{max} may not be different as compared to when the active uptake was not inhibited. Thus, in the present study, although RIF elevated the plasma concentrations of ATV, the unbound cell C_{max} was not different. The unbound cell C_{max} was slightly higher for BOS, perhaps due to inhibition of apical efflux of this drug in the RIF treated group. The sensitivity of active uptake clearance towards plasma concentrations is also dependent on the magnitude of this parameter compared to the diffusional clearance of the drug. Therefore, a similar extent of inhibition of active uptake clearance can have differential impact on the plasma and cell exposure of various drugs. In summary, the effect of inhibition of active uptake on unbound cell concentrations is governed by 1) the magnitude of the viable active uptake clearance relative to the organ blood flow and 2) the magnitude of the viable active uptake clearance relative to the organ passive diffusion clearance, assuming that the perpetrator is not inhibiting any other disposition pathway.

In summary, transporters complicate the understanding of drug disposition. Liver perfusion is a good experimental model to study hepatic disposition of drugs. Modeling

and simulation is a very powerful tool to improve the mechanistic understanding of drug disposition.

Future studies

Efficient inhibition of cyp mediated ATV metabolism provided valuable data for step-wise modeling using the 5-C model. However, inability to generate such type of data for the BOS group made the modeling challenging. The concentrations of RIF used for uptake inhibition in this project were detrimental to inhibition of other pathways like ATV metabolism or BOS apical efflux. The quality of data generated for similar future projects could be enhanced if cleaner and more specific enzyme and/or transporter inhibitors, which target only the specific pathway of interest can be used. Alternatively, knockout animal models for specific proteins of interest could also be used to address this issue. However, use of such highly sophisticated techniques could be prohibitively expensive.

Efficient inhibition of BOS metabolism could not be achieved, due to involvement of multiple enzymatic routes. Future studies could be conducted with dual inhibition of cyp2c9 and cyp3a1. Time dependent inactivation of cyp2c9 could be conducted with tienilic acid perfusions, similar to the ABT perfusion setup. RIF mediated BOS apical efflux inhibition could be confirmed by performing studies in inside-out rat mrp2 and P-gp vesicles.

From a DDI prediction perspective it would be helpful to define the transporter and enzyme interaction in the current models in a more mechanistic manner. For example, it

would be useful to define CL_{bu} as $V_{max}/(K_m+S)$. This way, mechanistic predictions for DDI can be made. It was not possible to perform this exercise in the current project since there were too many unknown parameters to begin with. But now that the magnitude of these clearance parameters is known, more granular modeling can be performed. Similar transporter and enzyme inhibition experiments can be performed in simpler and more practical systems like sandwich cultured rat hepatocytes for stepwise determination of individual clearance pathways involved in drug disposition. If IVIVC from this system is successful, then similar experiments can be performed in sandwich cultured human hepatocytes. The model can then be used to predict clinical DDIs.

REFERENCES

https://www.drugbank.ca/drugs/DB00559.

https://www.drugbank.ca/drugs/DB01076.

Adar Y, Stark M, Bram E, Nowak-Sliwinska P, Van Den Bergh H, Szewczyk G, Sarna T, Skladanowski A, Griffioen A, and Assaraf Y (2012) Imidazoacridinone-dependent lysosomal photodestruction: a pharmacological Trojan horse approach to eradicate multidrug-resistant cancers. *Cell death & disease* **3:**e293.

Akita H, Suzuki H, and Sugiyama Y (2001) Sinusoidal efflux of taurocholate is enhanced in Mrp2-deficient rat liver. *Pharmaceutical research* **18:**1119-1125.

Alrefai WA and Gill RK (2007) Bile acid transporters: structure, function, regulation and pathophysiological implications. *Pharmaceutical research* **24:**1803-1823.

Back D, Breckenridge A, Crawford F, MacIver M, Orme M, Park B, Rowe P, and Smith E (1979) The effect of rifampicin on norethisterone pharmacokinetics. *European journal of clinical pharmacology* **15:**193-197.

Backman JT, Karjalainen MJ, Neuvonen M, Laitila J, and Neuvonen PJ (2006) Rofecoxib is a potent inhibitor of cytochrome P450 1A2: studies with tizanidine and caffeine in healthy subjects. *British journal of clinical pharmacology* **62:**345-357.

Backman JT, Kyrklund C, Neuvonen M, and Neuvonen PJ (2002) Gemfibrozil greatly increases plasma concentrations of cerivastatin. *Clinical Pharmacology & Therapeutics* **72:**685-691.

Backman JT, Luurila H, Neuvonen M, and Neuvonen PJ (2005) Rifampin markedly decreases and gemfibrozil increases the plasma concentrations of atorvastatin and its metabolites. *Clinical pharmacology and therapeutics* **78:**154-167.

Bakos É, Evers R, Sinkó E, Váradi A, Borst P, and Sarkadi B (2000) Interactions of the human multidrug resistance proteins MRP1 and MRP2 with organic anions. *Molecular Pharmacology* **57:**760-768.

Balani SK, Zhu T, Yang TJ, Liu Z, He B, and Lee FW (2002) Effective dosing regimen of 1-aminobenzotriazole for inhibition of antipyrine clearance in rats, dogs, and monkeys. *Drug Metabolism and Disposition* **30:**1059-1062.

Ball SE, Maurer G, Zollinger M, Ladona M, and Vickers A (1992) Characterization of the cytochrome P-450 gene family responsible for the N-dealkylation of the ergot alkaloid CQA 206-291 in humans. *Drug Metabolism and Disposition* **20:**56-63.

Bentz J and Ellens H (2014) A structural model for the mass action kinetic analysis of P-GP mediated transport through confluent cell monolayers. *Enzyme Kinetics in Drug Metabolism: Fundamentals and Applications***:**289-316.

Black AE, Hayes RN, Roth BD, Woo P, and Woolf TF (1999) Metabolism and excretion of atorvastatin in rats and dogs. *Drug Metabolism and Disposition* **27:**916-923.

Blouin A, Bolender RP, and Weibel ER (1977) Distribution of organelles and membranes between hepatocytes and nonhepatocytes in the rat liver parenchyma. A stereological study. *The Journal of cell biology* **72:**441-455.

Bořek-Dohalský V, Huclova J, Barrett B, Němec B, Ulč I, and Jelinek I (2006) Validated HPLC–MS–MS method for simultaneous determination of atorvastatin and 2-

hydroxyatorvastatin in human plasma—pharmacokinetic study. *Analytical and bioanalytical chemistry* **386:**275-285.

Bossuyt X, Müller M, and Meier PJ (1996) Multispecific amphipathic substrate transport by an organic anion transporter of human liver. *Journal of hepatology* **25:**733-738.

Boyd RA, Stern RH, Stewart BH, Wu X, Reyner EL, Zegarac EA, Randinitis EJ, and Whitfield L (2000) Atorvastatin coadministration may increase digoxin concentrations by inhibition of intestinal P-glycoprotein-mediated secretion. *The Journal of Clinical Pharmacology* **40:**91-98.

Brown MW, Maldonado AL, Meredith CG, and Speeg K (1985) Effect of ketoconazole on hepatic oxidative drug metabolism. *Clinical Pharmacology & Therapeutics* **37:**290-297.

Chang JH, Ly J, Plise E, Zhang X, Messick K, Wright M, and Cheong J (2014) Differential effects of Rifampin and Ketoconazole on the blood and liver concentration of atorvastatin in wild-type and Cyp3a and Oatp1a/b knockout mice. *Drug Metabolism and Disposition* **42:**1067-1073.

Chapman MJ and Carrie A (2005) Mechanisms of Statin-Induced Myopathy, Am Heart Assoc.

Chiba M, Ishii Y, and Sugiyama Y (2009) Prediction of hepatic clearance in human from in vitro data for successful drug development. *The AAPS journal* **11:**262.

Choi M-K, Shin HJ, Choi Y-L, Deng J-W, Shin J-G, and Song I-S (2011) Differential effect of genetic variants of Na+-taurocholate co-transporting polypeptide

(NTCP) and organic anion-transporting polypeptide 1B1 (OATP1B1) on the uptake of HMG-CoA reductase inhibitors. *Xenobiotica* **41:**24-34.

Chu X, Korzekwa K, Elsby R, Fenner K, Galetin A, Lai Y, Matsson P, Moss A, Nagar S, and Rosania GR (2013) Intracellular drug concentrations and transporters: measurement, modeling, and implications for the liver. *Clinical Pharmacology & Therapeutics* **94:**126-141.

Chung JY, Cho JY, Yu KS, Kim JR, Oh DS, Jung HR, Lim KS, Moon KH, Shin SG, and Jang IJ (2005) Effect of OATP1B1 (SLCO1B1) variant alleles on the pharmacokinetics of pitavastatin in healthy volunteers. *Clinical Pharmacology & Therapeutics* **78:**342-350.

Cui Y, König J, and Keppler D (2001) Vectorial transport by double-transfected cells expressing the human uptake transporter SLC21A8 and the apical export pump ABCC2. *Molecular Pharmacology* **60:**934-943.

Cusato J, Allegra S, De Nicolò A, Boglione L, Fatiguso G, Abdi AM, Cariti G, Di Perri G, and D'Avolio A (2015) Intracellular accumulation of boceprevir according to plasma concentrations and pharmacogenetics. *International journal of antimicrobial agents* **45:**657-661.

De Duve C, De Barsy T, Poole B, and Tulkens P (1974) Lysosomotropic agents. *Biochemical pharmacology* **23:**2495IN12511-12510IN32531.

De Montellano PO and Mathews JM (1981) Autocatalytic alkylation of the cytochrome P-450 prosthetic haem group by 1-aminobenzotriazole. Isolation of an NN-bridged benzyne-protoporphyrin IX adduct. *Biochemical Journal* **195:**761-764.

DeGorter M, Xia C, Yang J, and Kim R (2012) Drug transporters in drug efficacy and toxicity. *Annual review of pharmacology and toxicology* **52:**249-273.

Dickinson BD, Altman RD, Nielsen NH, and Sterling ML (2001) Drug interactions between oral contraceptives and antibiotics. *Obstetrics & Gynecology* **98:**853-860.

Dingemanse J and van Giersbergen PL (2004) Clinical pharmacology of bosentan, a dual endothelin receptor antagonist. *Clinical pharmacokinetics* **43:**1089-1115.

Dollery C (2013) Intracellular drug concentrations. *Clinical Pharmacology & Therapeutics* **93:**263-266.

Duvvuri M and Krise JP (2005) Intracellular drug sequestration events associated with the emergence of multidrug resistance: a mechanistic review. *Front Biosci* **10:**1499-1509.

Eagling VA, Tjia JF, and Back DJ (1998) Differential selectivity of cytochrome P450 inhibitors against probe substrates in human and rat liver microsomes. *British journal of clinical pharmacology* **45:**107-114.

Eckford PD and Sharom FJ (2006) P-glycoprotein (ABCB1) interacts directly with lipid-based anti-cancer drugs and platelet-activating factors This paper is one of a selection of papers published in this Special Issue, entitled CSBMCB—Membrane Proteins in Health and Disease. *Biochemistry and cell biology* **84:**1022-1033.

Ellis LC, Hawksworth GM, and Weaver RJ (2013) ATP-dependent transport of statins by human and rat MRP2/Mrp2. *Toxicology and applied pharmacology* **269:**187-194.

Evers R, De Haas M, Sparidans R, Beijnen J, Wielinga P, Lankelma J, and Borst P (2000) Vinblastine and sulfinpyrazone export by the multidrug resistance protein MRP2 is associated with glutathione export. *British journal of cancer* **83:**375.

Fahrmayr C, König J, Auge D, Mieth M, Münch K, Segrestaa J, Pfeifer T, Treiber A, and Fromm M (2013) Phase I and II metabolism and MRP2-mediated export of bosentan in a MDCKII-OATP1B1-CYP3A4-UGT1A1-MRP2 quadruple-transfected cell line. *British journal of pharmacology* **169:**21-33.

Fattinger K, Funk C, Pantze M, Weber C, Reichen J, Stieger B, and Meier PJ (2001) The endothelin antagonist bosentan inhibits the canalicular bile salt export pump: a potential mechanism for hepatic adverse reactions. *Clinical Pharmacology & Therapeutics* **69:**223-231.

Floren LC, Bekersky I, Benet LZ, Mekki Q, Dressler D, Lee JW, Roberts JP, and Hebert MF (1997) Tacrolimus oral bioavailability doubles with coadministration of ketoconazole. *Clinical Pharmacology & Therapeutics* **62:**41-49.

Fouassier L, Kinnman N, Lefèvre G, Lasnier E, Rey C, Poupon R, Elferink RPO, and Housset C (2002) Contribution of mrp2 in alterations of canalicular bile formation by the endothelin antagonist bosentan. *Journal of hepatology* **37:**184-191.

Furberg CD and Pitt B (2001) Withdrawal of cerivastatin from the world market. *Trials* **2:**205.

Gallo SA, Sen A, Hensen ML, and Hui SW (2002) Temperature-dependent electrical and ultrastructural characterizations of porcine skin upon electroporation. *Biophysical journal* **82:**109-119.

Gasser R HR, Viger-Chougnet A (1995) Bosentan: metabolism Ro 47-0203 in human liver microsomes. *Basel: F HoffmannLa Roche Ltd*.

Gehin M, Sidharta PN, and Dingemanse J (2016) Bosentan Pharmacokinetics in Pediatric Patients with Pulmonary Arterial Hypertension: Comparison of Dried Blood Spot and Plasma Analysis. *Pharmacology* **98:**111-114.

Giacomini KM, Huang S-M, Tweedie DJ, Benet LZ, Brouwer KL, Chu X, Dahlin A, Evers R, Fischer V, and Hillgren KM (2010) Membrane transporters in drug development. *Nature reviews Drug discovery* **9:**215-236.

Gibbs MA, Thummel KE, Shen DD, and Kunze KL (1999) Inhibition of cytochrome P-450 3A (CYP3A) in human intestinal and liver microsomes: comparison of K i values and impact of CYP3A5 expression. *Drug Metabolism and Disposition* **27:**180-187.

Gibson D, Stern R, Abel R, and Whitfield L (1997) Absolute bioavailability of atorvastatin in man. *Pharm Res* **14:**253.

Goldman SD, Funk RS, Rajewski RA, and Krise JP (2009) Mechanisms of amine accumulation in, and egress from, lysosomes. *Bioanalysis* **1:**1445-1459.

Gomez DY, Wacher VJ, Tomlanovich SJ, Hebert MF, and Benet LZ (1995) The effects of ketoconazole on the intestinal metabolism and bioavailability of cyclosporine. *Clinical Pharmacology & Therapeutics* **58:**15-19.

Goosen TC, Bauman JN, Davis JA, Yu C, Hurst SI, Williams JA, and Loi C-M (2007) Atorvastatin glucuronidation is minimally and nonselectively inhibited by the

fibrates gemfibrozil, fenofibrate, and fenofibric acid. *Drug metabolism and disposition* **35:**1315-1324.

Gotink KJ, Broxterman HJ, Labots M, de Haas RR, Dekker H, Honeywell RJ, Rudek MA, Beerepoot LV, Musters RJ, and Jansen G (2011) Lysosomal sequestration of sunitinib: a novel mechanism of drug resistance. *Clinical Cancer Research* **17:**7337-7346.

Gottesman MM, Hrycyna C, Schoenlein PV, Germann U, and Pastan I (1995) Genetic analysis of the multidrug transporter. *Annual review of genetics* **29:**607-649.

Gottesman MM, Pastan I, and Ambudkar SV (1996) P-glycoprotein and multidrug resistance. *Current opinion in genetics & development* **6:**610-617.

Graham J and Northfield T (1987) Solubilization of lipids from hamster bile-canalicular and contiguous membranes and from human erythrocyte membranes by conjugated bile salts. *Biochemical Journal* **242:**825-834.

Greenblatt DJ, von Moltke LL, Daily JP, Harmatz JS, and Shader RI (1999) Extensive impairment of triazolam and alprazolam clearance by short-term low-dose ritonavir: the clinical dilemma of concurrent inhibition and induction, LWW.

Grub S, Bryson H, Goggin T, Lüdin E, and Jorga K (2001) The interaction of saquinavir (soft gelatin capsule) with ketoconazole, erythromycin and rifampicin: comparison of the effect in healthy volunteers and in HIV-infected patients. *European journal of clinical pharmacology* **57:**115-121.

Grube M, Köck K, Oswald S, Draber K, Meissner K, Eckel L, Böhm M, Felix SB, Vogelgesang S, and Jedlitschky G (2006) Organic anion transporting polypeptide

2B1 is a high-affinity transporter for atorvastatin and is expressed in the human heart. *Clinical Pharmacology & Therapeutics* **80:**607-620.

Guerrier M, Attili F, Alpini G, and Glaser S (2014) Prolonged administration of secretin to normal rats increases biliary proliferation and secretin-induced ductal secretory activity. *Hepatobiliary surgery and nutrition* **3:**118-125.

Hartman JC, Brouwer K, Mandagere A, Melvin L, and Gorczynski R (2010) Evaluation of the endothelin receptor antagonists ambrisentan, darusentan, bosentan, and sitaxsentan as substrates and inhibitors of hepatobiliary transporters in sandwich-cultured human hepatocytes This article is one of a selection of papers published in the two-part special issue entitled 20 Years of Endothelin Research. *Canadian journal of physiology and pharmacology* **88:**682-691.

Heimark LD, Gibaldi M, Trager WF, O'Reilly RA, and Goulart DA (1987) The mechanism of the warfarin-rifampin drug interaction in humans. *Clinical Pharmacology & Therapeutics* **42:**388-394.

Heimbach T, Lakshminarayana SB, Hu W, and He H (2009) Practical anticipation of human efficacious doses and pharmacokinetics using in vitro and preclinical in vivo data. *The AAPS journal* **11:**602.

Hennessy M and Spiers J (2007) A primer on the mechanics of P-glycoprotein the multidrug transporter. *Pharmacological research* **55:**1-15.

Herlevsen M, Oxford G, Owens CR, Conaway M, and Theodorescu D (2007) Depletion of major vault protein increases doxorubicin sensitivity and nuclear accumulation

and disrupts its sequestration in lysosomes. *Molecular Cancer Therapeutics* **6:**1804-1813.

Higgins JW, Ke AB, and Zamek-Gliszczynski MJ (2014) Clinical CYP3A inhibitor alternatives to ketoconazole, clarithromycin and itraconazole, are not transported into the liver by hepatic organic anion transporting polypeptides and organic cation transporter 1. *Drug Metabolism and Disposition* **42:**1780-1784.

Hill AV (1910) The possible effects of the aggregation of the molecules of haemoglobin on its dissociation curves. *J Physiol (Lond)* **40:**4-7.

Hillgren KM, Keppler D, Zur A, Giacomini KM, Stieger B, Cass CE, and Zhang L (2013) Emerging transporters of clinical importance: an update from the International Transporter Consortium. *Clinical Pharmacology & Therapeutics* **94:**52-63.

Hirano M, Maeda K, Shitara Y, and Sugiyama Y (2004) Contribution of OATP2 (OATP1B1) and OATP8 (OATP1B3) to the hepatic uptake of pitavastatin in humans. *Journal of Pharmacology and Experimental Therapeutics* **311:**139-146.

Hochman JH, Pudvah N, Qiu J, Yamazaki M, Tang C, Lin JH, and Prueksaritanont T (2004) Interactions of human P-glycoprotein with simvastatin, simvastatin acid, and atorvastatin. *Pharmaceutical research* **21:**1686-1691.

Holtzman CW, Wiggins BS, and Spinler SA (2006) Role of P-glycoprotein in Statin Drug Interactions. *Pharmacotherapy: The Journal of Human Pharmacology and Drug Therapy* **26:**1601-1607.

Honig PK, Wortham DC, Zamani K, Conner DP, Mullin JC, and Cantilena LR (1993) Terfenadine-ketoconazole interaction: pharmacokinetic and electrocardiographic consequences. *Jama* **269:**1513-1518.

Houston JB (1994) Utility of in vitro drug metabolism data in predicting in vivo metabolic clearance. *Biochemical pharmacology* **47:**1469-1479.

Hsiang B, Zhu Y, Wang Z, Wu Y, Sasseville V, Yang W-P, and Kirchgessner TG (1999) A novel human hepatic organic anion transporting polypeptide (OATP2) Identification of a liver-specific human organic anion transporting polypeptide and identification of rat and human hydroxymethylglutaryl-CoA reductase inhibitor transporters. *Journal of Biological Chemistry* **274:**37161-37168.

Hurwitz SJ, Terashima M, Mizunuma N, and Slapak CA (1997) Vesicular anthracycline accumulation in doxorubicin-selected U-937 cells: participation of lysosomes. *Blood* **89:**3745-3754.

Ismair MG, Stieger B, Cattori V, Hagenbuch B, Fried M, Meier PJ, and Kullak-Ublick GA (2001) Hepatic uptake of cholecystokinin octapeptide by organic anion-transporting polypeptides OATP4 and OATP8 of rat and human liver. *Gastroenterology* **121:**1185-1190.

Israili ZH (1979) Correlation of pharmacological effects with plasma levels of antihypertensive drugs in man. *Annual review of pharmacology and toxicology* **19:**25-52.

Istvan ES, Palnitkar M, Buchanan SK, and Deisenhofer J (2000) Crystal structure of the catalytic portion of human HMG-CoA reductase: insights into regulation of activity and catalysis. *The EMBO journal* **19:**819-830.

Iwatsubo T, Hirota N, Ooie T, Suzuki H, Shimada N, Chiba K, Ishizaki T, Green CE, Tyson CA, and Sugiyama Y (1997) Prediction of in vivo drug metabolism in the human liver from in vitro metabolism data. *Pharmacology & therapeutics* **73:**147-171.

Jacobsen W, Kuhn B, Soldner A, Kirchner G, Sewing K-F, Kollman PA, Benet LZ, and Christians U (2000) Lactonization is the critical first step in the disposition of the 3-hydroxy-3-methylglutaryl-CoA reductase inhibitor atorvastatin. *Drug Metabolism and Disposition* **28:**1369-1378.

Jones SA, Moore LB, Shenk JL, Wisely GB, Hamilton GA, McKee DD, Tomkinson NC, LeCluyse EL, Lambert MH, and Willson TM (2000) The pregnane X receptor: a promiscuous xenobiotic receptor that has diverged during evolution. *Molecular endocrinology* **14:**27-39.

Kalliokoski A and Niemi M (2009) Impact of OATP transporters on pharmacokinetics. *British journal of pharmacology* **158:**693-705.

Kameyama Y, Yamashita K, Kobayashi K, Hosokawa M, and Chiba K (2005) Functional characterization of SLCO1B1 (OATP-C) variants, SLCO1B1* 5, SLCO1B1* 15 and SLCO1B1* 15+ C1007G, by using transient expression systems of HeLa and HEK293 cells. *Pharmacogenetics and genomics* **15:**513-522.

Kandušer M, Šentjurc M, and Miklavčič D (2008) The temperature effect during pulse application on cell membrane fluidity and permeabilization. *Bioelectrochemistry* **74:**52-57.

Kantola T, Kivistö KT, and Neuvonen PJ (1998) Effect of itraconazole on the pharmacokinetics of atorvastatin. *Clinical Pharmacology & Therapeutics* **64:**58-65.

Karlgren M, Vildhede A, Norinder U, Wisniewski JR, Kimoto E, Lai Y, Haglund U, and Artursson P (2012) Classification of inhibitors of hepatic organic anion transporting polypeptides (OATPs): influence of protein expression on drug–drug interactions. *Journal of medicinal chemistry* **55:**4740-4763.

Katz DA, Carr R, Grimm DR, Xiong H, Holley-Shanks R, Mueller T, Leake B, Wang Q, Han L, and Wang PG (2006) Organic anion transporting polypeptide 1B1 activity classified by SLCO1B1 genotype influences atrasentan pharmacokinetics. *Clinical Pharmacology & Therapeutics* **79:**186-196.

Kazmi F, Hensley T, Pope C, Funk RS, Loewen GJ, Buckley DB, and Parkinson A (2013) Lysosomal sequestration (trapping) of lipophilic amine (cationic amphiphilic) drugs in immortalized human hepatocytes (Fa2N-4 cells). *Drug Metabolism and Disposition* **41:**897-905.

Kemp DC, Zamek-Gliszczynski MJ, and Brouwer KL (2005) Xenobiotics inhibit hepatic uptake and biliary excretion of taurocholate in rat hepatocytes. *Toxicological Sciences* **83:**207-214.

Knipp GT, Ho NF, Barsuhn CL, and Borchardt RT (1997) Paracellular diffusion in Caco-2 cell monolayers: Effect of perturbation on the transport of hydrophilic compounds that vary in charge and size. *Journal of pharmaceutical sciences* **86:**1105-1110.

Kobayashi K, Urashima K, Shimada N, and Chiba K (2002) Substrate specificity for rat cytochrome P450 (CYP) isoforms: screening with cDNA-expressed systems of the rat. *Biochemical pharmacology* **63:**889-896.

Koch-Weser J and Sellers EM (1976) Binding of drugs to serum albumin. *New England Journal of Medicine* **294:**311-316.

Kochansky CJ, McMasters DR, Lu P, Koeplinger KA, Kerr HH, Shou M, and Korzekwa KR (2008) Impact of pH on plasma protein binding in equilibrium dialysis. *Molecular pharmaceutics* **5:**438-448.

Koepsell H (2013) The SLC22 family with transporters of organic cations, anions and zwitterions. *Molecular aspects of medicine* **34:**413-435.

König J (2011) Uptake transporters of the human OATP family, in: *Drug Transporters*, pp 1-28, Springer.

Korzekwa K and Nagar S (2014) Compartmental models for apical efflux by P-glycoprotein: Part 2—A theoretical study on transporter kinetic parameters. *Pharmaceutical research* **31:**335-346.

Korzekwa K, Nagar S, Tucker J, Weiskircher EA, Bhoopathy S, and Hidalgo IJ (2012) Models to predict unbound intracellular drug concentrations in the presence of transporters. *Drug Metabolism and Disposition***:**dmd. 111.044289.

Kotegawa T, Laurijssens BE, von Moltke LL, Cotreau MM, Perloff MD, Venkatakrishnan K, Warrington JS, Granda BW, Harmatz JS, and Greenblatt DJ (2002) In vitro, pharmacokinetic, and pharmacodynamic interactions of ketoconazole and midazolam in the rat. *Journal of Pharmacology and Experimental Therapeutics* **302:**1228-1237.

Krishnamurthy P, Ross DD, Nakanishi T, Bailey-Dell K, Zhou S, Mercer KE, Sarkadi B, Sorrentino BP, and Schuetz JD (2004) The stem cell marker Bcrp/ABCG2 enhances hypoxic cell survival through interactions with heme. *Journal of Biological Chemistry* **279:**24218-24225.

Lancon A, Delma D, Osman H, Thénot J-P, Jannin B, and Latruffe N (2004) Human hepatic cell uptake of resveratrol: involvement of both passive diffusion and carrier-mediated process. *Biochemical and biophysical research communications* **316:**1132-1137.

Lau Y, Huang Y, Frassetto L, and Benet L (2007) Effect of OATP1B transporter inhibition on the pharmacokinetics of atorvastatin in healthy volunteers. *Clinical Pharmacology & Therapeutics* **81:**194-204.

Lau YY, Okochi H, Huang Y, and Benet LZ (2006a) Multiple transporters affect the disposition of atorvastatin and its two active hydroxy metabolites: application of in vitro and ex situ systems. *Journal of Pharmacology and Experimental Therapeutics* **316:**762-771.

Lau YY, Okochi H, Huang Y, and Benet LZ (2006b) Pharmacokinetics of atorvastatin and its hydroxy metabolites in rats and the effects of concomitant rifampicin

single doses: relevance of first-pass effect from hepatic uptake transporters, and intestinal and hepatic metabolism. *Drug metabolism and disposition* **34:**1175-1181.

Lausecker B, Hess B, Fischer G, Mueller M, and Hopfgartner G (2000) Simultaneous determination of bosentan and its three major metabolites in various biological matrices and species using narrow bore liquid chromatography with ion spray tandem mass spectrometric detection. *Journal of Chromatography B: Biomedical Sciences and Applications* **749:**67-83.

Lave T, Coassolo P, Ubeaud G, Brandt R, Schmitt C, Dupin S, Jaeck D, and Chou RC (1996) Interspecies scaling of bosentan, a new endothelin receptor antagonist and integration of in vitro data into allometric scaling. *Pharmaceutical research* **13:**97-101.

LeCluyse EL, Audus KL, and Hochman JH (1994) Formation of extensive canalicular networks by rat hepatocytes cultured in collagen-sandwich configuration. *American Journal of Physiology-Cell Physiology* **266:**C1764-C1774.

Ledwitch KV, Barnes RW, and Roberts AG (2016) Unravelling the complex drug–drug interactions of the cardiovascular drugs, verapamil and digoxin, with P-glycoprotein. *Bioscience reports* **36:**e00309.

Lee E, Ryan S, Birmingham B, Zalikowski J, March R, Ambrose H, Moore R, Lee C, Chen Y, and Schneck D (2005) Rosuvastatin pharmacokinetics and pharmacogenetics in white and Asian subjects residing in the same environment. *Clinical Pharmacology & Therapeutics* **78:**330-341.

Lepist E-I, Gillies H, Smith W, Hao J, Hubert C, Claire III RLS, Brouwer KR, and Ray AS (2014) Evaluation of the endothelin receptor antagonists ambrisentan, bosentan, macitentan, and sitaxsentan as hepatobiliary transporter inhibitors and substrates in sandwich-cultured human hepatocytes. *PloS one* **9:**e87548.

Leslie EM, Watkins PB, Kim RB, and Brouwer KL (2007) Differential inhibition of rat and human Na+-dependent taurocholate cotransporting polypeptide (NTCP/SLC10A1) by bosentan: a mechanism for species differences in hepatotoxicity. *Journal of Pharmacology and Experimental Therapeutics* **321:**1170-1178.

Lilja JJ, Kivistö KT, and Neuvonen PJ (1999) Grapefruit juice increases serum concentrations of atorvastatin and has no effect on pravastatin. *Clinical pharmacology and therapeutics* **66:**118-127.

Lindblad WJ, Schuetz EG, Redford KS, and Guzelian PS (1991) Hepatocellular phenotype in vitro is influenced by biophysical features of the collagenous substratum. *Hepatology* **13:**282-288.

Linder CD, Renaud NA, and Hutzler JM (2009) Is 1-aminobenzotriazole an appropriate in vitro tool as a nonspecific cytochrome P450 inactivator? *Drug Metabolism and Disposition* **37:**10-13.

Liu X, Brouwer KL, Gan L-SL, Brouwer KR, Stieger B, Meier PJ, Audus KL, and LeCluyse EL (1998) Partial maintenance of taurocholate uptake by adult rat hepatocytes cultured in a collagen sandwich configuration. *Pharmaceutical research* **15:**1533-1539.

Macintyre AC and Cutler DJ (1988) The potential role of lysosomes in tissue distribution of weak bases. *Biopharmaceutics & drug disposition* **9:**513-526.

Maeda K (2015) Organic anion transporting polypeptide (OATP) 1B1 and OATP1B3 as important regulators of the pharmacokinetics of substrate drugs. *Biological and Pharmaceutical Bulletin* **38:**155-168.

Maeda K, Ieiri I, Yasuda K, Fujino A, Fujiwara H, Otsubo K, Hirano M, Watanabe T, Kitamura Y, and Kusuhara H (2006) Effects of organic anion transporting polypeptide 1B1 haplotype on pharmacokinetics of pravastatin, valsartan, and temocapril. *Clinical Pharmacology & Therapeutics* **79:**427-439.

Maeda K, Ikeda Y, Fujita T, Yoshida K, Azuma Y, Haruyama Y, Yamane N, Kumagai Y, and Sugiyama Y (2011) Identification of the Rate-Determining Process in the Hepatic Clearance of Atorvastatin in a Clinical Cassette Microdosing Study. *Clinical Pharmacology & Therapeutics* **90:**575-581.

Mano Y, Usui T, and Kamimura H (2007) Effects of bosentan, an endothelin receptor antagonist, on bile salt export pump and multidrug resistance–associated protein 2. *Biopharmaceutics & drug disposition* **28:**13-18.

Masyuk TV, Ritman EL, and LaRusso NF (2001) Quantitative assessment of the rat intrahepatic biliary system by three-dimensional reconstruction. *The American journal of pathology* **158:**2079-2088.

Matsunaga N, Kaneko N, Staub AY, Nakanishi T, Nunoya K-i, Imawaka H, and Tamai I (2015) Analysis of metabolic pathway of bosentan and cytotoxicity of bosentan metabolites based on a quantitative modeling of metabolism and transport in

sandwich-cultured human hepatocytes. *Drug Metabolism and Disposition***:**dmd. 115.067074.

Mayer LD, Lim KT, and Hartley D (2002) Identification of two distinct intracellular sites that contribute to the modulation of multidrug resistance in P388/ADR cells expressing P-glycoprotein. *Journal of Experimental Therapeutics and Oncology* **2:**107-120.

Ménochet K, Kenworthy KE, Houston JB, and Galetin A (2012) Simultaneous assessment of uptake and metabolism in rat hepatocytes: a comprehensive mechanistic model. *Journal of Pharmacology and Experimental Therapeutics* **341:**2-15.

Meyer J and Brandt R (1996) In vitro binding of the endothelin receptor antagonist ro 47-0203 to plasma proteins in man and animals, and red blood cell/plasma partitioning. *Basel: F Hoffmann-La Roche Ltd*.

Michniewicz B, Black A, Sinz M, and Woolf T (1994) In vitro and in vivo metabolism of atorvastatin (CI-981), in: *ISSX Proc*, pp 93.

Miyauchi S, Sugiyama Y, Sawada Y, Morita K, Iga T, and Hanano M (1987) Kinetics of hepatic transport of 4-methylumbelliferone in rats. Analysis by multiple indicator dilution method. *Journal of pharmacokinetics and biopharmaceutics* **15:**25-38.

Moore JT and Kliewer SA (2000) Use of the nuclear receptor PXR to predict drug interactions. *Toxicology* **153:**1-10.

Mosca P, Bonazzi P, Novelli G, Jezequel A, and Orlandi F (1985) In vivo and in vitro inhibition of hepatic microsomal drug metabolism by ketoconazole. *British journal of experimental pathology* **66:**737.

Nagar S and Korzekwa K (2012) Nonspecific Protein Binding Versus Membrane Partitioning-It Is Not Just Semantics. *Drug Metabolism and Disposition***:**dmd. 112.046599.

Nagar S, Tucker J, Weiskircher EA, Bhoopathy S, Hidalgo IJ, and Korzekwa K (2014) Compartmental models for apical efflux by P-glycoprotein—part 1: evaluation of model complexity. *Pharmaceutical research* **31:**347-359.

Nawrocki JW, Weiss SR, Davidson MH, Sprecher DL, Schwartz SL, Lupien P-J, Jones PH, Haber HE, and Black DM (1995) Reduction of LDL cholesterol by 25% to 60% in patients with primary hypercholesterolemia by atorvastatin, a new HMG-CoA reductase inhibitor. *Arteriosclerosis, thrombosis, and vascular biology* **15:**678-682.

Niemi M, Backman JT, Kajosaari LI, Leathart JB, Neuvonen M, Daly AK, Eichelbaum M, Kivistö KT, and Neuvonen PJ (2005) Polymorphic organic anion transporting polypeptide 1B1 is a major determinant of repaglinide pharmacokinetics. *Clinical Pharmacology & Therapeutics* **77:**468-478.

Niemi M, Pasanen MK, and Neuvonen PJ (2011) Organic anion transporting polypeptide 1B1: a genetically polymorphic transporter of major importance for hepatic drug uptake. *Pharmacological reviews* **63:**157-181.

Nies AT, Koepsell H, Damme K, and Schwab M (2011) Organic cation transporters (OCTs, MATEs), in vitro and in vivo evidence for the importance in drug therapy, in: *Drug Transporters*, pp 105-167, Springer.

Nozawa T, Minami H, Sugiura S, Tsuji A, and Tamai I (2005) Role of organic anion transporter OATP1B1 (OATP-C) in hepatic uptake of irinotecan and its active metabolite, 7-ethyl-10-hydroxycamptothecin: in vitro evidence and effect of single nucleotide polymorphisms. *Drug Metabolism and Disposition* **33:**434-439.

Oliven A and Bassan H (1986) Effects of rifampin and isoniazid on the isolated perfused rat liver. *Chemotherapy* **32:**159-165.

Pahnke J, Wolkenhauer O, Krohn M, and Walker LC (2008) Clinico-pathologic function of cerebral ABC transporters-implications for the pathogenesis of Alzheimer's disease. *Current Alzheimer research* **5:**396-405.

Paine SW, Parker AJ, Gardiner P, Webborn PJ, and Riley RJ (2008) Prediction of the pharmacokinetics of atorvastatin, cerivastatin, and indomethacin using kinetic models applied to isolated rat hepatocytes. *Drug Metabolism and Disposition* **36:**1365.

Pang KS and Rowland M (1977) Hepatic clearance of drugs. I. Theoretical considerations of a “well-stirred” model and a “parallel tube” model. Influence of hepatic blood flow, plasma and blood cell binding, and the hepatocellular enzymatic activity on hepatic drug clearance. *Journal of pharmacokinetics and biopharmaceutics* **5:**625-653.

Pardridge WM, Sakiyama R, and Fierer G (1983) Transport of propranolol and lidocaine through the rat blood-brain barrier. Primary role of globulin-bound drug. *Journal of Clinical Investigation* **71:**900.

Parekh JM, Shah DK, Sanyal M, Yadav M, and Shrivastav PS (2012) Development of an SPE-LC–MS/MS method for simultaneous quantification of bosentan and its active metabolite hydroxybosentan in human plasma to support a bioequivalence study. *Journal of pharmaceutical and biomedical analysis* **70:**462-470.

Parrish KE, Mao J, Chen J, Jaochico A, Ly J, Ho Q, Mukadam S, and Wright M (2016) In vitro and in vivo characterization of CYP inhibition by 1-aminobenzotriazole in rats. *Biopharmaceutics & drug disposition* **37:**200-211.

Patilea-Vrana G and Unadkat JD (2016) Transport vs. Metabolism: What Determines the Pharmacokinetics and Pharmacodynamics of Drugs? Insights From the Extended Clearance Model. *Clinical Pharmacology & Therapeutics* **100:**413-418.

Pfeifer ND, Harris KB, Yan GZ, and Brouwer KL (2013) Determination of intracellular unbound concentrations and subcellular localization of drugs in rat sandwich-cultured hepatocytes compared with liver tissue. *Drug Metabolism and Disposition* **41:**1949-1956.

Plise EG, Halladay JS, Cheong J, Sodhi J, and Salphati L (2010) Commonly used inhibitors of drug metabolizing enzymes: do they also inhibit drug transporters?, in: *Drug Metabolism Reviews*, pp 139-139, TAYLOR & FRANCIS INC 325 CHESTNUT ST, SUITE 800, PHILADELPHIA, PA 19106 USA.

Prueksaritanont T, Subramanian R, Fang X, Ma B, Qiu Y, Lin JH, Pearson PG, and Baillie TA (2002) Glucuronidation of statins in animals and humans: a novel mechanism of statin lactonization. *Drug Metabolism and Disposition* **30:**505-512.

Quinn PJ (1988) Effects of temperature on cell membranes, in: *Symp Soc Exp Biol*, pp 237-258.

Quinney SK, Zhang X, Lucksiri A, Gorski JC, Li L, and Hall SD (2009) Physiologically-based pharmacokinetic model of mechanism-based inhibition of CYP3A by clarithromycin. *Drug Metabolism and Disposition***:**dmd. 109.028746.

Reinoso RF, Telfer BA, Brennan BS, and Rowland M (2001) Uptake of teicoplanin by isolated rat hepatocytes: comparison with in vivo hepatic distribution. *Drug Metabolism and Disposition* **29:**453-459.

Renard D, Bouillon T, Zhou P, Flesch G, and Quinn D (2015) Pharmacokinetic interactions among imatinib, bosentan and sildenafil, and their clinical implications in severe pulmonary arterial hypertension. *British journal of clinical pharmacology* **80:**75-85.

Richardson PD and Withrington PG (1982) Physiological regulation of the hepatic circulation. *Annual review of physiology* **44:**57-69.

Roch-Ramel F, Besseghir K, and Murer H (1992) Renal excretion and tubular transport of organic anions and cations. *Comprehensive Physiology*.

Rubin K, Höök M, and Timpl R (1981) Substrate adhesion of rat hepatocytes: mechanism of attachment to collagen substrates. *Cell* **24:**463-470.

Ruth A, Stein WD, Rose E, and Roninson IB (2001) Coordinate changes in drug resistance and drug-induced conformational transitions in altered-function mutants of the multidrug transporter P-glycoprotein. *Biochemistry* **40:**4332-4339.

Schneck DW, Birmingham BK, Zalikowski JA, Mitchell PD, Wang Y, Martin PD, Lasseter KC, Brown CD, Windass AS, and Raza A (2004) The effect of gemfibrozil on the pharmacokinetics of rosuvastatin. *Clinical Pharmacology & Therapeutics* **75:**455-463.

Shah RP, Kumar V, and Singh S (2008) Liquid chromatography/mass spectrometric studies on atorvastatin and its stress degradation products. *Rapid Communications in Mass Spectrometry* **22:**613-622.

Shah VP, Midha KK, Findlay JW, Hill HM, Hulse JD, McGilveray IJ, McKay G, Miller KJ, Patnaik RN, and Powell ML (2000) Bioanalytical method validation—a revisit with a decade of progress. *Pharmaceutical research* **17:**1551-1557.

Shigehara E, Tokui T, Koga T, Ishigami M, Kuroiwa C, and Horiuchi S (1992) Carrier-mediated uptake of pravastatin by rat hepatocytes in primary culture. *Biochemical pharmacology* **43:**667-670.

Shimada S, Fujino H, Morikawa T, Moriyasu M, and Kojima J (2003) Uptake mechanism of pitavastatin, a new inhibitor of HMG-CoA reductase, in rat hepatocytes. *Drug metabolism and pharmacokinetics* **18:**245-251.

Shou M, Hayashi M, Pan Y, Xu Y, Morrissey K, Xu L, and Skiles GL (2008) Modeling, prediction, and in vitro in vivo correlation of CYP3A4 induction. *Drug Metabolism and Disposition* **36:**2355-2370.

Smith PJ, Sykes HR, Fox ME, and Furlong IJ (1992) Subcellular distribution of the anticancer drug mitoxantrone in human and drug-resistant murine cells analyzed by flow cytometry and confocal microscopy and its relationship to the induction of DNA damage. *Cancer research* **52:**4000-4008.

Sohlenius-Sternbeck A-K (2006) Determination of the hepatocellularity number for human, dog, rabbit, rat and mouse livers from protein concentration measurements. *Toxicology in vitro* **20:**1582-1586.

Somogyi A and Gugler R (1983) Clinical pharmacokinetics of cimetidine. *Clinical pharmacokinetics* **8:**463-495.

Song I-S, Lee DY, Shin M-H, Kim H, Ahn YG, Park I, Kim KH, Kind T, Shin J-G, and Fiehn O (2012) Pharmacogenetics meets metabolomics: discovery of tryptophan as a new endogenous OCT2 substrate related to metformin disposition. *PLoS One* **7:**e36637.

Spears KJ, Ross J, Stenhouse A, Ward CJ, Goh L-B, Wolf CR, Morgan P, Ayrton A, and Friedberg TH (2005) Directional trans-epithelial transport of organic anions in porcine LLC-PK1 cells that co-express human OATP1B1 (OATP-C) and MRP2. *Biochemical pharmacology* **69:**415-423.

Sun H and Pang KS (2008) Permeability, transport, and metabolism of solutes in Caco-2 cell monolayers: a theoretical study. *Drug Metabolism and Disposition* **36:**102-123.

Suzuki H and Sugiyama Y (2002) Transporters for bile acids and organic anions, in: *Membrane Transporters as Drug Targets*, pp 387-439, Springer.

Suzuki H, Terasaki T, and Sugiyama Y (1997) Role of efflux transport across the blood-brain barrier and blood-cerebrospinal fluid barrier on the disposition of xenobiotics in the central nervous system. *Advanced drug delivery reviews* **25:**257-285.

Ternberg JL and Butcher HR (1965) Blood-flow relation between hepatic artery and portal vein. *Science* **150:**1030-1031.

Tirona RG and Kim RB (2007) Organic anion-transporting polypeptides. *Drug Transporters***:**75-104.

Trauner M and Boyer JL (2003) Bile salt transporters: molecular characterization, function, and regulation. *Physiological reviews* **83:**633-671.

Treiber A, Schneiter R, Delahaye S, and Clozel M (2004) Inhibition of organic anion transporting polypeptide-mediated hepatic uptake is the major determinant in the pharmacokinetic interaction between bosentan and cyclosporin A in the rat. *Journal of Pharmacology and Experimental Therapeutics* **308:**1121-1129.

Treiber A, Schneiter R, Häusler S, and Stieger B (2007) Bosentan is a substrate of human OATP1B1 and OATP1B3: inhibition of hepatic uptake as the common mechanism of its interactions with cyclosporin A, rifampicin, and sildenafil. *Drug metabolism and disposition* **35:**1400-1407.

van Giersbergen PL, Halabi A, and Dingemanse J (2002) Single-and multiple-dose pharmacokinetics of bosentan and its interaction with ketoconazole. *British journal of clinical pharmacology* **53:**589-595.

VanWert AL, Gionfriddo MR, and Sweet DH (2010) Organic anion transporters: discovery, pharmacology, regulation and roles in pathophysiology. *Biopharmaceutics & drug disposition* **31:**1-71.

Vavricka SR, Van Montfoort J, Ha HR, Meier PJ, and Fattinger K (2002) Interactions of rifamycin SV and rifampicin with organic anion uptake systems of human liver. *Hepatology* **36:**164-172.

Vignati LA, Bogni A, Grossi P, and Monshouwer M (2004) A human and mouse pregnane X receptor reporter gene assay in combination with cytotoxicity measurements as a tool to evaluate species-specific CYP3A induction. *Toxicology* **199:**23-33.

Vildhede A, Karlgren M, Svedberg EK, Wisniewski JR, Lai Y, Norén A, and Artursson P (2014) Hepatic uptake of atorvastatin: influence of variability in transporter expression on uptake clearance and drug-drug interactions. *Drug metabolism and disposition***:**dmd. 113.056309.

Wang B, You G, and Morris ME (2007) *Drug transporters: molecular characterization and role in drug disposition*. John Wiley & Sons.

Watanabe T, Kusuhara H, Maeda K, Kanamaru H, Saito Y, Hu Z, and Sugiyama Y (2009a) Investigation of the rate-determining process in the hepatic elimination of HMG-CoA reductase inhibitors in rats and humans. *Drug Metabolism and Disposition***:**dmd. 109.030254.

Watanabe T, Kusuhara H, Maeda K, Shitara Y, and Sugiyama Y (2009b) Physiologically based pharmacokinetic modeling to predict transporter-mediated clearance and

distribution of pravastatin in humans. *Journal of Pharmacology and Experimental Therapeutics* **328:**652-662.

Watanabe T, Kusuhara H, Watanabe T, Debori Y, Maeda K, Kondo T, Nakayama H, Horita S, Ogilvie BW, and Parkinson A (2011) Prediction of the overall renal tubular secretion and hepatic clearance of anionic drugs and a renal drug-drug interaction involving organic anion transporter 3 in humans by in vitro uptake experiments. *Drug Metabolism and Disposition* **39:**1031-1038.

Watanabe T, Maeda K, Kondo T, Nakayama H, Horita S, Kusuhara H, and Sugiyama Y (2009c) Prediction of the hepatic and renal clearance of transporter substrates in rats using in vitro uptake experiments. *Drug Metabolism and Disposition* **37:**1471-1479.

Watanabe T, Miyake M, Shimizu T, Kamezawa M, Masutomi N, Shimura T, and Ohashi R (2015) Utility of bilirubins and bile acids as endogenous biomarkers for the inhibition of hepatic transporters. *Drug Metabolism and Disposition* **43:**459-466.

Weber C, Gasser R, and Hopfgartner G (1999a) Absorption, excretion, and metabolism of the endothelin receptor antagonist bosentan in healthy male subjects. *Drug Metabolism and Disposition* **27:**810-815.

Weber C, Schmitt R, Birnboeck H, Hopfgartner G, Eggers H, Meyer J, Marle S, Viischer HW, and Jonkman JH (1999b) Multiple-Dose Pharmacokinetics, Safety, and Tolerability of Bosentan, an Endothelin Receptor Antagonist, in Healthy Male Volunteers. *The Journal of Clinical Pharmacology* **39:**703-714.

Weber C, Schmitt R, Birnboeck H, Hopfgartner G, Marle SP, Peeters PA, Jonkman JH, and Jones CR (1996) Pharmacokinetics and pharmacodynamics of the endothelin-receptor antagonist bosentan in healthy human subjects. *Clinical Pharmacology & Therapeutics* **60:**124-137.

Woodward OM, Köttgen A, Coresh J, Boerwinkle E, Guggino WB, and Köttgen M (2009) Identification of a urate transporter, ABCG2, with a common functional polymorphism causing gout. *Proceedings of the National Academy of Sciences* **106:**10338-10342.

Xiang X, Jada SR, Li HH, Fan L, San Tham L, Wong CI, Lee SC, Lim R, Zhou QY, and Goh BC (2006) Pharmacogenetics of SLCO1B1 gene and the impact of* 1b and* 15 haplotypes on irinotecan disposition in Asian cancer patients. *Pharmacogenetics and genomics* **16:**683-691.

Xiong H, Callaghan D, Jones A, Bai J, Rasquinha I, Smith C, Pei K, Walker D, Lue L-F, and Stanimirovic D (2009) ABCG2 is upregulated in Alzheimer's brain with cerebral amyloid angiopathy and may act as a gatekeeper at the blood–brain barrier for Aβ1–40 peptides. *Journal of Neuroscience* **29:**5463-5475.

Yabe Y, Galetin A, and Houston JB (2011) Kinetic characterization of rat hepatic uptake of 16 actively transported drugs. *Drug Metabolism and Disposition***:**dmd. 111.040477.

Yamashiro W, Maeda K, Hirouchi M, Adachi Y, Hu Z, and Sugiyama Y (2006) Involvement of transporters in the hepatic uptake and biliary excretion of

valsartan, a selective antagonist of the angiotensin II AT1-receptor, in humans. *Drug metabolism and disposition* **34:**1247-1254.

Zhang W, He YJ, Han CT, Liu ZQ, Li Q, Fan L, Tan ZR, Zhang WX, Yu BN, and Wang D (2006) Effect of SLCO1B1 genetic polymorphism on the pharmacokinetics of nateglinide. *British journal of clinical pharmacology* **62:**567-572.

Zhang X, Galinsky RE, Kimura RE, Quinney SK, Jones DR, and Hall SD (2010) Inhibition of CYP3A by erythromycin: in vitro-in vivo correlation in rats. *Drug Metabolism and Disposition* **38:**61-72.

Ziemniak JA, Shank RG, and Schentag JJ (1984) The partitioning of cimetidine into canine cerebrospinal fluid. *Drug metabolism and disposition* **12:**217-221.

Zou P, Yu Y, Zheng N, Yang Y, Paholak HJ, Lawrence XY, and Sun D (2012) Applications of human pharmacokinetic prediction in first-in-human dose estimation. *The AAPS journal* **14:**262-281.

APPENDIX A

SENSITIVITY ANALYSIS FOR BOS LIVER PERFUSION MODELING

Sensitivity analysis was conducted for testing the effect of CL_m, CL_{aec}, CL_{aem} and "a" on CL_i, total tissue concentrations and amount recovered in the bile for BOS using BOS + RIF dataset, observed tissue concentrations: 136 µM, observed amount recovered in bile 0.012 µmoles, the predicted values falling outside the 20% cut-off are denoted in red

Table A1. Effect of CL_m on CL_i, total tissue concentrations and amount recovered in the bile for BOS using BOS + RIF dataset; Fixed parameters: CL_{aec} = 49.9 L/min, CL_{aem} = 0.00045 L/min, a = 0.2 and CL_m

CL_m (L/min)	0.029	0.058	0.115	0.014	0.007
CL_i estimate ± standard error (L/min)	5.52 ± 1.02	7.03 ± 2.63	8.01 ± 8.47	4.9 ± 0.72	4.62± 0.47
R^2	0.94	0.90	0.774	0.95	0.96
Adjusted R^2	0.93	0.88	0.742	0.95	0.95
Predicted liver concentration (µM)	135.4	95.96	57.42	157.6	168.9
Predicted amount in bile (µmoles)	0.0113	0.0085	0.0057	0.0127	0.0135
Predicted unbound cell concentration at 50 min (µM)	0.251	0.216	0.143	0.264	0.270

The predicted values falling outside the 20% cut-off are denoted in red

Table A2. Effect of CL_{aec} on CL_i, total tissue concentrations and amount recovered in the bile for BOS using BOS + RIF dataset; Fixed parameters: CL_m = 0.029 L/min or 0.0143 L/min, CL_{aem} = 0.00045 L/min, a = 0.2 and CL_{aec}

	CL_m = 0.029 L/min					CL_m = 0.0143 L/min	
CL_{aec} (L/min)	99.89	199.78	24.97	12.49	9.99	199.78	9.99
CL_i estimate ± standard error (L/min)	11.26 ± 2.01	22.77 ± 4.44	2.66 ± 0.58	1.27 ± 0.36	0.99 ± 0.31	20.1 ± 2.37	0.9124 ± 0.2331
R^2	0.95	0.95	0.94	0.92	0.91	0.96	0.92
Adjusted R^2	0.94	0.94	0.93	0.91	0.90	0.954	0.9055
Predicted liver concentration (µM)	135.05	134.70	136.29	136.42	136.30	157.5	155.2
Predicted amount in bile (µmoles)	0.0111	0.0109	0.0118	0.0129	0.0134	0.0123	0.015
Predicted unbound cell concentration at 50 min (µM)	0.254	0.256	0.245	0.235	0.231	0.27	0.245

The predicted values falling outside the 20% cut-off are denoted in red

Table A3. Effect of CL_{aem} on CL_i, total tissue concentrations and amount recovered in the bile for BOS using BOS + RIF dataset; Fixed parameters: CL_m = 0.029 L/min or 0.0143 L/min, CL_{aec} = 49.9 L/min, a = 0.2

	CL_m = 0.029 L/min					CL_m = 0.0143 L/min	
CL_{aem}* (L/min)	0.000905	0.002714	0.004524	0.000113	0	0	0.002714
CL_i estimate ± standard error (L/min)	5.53 ± 0.99	5.55 ± 1.02	5.65 ± 1.11	5.52 ± 1.01	5.46 ± 1.01	4.89 ± 0.652	4.922 ± 0.66
R^2	0.94	0.94	0.94	0.94	0.94	0.957	0.956
Adjusted R^2	0.94	0.94	0.94	0.94	0.94	0.951	0.950
Predicted liver concentration (µM)	135.37	134.89	133.80	135.56	136.03	157.8	156.94
Predicted amount in bile (µmoles)	0.01178	0.01355	0.0151	0.01099	0.0109	0.0122	0.0156
Predicted unbound cell concentration at 50 min (µM)	0.251	0.251	0.253	0.251	0.250	0.264	0.264

The predicted values falling outside the 20% cut-off are denoted in red

Table A4. Effect of a (back diffusion from bile) on CL_i, total tissue concentrations and amount recovered in the bile for BOS using BOS + RIF dataset; Fixed parameters: CL_m = 0.029 L/min or 0.0143 L/min, CL_{aec} = 49.9 L/min, CL_{aem} = 0.00045 L/min

	CL_m = 0.029 L/min				CL_m = 0.0143 L/min	
A	1	0.5	0.1	0.05	0.05	1
CL_i estimate ± standard error (L/min)	5.446 ± 0.98	5.47 ± 0.87	5.63 ± 1.08	5.84 ± 1.38	5.17 ± 0.73	4.82 ± 0.62
R^2	0.945	0.945	0.942	0.939	0.953	0.958
Adjusted R^2	0.937	0.937	0.934	0.930	0.946	0.952
Predicted liver concentration (µM)	137.6	137.13	132.7	127.7	148.83	160.22
Predicted amount in bile (µmoles)	0.00229	0.00458	0.022	0.04307	0.0487	0.0026
Predicted unbound cell concentration at 50 min (µM)	0.252	0.252	0.250	0.248	0.261	0.265

The predicted values falling outside the 20% cut-off are denoted in red

Table A5. Effect of CL_{aem} and CL_{aec} on CL_i, total tissue concentrations and amount recovered in the bile for BOS using BOS + RIF dataset; Fixed parameters: CL_m = 0.029 L/min and a = 0.2

CL_{aec} (L/min)	199.78	9.99	199.78	9.99
CL_{aem}^* (L/min)	0	0	0.002714	0.002714
CL_i estimate ± standard error (L/min)	23.33 ± 3.62	0.33 ± 0.01805	22.79 ± 3.78	1.03 ± 0.32
R^2	0.946	0.912	0.946	0.911
Adjusted R^2	0.939	0.899	0.939	0.898
Predicted liver concentration (µM)	133.7	136.3	134.64	132.8
Predicted amount in bile (µmoles)	0.0107	0.0109	0.0115	0.0249
Predicted unbound cell concentration at 50 min (µM)	0.259	0.233	0.256	0.232

The predicted values falling outside the 20% cut-off are denoted in red

Table A6. Effect of CL_{aec} and a on CL_i, total tissue concentrations and amount recovered in the bile for BOS using BOS + RIF dataset; Fixed parameters: CL_m = 0.029 L/min and CL_{aem} = 0

CL_{aec} (L/min)	199.78	9.99	199.78	9.99
A	0.05	1	0.05	1
CL_i estimate ± standard error (L/min)	23.75 ± 4.35	1.06 ± 0.37	22.37 ± 3.69	0.99 ± 0.30
R^2	0.942	0.910	0.948	0.912
Adjusted R^2	0.933	0.896	0.940	0.899
Predicted liver concentration (µM)	127.74	128.7	137.05	138
Predicted amount in bile (µmoles)	0.0414	0.0410	0.0023	0.0022
Predicted unbound cell concentration at 50 min (µM)	0.251	0.231	0.257	0.233

The predicted values falling outside the 20% cut-off are denoted in red

APPENDIX B

INDIVIDUAL PK PROFILES IN DIFFERENT EXPERIMENTAL GROUPS FOR INHIBITION OF ATV METABOLISM BY ABT AND KETO

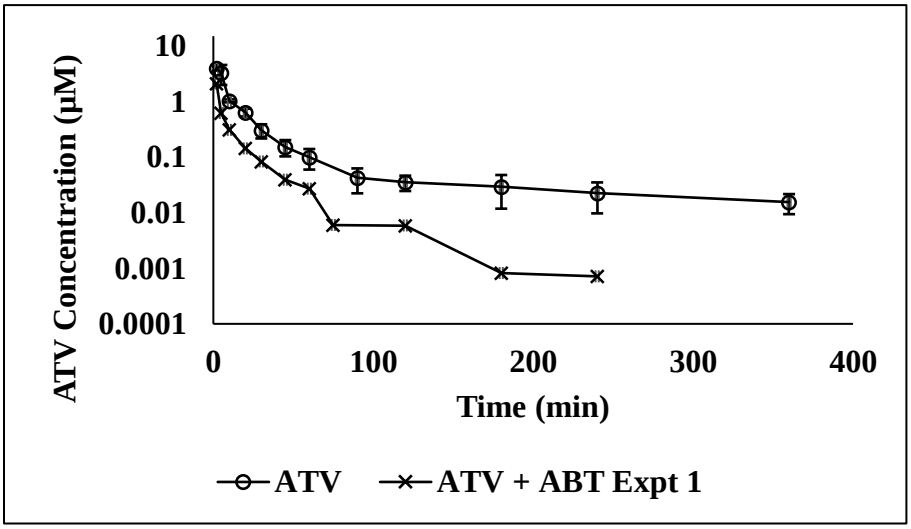

Figure B1 Effect of inhibition of ATV metabolism by ABT (experiment 1). ATV: n=3, ATV + ABT Experiment 1: n=3; Data are presented as mean ± SD

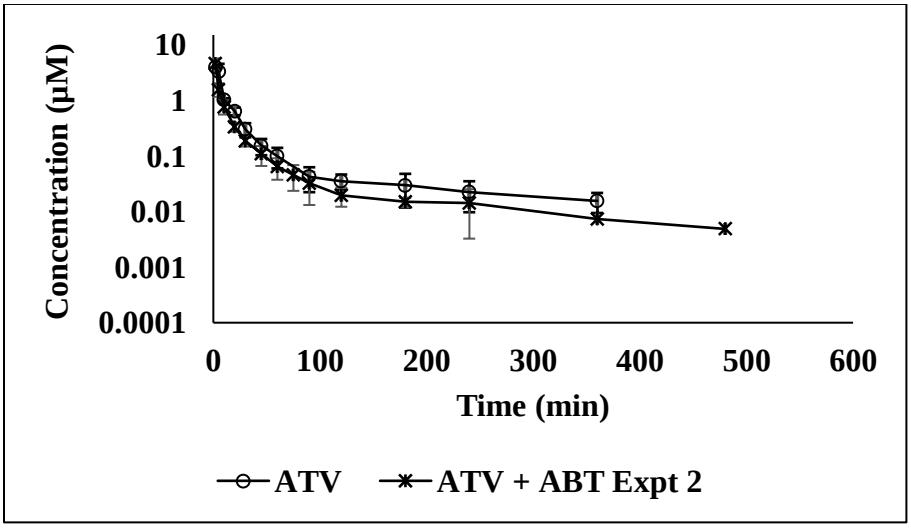

Figure B2 Effect of inhibition of ATV metabolism by ABT (experiment 2). ATV: n=3, ATV + ABT Experiment 2: n=3; Data are presented as mean ± SD

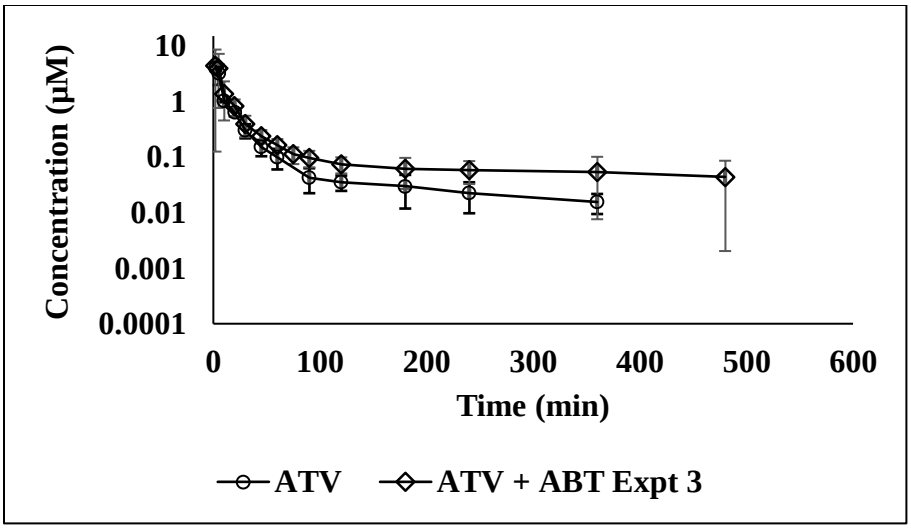

Figure B3 Effect of inhibition of ATV metabolism by ABT (experiment 3). ATV: n=3, ATV + ABT Experiment 3: n=3; Data are presented as mean ± SD

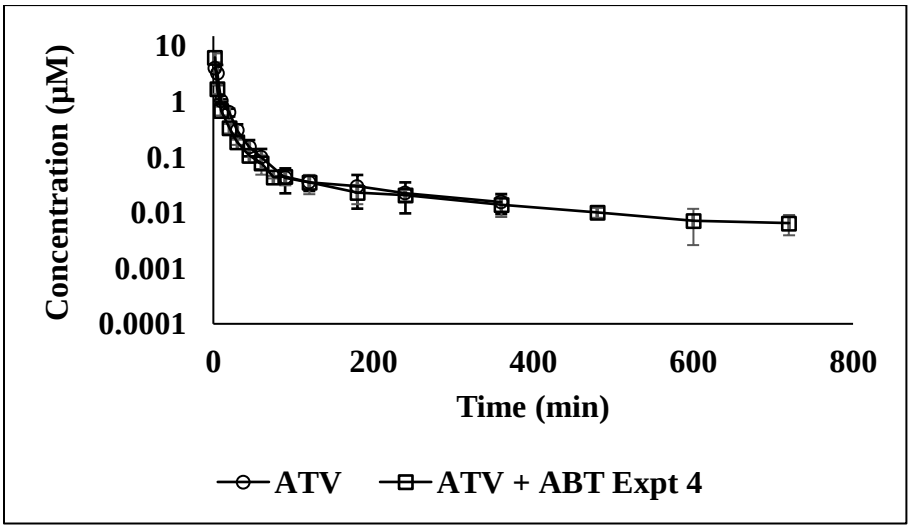

Figure B4 Effect of inhibition of ATV metabolism by ABT (experiment 4). ATV: n=3, ATV + ABT Experiment 4: n=3; Data are presented as mean ± SD

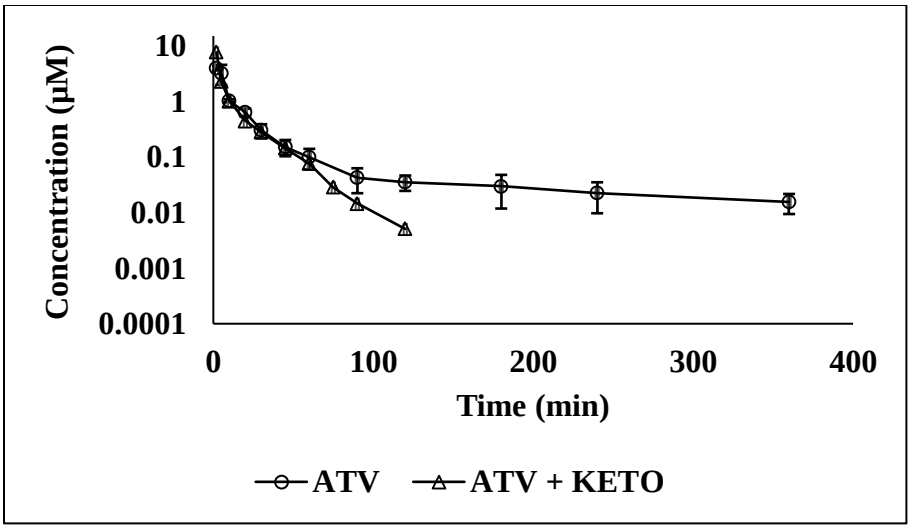

Figure B5 Effect of inhibition of ATV metabolism by KETO. ATV: n=3, ATV + KETO: n=3; Data are presented as mean ± SD

APPENDIX C

COMPARTMENTAL ANALYSIS FOR BOS PK DATA FROM BOS + ABT GROUP

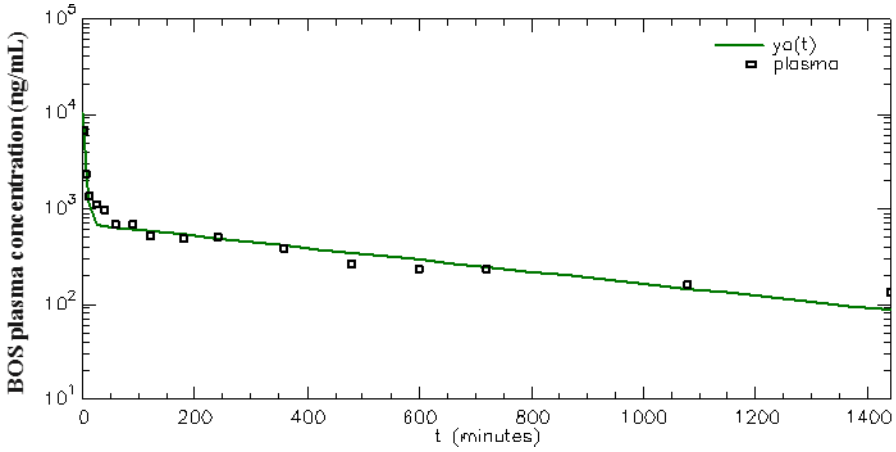

Figure C1 2-C model analysis of BOS PK data from BOS + ABT group. BOS PK profile predicted by 2-C model (green line) overlaid on experimental PK data (Open squares)

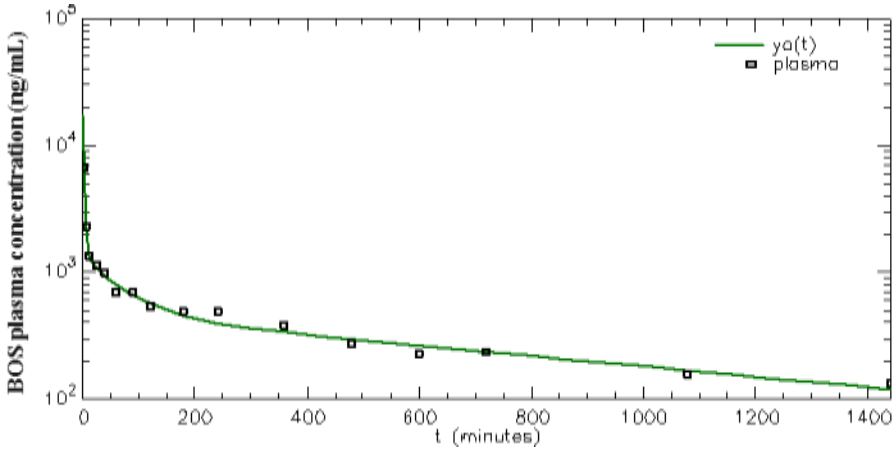

Figure C2 3-C model analysis of BOS PK data from BOS + ABT group. BOS PK profile predicted by 3-C model (green line) overlaid on experimental PK data (Open squares)

Table C1. Compartmental analysis of BOS PK from BOS + ABT group

	CL (mL/min)	**V_{ss} (mL)**	**$t_{1/2}$ (min)**
BOS + ABT (2C analysis)	1.9 ± 0.16	758 ± 80	479 ± 65
BOS + ABT (3C analysis)	1.7 ± 1.06	921 ± 85	729 ± 107

APPENDIX D

ANALYSIS OF BOS PK DATA FROM BOS + RIF GROUP USING THE 2-C HYBRID MODEL, WITHOUT THE ASSUMPTION OF INHIBITION OF APICAL EFFLUX.

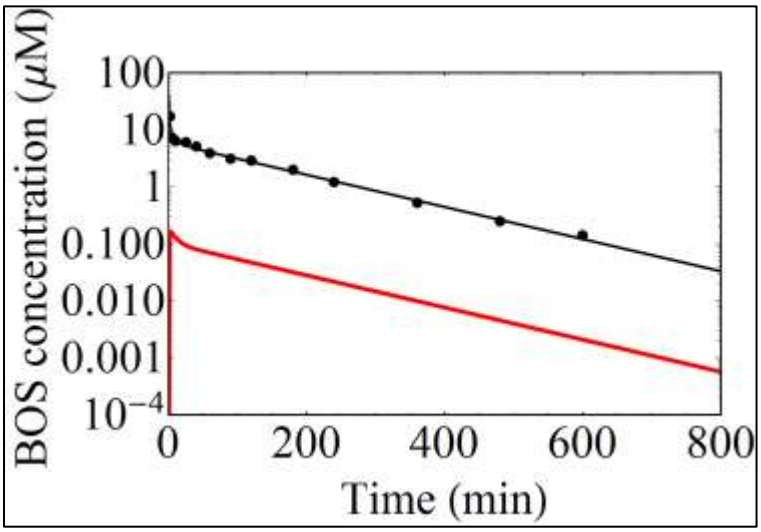

Figure D1 Fitted BOS concentration-time profiles for BOS + RIF group using the semi-physiological model without the assumption of apical efflux. Solid circles are experimental data for plasma concentrations, black solid line represents model fitted plasma profile, and red solid line represents model predicted unbound intracellular concentration-time profile

Table D1 Parameter estimates obtained by analysis of BOS data with the 2-C hybrid model without inhibition of apical efflux

Parameter	**BOS + RIF (without apical efflux inhibition)**
K_{12}	0.184 ± 0.39
K_{21}	0.006 ± 0.02
$V_{central}$ (liters)	0.027 ± 0.044
A	0.0007 ± 0.012

APPENDIX E

PERMISSION TO REPRODUCE COPYRIGHTED MATERIAL

March 16, 2017

Priyanka Kulkarni
Pharmaceutical Sciences Department
Temple University
3307 N Broad Street
Philadelphia, PA 19140

Email: priyanka.k@temple.edu

Dear Priyanka Kulkarni:

This is to grant you permission to reproduce selected text, Figures 1-5, and Tables 1-3 in your dissertation entitled "Intracellular unbound concentrations of atorvastatin and bosentan - Prediction using modeling and simulation, and effect of metabolism and transport" for Temple University:

> Selected text, Figures 1-5, and Tables 1-3 from P Kulkarni, K Korzekwa, and S Nagar (2016) Intracellular Unbound Atorvastatin Concentrations in the Presence of Metabolism and Transport, *J Pharmacol Exp Ther*, 359(1):26-36; DOI: https://doi.org/10.1124/jpet.116.235689

Permission to reproduce the material is granted for worldwide use in all languages, translations, and editions, and in any format or medium including print and electronic. The authors and the source of the materials must be cited in full, including the article title, journal title, volume, year, and page numbers.

Sincerely yours,

Richard Dodenhoff
Journals Director

9650 Rockville Pike | Bethesda | MD | 20814-3995
P: (301) 634-7060 | F: (301) 634-7061 | E: info@aspet.org | www.aspet.org